INVESTIGATION ON MECHANICAL, MICROSTRUCTURAL AND THERMAL PROPERTIES OF Sn-0.7Cu AND Sn-1Ag-0.5Cu SOLDER ALLOYS BEARING Fe AND Bi

MOHAMMAD HOSSEIN MAHDAVIFARD

FACULTY OF ENGINEERING
UNIVERSITY OF MALAYA
KUALA LUMPUR

2017

INVESTIGATION ON MECHANICAL, MICROSTRUCTURAL AND THERMAL PROPERTIES OF Sn-0.7Cu AND Sn-1Ag-0.5Cu SOLDER ALLOYS BEARING Fe AND Bi

MOHAMMAD HOSSEIN MAHDAVIFARD

THESIS SUBMITTED IN FULFILMENT OF THE REQUIREMENTS FOR THE DEGREE OF DOCTOR OF PHILOSOPHY

FACULTY OF ENGINEERING
UNIVERSITY OF MALAYA
KUALA LUMPUR

2017

UNIVERSITY OF MALAYA

ORIGINAL LITERARY WORK DECLARATION

Name of Candidate: **Mohammad Hossein Mahdavifard**

Registration/Matric No: **KHA130085**

Name of Degree: **Ph.D.**

Title of Project Paper/Research Report/Dissertation/Thesis ("this Work"):

INVESTIGATION ON MECHANICAL, MICROSTRUCTURAL AND THERMAL PROPERTIES OF Sn-0.7Cu AND Sn-1Ag-0.5Cu SOLDER ALLOYS BEARING Fe AND Bi

Field of Study: **Advanced materials/Nanomaterials**

I do solemnly and sincerely declare that:

(1) I am the sole author/writer of this Work;
(2) This Work is original;
(3) Any use of any work in which copyright exists was done by way of fair dealing and for permitted purposes and any excerpt or extract from, or reference to or reproduction of any copyright work has been disclosed expressly and sufficiently and the title of the Work and its authorship have been acknowledged in this Work;
(4) I do not have any actual knowledge nor do I ought reasonably to know that the making of this work constitutes an infringement of any copyright work;
(5) I hereby assign all and every rights in the copyright to this Work to the University of Malaya ("UM"), who henceforth shall be owner of the copyright in this Work and that any reproduction or use in any form or by any means whatsoever is prohibited without the written consent of UM having been first had and obtained;
(6) I am fully aware that if in the course of making this Work I have infringed any copyright whether intentionally or otherwise, I may be subject to legal action or any other action as may be determined by UM.

Candidate's Signature Date:

Subscribed and solemnly declared before,

Witness's Signature Date:

Name:

Designation:

ABSTRACT

Low-Ag Sn-Ag-Cu (SAC) alloys such as Sn-1 wt.%Ag-0.5 wt.% Cu (SAC105) have been considered as a solution to both the cost and poor drop impact reliability issues of high Ag SAC solders. Moreover, alloying elements have been added into SAC solder alloys to refine the microstructure, and improve the wettability and mechanical properties. In the present study, Fe and Bi were added together to the low Ag solder, Sn-1 wt.%Ag-0.5 wt.% Cu (SAC105), and without Ag, Sn-0.7Cu(SC07) to investigate the effect of these two elements on the bulk alloy microstructure, tensile and thermal properties. Fe and Bi have different role to improve reliability of solder alloy. Fe improve and stabilize mechanical properties and drop reliability, whereas Bi strengthen solder by solid solution effect, decrease melting temperature and improve wetting properties. On the basis of the previous works, 0.05wt%Fe added to SAC105 or SC07 because by increasing Fe more than 0.1wt% it makes large $FeSn_2$ intermetallic in bulk of solder which deteriorate mechanical properties. Also, selected 1 and 2wt% Bi to add to SAC105 or SC07 because Liu et al. showed that more than 3wt% Bi make solder too brittle. Addition of Bi to SAC105-Fe and SC07-Fe increased yield strength and ultimate tensile strength while decreased total elongation. Bi degenerated the eutectic region into a chain-like arrangement, which decreased Cu_6Sn_5 and increased β-Sn in solder. 0.05wt%Fe made few $FeSn_2$ IMC particles in the solder which does not have considerable effect on mechanical and microstructural properties. 1wt% or 2wt%Bi scattered in the whole of solder without concentration at any position and strengthen solder by a solid solution effect. The surface fracture of solder does not show necking by addition of Bi. Moreover, the solidus temperature of SAC105Fe-2Bi is 214°C, which is 5°C less than SAC105. The addition of 2 wt.% Bi to SC07-Fe decreases the solidus temperature of SC07 from 227.6°C to 223.8°C. After aging at 125 °C for 30 days, UTS (ultimate tensile strength)

and yield strength decreased for SAC105 or SC07 by coarsening of IMCs whereas total elongation increased. Scanning electron microscope (FESEM) and energy dispersive X-ray (EDX) indicated that the growth and spheroidization of [Cu_6Sn_5 and Ag_3Sn] for SAC105 or Cu_6Sn_5 for SC07 after aging controlled by Gibbs-Thomson effect and Ostwald ripening process. Therefore, IMCs and β-Sn grains coarsened. Addition of Bi strengthen solder by scattering in the bulk of SAC105-Fe solder alloy, increased β-Sn and degenerated Cu_6Sn_5 and Ag_3Sn into a chain-like arrangement due to the solid solution and precipitation strengthening effects by Bi in the Sn-rich phase. Partially substitution of Fe in the Cu_6Sn_5 on the basis of Darken-Gurry ellipse decreased microstructure coarsening rate. UTS, Yield strength, and total elongation are approximately constant for SAC105-Fe-Bi and SC07-Fe-Bi after aging which means stable properties of solder. The nanoindentation results for SC07 and SAC105 solder alloys after addition of Bi and Fe showed a remarkable increase in Er (reduced elastic modulus) and hardness. Wetting angle of SC07 and SAC105 with RMA (rosin mildly activated) flux after addition of Fe and Bi decreased, whereas spreading rate increased.

ABSTRAK

Aloi Sn-Ag-Cu yang berkandungan Ag rendah seperti Sn-1 wt.%Ag-0.5 wt.% Cu (SAC105) difikirkan sebagai penyelesaian kepada kedua-dua masalah kos dan kebolehpercayaan impak jatuh yang teruk untuk pateri SAC yang mempunyai kandungan Ag yang tinggi. Lebih-lebih lagi, aplikasi aloi SAC dihadkan oleh elemen pengaloian yang kasar ditambah ke dalam aloi SAC untuk memperhalusi struktur mikro, dan menambah baik sifat-sifat kebolehbasahan dan mekanikal. Dalam kajian ini, Fe dan Bi ditambah bersama-sama ke dalam aloi pateri Ag rendah, Sn-1 wt.%Ag-0.5 wt.% Cu (SAC105), dan tanpa Ag, Sn-0.7Cu(SC07) untuk menyiasat kesan kedua-dua elemen ini kepada sifat-sifat mikrostruktur pukal aloi, tegangan dan termal. Fe dan Bi mempunyai fungsi yang berbeza dalam menambah baik kebolehpercayaan aloi pateri. Fe memperbaiki dan menstabilkan sifat mekanikal dan ketahanan jatuh, manakala Bi menguatkan pateri dengan kesan larutan pepejal, merendahkan takat lebur dan menambah baik sifat kebolehbasahan. Berasaskan kepada kajian lalu, hanya 0.05wt%Fe ditambah ke dalam SAC105 kerana meningkatkan Fe lebih daripada 0.1wt% menghasilkan antara logam $FeSn_2$ yang besar dalam pateri pukal yang mana menyebabkan sifat mekanikal merosot. 1 dan 2wt% Bi juga dipilih untuk ditambah ke dalam SAC105 kerana Liu et al. telah tunjukkan bahawa lebih daripada 3wt% Bi menjadikan pateri terlalu rapuh. Tambahan Bi ke dalam SAC105-Fe dan SC07-Fe meningkatkan kekuatan alah dan kekuatan tegangan muktamad di samping mengurangkan pemanjangan keseluruhan. Bi mengurangkan bahagian eutektik kepada susunan seperti rantai,yang mana Cu_6Sn_5 dan meningkatkan β-Sn dalam pateri. 0.05wt%Fe menghasilkan beberapa zarah IMC $FeSn_2$ dalam pateri yang mana tidak meninggalkan kesan ketara ke atas sifat-sifat mekanikal dan struktur mikro. 1wt% atau 2wt%Bi pula tersebar keseluruh pateri tidak tertumpu pada mana-mana posisi dan menguatkan pateri melalui kesan larutan pepejal. Retakan permukaan pateri tidak menunjukkan perleheran dengan tambahan Bi. Tambahan pula,

suhu solidus SAC105Fe-2Bi ialah 214°C, ianya kurang 5°C dari SAC105. Tambahan 2 wt.% Bi kepada SC07-Fe merendahkan suhu solidus SC07 dari 227.6°C ke 223.8°C. Selepas penuaan suhu pada 125 °C selama 30 hari, kekuatan tegangan muktamad (UTS) dan kekuatan alah menurun untuk SAC105 atau SC07 melalui pengasaran IMC yang mana pemanjangan keseluruhan meningkat. Mikroskop elektron pengimbas (FESEM) dan tenaga x-ray terserak (EDX) menunjukkan pertumbuhan dan sferoidisasi Cu_6Sn_5 dan Ag_3Sn untuk SAC105 atau Cu_6Sn_5 untuk SC07 selepas penuaan dikawal oleh kesan Gibbs-Thomson dan proses pematangan Ostwald. Dengan itu, butiran IMC dan β-Sn menjadi kasar. Tambahan Bi menguatkan aloi pateri dengan tersebar di dalam aloi pateri pukal SAC105-Fe, meningkatkan β-Sn dan menjadikan Cu_6Sn_5 dan Ag_3Sn kepada susunan seperti rantai disebabkan larutan pepejal dan kesan penguatan pemendakan oleh Bi dalam fasa kaya Sn. Penggantian separa Fe dalam Cu_6Sn_5 berasaskan elips Darken-Gurry mengurangkan kadar pengasaran struktur mikro. UTS, kekuatan alah, dan pemanjangan keseluruhan adalah malar selepas penuaan. Keputusan indentasi nano untuk aloi pateri SC07 dan SAC105 selepas tambahan Bi dan Fe menunnjukkan peningkataan dalam Er (modulus elastik terturun) dan kekerasan. Sudut pembasahan SC07 dan SAC105 dengan fluks RMA (rosin teraktif lembut) selepas tambahan Fe dan Bi berkurang, manakala kadar penghamparan meningkat.

ACKNOWLEDGEMENTS

Special thanks to my dear parents and my dear sister who are close to my heart and deserve the highest appreciation for their support and patience.

I express my deep and sincere gratitude to my supervisor, Prof. Dr. Mohd Faizul Mohd Sabri for his support, technical advices, recommendation and constructive comment throughout this thesis.

I express my sincere thanks to my co-supervisors Prof. Dr. Irfan Anjum Badruddin, and Dr. Shaifulazuar Rozali, as well as Prof. Dr. Suhana Mohd Said for all their support, advices, and cooperation.

I would like to thanks all technician who assist me during my experiments at mechanical department of university of Malaya, MIMOS Berhad, and Accurus Scientific Co.

I would like to thanks to my dear friends and colleagues. Special thanks to all members of NME (Nano-micro-electronic) and LCD (Liquid-crystal-display) groups for their help and friendly environment for research.

I acknowledge the financial supports provided by University of Malaya under PPP Fund project No: PG079/2014A and UMRG Fund project No: RP003A-13AET.

TABLE OF CONTENTS

LIST OF FIGURES

LIST OF TABLES

LIST OF SYMBOLS AND ABBREVIATIONS

DSC	:	Differential Scanning Calorimeter
SEM	:	Scanning Electron Microscopy
FESEM	:	Field Emission Scanning Electron Microscopy
SPM	:	Scanning Probe Microscopy
EDX (EDS)	:	Energy Dispersive X-Ray Spectroscopy
FIB	:	Focused Ion Beam
XRD	:	X-ray Diffraction
TEM	:	Transmission Electron Microscopy
AES	:	Atomic Emission Spectrometry
DTA	:	Differential Thermal Analysis
BGA	:	Ball Grid Array
ENIG	:	Electroless nickel immersion gold surface finish
IMCs	:	Intermetallic compounds
CTE	:	coefficient of thermal expansion
TMF	:	Thermomechanical Fatigue
Wt.%	:	Weight percent
HV	:	Vickers Hardness
RMA	:	Rosin Mildly Activated
ICP-OES	:	Inductive Couple Plasma- Optical Emission Spectrometer
IC	:	Integrated Circuit
PCB	:	Printed Circuit Board
FC	:	Flip Chip
SMT	:	Surface Mount Technology
WEEE	:	Waste Electrical and Electronic Equipment

USEPA	:	United States Environmental Protection Agency
NEMI	:	National Electronics Manufacturing Initiative
NCMS	:	National Center for Manufacturing Science
RoHS	:	Restriction of Hazardous Substance Directives
OSP	:	Organic Solderability Preservative
PIH	:	Pin in Hole
PTH	:	Pin through Hole
Sn	:	Tin
Pb	:	Lead
Mo	:	Molybdenum
Cu	:	Copper
Ag	:	Silver
Bi	:	Bismuth
Au	:	Gold
Zn	:	Zinc
Sb	:	Antimony
Ge	:	Germanium
In	:	Indium
Al	:	Aluminium
Mn	:	Manganese
Ce	:	Cerium
Fe	:	Iron
H_2SO_4	:	Sulphuric acid
HCL	:	Hydrochloric acid
SiC	:	Silicon carbide
nm	:	Nanometer

μm	:	Micrometer
σ	:	Engineering stress
ε	:	Engineering strain
E	:	Young's modulus
ρ	:	Density
F	:	Force
E_r	:	Reduced Young's modulus
UTS	:	Ultimate tensile strength
SAC	:	Sn-Ag-Cu solder
SAC305	:	Sn- 3wt.% Ag- 0.5wt.% Cu
SAC105	:	Sn- 1wt.% Ag- 0.5wt.% Cu
SAC105-0.05Fe-1Bi	:	Sn-1wt.% Ag-0.5wt.% Cu-0.05wt.% Fe-1wt.% Bi
SAC105-0.05Fe-2Bi	:	Sn-1wt.% Ag-0.5wt.% Cu-0.05wt.% Fe-2wt.% Bi
SC07	:	Sn-0.7wt.% Cu
SC07-0.05Fe	:	Sn-0.7wt.% Cu-0.05wt.%Fe
SC07-0.05Fe-1Bi	:	Sn-0.7wt.% Cu-0.05wt.%Fe-1wt.%Bi
SC07-0.05Fe-2Bi	:	Sn-0.7wt.% Cu-0.05wt.%Fe-2wt.%Bi
T_c	:	Onset solidification temperature
T_s	:	Solidus temperature

CHAPTER 1: INTRODUCTION

1.1 Background

The eutectic Sn–Pb solder has been a dominant alloy for surface mount technology (SMT) or wave soldering in electronic application (Abtew et al., 2000; Hu et al., 2013; Osório et al., 2013). However, Pb-free solders has been developed due to the health and environmental concerns for toxicity of Pb (Hu et al., 2015). The eutectic Sn-0.7Cu or Low Ag Sn-1Ag-0.5Cu (SAC) solder alloys with superior properties such as: low-cost, comparable electrical performance, prohibiting dissolution of Cu substrate and availability is considered proper candidate for wave soldering in electronic application (Chen et al., 2002). However, microelectronic solders based on Sn-Cu or SAC are generally exposed to microstructural coarsening during service or storage due to the coarsening of Cu_6Sn_5 IMC particles. In addition, the melting point of Sn-Cu solders are relatively high (~227˚C) in compare to the Sn-Pb solder alloy (183˚C) (Wu et al., 2002; Yang et al., 2015). Some alloying elements, such as Ni, Co, Ce, Fe, Ag, Sb and Zn (Anderson, 2007; Bui et al., 2013; Hodúlová et al., 2011; Laurila et al., 2009; Song et al., 2010; Wang et al., 2009) have been added to Sn-based solder alloys to reduce melting point and improve the microstructural and mechanical properties of the solder alloys. There have been dedicated effort on alternative lead-free solders, based on the following criteria:

1) Low melting point: The melting point of the lead-free alloy joints should be low enough to avoid thermal damage to the packages and close to eutectic Sn-Pb (183°C).
2) Mechanical and microstructural properties: solder alloys should have reliable mechanical and microstructural properties. On the basis of previous studies one method to improve these properties is micro alloying.

3) Wettability: solder should readily wet the bond pads to provide reliable bonding between components.
4) Availability and cost: The sufficient supplies with low cost should be available. The microelectronic industry is extremely cost conscious. Low Ag solder and Sn-Cu solder selected to satisfy this criterion. Furthermore, low Ag solder have better drop test properties.

Previous studies showed that adding Fe to Sn-Ag-Cu solders increased its yield strength and UTS, and decreased elongation (Kim et al., 2003). Also, Fe stabilized the mechanical properties of solder with aging and improved drop impact reliability. In addition, Fe suppress formation of Kirkendall voids at interface (Kim et al., 2013). The Fe-doped solder alloys have higher melting temperature and lower wettability in compare to the high-Ag-content Sn-3Ag-0.5Cu solder alloy (Anderson, 2007). Bi doping can be used to form a lead-free solder with low melting temperature. It was reported that doping different amounts of Bi to the solder alloy decreased melting temperature (El-Daly et al., 2015; Zhou et al., 2005). There have been several investigations on the effects of Bi doping on the solder alloys. Pandher et al. (Pandher et al., 2008) reported that the growth rate of the Cu_3Sn IMC layer on substrate hampered by additions of Bi (up 2 wt.%) to Sn-0.3Ag-0.7Cu solder. Also, Hodulova et al. (Hodúlová et al., 2011) reported that Cu_3Sn growth on Cu substrate during solid-state aging hindered by addition of 1 wt.% Bi to Sn-1Ag-0.5Cu solder. It was concluded that Bi can substitute for Sn in IMCs, where they are able to inhibit Sn diffusion to the Cu_3Sn. Therefore, Bi doping can prevent growth rates of the Cu_3Sn. Also reported that Bi addition improved solder wetting properties because of better solder spreading as a result of the segregation of Bi on the solder surface in the liquid state by decreasing the surface tension of the molten solder (Pandher et al., 2007). Bi-doped Sn-0.3Ag-0.7Cu has lower interfacial fracture due to the growth suppression of the Cu_3Sn IMC layers and better wettability (Pandher & Healey, 2008; Pandher et al.,

2007). Also, Liu et al. (Liu et al., 2011) showed that melting temperature reduce by additions of Bi (1 wt.% to 4.5 wt.%) to Sn-0.3Ag-0.7Cu solder. Furthermore, Bi addition increase tensile strength and decreases the ductility. Thus, the optimum addition of Bi can improve bulk solder strength, otherwise excess of it reduces the bulk compliance. In addition, fillet lifting can occur because the excess Bi segregates towards the solder–pad interface and make the Cu pads brittle (Kariya et al., 1998). Moreover, Bi doping to the bulk of solders increases the strength through precipitation hardening and refines the grain structure (He et al., 2006; Pandher & Healey, 2008; Pandher et al., 2007).

The aim of this study is making novel low-Ag or without Ag solder alloy which is reliable (desirable mechanical properties, stabilized mechanical properties after aging, low melting temperature, and low wetting angle) and affordable. In a nutshell, Fe and Bi have different role to improve reliability of solder alloy. Fe stabilize mechanical properties after aging and improve drop reliability, whereas Bi strengthen solder by solid solution effect, decrease melting temperature and improve wetting properties. Therefore, this work compare Fe and Bi bearing Sn-1Ag-0.5Cu and Sn-0.7Cu with low Ag SAC and other conventional solder alloy to investigate the beneficial effects of Fe and Bi on the microstructural, mechanical, and thermal properties, as well as the fracture behavior and wetting properties.

1.2 Research Objectives

1. Investigate the effect of alloying addition of Fe and Bi to the Sn-1Ag-0.5Cu(SAC105) and Sn-0.7Cu(SC07) solder alloys on mechanical and microstructure properties.
2. Analysis the thermal behavior of Sn-1Ag-0.5Cu-xFe-YBi and Sn-0.7Cu-xFe-YBi solder alloys (x= 0.05 and 0.1 wt.%, Y= 1 and 2).

3. Investigate aging effect on mechanical and microstructural properties of SAC105 and SC07 solder alloys by adding Fe and Bi.
4. Measure the wetting properties of the solder joints, nanoindentation and hardness of (Fe and Bi)-bearing Sn-1Ag-0.5Cu and Sn-0.7Cu solder alloys.

1.3 Organization of the dissertation

The purpose of this study is presented in Chapter 1. Chapter 2 presents the background and literature review relevant to this study. The literature reviews primarily focus on the properties of lead-free solder alloys and microalloying to improve solder reliability. Chapter 3 describes the methodology and experimental study by explaining the steps of fabrication, testing and characterization of solder alloys. Chapter 4 compares the (Fe and Bi)-bearing Sn-1Ag-0.5Cu and Sn-0.7Cu with Sn-1Ag-0.5Cu and Sn-0.7Cu and other conventional solder alloys to understand the beneficial effects of Fe and Bi on the microstructural, mechanical, and thermal properties, as well as the fracture behavior, aging effect and wetting properties. General conclusions and potential future research are presented in Chapter 5.

CHAPTER 2: LITERATURE REVIEW

2.1 Microelectronic Packaging

The modern types of electronic equipment are very complex and consist of a large number of components which they are combined together through levels of package to make integrated equipment. These three levels shown in Figure 2.1. Electronic packaging technology involves material science, package technology, reliability assessment and so on.

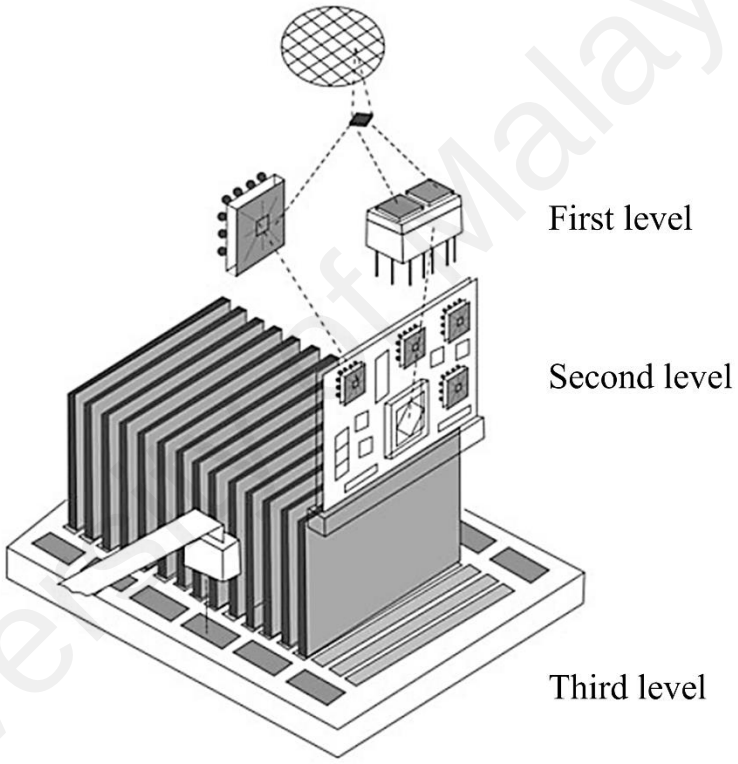

Figure 2.1: First, second and third level of electronic packaging(Datta et al., 2004).

So many technologies are used in each levels of electronic package. Most connection are in the first and second level package which is known as the microjoining technology. The size of joining play important role in the microelectronic joining which is different from welding technology. The characteristics of microelectronic joining are as follow:

(1) Small, thin, and light components joint together.

(2) The materials being jointed are nonferrous metals.

(3) For high quality joining the thickness of diffusion layer, surface tension, and dissolved quantity are noticeably important.

(4) The high level of accuracy is required in microelectronic joining.

(5) The electronic components should not be affected by joining process (Greig, 2007).

2.2 Soldering technology and their metallurgy

Precise soldering is the most popular microelectronic joining technology. Soldering is utilizing a molten filler metal to wet the surfaces of a joints, by or without applying flux, which lead to form metallurgical bonds between the filler and the particular constituent. The surfaces of the specimen are "eroded" as a result of the reaction between the molten filler metal and the surface. Although the amount of this "erosion" is less than 100μm (Humpston et al., 2004).

The criteria for compatible solder with parent materials are:

1. The solder materials should have a lower liquidus temperature in compare to the melting point (solidus temperature) of the base materials and should produce solder joint at the temperature that does not degrade the properties of parent materials
2. The base materials or coated layer on it should be able to wet properly for reliable adhesion by forming the metallic bonds.
3. Any impurities which can embrittle or weaken the joint should be eliminated
4. The erosion of the base material at the joint interface should be limited (Humpston & Jacobson, 2004).

Soldering has a key role in electronic packaging industries at several levels such as, wire bonding in surface mount technology(SMT), solder ball connection in ball grid

arrays (BGA), integrated circuit (IC) package assembly in printed circuit board (PCB) or flip chip (FC) connections (Kang et al., 1994). Solder joints should provide the electrical connections between the component in addition to the thermal, physical and mechanical support; if not the reliability of the system is endangered and perhaps cause a failure or damage the package.

The eutectic Sn-Pb has a melting point of 183°C. The ability to form a metallic bond with Cu substrate at such a low temperature is the key reason to used Sn-Pb solders worldwide for so long (Tu, 2010). Because of the miniaturization trend in the electronic devices, their requires smaller solder joint and fine pitch interconnections (Shen et al., 2009). On the other hand, functional density enhancement and reliability issue are the key concerns in the electronic industries for the market demand. Therefore ball grid array (BGA) and flip chip (FC) packaging technologies are being used in the electronic industries for having higher input/output connections in a certain area (M. Arden, 2002). High localized temperature during service as a result of ultra-fine solder joints in BGA and FC packaging leads to coarsening the solder microstructure and deteriorate the reliability. It has become the main technological issue for electronic packaging and soldering.

Reflow and wave soldering processes are being used in the electronic industries for the preparation of solder joints (Suganuma, 2001). In reflow soldering process solder is applied as paste by using a stencil mask and then heated to the reflow temperature. This soldering process as shown in Figure 2.2 is quite common in surface mount technology (SMT) process on printed circuit boards (PCBs) (Jianbiao et al., 2004).Wave soldering is also used for pin-in-hole (PIH) or pin-through-hole (PTH) types of assemblies where molten solder is used in the bottom side of PCB and then heated to the reflow temperature. Selection proper material for technological demand and reliability is very crucial in both reflow and wave soldering process. In the near future it is required to overcome more challenges for

manufacturing of miniaturized, higher performance and multifunctional electronic device, especially in the metallurgical aspects(Zhang, 2015).

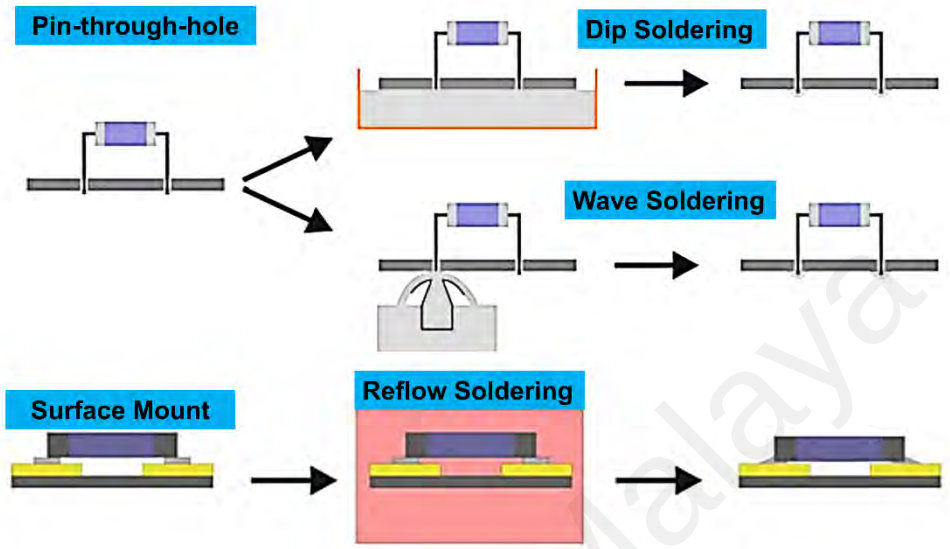

Figure 2.2 : Dip soldering and wave soldering in Pin-through-hole package, reflow soldering in surface mount package (Zhang, 2015).

2.2.1 Health and Environmental Effects of Pb

Pb(lead) is one of the top 17 chemicals posing the greatest threat to human life and the environment on the basis of the United States Environmental Protection Agency (USEPA) (Wood et al., 1994). Pb in the electronic industries is considered as hazardous material for the environment. Wastes of electronic products are usually disposed to the landfills contaminates the soil, water, human body and food-chain in ecosystem (Glazer, 1994). Therefore "green" electronic products completely free of toxic materials such as Pb are being widely grabbed researcher's attention (Harrison et al., 2001).

2.2.2 Reliability of solders

From manufacturing to the start of the equipment life is considered quality. Several factors effect quality such as defects during assembly process and the quality of each component before assembly. Defected components or not accurate assembly temperature profile or any other defect before sending electronic circuit board to the field are considered quality issues and not reliability issues.

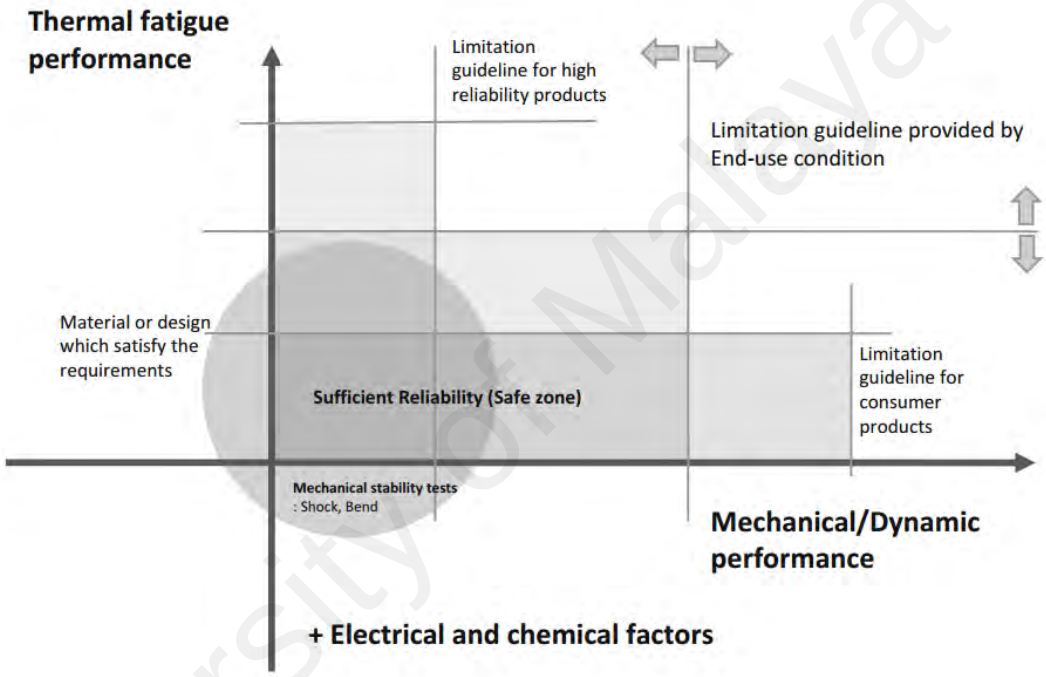

Figure 2.3 : Thermal, mechanical, electrical and chemical factors of solder reliability(Lee et al., 2015)

The life of products starts when they passed all the required tests and be qualified for market. Designer and user expect different procedure to deteriorate the equipment life and its failure by start of product life in their functional environment. Therefore, when all quality expectations are met, reliability is the natural behavior of the electronic device. Reliability of solder interconnect are depending on the several external factors such as electrical, mechanical, thermal, and chemical aspects in different application products (Lee et al., 2015), Figure 2.3.

2.3 Pb-Free Solder

Most of the the eutectic lead-free solders are Sn-based. The eutectic alloys consisting of Sn and other metals such as Au, Ag, Cu, Bi, In, Zn, Sb, and Ge have been considered as the binary lead-free solder systems. Their eutectic temperature are shown in Table 2.1. By comparing the eutectic temperatures of Pb-free alloys with the Pb-Sn eutectic solders the temperature gap between them is clear (exception Sn-Zn system:198.5ºC) (Tu, 2010).

Zinc forms a stable oxide which leads to drossing during wave soldering, and due to that shows poor wetting behaviour. Thus, a forming gas ambient is required during soldering. However, Zn is not expensive and is available for widespread use. Moreover, the eutectic Sn-Zn has a closest melting point to that of eutectic Sn-Pb in compare to other eutectic Pb-free solders.

Table 2.1: Binary Pb-free eutectic solders (Tu, 2010).

system	Eutectic temp. (°C)
Sn-0.7Cu	227
Sn-3.5Ag	221
Sn-10Au	217
Sn-9Zn	198.5
Sn-38.1Pb	183
Sn-57Bi	139
Sn-51In	120

The eutectic Sn-Bi solder has been used widely in pin-through-hole assembly. Basically Bismuth provide good wetting properties. However, the primary source of Bi is a by-product in Pb refining. Therefore, its availability limited by the restrictions on Pb(lead). Thus, due to less availability of Bi it is not sufficient for 57wt.% Bi for Sn-57Bi. United Nations Environment Program recognized Antimony (Sb) as dangerous element for environment, therefore it is not suggested as a base replacement of Pb. Due to high reactivity of Germanium (Ge), it is used just as a minor alloying element. Indium (In) forms oxide easily and it is not available and its too expensive.

Sn-noble metal (Ag, Au, …) solder alloys have higher melting point and higher concentration of Sn in compare to the eutectic Sn-Pb. Thus, these alloys have higher reflow temperature, by about 40°C. Therefore, the rate of intermetallic compound formation with Cu and Ni substrate is higher due to higher dissolution rate and solubility of Cu and Ni in the molten solder. Moreover, the surface energies of Sn-noble metal solder alloys are higher than that of Sn-Pb which leads to a larger wetting angle.

While the microstructure of Sn-Pb solder alloys has no IMCs, the microstructure of Sn-noble metal eutectic solders is a mixture of Sn and intermetallic compounds (IMCs) due to high concentration of Sn. The mechanical properties of Sn are anisotropic because of its body-centered tetragonal crystal and its deforming by twining. Therefore, the inhomogeneous microstructures form due to the IMCs in structure especially Ag_3Sn. (Tu, 2007).

Among the numerous lead-free solder options available, the following families are of particular interest and are the prevailing choices of industry: eutectic Sn-Ag, eutectic Sn-Cu, eutectic Sn-Ag-Cu, eutectic Sn-Zn, eutectic Bi-Sn, and their modifications, as shown in Figure 2.4 with their applications.

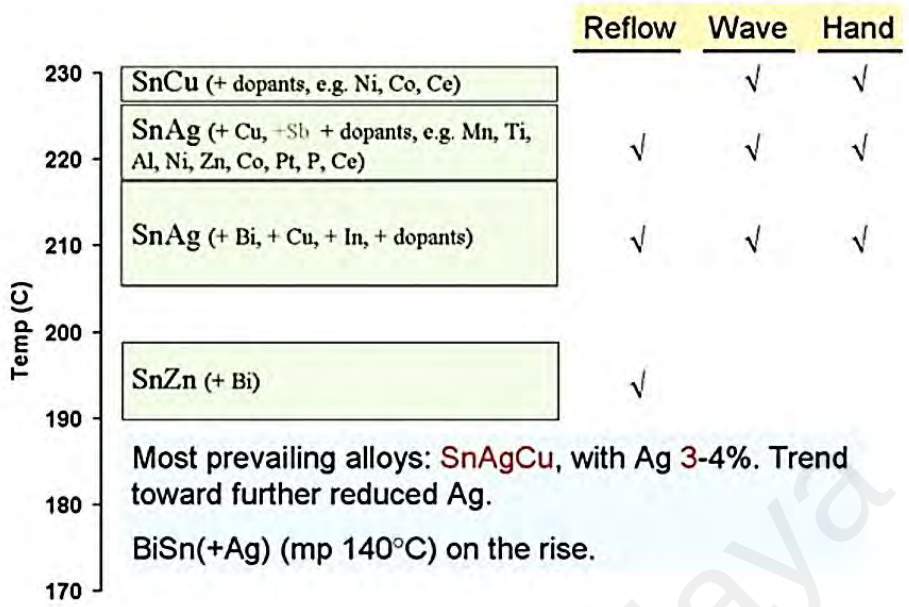

Figure 2.4: Common Pb-free solder alloys and their applications(Lu et al., 2009)

Near eutectic Sn-Ag-Cu lead-free solders, such as Sn-4wt.%Ag-0.5wt.%Cu (SAC405) or Sn-3wt.%Ag-0.5wt.%Cu (SAC305), suggested as a promising replacement for Sn-Pb solder alloy because of their low melting temperature, and favorable thermal–mechanical fatigue properties. However, because of the rigidity of the high-Ag-content Sn-Ag-Cu (SAC) alloys, portable electronic products that contain these high-Ag-SAC solder joints are more prone to failure due to drop and high impact applications. Moreover, the high Ag content in Sn-Ag-Cu alloys results in a relatively high cost for these solder alloys. Low-Ag-content Sn-Ag-Cu alloys such as Sn-1 wt.%Ag-0.5 wt.% Cu (SAC105) or Sn-0.7wt.%Cu have been considered as a solution to both the cost and poor drop impact reliability issues (Chen et al., 2002), which will be discussed their properties in the following.

2.3.1 Sn-0.7Cu

The eutectic Sn-0.7Cu is one of the reliable solder alloy for reflow and wave soldering applications (Boettinger et al., 2005). The cost of this solder is much lower comparing other solders since it does not contain any expensive elements such as Ag.

Sn-Cu is one of the cheap Pb-free alloys and is widely considered for low-cost applications within electronics assembly and in other industrial applications such as plumbing. The Sn-0.7wt.%Cu is eutectic composition and form at approximately 227°C. If the Cu level is raised above 0.7wt.% then the liquidus increase sharply to high temperature. Therefore, the liquidus temperature can be effected when Cu dissolute from the board. Thus during wave soldering severe control on composition of solder bath is required (Suganuma, 2003).

The Cu-Sn phase diagram has shown in Figure 2.5. Figure 2.6 shows microstructure of Sn-0.7Cu solder which consists of the rich β-Sn phase with dispersed Cu_6Sn_5 IMCs. Cu_6Sn_5 tends to precipitate in the form of hollow rods however practically small particle are more common due to high cooling rate. The addition of Cu to Sn can provide limited solid solution strengthening due to limited solution in the region of 0.001%. Although, the microstructure of Sn-0.7Cu is similar to the Sn-3.5Ag alloy, but the difference in intermetallic type, size, and dispersion leads to lower strengthening by the particles. Thus, the strength of the Sn-0.7Cu is limited and generally tensile strength is lower than Sn–Pb at room temperature while it has a relatively high ductility over a range of temperatures (Wood & Nimmo, 1994).

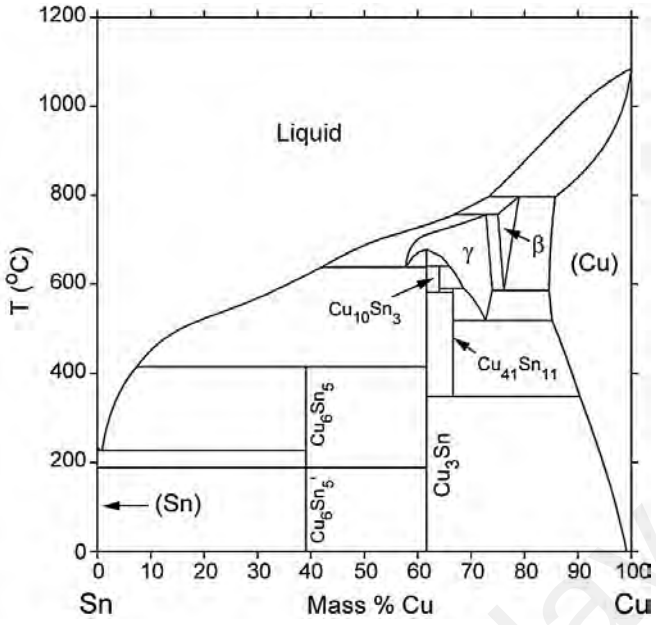

Figure 2.5: Sn-Cu phase diagram (Okamoto, 2002).

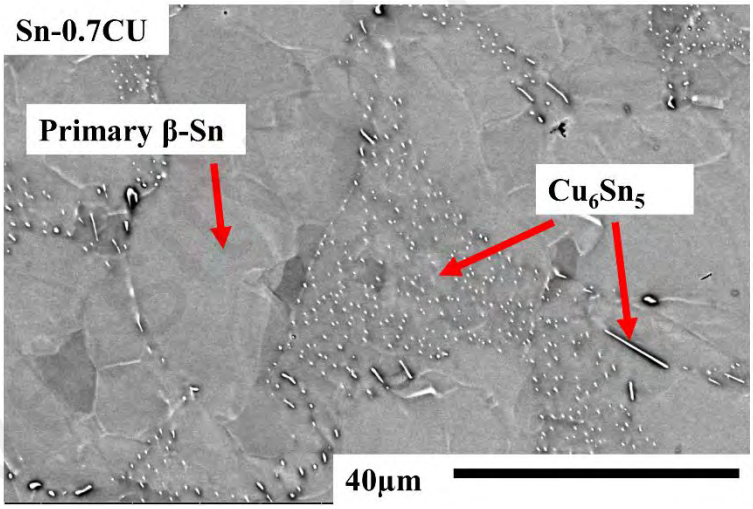

Figure 2.6: Sn-0.7 Cu microstructure includes Cu_6Sn_5 and primary β-Sn.

The wetting achieved with this solder is sufficient for most purposes, but due to high melting point the proper flux should be selected to maintain activation at appropriate temperature. Dependent on the wave soldering production conditions, the wetting and flow characteristics of Sn–0.7Cu can be unsatisfactory, with poor penetration of plated-through holes and dull grainy joints(Suganuma, 2003).

2.3.2 The Sn-Ag-Cu lead-free solder

The National Electronic Manufacturing Initiative (NEMI) recommended to replace eutectic Sn-Pb solder by near eutectic Sn-Ag-Cu alloys. This family of Pb-free Sn-Ag-Cu alloys has shown high promise in the electronic industries due to having good wetting characteristics with substrate, proper fatigue resistance, high joint strength etc.

Most of the ternary and higher order solders are based on the binary eutectic Sn-Ag, Sn-Cu, Sn-Zn, or Sn-Bi alloys. On the basis of all research which have done Sn-Ag-Cu is the most promising Pb-free solder. Based on differential scanning calorimetry measurements, and thermal analysis results the eutectic composition was estimated at Sn-(3.5±0.3) wt.% Ag-(0.9±0.2) wt.% Cu and eutectic temperature has been determined to be about 217°C. The eutectic Sn-Ag-Cu alloy forms good quality joints with copper. It has a superior thermo-mechanical property in compare to Sn-Pb solder.

The phase transformation of Sn-Ag-Cu system is evaluated based on the following binary systems: Sn-Cu (Figure 2.5), Sn-Ag and Ag-Cu (Moon et al., 2000). The calculated binary phase diagrams for the binary system Sn-Ag and Ag-Cu are shown in Figure2.7 (a) and (b). The ternary phase diagram of Sn-Ag-Cu are shown in Figure 2.7 (c).

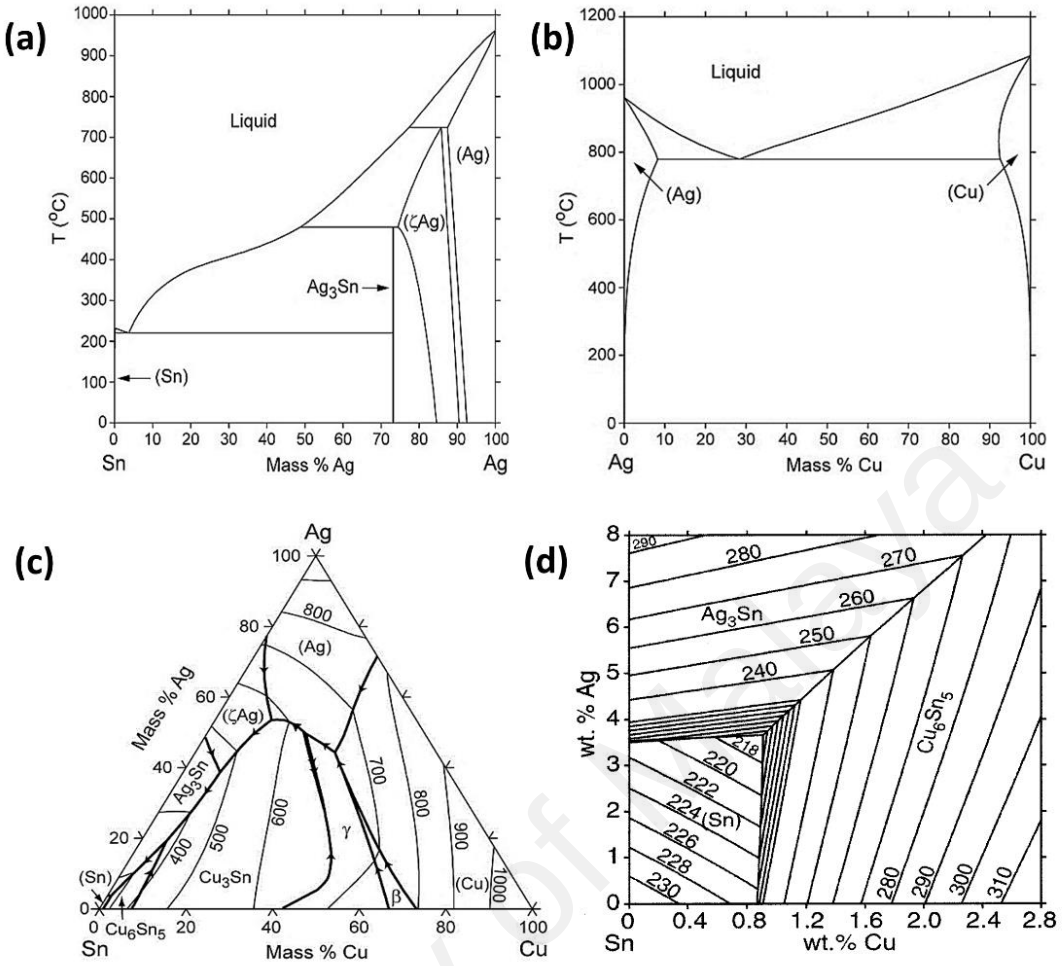

Figure 2.7: (a) Sn-Ag (Karakaya et al., 1987) and (b) Ag-Cu system (Xie et al., 1998) (c) Sn-Ag-Cu ternary phase diagram (d) Calculated liquidus surface of the Sn rich region of Sn-Ag-Cu alloy system (Moon et al., 2000).

The National Center for Manufacturing Sciences (NCMS), Michigan, USA suggested that the solder liquidus temperature should be less than 225ºC with a maximum 30ºC difference between solidus and liquidus temperature (Bath, 2010). Obviously the ternary eutectic or near eutectic Sn-Ag-Cu alloys meet the first two criterions since the melting temperature of the ternary eutectic Sn-Ag-Cu alloy is 217ºC (Moon et al., 2000). Depending on particular applications the operating temperature of electronic equipments may be as high as 150ºC (Suganuma, 2001). So the ternary eutectic or near eutectic Sn-Ag-Cu alloys are one of the best candidates for Pb-free solder alternatives. The calculated eutectic composition of the Sn-Ag-Cu system is 3.66 wt.% Ag, 0.91 wt.% Cu as it is seen in Figure 2.7 (d). But the

experimentally determined value of the Sn-Ag-Cu system is 3.5 wt% Ag, 0.9 wt% Cu which differs a little from the calculated value.

2.3.2.1 Low Ag Sn-Ag-Cu

Due to the rigidity of high-Ag-content SAC alloys in compare to Sn-Pb solder alloy, more failures may occur in drop and high-impact applications in portable electronic equipments that contain these high-Ag-content SAC solder joints (Kotadia et al., 2014).

Moreover, the high Ag content in SAC alloys results in a relatively high cost for these solder alloys, and market has trouble to sustain the supply of Ag for the solder industry. Low-Ag-content SAC alloys, such as Sn-1wt.% Ag-0.5wt.% Cu (SAC105), have been considered as a solution to both cost and poor drop-impact reliability factors(Suh et al., 2007). Reducing the Ag content of SAC alloy has increased its bulk compliance and plastic energy dissipation ability, which have been identified as key factors for improving the drop resistance(You et al., 2009).

However, the decrease in Ag content for improvement in drop-impact performance also has the consequence of compromising the thermal–mechanical fatigue properties (Kariya & Otsuka, 1998; Terashima et al., 2004). Moreover, electronic industry demand Pb-free solder alloys with lower cost while improving both the drop-impact reliability and thermal-mechanical fatigue properties.

2.4 Properties of Lead-Free Solder Alloys

2.4.1 Mechanical properties of lead- free solder alloys

Solder is used by the microelectronics industry and is usually available in three basic forms: bulk solders for operations such as wave soldering, solder paste for operations such as surface mount reflows, and solder balls or solder columns for applications such as ball grid array, column grid array and flip chip packages. Solder paste contains solder

particles that typically range from 4 to 8 μm in diameter, formulated with flux. Solder balls typically range from 0.3 to 0.75 μm in diameter. Since solder used in electronic industry exists in various forms, the design of specimen plays an important role in the representability and validity of the research result. The specimen design is the first important aspect for a test method. The specimens currently used to test the thermal mechanical properties and the fatigue life of solder joints can be divided into three categories as: bulk solder, simplified shear sample and SMT solder joints.

The "dog-bone" shaped bulk sample is the conventional tensile specimen, which is used extensively for tensile testing. The specimen is annealed in an oven at a specified temperature for a determined period of time and then cooled in air to stabilize the microstructure and relieve residual stress. The mechanical properties obtained are useful as the reference data for the correlated tests. The material properties, such as yield strength, ultimate tensile strength, CTE and elastic modulus for wide variability of lead-free solders are listed in Table 2.2.

Also, solder alloys should be resistance to thermomechanical fatigue (TMF). The lead-free solder alloys should be able to withstand different amounts, types, and rates of loading which are dependent upon the different coefficients of thermal expansion (CTE) and mechanical properties of the board, components, and alloys, residual stresses, solder joint geometry, and specially solder microstructure.

High modulus and high tensile strength solders are not preferable for flip-chip applications, thus high-solute solders or near-ternary eutectic Sn-Ag-Cu solders are not chosen for this application. Low-Ag SAC solders is popular for solder interconnects which required low strength and high ductility (Seo et al., 2008).

Table 2.2: Physical properties of lead-free solder alloys(Lee et al., 2005; Puttlitz et al., 2004).

Alloy composition (Wt%)	Liquidus (°C)	Solidus (°C)	Ultimate Tensile Strength (MPa)	0.2% Yield Strength (MPa)	Elongation (%)	Elastic modulus (Gpa)	CTE (µm/m°C)
Sn-37Pb	183	183	31	27	48	-	26
Sn-3.5Ag	221	221	27	23	24	26	22
Sn-3Ag-2Bi	220	216	55	38	30	-	22
Sn-3.1Ag-1.5Cu	216	217	-	39	-	47	-
Sn-3.5Ag-1.5Bi	220	214	32	34	26	-	22
Sn-58Bi	139	139	35	26	46	12	17
Sn-50In	118	125	20	-	25	-	-
Sn-2Bi-3Sb-1.5Cu	231	225	65	51	28	-	-
Sn-3Ag-10Sb	231	228	-	-	-	26	-
Sn-2Ag-64Bi-4Cu	146	137	69	67	3	-	14
Sn-7.5Bi-2Ag-0.5Cu	238	229	67	51	19	-	-
Sn-2Cu-0.8Sb-0.2Ag	230	219	30	26	27	-	-
Sn-8In-7Zn	195	178	44	42	14	-	-
Sn-55Bi-3Ag-1.5Sb	147	137	68	62	27	-	13

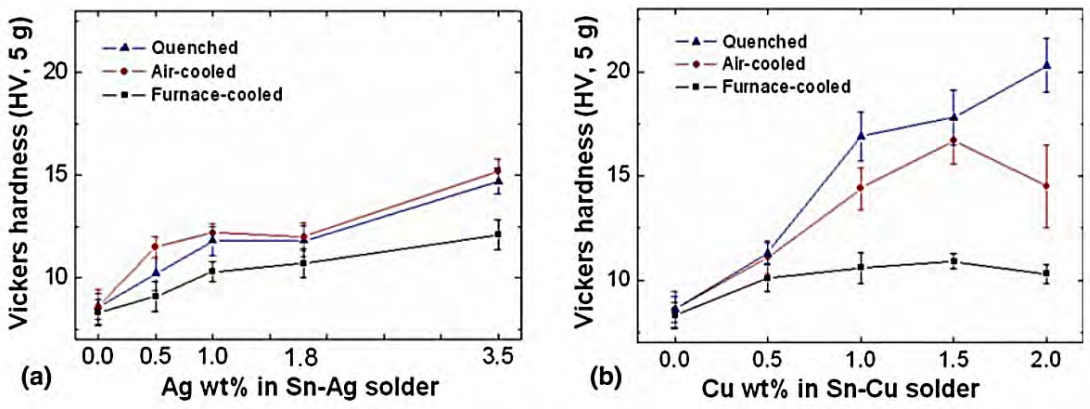

Figure 2.8: Microhardness data of (a) Sn-Ag and (b) Sn-Cu solders(Seo et al., 2008)

Figure 2.8 exhibits the micro hardness data of Sn-Ag and Sn-Cu, measured in terms of alloy composition and cooling rate. Generally due to the structure–property relationship, more alloy addition and faster cooling resulted in a higher hardness. Sn-Cu follow the general structure–property relationship. Figure 2.9 shows Cross-polarized images of Sn-Cu solder balls (380 μm diameter) as a function of cooling rate and Cu composition. While Sn-Ag solders do not follow this relation with regard to cooling rate; the rapidly quenched Sn-Ag solder exhibit a less hardness than air-cooled Sn-Ag solders, as shown in Figure 2.8a. Sn-Ag quenched solders have a fine twin structure, while air-cooled Sn-Ag have a relatively coarse micro structure revealed by the cross polarized images in Figure 2.10. On the basis of Hall–Petch relationship, for metals and alloys a finer grain structure is responsible for a higher yield strength (or higher hardness) due to the grain-boundary strengthening mechanism. While the fine twin structure observed in Sn-Ag solders seems to not contribute for the hardening of Sn-rich solders. Therefore, based on previous reports microhardness data of Sn-Ag and Sn-Cu can be better interpreted with the quantity, size and distribution of IMC particles rather than Sn grain or twin size revealed in crosspolarizing images.

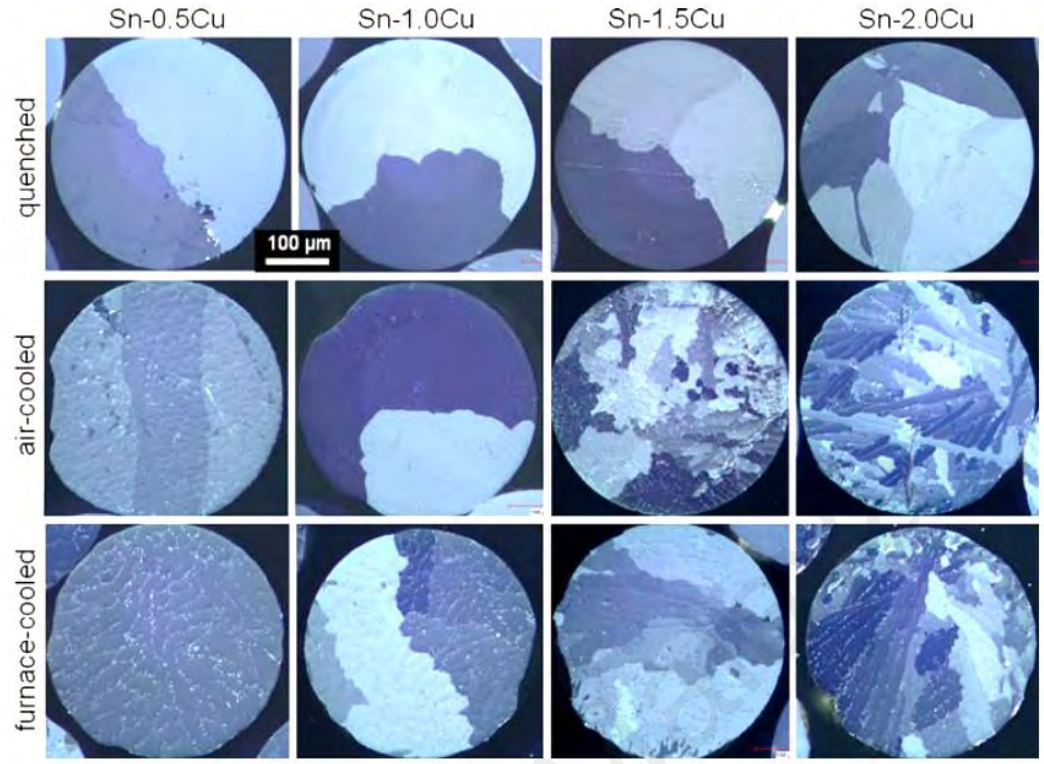

Figure 2.9: Cross-polarized images of Sn-Cu solder balls (380 µm diameter) as a function of cooling rate and Cu composition (Seo et al., 2008).

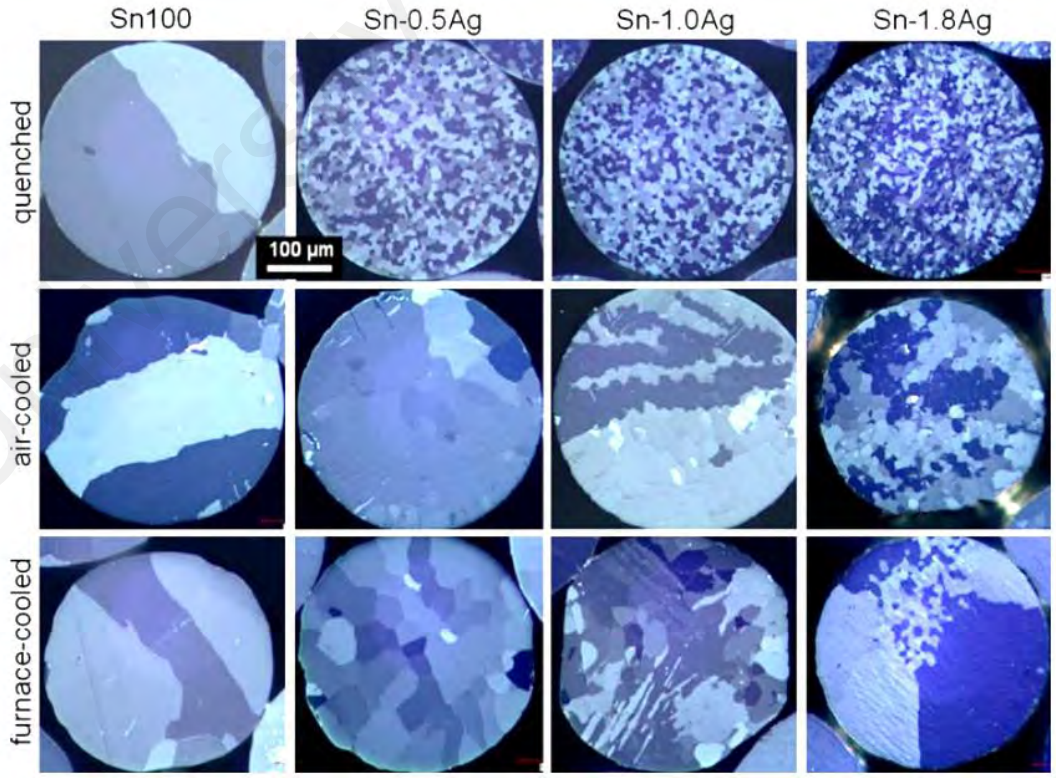

Figure 2.10: Cross-polarized images of Sn-Ag solder balls (380 µm diameter) as a function of cooling rate and Ag composition(Seo et al., 2008).

As shown in Figure 2.8, the addition of Cu solute atoms to Sn matrix is much more effective than Ag to Sn on the hardness of the solder composition at the same cooling rate. It can be interpreted by two reasons. First, for the same wt.% of Cu or Ag, the volume fraction of Cu_6Sn_5, formed at 220°C, just below the eutectic temperature, is estimated to be always larger than Ag_3Sn. Second, that the bulk hardness of Cu_6Sn_5 (4.5 GPa) is much higher than Ag_3Sn (1.5 GPa). Hence, Sn-Cu solders are expected to be harder than Sn-Ag, for the same amount of Ag or Cu, assuming each IMC system has a similar size and distribution characteristics.

2.4.2 Microstructure of lead-free solder alloys

The mechanical properties of Pb-free solder are correlated to the microstructure, which is affected by alloy compositions, aging conditions and cooling rates. The Sn content in most Pb-free solder alloys is in excess of 90 atomic percent, thus the solidification characteristics of these solder alloys are critically affected by the solidification behavior of Sn. Sn is characterized by a striking solidification behavior. The solidification of Sn is marked with significant undercooling and high growth rates. In fact, the microstructure of solidified pure Sn is characterized by large Sn dendrites growing primarily in the [110] and $[1\bar{1}0]$ directions, while the [001] is the slow growth direction (Abbaschian et al., 1975; Kim et al., 2003; Moon et al., 2000; Rosenberg et al., 1954).

In Sn–Ag–Cu alloys, two kinds of large IMCs of Ag_3Sn and Cu_6Sn_5 can be formed depending on phase diagrams, Figure 2.11. These large IMCs are quite brittle, which may lead to serious problems under stressed conditions in the actual service for printed wiring boards. It has been reported that the long Cu_6Sn_5 whisker like IMCs formed in solder/Cu joints have a great effect on their tensile fracture characteristics. They decreased elongation at lower temperatures by providing the origin of tensile failure (Frear, 1996, 2007; Kim et al., 2003).

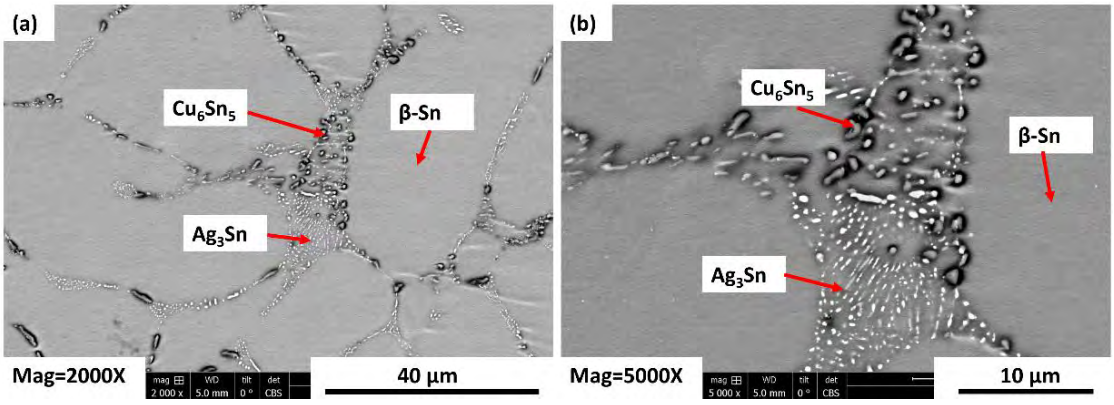

Figure 2.11: FSEM micrographs of eutectic structures, shows β-Sn, Ag_3Sn and Cu_6Sn_5 (a) at 2000x magnification (b) at 5000x magnification.

The microstructure strongly influences the fatigue resistance and other mechanical properties of a solder alloy. As a whole, the solder microstructure is determined by the solidification behavior of the solder and the reaction at the solder and base-metal interface. If the solder is used at a high homologous temperature, as it ordinarily is, the microstructure may evolve during service (Amagai et al., 2002; Kim et al., 2003; Wade et al., 2001; Zribi et al., 2001).

For Sn-3.5Ag eutectic solder alloy, Chawla et al. showed that first Ag_3Sn plates form by cooling from above the eutectic temperature, because the high Sn-alloys do not solidify with a classic eutectic structure due to the difficulty in nucleating the β-Sn. The cooling rate affect the size of the platelets. Once the β-Sn phase is able to nucleate, β-Sn dendrites form with interdendritic Ag_3Sn of an intermediate scale and sub-100nm Ag_3Sn particles within the dendrites, with the size of all features depending on cooling rate. Kerr and Chawla have explained the role of sub-100nm Ag_3Sn precipitates on creep and grain boundary and dislocation motion in Sn-3.5Ag, as seen in Figure 2.12. Figure 2.12a illustrates Ag_3Sn precipitates in β-Sn that pin the grain boundary in the as-solidified state and following deformation. After creep deformation, dislocations pinned by Ag_3Sn particles with bowed dislocation segments recognized between the pinned dislocation

segments, Figure 2.12b. High stress exponents were observed due to the resisting stress on dislocations from the hard Ag_3Sn particles.

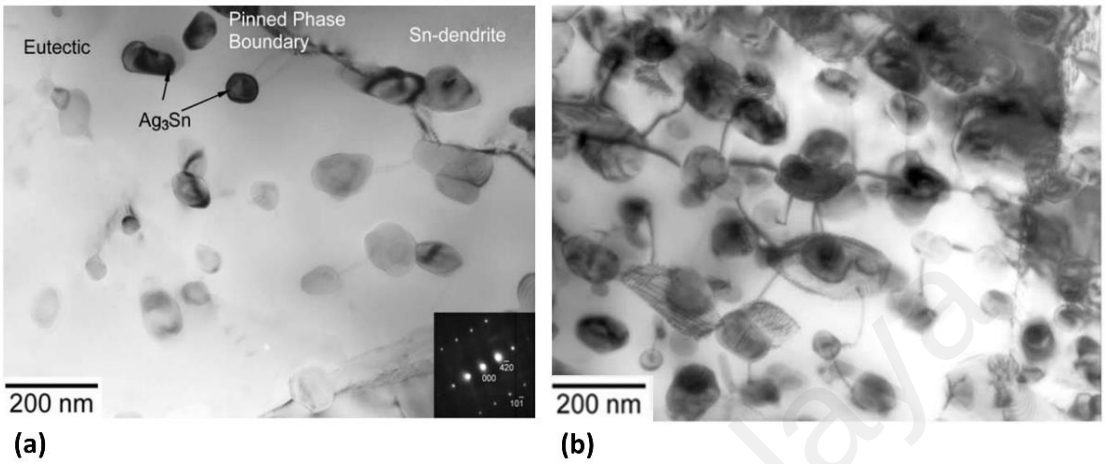

Figure 2.12: (a)TEM micrograph illustrating the Ag_3Sn particles, Sn–dendrite, and the pinned boundary between the two phases(b) Dislocations pinned by Ag_3Sn particles in the eutectic mixture after creep deformation (Kerr et al., 2004).

2.4.3 Thermal Behavior (melting and solidification)

Single element systems have a single melting point where the material changes from a single-phase solid material to a single-phase liquid material. During the procedure heat is absorbed and temperature remain constant to dissociate the solid-state atoms into a liquid state. For instance, pure Ag melts at 961°C, while pure Sn melts at 232°C. However due to thermodynamic considerations, the melting point of the alloy (mixture of pure metal and other elements) may be depressed and/or additional eutectic and peritectic reactions can occur. For example, when Ag and Sn are combined, there is a single composition 96.5wt.%Sn–3.5wt.%Ag, where the two-phase solid transforms to a single phase liquid at a single temperature (221°C), much like a pure element. This is called the eutectic temperature. Otherwise, when the composition deviate from eutectic composition the change from solid to liquid occur over a range of temperatures which referred as a mushy/pasty zone. The point where the first liquid begins to form or the bottom temperature of the mushy zone is solidus. On the other side, the point where the last solid

melts into liquid or the point at the top of the mushy zone is the liquidus. Multiple component systems are more complicated and have more phases that can form, including even lower temperatures where eutectic liquidus can exist (Bradley III et al., 2001).

During solidification of solder joint the cooling rate is too fast (just few degrees per minute) for SAC solder alloys to maintain phase equilibria. The solder microstructure affected by nonequilibrium cooling due to undercooling effects into the solidification process (Kang et al., 2007; Lee et al., 2015). In order to form a solid embryo, liquid should be cooled below its solidification temperature to obtain sufficient free energy for solidification to overcome the interface energy required for creation of the liquid–solid interface. Undercooling affects the phase equilibria, solidification process, and microstructure in many different ways. Undercooling can change the composition for the eutectic reaction by expanding one or both primary phase fields due to lower eutectic temperature. There are three solid phases in a ternary eutectic system with different interfacial energy. The phase that has higher interfacial energy in compare to other phases will control the whole solidification sequence which results in microstructures where the phase fraction and the type of phases are different from the phase diagram and are metastable. Because of difficulty in nucleating of the β-Sn phase, SAC solder alloys behave in this way.

β-Sn has difficulty to nucleate during cooling of solders from the process temperature. It leads to formation of metastable phases, supercooling of the liquid phase well below where it is stable at equilibrium, and rapid formation of Sn dendrites once nucleation has occurred. Therefore, SAC alloys are predominantly β-Sn, with small amounts of Cu_6Sn_5 and Ag_3Sn intermetallics.

Composition determine the first solid phase forming in SAC alloys during cooling from the molten state. For Sn-3.9Ag-0.6Cu solder alloy, the first phase that forms on

cooling is Ag_3Sn. On the basis of equilibrium thermodynamics calculations next phases are expected to be Ag_3Sn and β-Sn. If β-Sn does not nucleate, the equilibrium phase diagram in Figure 2.7d cannot be used to predict the phases forming during cooling. Therefore, a metastable phase diagram, Figure 2.13, should be constructed to take into account the difficulty in nucleating β-Sn and the temperature at which β-Sn nucleation finally occurs. In the metastable transformation for Sn-3.9Ag-0.6Cu, Ag_3Sn continues to form as the supercooled liquid by decreasing Ag concentration. The next stable phase to form in addition to Ag_3Sn is Cu_6Sn_5 when the composition reaches the metastable liquidus valley (line of two-fold saturation). The supercooled liquid continues to reduce the amount of Ag and Cu as the two intermetallics form. For alloys that start in the Ag_3Sn phase field, this means that there are large Ag_3Sn plates that form beginning at the liquidus surface and these continue to grow from the supercooled liquid below the eutectic temperature. The supercooled liquid is sufficiently supersaturated at some temperature below the eutectic temperature to finally nucleate β-Sn in the presence of local heterogeneous nucleation sites in the alloy. At this point, β-Sn forms as dendrites from a small number of nuclei and the solder joint solidifies completely with the remaining ternary alloy liquid forming regions with different phases and morphologies (Moon et al., 2000).

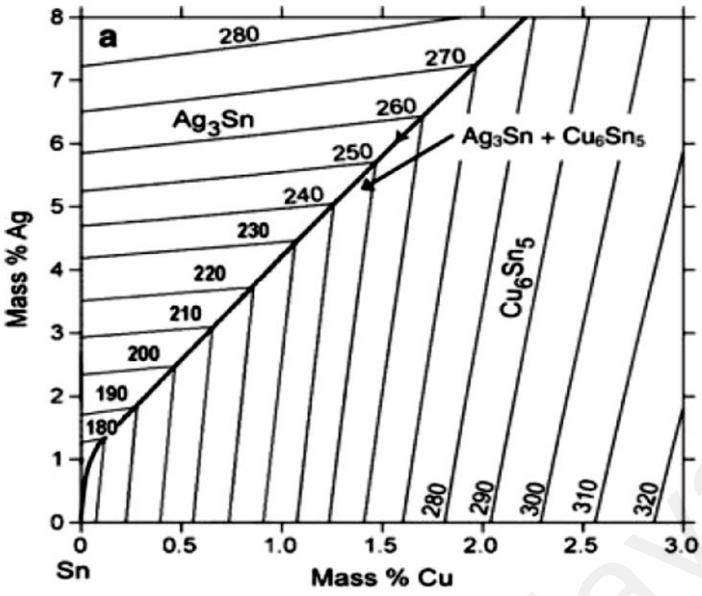

Figure 2.13: Metastable Sn-Ag-Cu phase diagram showing no formation of β-Sn until a notably lower temperature and with a lower Ag and copper concentration than the equilibrium ternary eutectic temperature and composition(Swenson, 2007).

Moreover, Lehman et al. presented the effect of undercooling on the phase type and fraction of SAC alloy microstructure using the case of the Sn-3.9Ag-0.6Cu alloy and a 3D phase diagram displaying liquidus surfaces of β-Sn, Cu_6Sn_5, and Ag_3Sn as a function of temperature and composition, Figure. 2.14. In this plot, the liquidus surfaces for β-Sn, Cu_6Sn_5, and Ag_3Sn are extrapolated below the eutectic temperature to consider effects of undercooling. The red trajectory superimposed on the liquidus surfaces represents the change in composition and temperature of the liquid under equilibrium cooling. The white trajectory represents the case of more realistic cooling where a sizable degree of undercooling occurs during the solidification process.

Many factors affect nucleation process such as size and purity of the melt, cooling rate, and substrate types which determine the degree of undercooling in SAC alloys. Normally, 20–30 °C of undercooling is reported in SAC solder alloys during reflow process(Anderson et al., 2001). More than 20 °C undercooling consider high due to their low melting temperature.

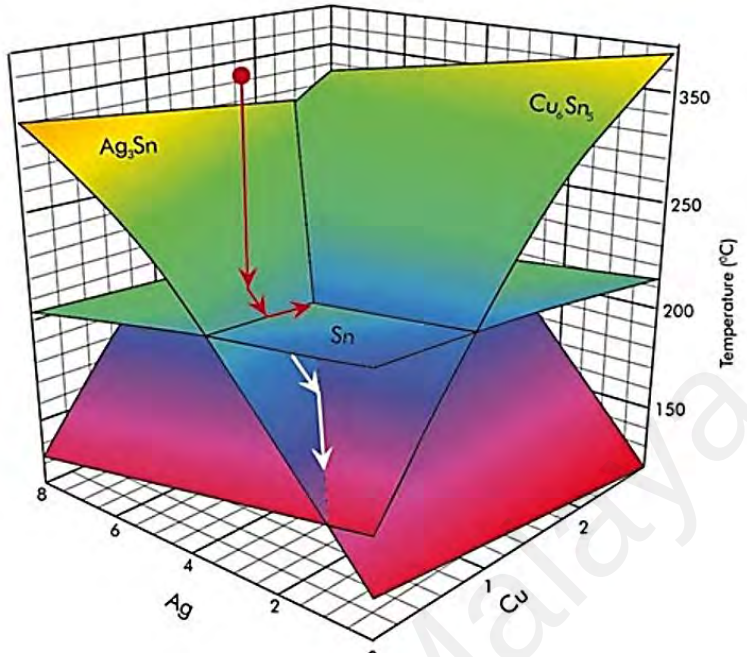

Figure 2.14: A 3D phase diagram showing the liquid surface projection of Sn rich side Sn-Ag-Cu ternary system. Liquidus surfaces of Sn, Ag_3Sn, and Cu_6Sn_5 are extrapolated below the equilibrium to illustrate the undercooling effect. The red trajectory corresponds to the solidification without undercooling, while the white trajectory related to the solidification with undercooling(Lee et al., 2015; Lehman et al., 2004).

Differential Thermal Analysis (DTA) in Figure 2.15 illustrates heat evolution during cooling for Sn-4.7wt.%Ag-1.7wt.%Cu from the liquid state, the first phases to form are Ag_3Sn and Cu_6Sn_5 at 244°C. Since β-Sn is difficult to nucleate, the liquid supercools by approximately 20°C while Ag_3Sn and Cu_6Sn_5 continue to form until the remaining liquid solidifies at 198.5°C. The latent heat (or heat of fusion) is released, leading to the solder self-heating to 217°C, the eutectic temperature (recalescence). Supercooling can also be exhibited in the Sn-Pb system, but typically with a supercooling of 5°C.

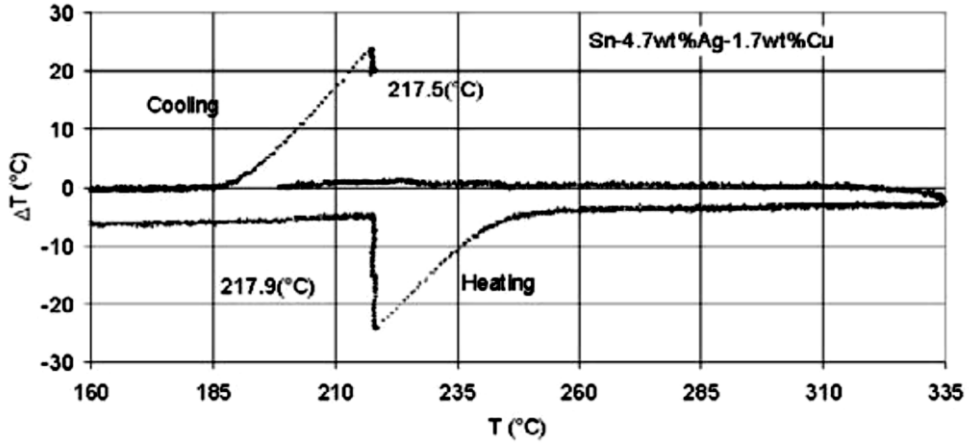

Figure 2.15: DTA heating and cooling curves for Sn-4.7Ag-1.7Cu (Moon et al., 2000).

Table 2.3 presents the amount of the undercooling measured with several Pb-free solders. The undercooling of Sn-rich solders, such as, Sn-Cu, Sn-Ag and Sn-Ag-Cu, is not remarkably affected by varying Cu or Ag content or both. Thus, Cu and Ag solute atoms or their intermetallic compounds, such as Cu_6Sn_5 or Ag_3Sn, may not provide preferential nucleation sites for β-Sn solidification.

Table 2.3: The amount of the undercooling measured by DSC with Pb-free Solders(Kang et al., 2007).

Composition (wt%)	Onset Temp (heating) (T_1)	Onset Temp (cooling) (T_2)	ΔT ($T_1 - T_2$)	Peak Temperatures[a]
Sn-0.9Cu	228.6	199.7	28.9	230.5 (H), 202.0 (C)
Sn-2Ag	228.7	201.5	27.2	230.2(H), 204.5(C)
Sn-l.OAg-0.9Cu	218.2	192.3	25.9	220.2. 226.0(H). 195.6 (C)
Sn-0.9Cu-0.6Zn	226.8	220.0	6.8	228.7(H) 223.0(C)
Sn-lAg-0.9CU-lZn	217.4	219.2	(−1.8)	219.2, 224.8 (H) 213.0, 219.6(C)
Sn-0.9Cu-0.3Fe	228.7	208.5	20.2	230.8 (H), 211.9 (C)
Sn-0.9Cu-0.2Co	229.4	224.7	4.7	231.3 (H), 226.3 (C)
Sn-3.0A_2-0.5Cu[a]	218.7	195.0	23.7	219.7 (H), 195.2 (C)

[a] DSC 22OC, Seiko, heating at 6 °C/min, cooling at 6 °C/min.
[b] All solder balls are 1.27 mm (50 mil) diameter (~8 mg), except for Sn-3.0Ag-0.5Cu, 25 mil diameter (~1 mg).

However, the addition of a small amount of Co, Fe, or Zn is found to be very effective to reduce the undercooling by more than 20°C. For example, a typical DSC (differential scanning calorimetry) thermal profiles during the heating and cooling cycle of one solder ball of Sn-0.9Cu and Sn-0.9Cu-0.2Co are shown in Figure 2.16, Which illustrate addition of 0.2wt.%Co to Sn-0.9Cu decrease undercooling from 28.9°C to 20.2°C.

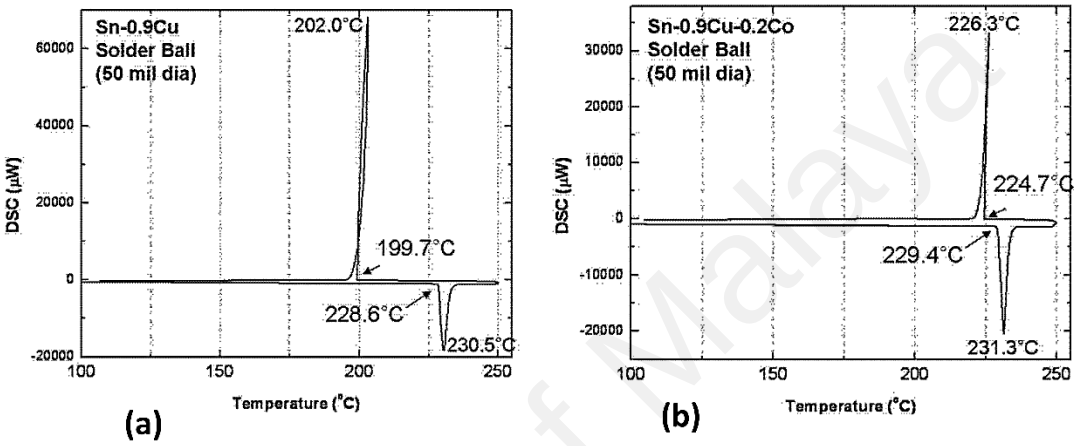

Figure 2.16: A typical DSC thermal profile recorded during the heating and cooling cycle of one solder ball of (a) Sn-0.9Cu, (b) Sn 0.9Cu-0.2Co (Kang et al., 2007).

In the eutectic Sn-Ag-Cu system, the undercooling for the nucleation of the solid Ag_3Sn phase is small, 7.2°C with differential scanning calorimetry (DSC) in the Sn-3.8wt.%Ag-0.7wt.%Cu alloy. But the formation of the Ag_3Sn does not facilitate the nucleation of the β-Sn phase. The β-Sn does not wet on the previously formed Ag_3Sn, therefore; it will not nucleate heterogeneously on the Ag_3Sn. The undercooling for the β-Sn phase is 29 °C in the same alloy. It was observed that the large undercooling of the β-Sn phase in the presence of large Ag_3Sn intermetallic particles and the same conclusion was reached, that the intermetallics particles are ineffective as heterogeneous nucleation substrates for Sn (Moon et al., 2000).

The eutectic Sn-3.5Ag, Sn-0.7Cu, and Sn-3.5Ag-0.9Cu alloys are anomalous. The difference in the melting point between Sn and Ag (or Cu) is large; the difference in the volume fraction of the constituent phases, β-Sn and Ag_3Sn (or Cu_6Sn_5), is also large. More importantly, the Ag_3Sn and Cu_6Sn_5 are faceting phases, while β-Sn is a non-faceting phase. During solidification, the faceting phase, Ag_3Sn or Cu_6Sn_5, grows by layer deposition involving the lateral propagation of a step across the liquid/solid interface. On the other hand, the non-faceting phase, β-Sn, advances into the liquid phase by tree-like, non-faceted dendrites. Because of the different growth mechanisms, the growth rates of the β-Sn and Ag_3Sn (or Cu_6Sn_5) are quite different. Therefore, the growths of the β-Sn, and Ag_3Sn (or Cu_6Sn_5) are independent or only loosely coupled (Shangguan, 2005).

2.4.4 Anisotropy of Sn

Sn is one of the most anisotropic metals. The crystal structure of Sn is body-centered tetragonal as shown in Figure 2.17, which is a central atom with tetrahedral bonding to the atoms on the four faces. Sn-based solder joints usually form large or single-crystal joints, hence the anisotropic properties of Sn provide an initial force for heterogeneous microstructural evolution, and thus the properties of solder joints evolve in a complex manner.

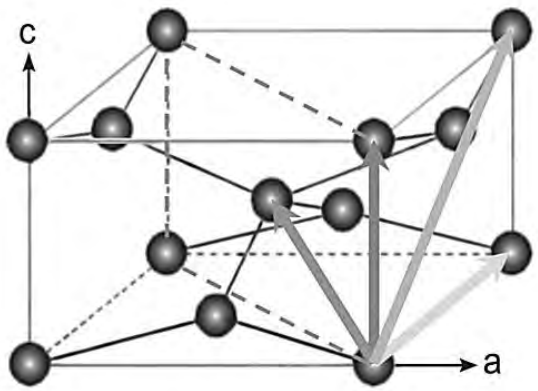

Figure 2.17: Crystal structure of pure Sn with lattice parameters a =5.8315 Å, c=3.1814 Å; c /a = 0.5456 (Telang et al., 2005).

In particular, the anisotropy of the coefficient of thermal expansion (CTE) is important. The CTE rises with temperature which at all temperatures it is twice as large in the *c* direction than the *a* direction, Figure 2.18(a). The 3-dimensional(3D) CTE surface that describes this property with respect to the crystal directions illustrates in Figure2.18a with an ellipsoid appearance. Therefore, the CTE is isotropic in the x–y plane while shows the maximum anisotropy in any plane containing the z axis.

The elastic anisotropy shown as a surface of Young's modulus values in 3D in Figure 2.18(b). This figure is shown at two temperatures, the upper half at 150°C and the lower half at -45°C, which are common application temperatures for most electronic systems. Sn is most compliant in the <100> directions and stiffest in the [001] direction and almost as stiff in the <110> directions (thus, Sn is nearly isotropic on {110} planes). At low temperatures, the maximum anisotropy ratio is approximately 2, whereas this ratio rises to around 5 at the highest temperatures. An important results of the stiffness and CTE is that Sn is stiffest in the direction that the CTE is highest. Therefore, there will be remarkable disagreements at grain boundaries where dislocations are generated, leading to localized plastic deformation of the crystal. Thus, the amount of diffusion or dislocation generation required will be in proportion to the magnitude of the disorientation between the two crystals and the change in stress or temperature.

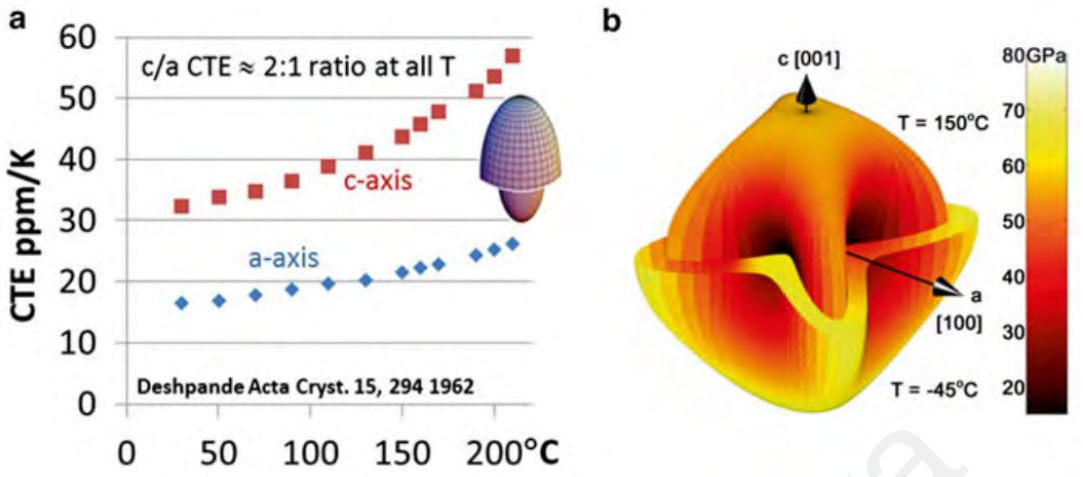

Figure 2.18: (a) Temperature dependence of the coefficient of thermal expansion (CTE) with temperature (ellipses show relative difference in CTE magnitude at 25°C and 210°C). (b) Anisotropy of Young's Modulus at −45°C and 150°C(Lee et al., 2015).

2.4.5 Isothermal Aging

As a result of isothermal aging the microstructure, mechanical property, and failure mechanisms of Sn-based solder joints are continually changing (Medvedev, 1956). Generally thermal aging has a detrimental effect on reliability such as reductions in stiffness, yield stress, ultimate strength, and strain to failure, as well as highly accelerated creep(Lampe, 1976; Ma et al., 2009; Xiao et al., 2004).

Thermal activation leads to microstructural evolution into structures with less interfacial energy and probably changes in crystal structure of the IMCs due to metastable solidification microstructure. For instance, Cu_6Sn_5 has a monoclinic structure in its equilibrium structure, however it initially forms in a metastable hexagonal structure which can transform into the monoclinic structure, based on microalloying present in the alloy and thermomechanical history. However some elements microalloying can stabilize the hexagonal structure (Nogita et al., 2008).

Figure 2.19(a) and (c) shows the initial dendritic microstructure after solidification. This microstructure contains Sn and areas surrounding it that contain fine particles which are effective in pinning dislocations. Thus, microstructure is a composite material with hard regions and soft regions. In the backscattered electron image within the β dendrites, low-angle boundaries with small orientation differences are usually observed, Figure 2.19(c). Furthermore, individual dislocations or dislocation sub-grain walls can be recognized by optimizing tilting condition. Based on the initial solder composition and the time and temperature history in the liquid state some of the larger particles can be observed within the nanoscale Ag_3Sn precipitates. With a slower solidification rate, such as in larger sample volumes (e.g., cast bulk tensile samples), the Ag_3Sn particles are larger and more cylindrical than spherical, and the dendritic structure is more clearly defined (Yazzie et al., 2012).

By aging an as-cast sample can simulate the microstructure that develops with years of service conditions which transform the eutectic microstructure regions into Sn with approximately distributed larger particles (Fig. 2.19(b)). The coarsening of Ag_3Sn particles facilitate by existence of dislocations within the β-Sn dendrite which provide dislocation pipes. As a result of coarsening process the spacing between particles rises. Therefore, the stress needed to cause dislocation motion throughout the joint decreases. The stress reduction in thermal cycling experiments occurs exponentially over the first several hundred cycles, depending on the strain magnitude. Aging can lead to coarsening similar to the thermal cycling, however there is the significant difference between them. In thermal cycling the stress changes continually, leading to dislocation generation and recovery, and changing the temperature which make easier the dissolution of precipitates at high temperature and re-precipitation of dissolved elements in solution back onto existing precipitates, whereas this process does not occur during long-term aging.

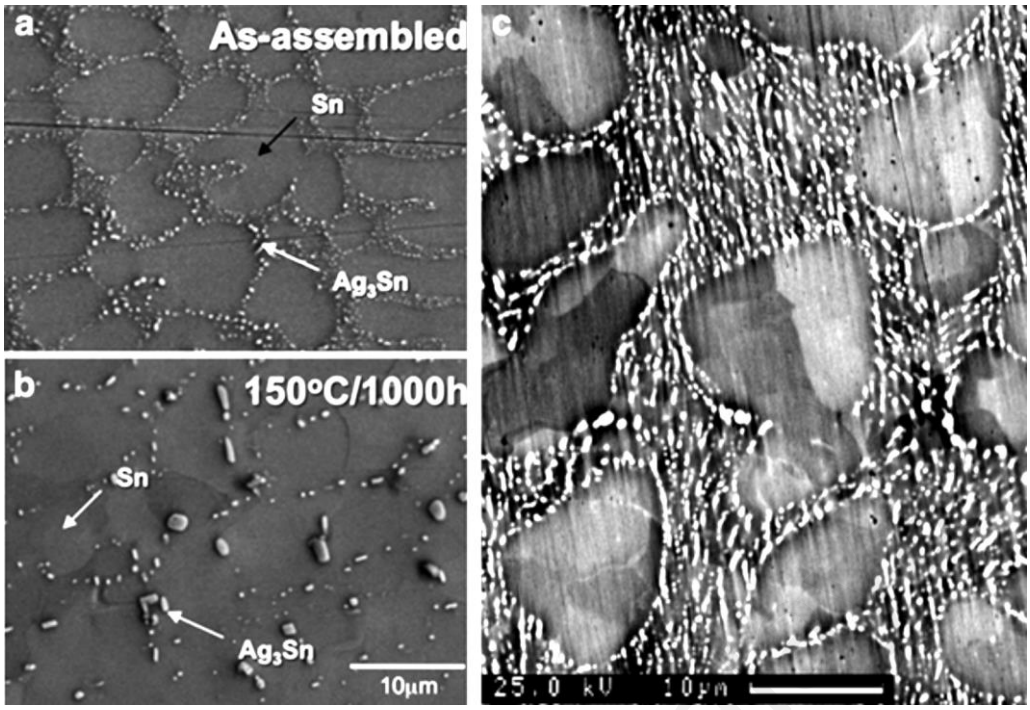

Figure 2.19: (a)Secondary electron image of as-fabricated SAC305 solder microstructure, and (b) the coarsened microstructure after aging. (c) Backscattered electron micrograph of as-solidified eutectic Sn–Ag solder illustrating subgrain boundaries within β tin dendrites(Zhou et al., 2016).

Isothermal aging resulted in the degradation of strength and increasing in the creep rate. The consequence of microstructure and IMC precipitate coarsening after aging will be the reduction in strength. By increasing temperature during aging process, there is stress relaxation arising from CTE and anisotropic stiffness effects, resulting in decreasing creep rate exponentially. Dislocation nucleation, mobility, and grain size control creep behavior (Mathew et al., 2005). As a result of more grain boundary due to finer grains, sliding will be easier by absorption of dislocations into boundaries, which lead to grain boundary diffusion and hence accelerate creep deformation and stress relaxation. More distances between particles due to particle coarsening result in more shear strain by bowing of dislocations that are pinned by particles. The pinning effect of particles on grain boundary motion degraded by fewer and larger particles. Therefore, the effect of dislocation motion on elastic modulus will increase by coarse grain and particle size. Thus, isothermal aging can lead to a reduction in the apparent elastic modulus (Ma,

2009). Isothermal aging results also show that after an initial tensile strength drop, Sn–Pb eutectic solder reaches a relatively stable condition after about 200 h of aging. However, for SAC, both the tensile and creep properties continuously change with increasing aging time. It is noteworthy that the creep deformation of SAC is only lower (better than) Sn–Pb at room temperature and shorter aging times(Ma et al., 2007).

2.4.6 Wetting and Solderability

Wetting of a liquid on a solid is determined by the relative energies of the liquid-vapor surface tension, the solid-liquid interfacial energy, and the solid-vapor interfacial energy, as represented by Young's Equation($\gamma_{SV} = \gamma_{SL} + \gamma_{LV}\cos\theta$, interfacial energy between solid liquid phase γ_{SL}, liquid vapor phase γ_{LV}, and solid vapor phase γ_{SV}) (Lea, 1993). Figure 2.20 illustrates the large and small wetting angles. The thermodynamics of an alloy play a central role in determining its intrinsic liquid-vapor surface tension. The surface tension of pure Sn is significantly higher than Sn-Pb eutectic (White, 1971). The surface tension of high-Sn lead-free solder alloys are higher than Sn-Pb solder alloys which leads to higher contact angles for lead-free solder alloys (White, 1971). The effects of different solderability factors, such as flux, temperature, and substrate conditions, and for screening materials and soldering conditions can be separated by wetting balance and spreading rate of solder. Generally, wetting characteristics of lead-free solder alloys on a specific metal substrate depend on the composition and temperature of the solder and the substrate, as well as the size and thermal conductivity of the substrate, the liquidus temperature of the solder, the surface condition of the substrate, the gaseous experimental environment (oxygen, air, nitrogen), and, last but not least, the flux.

Generally wetting quality on substrate can be evaluated by contact angle. Normally, when the value is between $0° < \theta < 20°$, the wetting quality is very good. For the value

20° < θ < 30° and 30° <θ < 40° it is good and acceptable. When the value of θ > 40°, the wetting behavior is bad and not acceptable (Kripesh et al., 2001).

Figure 2.20: Large and small wetting angles of solder on substrate.

2.4.7 Interfacial Reactions of lead-free Solder with Substrate

As a result of reactions between the solder and substrate during the soldering process intermetallic compounds (IMCs) form between them. A uniform IMC layer between the solder and substrate is essential for good metallurgical bond. However, the thickness of IMC strongly affects the reliability and mechanical properties of the solder joint. A thick IMC hamper the interface integrity because of its brittle nature and creates mismatch in physical properties such as elastic modulus, thermal expansion etc (Lee et al., 1997; Pang et al., 2004). For this reason, the interfacial reaction should be controlled to ensure the reliable properties of the solder to have an optimized interfacial IMC. The interfacial reaction between the solder and substrate can be during reflow process, or during high temperature aging. The former process is encountered during the reflow and wave soldering processes and the latter happens during service or high temperature aging test. During service or high temperature aging the thickness of interfacial IMC increases due to diffusion of Sn from the bulk solder to the substrate(Sivasubramaniam et al., 2008).

Cu and Ni thin films are used widely as on-chip under-bump metallization (UBM), but they can be reacted and dissolved away by molten solder during reflow, resulting in spalling of IMC(Laurila et al., 2005). There are many surface finishes such as, Electroless

Nickel/Immersion Gold (ENIG) and Organic Solderability Preservative (OSP), which are being implemented to meet the requirements of lead-free solder substrate (Rizvi et al., 2007).

Cu is the most common conductor metal, which is utilized in contact with solders owing to its good solderability characteristic and excellent thermal conductivity performance (Rizvi et al., 2007). The whole interfacial layer of the IMCs will tend to become planar with increasing reflow time (Moon et al., 2000). The IMC layer are composed of two layers, the light gray regions are Cu_6Sn_5 and thin dark gray layer beneath is Cu_3Sn, the thickness of which is very thin, as shown in Figure 2.21 (Peng et al., 2007). But after reflow most of the time this thin Cu_3Sn layer is not visible under SEM in the cross-sectional view. In general, for most of the Sn-based solder Cu_3Sn IMC layer grows at the side of Cu substrate during reflowing (Gong et al., 2009; Shang et al., 2009).

Moreover, Ag_3Sn IMC was found dispersed uniformly in the solder after reflow. The planar Ag_3Sn which formed near the interface have changed remarkably and merged together to large platelets with increasing thermal cycles or aging (Pang et al., 2004). Large Ag_3Sn needles can cause reliability concern when they form in a high stress concentration area, such as the corner between solder and copper substrate. Fatigue cracks can initiate and propagate along the interface between the Ag_3Sn and solder matrix, as leading to mechanical failure (Schoeller et al., 2009).

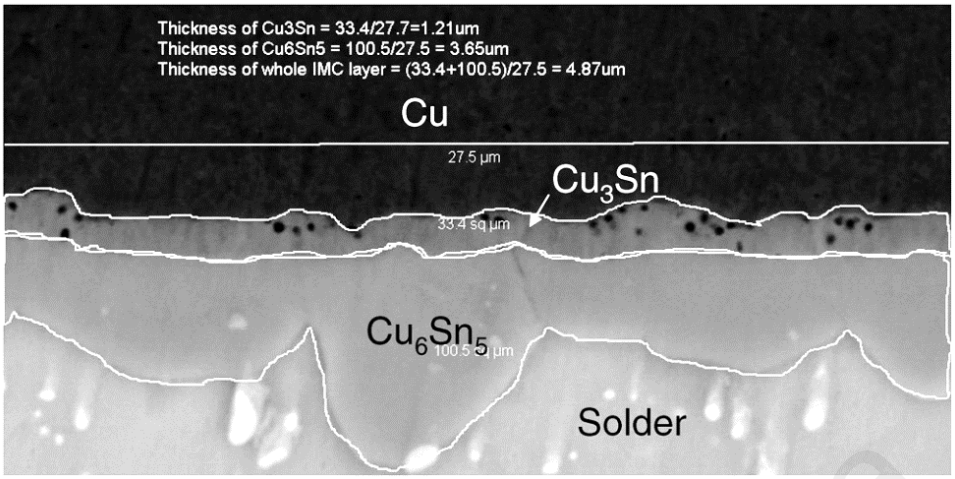

Figure 2.21: IMC layers formed between the solder and Cu substrate after soldering(Peng et al., 2007).

In electronic products, Ni is one of the most common metals to be in direct contact with the solders(Ho et al., 2002). Nickel is used as a solderable diffusion barrier in several types of surface finishes for components and printed circuit boards, since the reaction rate of Ni with molten solder is smaller than Au, Ag, and Cu (Bader, 1975).

Sn-Ag-Cu solder reflowed on pure Ni substrates showed distinctly different from those observed for Sn-Ag-Cu/Cu solder joint. Figure 2.22 shows that the reaction between Ni and Sn-3Ag-0.6Cu make $(Cu,Ni)_6Sn_5$ in bulk of solder and at interface near to the solder, whereas $(Ni,Cu)_3Sn_4$ observed between Ni and $(Cu,Ni)_6Sn_5$. Further work revealed that a different phase was growing at the interface due to the different Cu concentration in solder composition, thus with a composition of $Cu_xNi_ySn_{45}$, where the Cu concentration (x), varied between 44 and 53 atomic percent, and the Ni concentration (y) between 1 and 10 atomic percent. These compositions are consistent with the stoichiometry of the compound $(Cu,Ni)_6Sn_5$ (Zribi et al., 2001).

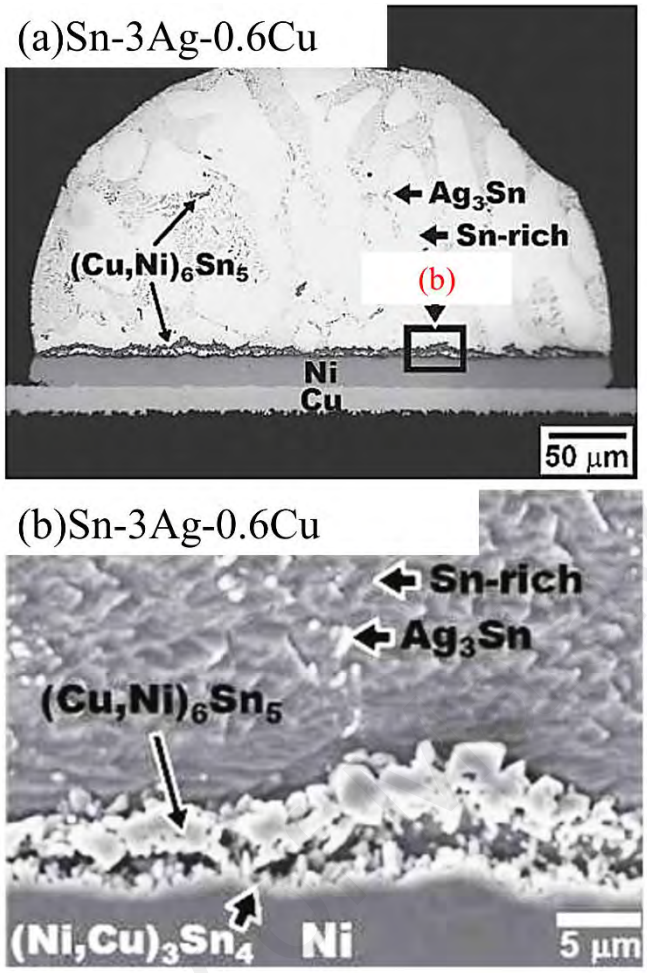

Figure 2.22: (a)Interface between Sn-3.0Ag-0.6Cu solder ball and Ni/Cu substrate (b) Zoom-in view of (a)(Ho et al., 2006).

The atomic diffusion from the substrate through the IMC is the main controlling process for IMC growth on substrate (Guowei et al., 2000; Zhuo-Ming et al., 2000). However, for IMC growth in bulk solder the dominant process is the diffusion of Cu to the interface between the IMC and solder.

2.4.8 Effect of Ag on solder alloys

The effect of adding Ag up to 1 mass% on the microstructural and mechanical properties of Sn–Cu eutectic solder alloy was examined by Huh et.al (Huh et al., 2001). Without Ag, primary β–Sn grains are surrounded by the eutectic network band of Cu_6Sn_5 needle precipitates/β–Sn. With increasing Ag content, the primary β–Sn grain size and

the eutectic network size become finer. In the eutectic band fine Ag_3Sn particles appear in addition to Cu_6Sn_5 precipitates. The 0.2% proof stress and tensile strength decrease with the addition of 0.1 mass %Ag and then gradually increase up to 1 mass %Ag. Even with 1% Ag, they are less than the values for a Sn–0.7Cu binary alloy. In contrast, by increasing Ag content up to 1% elongation increases. Therefore, the addition of Ag to Sn–0.7Cu alloy can effectively improve its ductility. The strain rate dependence of 0.2% proof stress of Sn–0.7Cu–0.5Ag is similar to that of Sn–Ag eutectic alloy but is different from that of Sn–Cu eutectic alloy. A small amount of added Ag results in a change of the deformation mechanism of Sn–Cu alloy.

The failure mode during drop-impact loading conditions for high-Ag-content SAC solder joints was manifested by cracking along the interface between the IMC layer and the solder (packaging side) and through the IMC layer (board side)(Kim et al., 2007; Kim et al., 2007; Syed et al., 2006). In either case, the drop-impact failure was characterized by a lack of bulk solder deformation and an absence of bulk solder cracking. The lack of bulk solder deformation during the drop-impact loading conditions was attributed to the strain-rate sensitivity of the solder(Frear, 1999; Pang et al., 2006; Suh et al., 2007).

Metallic materials including solders typically become stronger with increasing strain rates. In other words, the flow stress increases with increasing strain rates. The strain-rate sensitivity is a function of the homologous temperature (T_{hom}), which is considerably higher for solders due to their low melting temperatures. As a result of the high strain rate sensitivity, the yield strength of the SAC solders increases rapidly with strain rate. This increased yield strength suppresses any plastic deformation and prevents the drop-impact energy from dissipating through the bulk solder, thereby transferring more dynamic stress to the interface, which then causes interfacial fractures(Kim et al., 2007; Pang & Che,

2006). Thus, the drop impact reliability of the solder joints is influenced by a complex combination of the bulk solder and interface IMC layer properties.

The first approach for improvement of the drop impact performance of the SAC solder joints was to optimize the bulk solder properties by reducing the Ag content as low as<2 wt.%. Reducing the Ag content causes the bulk solder to exhibit low elastic modulus and yield strength as well as high elongation, which in turn increases the bulk compliance and ductility of the solder joint(Lee et al., 2007; Pandher et al., 2007; Suh et al., 2007). In other words, a solder alloy with higher elastic compliance is expected to exhibit longer critical strain to failure than a solder alloy with lower elastic compliance. Therefore, the low-Ag-content solder joints are much more likely to deform in bulk under high-strain-rate loading conditions. For example, in contrast to SAC405, which predominantly shows interfacial fracture during drop testing, SAC105 shows considerable amount of cohesive failure through solder bulk, as shown in Figure 2.23 (~50% of joint failure was identified as cohesive fracture in SAC105.). The cohesive fracture through solder bulk obviously represents higher energy dissipation than interfacial fracture(Suh et al., 2007).

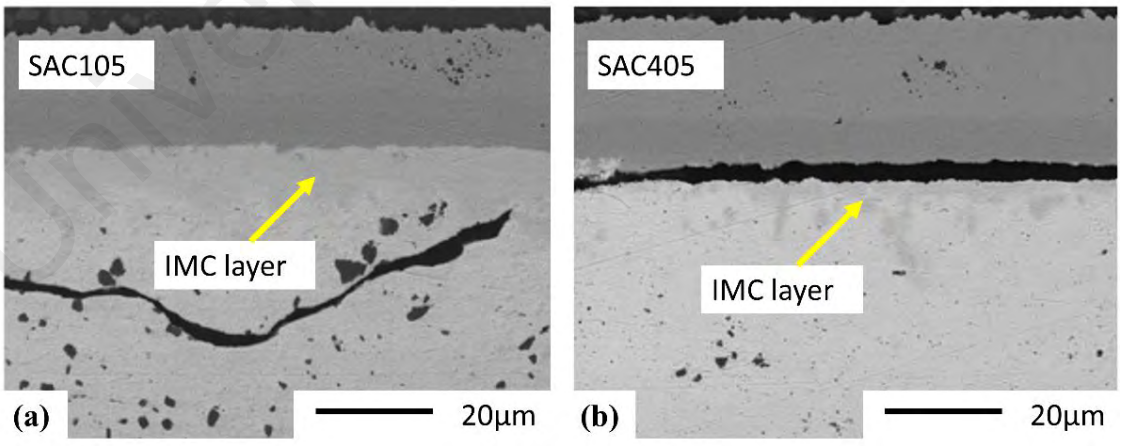

Figure 2.23: SEM micrographs of different drop testing failure modes of (a) SAC105 and (b) SAC405 on electrolytic Ni/Au (Suh et al., 2007).

The elastic compliance and plastic energy dissipation ability are identified as key material properties to be optimized for extrinsic toughening mechanisms, which are

believed to play an important role in the drop-impact performance enhancement. Extrinsic toughening refers to a toughening mechanism that is attained by reducing the effective crack driving force experienced by the crack tip during various energy dissipation processes, without increasing the inherent fracture resistance of the material or the interface. Specifically, high elastic compliance and high plastic energy dissipation abilities effectively toughen the crack tip during crack propagation and prolong the time required to reach the critical stress for fracture under high-strain-rate loading conditions (Ritchie, 1988). Therefore, the low Ag-content SAC alloys can dissipate more dynamic energy through bulk solder deformation, and consequently, they reduce the dynamic stress transferred to the interface IMC layers.

2.4.9 Reliability of solder joints

Reliability of solder joint has been a concern for a long time, such as, the low cycle fatigue of Sn-Pb solder joints in flip chip technology due to the cyclic thermal stress between a Si (silicon) chip and its substrate. At present, the risk of fatigue has been much reduced by the innovative application of underfill of epoxy between the chip and its substrate. On the other hand, to replace of Sn-Pb solders by Pb-free solders, new reliability issues have appeared, mostly because the Pb-free solders have a very high concentration of Sn. Furthermore, due to the demand of greater functionality in portable consumer electronic products, electromigration is becoming a current serious reliability issue. This is because of the increase of current density to be carried by the power solder joints (Tu, 2010).

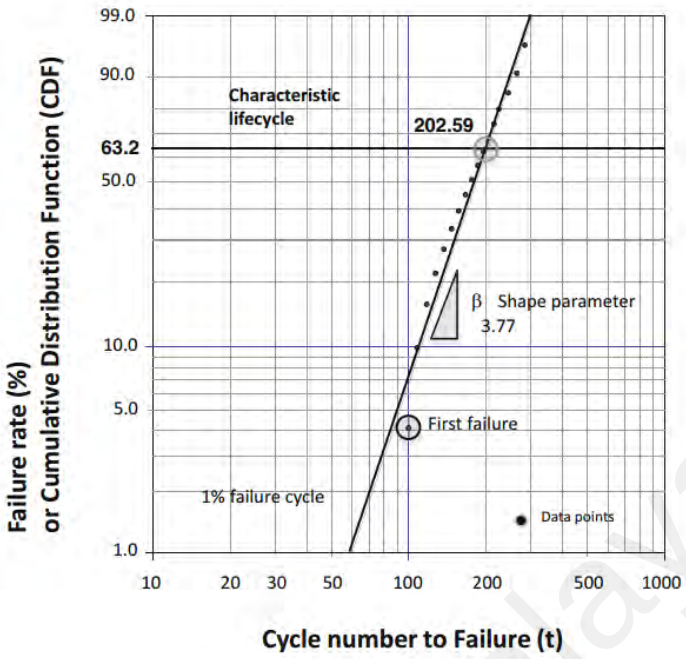

Figure 2.24: Typical Weibull plot (Lee et al., 2015).

The common industrial choice for the statistical analysis of failure is the Weibull model, known as Weibull distribution. The horizontal scale is the cycle or time (t) parameter to failure, with a logarithmic scale. The vertical scale is the cumulative distribution function (CDF) that defines the proportion of the parts that will fail up to cycle number (t) in percent. The two defining parameters of the Weibull plot are the slope, beta (β), and the characteristic life, eta (η). Typical Weibull plot are shown in Figure 2.24.

As shown in Figure 2.25, Syed et al. showed that SAC105 has better performance than SAC305 under drop loading conditions. However, the trend is reversed for temperature cycle test. A slight reduction in performance. A similar trend was observed when eutectic SnAg solder alloy was compared with SAC105 solder alloy for temperature cycle, drop, and bend cycling conditions.

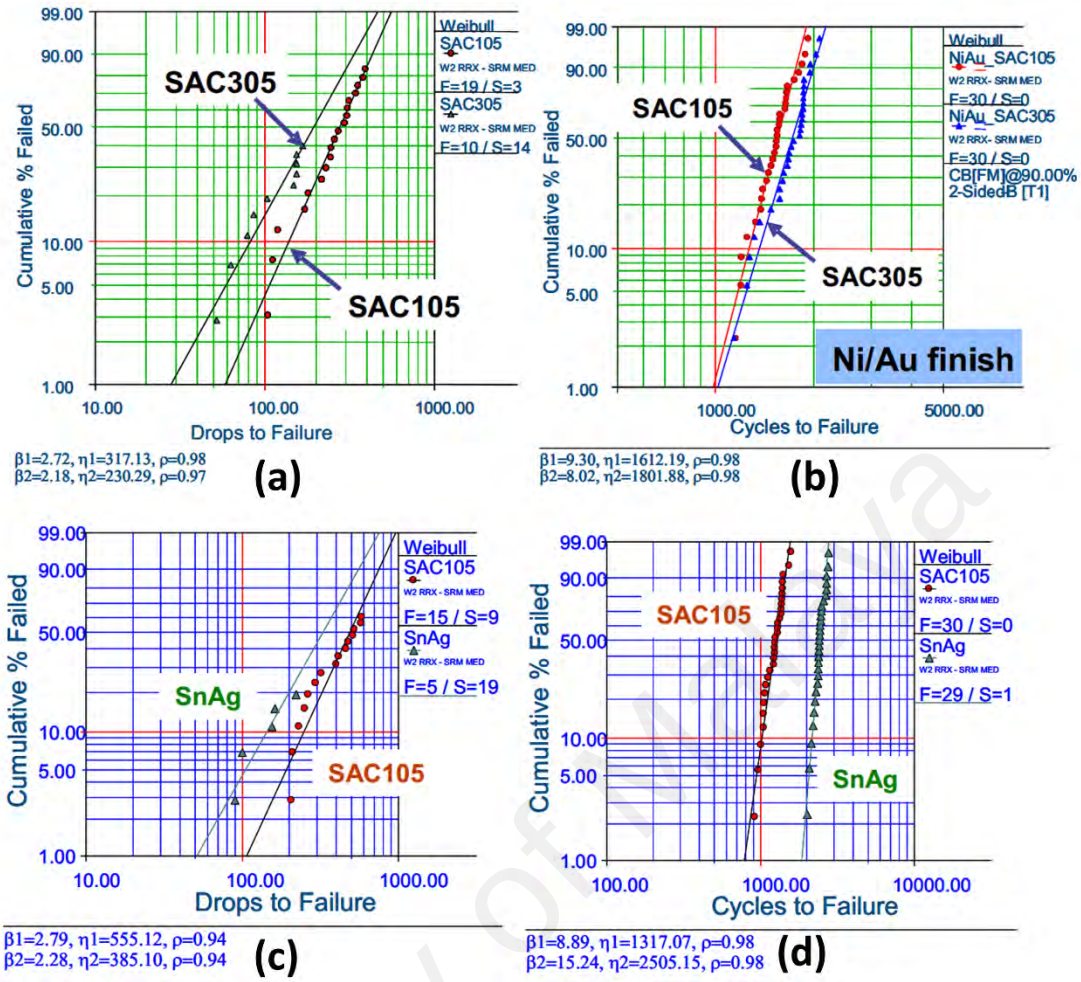

Figure 2.25 : (a) and (b) compare SAC105 and SAC305. (c) and (d) compare SAC105 and Sn-Ag. (a) and (c) shows Drops to failure, whereas (b) and (d) shows Temperature cycle to failure for NiAu finish packages.

2.5 Microalloying of Solders to Improve Reliability

Some alloying elements, such as Ni (Hammad, 2013), Co (Wang et al., 2009), Ce (Xie et al., 2012), Fe (Laurila et al., 2009), Ag (Yang, 2013), Sb (El-Daly et al., 2013) and Zn (El-Daly et al., 2013) etc. have been added into SAC alloys to refine the microstructure, and improve the wettability and mechanical properties. The net result of minor alloying addition is to (1) change the bulk alloy microstructure and mechanical properties, and/or (2) control the interfacial intermetallic layer(s)(Wu et al., 2002).

2.5.1 Effects of addition of Mn, Ti, In, Sb, Ni, Ge, Ce and Co

Eutectic Sn-0.7Cu exhibits a melting temperature at 227ºC. Sn-0.7Cu is lower in tensile strength but higher in elongation than both eutectic Sn-Ag and Sn-Pb, reflecting the softness and ductility of Sn-Cu (Lau et al., 2003). The creep strength of eutectic Sn-Cu is higher than Sn100, but lower than eutectic Sn-Ag and Sn-Ag-Cu at both 20ºC and 100ºC. Wetting balance test results by Hunt et al. indicated that the wetting ability decreased in the following order: eutectic Sn-Pb > Sn-Ag-Cu > Sn-Ag > Sn-Cu when an unactivated flux was used (Hunt et al., 2000). Eutectic Sn-Cu is commonly used at wave soldering and hand soldering. The mechanical and wetting properties of eutectic Sn-Cu were enhanced by addition of small amount of dopants such as Ni, Ge, Co, and Ce. Sn-0.7Cu-0.05Ni (Lee, 2009) and Sn-0.7Cu-0.05Co (Lee, 2009) were reported to exhibit a reduced wetting time, copper dissolution rate, and a more shiny smooth solder joint surface at wave soldering. Sn99.3Cu0.7Ce0.02 was reported to have enhanced elongation performance and drop test performance (Liu et al., 2006).

For Sn-Ag-Cu, its hardness, tensile strength, yield strength, shear strength, impact strength, and creep resistance are all higher than eutectic Sn-Pb (Sn63) (Lau et al., 2003). The wetting performance is better than both eutectic Sn-Cu and eutectic Sn-Ag, although poorer than that of Sn63 (Huang et al., 1999). Addition of Sb into SAC, Sn96.2Ag2.5Cu0.8Sb0.5 (CASTIN), was reported to exhibit a slower intermetallic compound growth rate (Lee, 2009). Due to its high hardness, lead-free solder joints typically suffer fragility issue upon drop test. This is a particular concern for portable electronic devices. Reducing Ag content, such as Sn98.5Ag1.0Cu0.5 (SAC105), Sn99Ag0.3Ag0.7 (SAC0307), and Sn98.9Ag1.0Cu0.1 (SAC101) (Lee, 2009), improves the nonfragility (Date et al., 2005). This approach often results in an elevated liquidus temperature up to around 227°C.

2.5.2 Effects of addition of Fe

On the basis of phase diagrams of Sn-Fe, Cu-Fe, and Ag-Fe just $FeSn_2$ intermetallic compound can be exist in the eutectic area with an irregular shape.

Previous research showed that Fe can decrease the size of IMC in interface by retarding the growth of interfacial Cu_6Sn_5 and Cu_3Sn layer during liquid state(Laurila et al., 2009). Fe does not dissolve in IMC's, also does not alter the ratio of Cu_6Sn_5–Cu_3Sn layer in the system and only slightly decreased the total IMC layer thickness(Laurila et al., 2009), Figure 2.26.

Also previous research on Sn-1Ag-0.5Cu showed that doping Fe decrease yield strength and UTS, whereas doesn't have considerable effect on elongation, Figure 2.27 shows strass-strain curve. On the other hand Fe improved drop impact reliability and also stabilize the mechanical properties of solder with aging as shown in Figure 2.28 (Kantarcıoğlu et al., 2014).

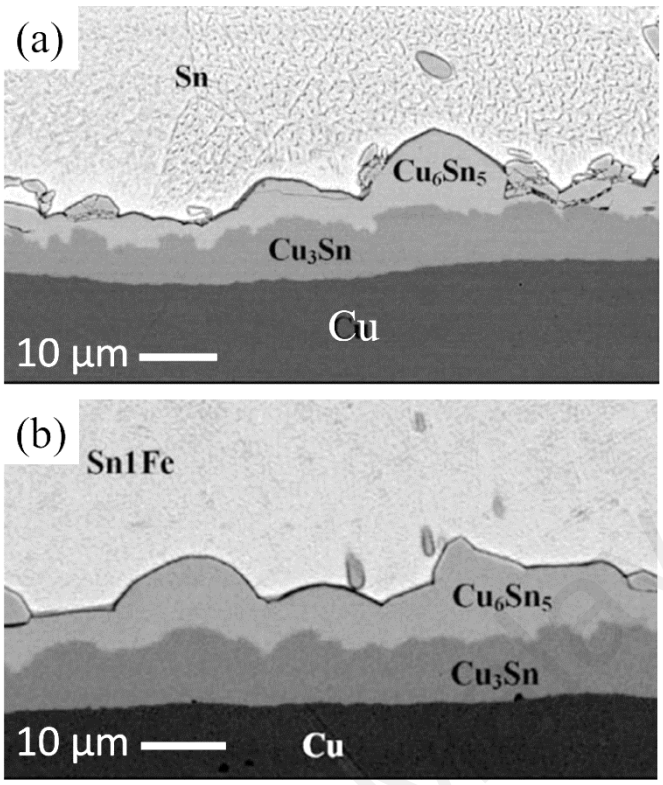

Figure 2.26: (a) Reaction layers formed in the reaction between(a) pure 100Sn and Cu after annealing at 150°C for 2560 h (b) Sn-1wt.%Fe and Cu after annealing at 150°C for 2560 h(Laurila et al., 2009).

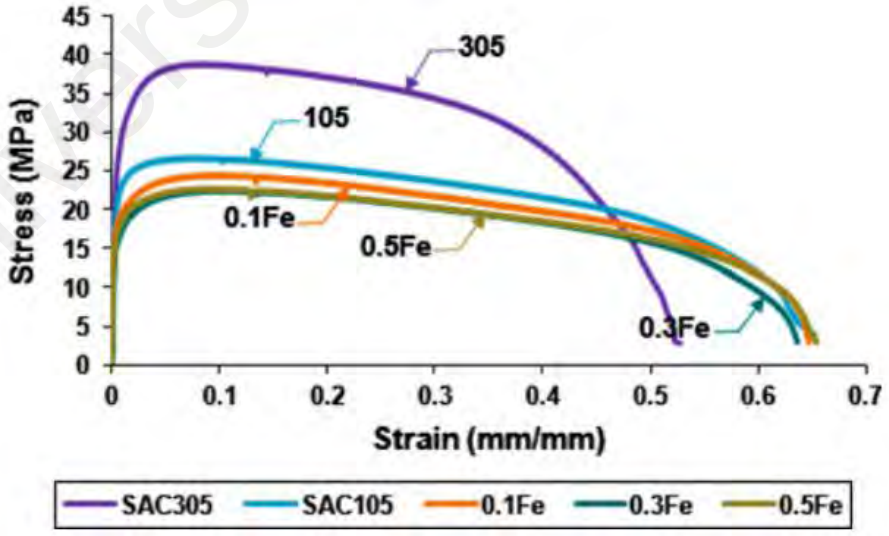

Figure 2.27: Stress-strain curve of SAC305, SAC105, SAC105-0.1Fe, SAC105-0.3Fe, and SAC105-0.5Fe solders alloys(Shnawah et al., 2012).

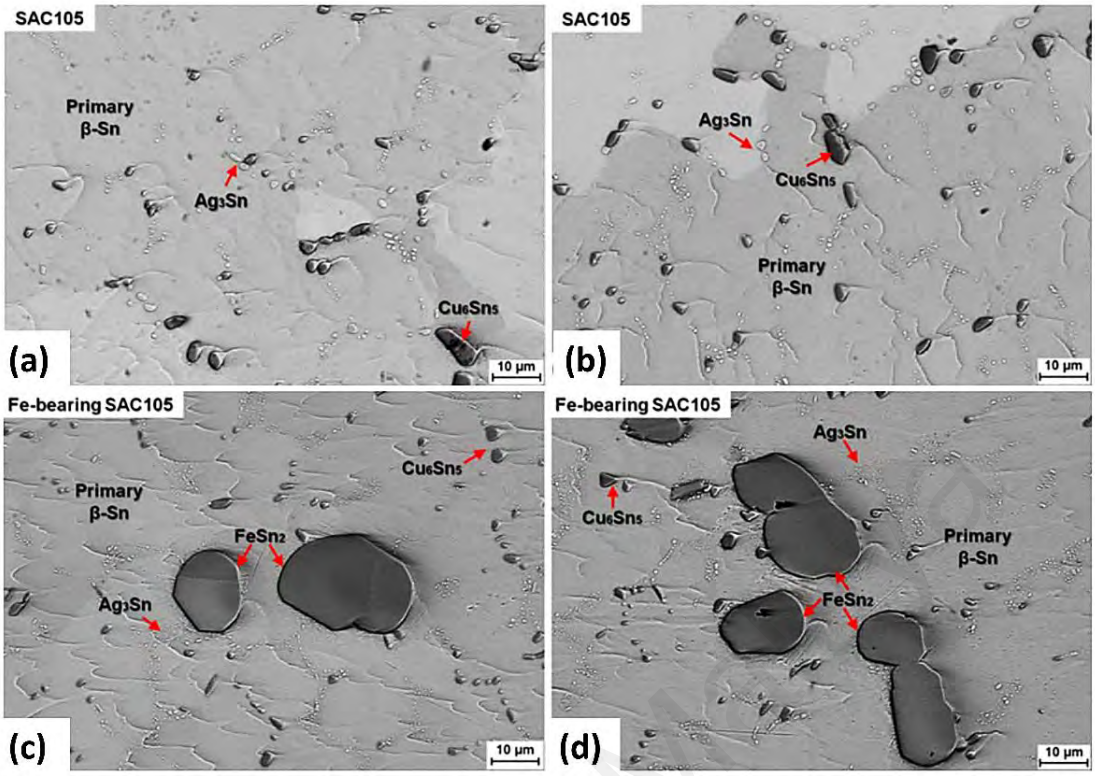

Figure 2.28: SEM micrographs of SAC105 and Fe-bearing SAC105 solder alloy (a,c) after 720 h of aging at 100 °C and (b,d) after 24 h of aging at 180 °C (Shnawah et al., 2013).

Fe addition to the Sn–1Ag–0.5Cu solder alloy suppresses the coarsening of Ag_3Sn intermetallics. The lattice strain in the Ag_3Sn intermetallics and the blocking effect on Ag diffusivity in Sn matrix are the possible mechanisms for the coarsening suppression of the Ag_3Sn intermetallics in Fe-modified solder alloy. Figure 2.29 shows a cross-sectioned TEM photograph of the as-cast Fe-modified SAC105 solder alloy with micro-electron-beam diffraction pattern. There are two distinctly different areas in contrast, where the IMC particles and primary β-Sn could be well determined by means of the micro-element analysis. From the EDX analysis, the composition of the IMC particles is determined as 8.24Fe–61.87Ag–29.89Sn (in atomic percent, the standard atomic deviation is 2.0%). Combined with micro-electron-beam diffraction patterns taken from the IMC particles, these particles were further determined to be Ag_3Sn IMC particles containing a small amount of Fe.

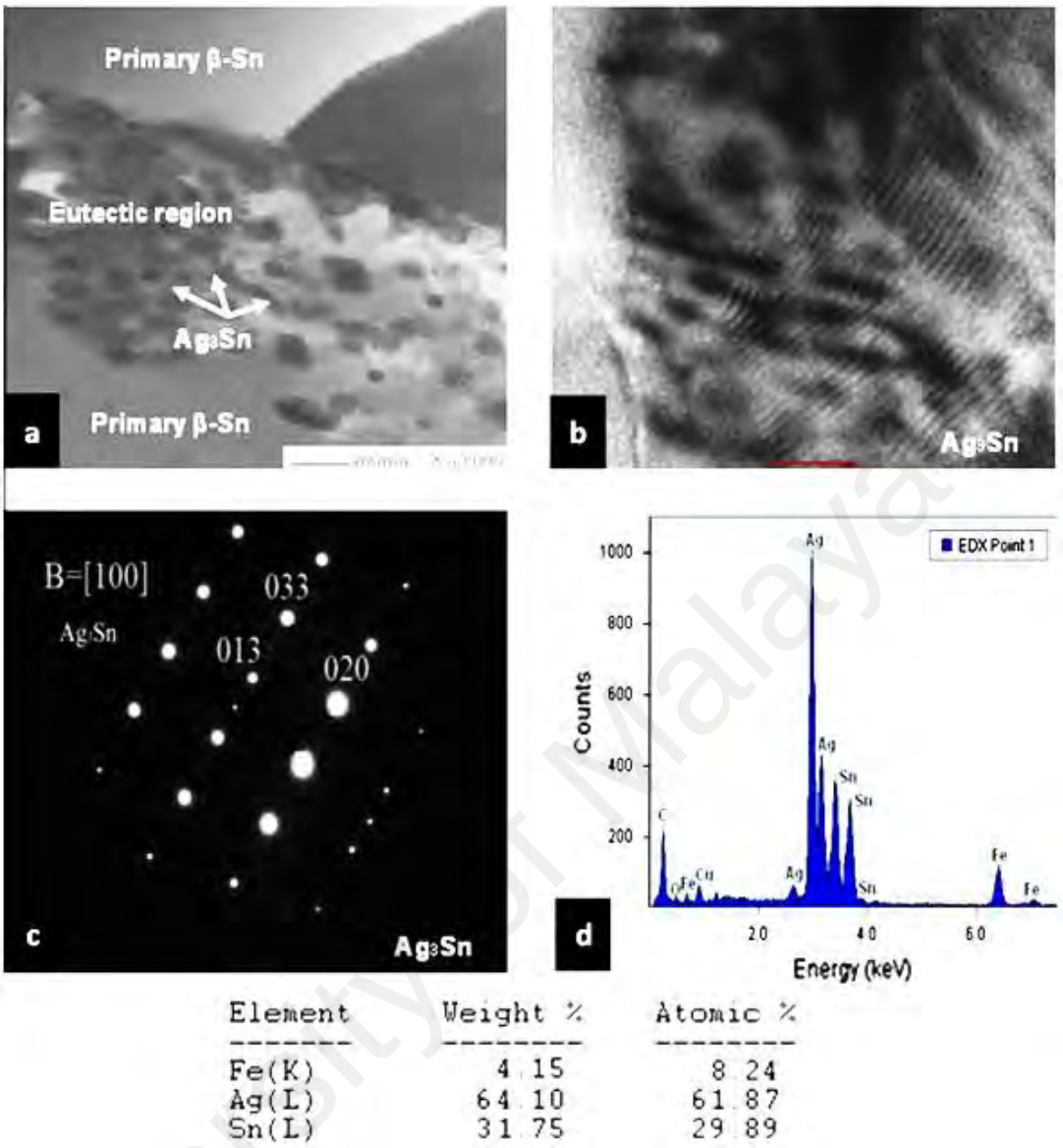

Figure 2.29: TEM analysis of the Ag_3Sn IMC particles formed at the eutectic region in the as-cast Fe-modified solder alloy: (a) TEM image, (b) high resolution TEM image, (c) microelectron-beam diffraction pattern, and (d) TEM-EDX spectrum(Shnawah et al., 2015).

In the second mechanism, the presence of Fe solute atoms in the Sn matrix in the eutectic regions significantly reduces the diffusivities of Ag, which significantly reduces the effect of the Ostwald ripening process. Such a trend can be attributed to the blocking effect: the diffusivity of Fe in the Sn matrix is extremely slower than the diffusivity of Ag in the Sn matrix (Shimotomai et al., 1978). This difference in diffusivity makes the lattice sites occupied by Fe solute atoms blocking sites to the diffusion of Ag atoms in the Sn matrix during aging. The Fe solute atoms in the Sn matrix act as obstacles to the

movements of Ag atoms from the Sn matrix surrounding the smaller Ag_3Sn IMC particles towards the Sn matrix surrounding the larger Ag_3Sn IMC particles, which significantly reduces the supply of Ag required for the Ag_3Sn coarsening. Thus, Fe can promote microstructural stability and stabilize mechanical properties by modification of the coarsening behavior of a solder-joint during high temperature aging.

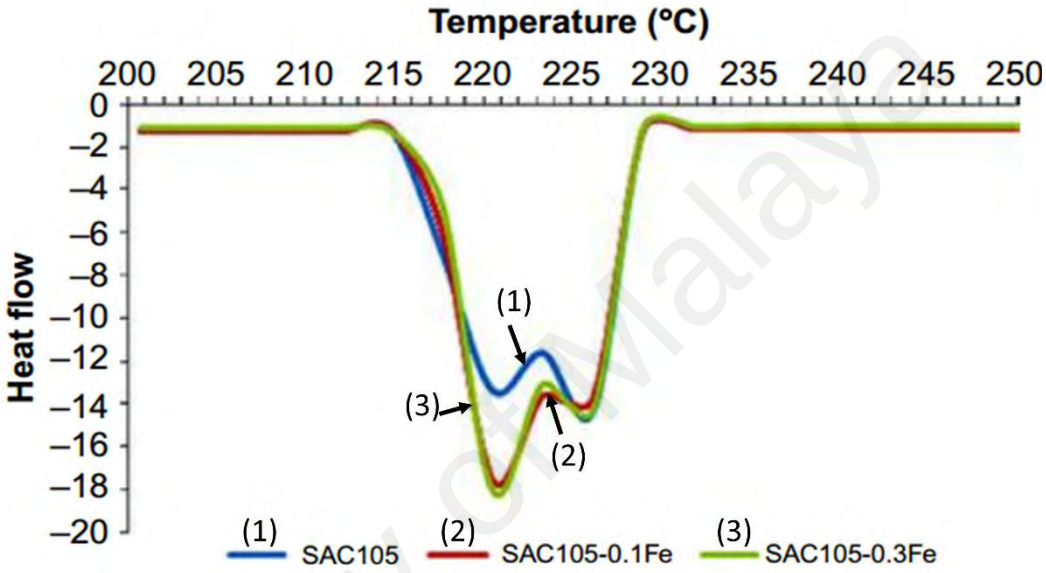

Figure 2.30: DSC thermographs of (a) Sn-1Ag-0.5Cu, (b) Sn-1Ag- 0.5Cu-0.1Fe and (c) Sn-1Ag-0.5Cu-0.3Fe (Shnawah et al., 2012).

The additions of Fe to the Sn-1Ag-0.5Cu solder did no affect the mode of fracture; all tested solders showed large ductile-dimples on their fracture surfaces. Figure 2.30 shows DSC thermographs, the additions of Fe did not cause any significant effect on the melting behaviour, hence allowing the use of the Fe-containing Sn-1Ag-0.5Cu alloy to be consistent with the use conditions for conventional Sn-Ag-Cu solder alloys(Shnawah et al., 2012).

Fe is able to suppress formation of Kirkendall voids (Kim & Yu, 2013).The formation of Kirkendall voids at solder joints creates serious reliability issues for the microelectronics industry Yu et al. showed that residual S, coming from sodium

sulfopropyl-disulfide (SPS) as an additive in a Cu bath, was segregated at the Cu_3Sn/Cu interface and accelerated the nucleation of voids (Kim et al., 2008), and also demonstrated that those nucleated voids grew due to the tensile stress arising from the Kirkendall effect(Yu et al., 2008). Kim and Yu showed that Kirkendall voiding propensity decreased with an increase in the Fe content dissolved in the solder and in the Cu under bump metallization (UBM) because Fe is a sulfide-forming element (FeS) and scavenging of S originating from the additive as shown in Figure 2.31.

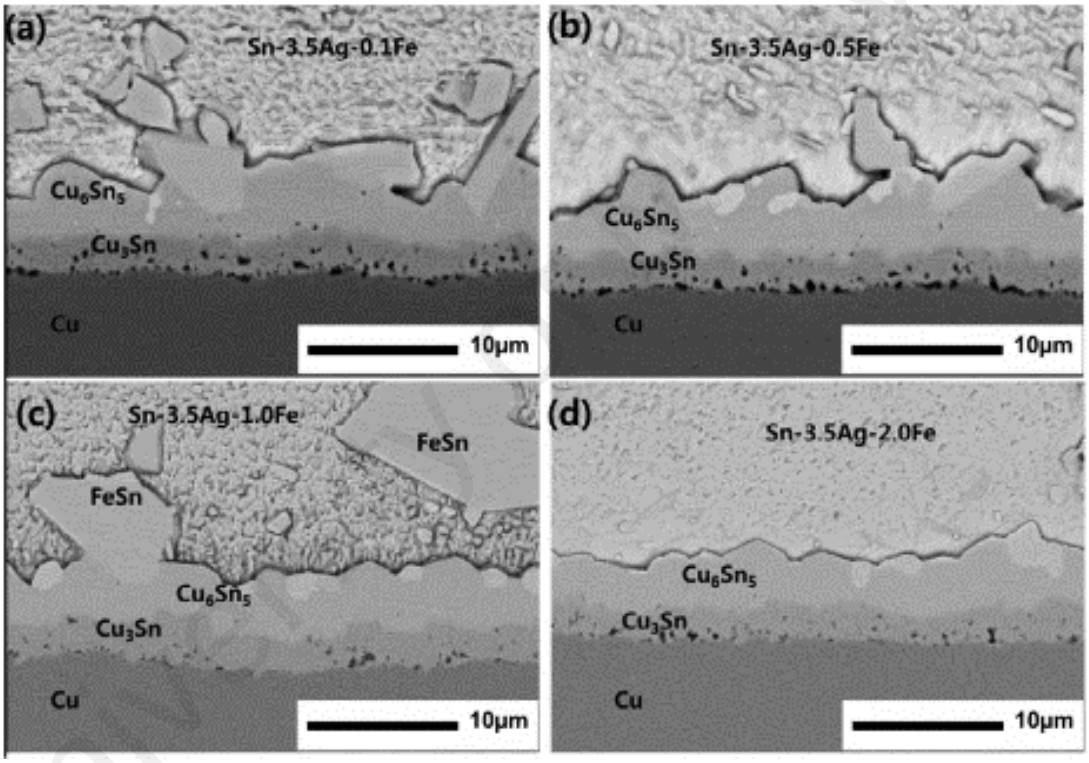

Figure 2.31: SEM micrographs of Sn–3.5Ag–xFe/Cu joints after aging at 150 °C for 240 h: (a) 0.1Fe, (b) 0.5Fe, (c) 1.0Fe and (d) 2.0Fe(Yu & Kim, 2008).

Anderson et al. reported for Fe-modified SAC solder alloys that all solder joints in the as-soldered and 100-h aged condition experienced shear failure in a ductile manner by either uniform shear of the solder matrix (in the highest strength solders) or by a more localized shear of the solder matrix adjacent to the Cu_6Sn_5 interfacial layer. After aging for 1000 h only ductile failure was observed in all solder joints made from the Fe-

modified SAC alloys. Initial analysis indicates that substitutional alloying of Fe into the intermetallic layers between the solder matrix and the Cu substrate appears to depress the diffusion rate of Sn and to minimize the formation and coalescence of voids at the Cu_3Sn/Cu interface, preventing interfacial weakening. Thus, the strategy of modifying a strong SAC solder alloy with a substitutional alloy addition for Cu seems to be effective for producing a solder joint with Cu that retains both strength and ductility for extremely long periods of isothermal aging (to at least 1000 h) at high temperatures (up to 150°C) (Anderson et al., 2004).

2.5.3 Effects of addition of Bi

Lead-free alloys with Bi are typically better in wetting than other lead-free alloys (Huang & Lee, 1999), presumably due to the low surface tension of Bi (0.376 N/m for Bi versus 0.537 N/m for Sn) (Lee, 2007). Addition of Bi to SAC0307 solder on an OSP surface finish has also been reported to improve the wetting properties due to the surface segregation of the added Bi (Figure 2.32 a and b) Segregation of Bi on the solder surface in the liquid state improves the solder spreading, possibly by decreasing the surface tension of the molten solder(Liu et al., 2008).

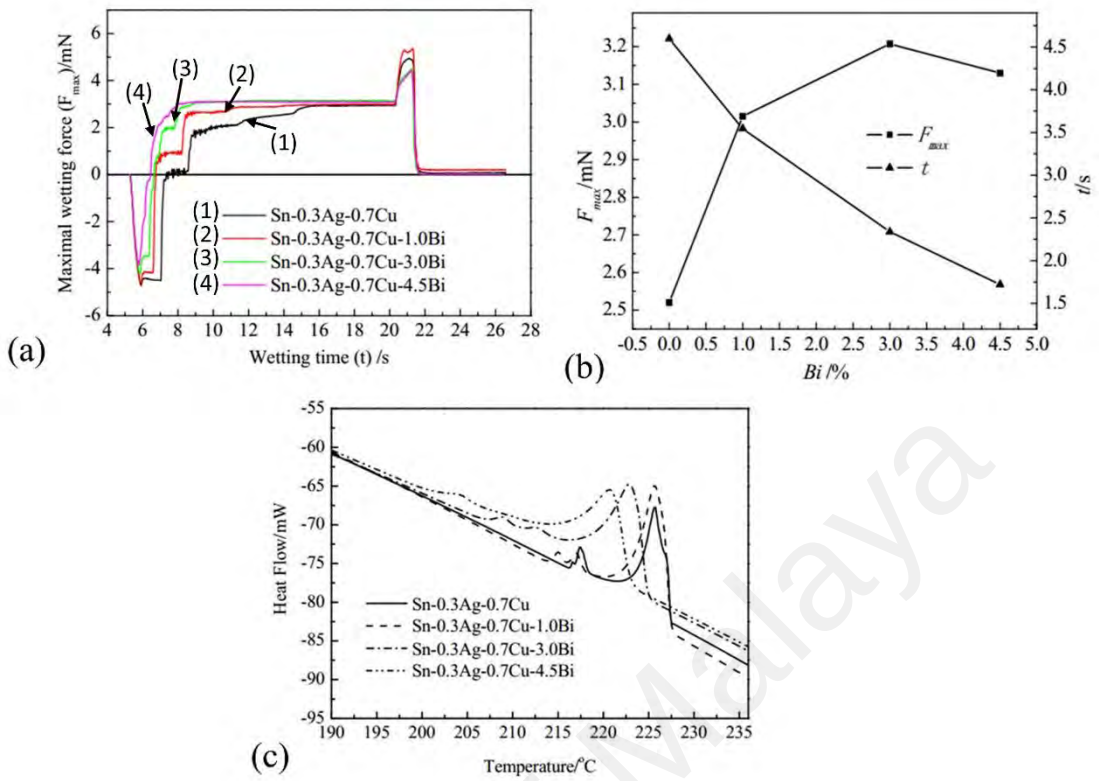

Figure 2.32: (a) Wetting Curves of Sn-0.3Ag-0.7Cu-xBi at 240°C (b) Wetting results of Sn-0.3Ag-0.7Cu-xBi at 240°C (c) Sn-0.3Ag-0.7Cu-xBi DSC melting profile (Liu et al., 2008).

Liu et.al showed that Bi addition has a positive effect on decreasing the melting point of Sn-0.3Ag-0.7Cu solder (222.6°C). The melting point of Sn-0.3Ag-0.7Cu-3.0Bi low-Ag solder has decreased to 217.3°C, which is almost equal to that of recommendatory lead free solders, Figure 2.32c. However, Bi addition also increased the melting range between liquidus and solidus, which may lead to the initiation of solidification crack of the solder joints.

Both tensile and shear strength of the solder interconnects increased with the adding amount of Bi element obviously, Figure 2.33. However, solder tensile elongation decreases with the adding of Bi elements significantly. That indicates the Bi addition will make the low-Ag solder get worse in ductility Bi addition can also restrain the intermetallic compound growth rate during thermal aging. The shear test results after

thermal aging also shows that Bi addition prevent the severe degradation of solder mechanical property.

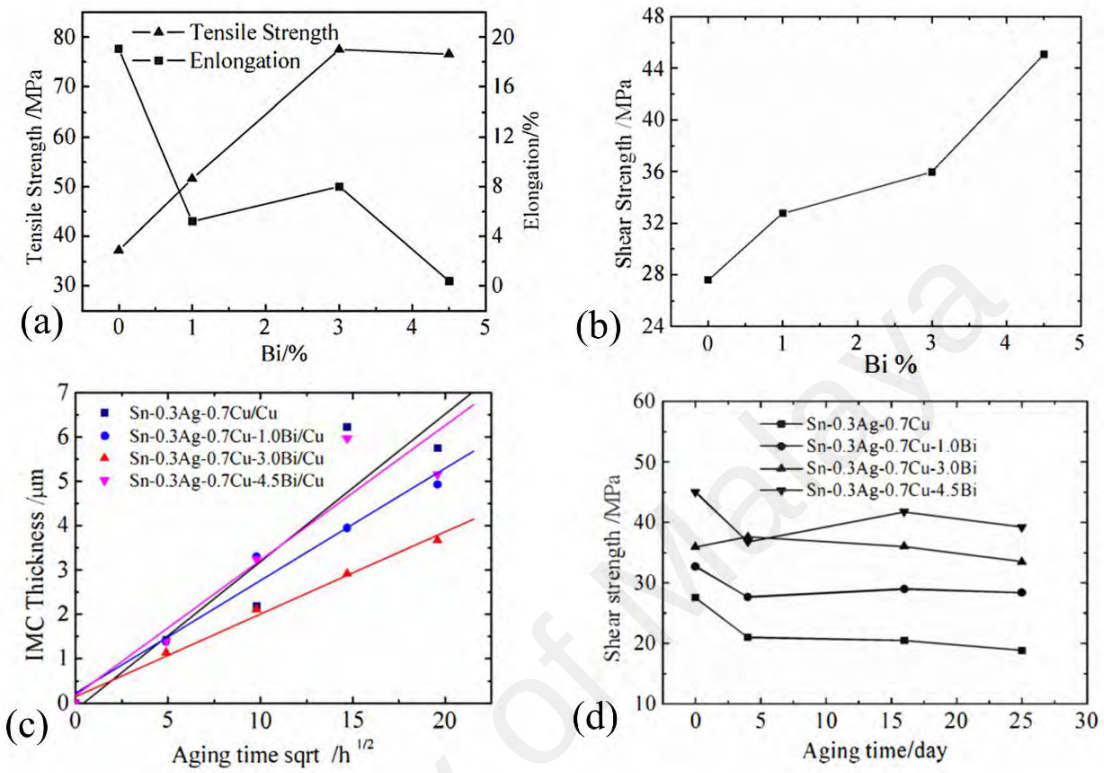

Figure 2.33: Sn-0.3Ag-0.7Cu-XBi solder alloy (a) Tensile strength (b) shear strength (c) IMC thicknesses change with aging time sqrt (d) Shear Strength after thermal (Liu et al., 2010).

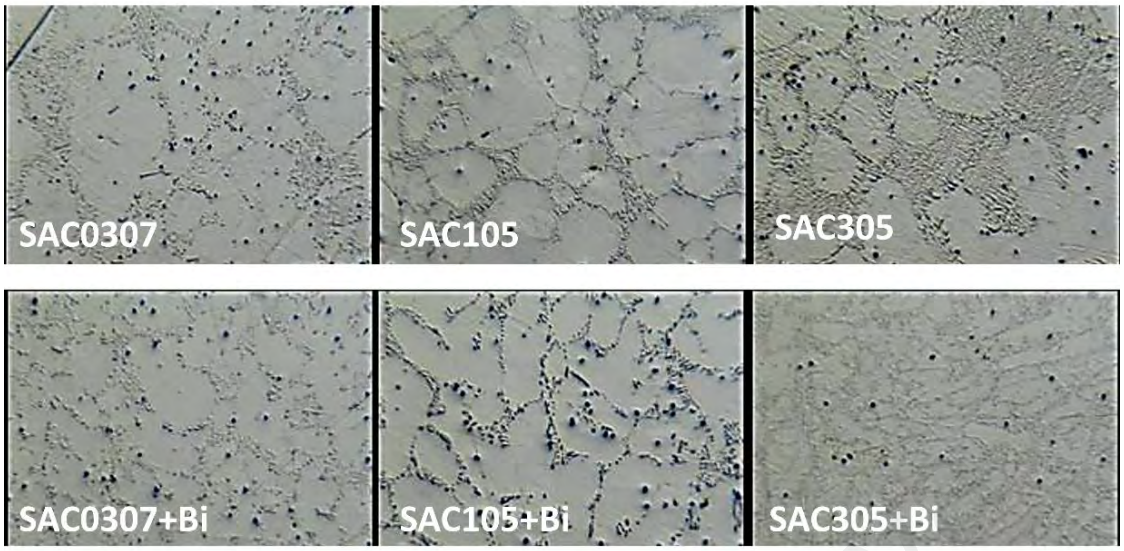

Figure 2.34: Effect of Bi addition on the microstructure of SAC alloys(Pandher & Healey, 2008).

Addition of Bi to Sn-Ag-Cu system also refines the intermetallic compound (IMC) grain size and retards the excessive growth of IMC (Li et al., 2006). Pandher & Healey (2008) showed that Bi addition has significant grain refining effect that improves the temperature cycling performance, Figure 2.34. Also, they showed Bi addition improve drop shock performance in low-Ag alloys because of its effect to control and hinder interfacial IMC(Cu_3Sn) in SAC0307, even though it acts to strengthen the solder matrix. Hodulova et al. (2011) studied the effect of addition of Bi to SAC during solid state aging. They observed Cu_3Sn growth rate was decreased by Bi addition in the lead-free solder, Figure 2.35. Because bismuth can substitute Sn in IMC and $Cu_3(Sn,Bi)$ compounds may form at Cu_3Sn grain boundaries where inhibit Sn diffusion (Hodúlová et al., 2011).

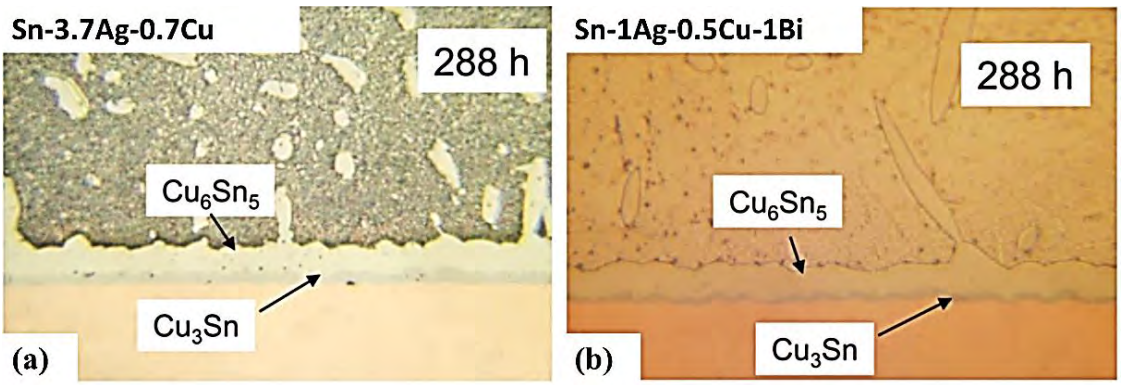

Figure 2.35 Microstructure interface after soldering and solid state ageing at 150 ◦C for 288 h, (a) Sn-3.7Ag-0.7Cu (b) Sn-1Ag-0.5Cu-1Bi at Cu substrate (Hodúlová et al., 2011).

The Bi addition resulted in a significant linear increase of the ultimate tensile strength (UTS) of solders, which is attributed to a solid-solution hardening mechanism. The Bi addition significantly, linearly increased the UTS of Bi-containing lead-free solders. Consequently, the solder would become "strong and brittle." The strong strengthening effect of Bi was attributed to a solid-solution hardening mechanism, referring to the microstructure analysis of Bi-containing lead-free solders (Huang et al., 2005).

Figure 2.36 shows that Bi addition to SAC307 improves drop shock performance in low-Ag alloys because of its effect to control interfacial IMC, even though it acts to strengthen the solder matrix(Pandher & Healey, 2008).

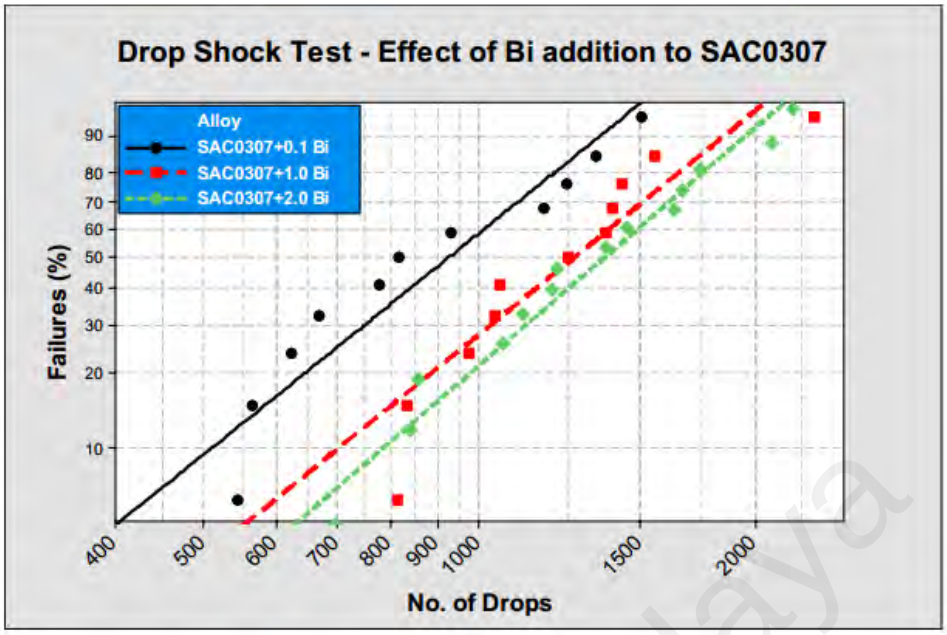

Figure 2.36: Effect of different levels of Bi addition to SAC0307 on drop shock performance (Pandher & Healey, 2008).

2.5.4 Effects of Alloying Elements on the Interfacial IMCs

Based on a summary of the previous research, the addition of alloying elements to the solder can affect the interfacial IMCs in the following three ways (Zeng et al., 2010):

1. Alloying elements can increase or decrease the thickness of interfacial IMCs.
2. The physical and chemical properties of the interfacial IMCs can be altered due to the addition of alloying elements.
3. Additional reaction layer can form at the interface between the solder and substrate.

Based on the solubility of the alloying elements in the IMC layers these elements can be divided into two categories: (i) alloying elements that do not dissolve in either Cu_6Sn_5 or Cu_3Sn, such as Al, Bi, P, Ti, S, rare earth elements, and (ii) elements that exhibit significant solubility in (usually) Cu_6Sn_5 and (possible) to Cu_3Sn, such as Ni, Co, Au, Sb, In, etc. It was shown that the latter group of elements have markedly stronger effect on the growth behavior of IMC's in the Sn–Cu system than those belonging to the first group,

because these (that do not dissolve in IMC's) can influence diffusion fluxes in the layers only indirectly through the activity of Sn. On the other hand, if the element dissolves in IMC layer it can alter its stability and probably also its microstructure, thus influencing the growth kinetics directly (Laurila et al., 2010).

Between alloying elements, Ni and Co has a prominent solubility on the interfacial IMCs. It is found that the addition of Ni and Co as an alloying element to the solder increases the total IMC thickness but the Cu_3Sn IMC thickness is decreased during reflow and aging compared to the pure solder (Wang et al., 2009). Also Nogita and Nishimura showed that nickel stabilizes the hexagonal close packed (hcp) form of the Cu_6Sn_5. In the absence of nickel, hcp Cu_6Sn_5 transformed to the monoclinic form upon cooling below about 190 ° C. This transformation was accompanied by a 26% volume change that could lead to cracking in the IMC. Small additions of nickel in the solder alloy concentrated in the IMC would stabilize the hcp form of Cu_6Sn_5, leading to an IMC without mechanical damage (Nogita & Nishimura, 2008).

It is observed that the addition of Au (less than 0.25 wt %) to the near eutectic SAC solder results scallop type $(Cu,Au)_6Sn_5$ IMC after reflow. However, if the Au content is more than 0.25 wt% the morphology of the interfacial IMC is changed with the formation of two phase layer [$((Cu,Au)_6Sn_5)$+Sn] (Park et al., 2003). The addition of Au reduces the Cu_3Sn IMC, but the effect of Au is weaker compared Ni and Co because of having lower solubility in Cu_3Sn IMC (Zakel et al., 1991). On the contrary, though Sb has a strong effect on solid solution strengthening of Sn, it has virtually no effect on the interfacial IMC (Laurila et al., 2010).

Addition of elements that do not show marked solubility on the interfacial Cu-Sn IMC like Al is found to increase the mechanical properties such as microhardness, strength etc. to the SAC solder (Liu et al., 2008).

Hu et al. found that addition of Bi into the Sn-0.7Cu eutectic solder caused the excessive formations of IMCs during the soldering reaction and thereafter in aging condition. The interfacial IMC layer was composed of Cu_6Sn_5 and Cu_3Sn layers after liquid soldering for Sn-0.7Cu/Cu, Sn-0.7Cu-0.7Bi/Cu and Sn-0.7Cu-1.3Bi/Cu joints, Figure 2.37. With the increasing soldering temperature, the thickness of IMC layers (including Cu_6Sn_5 and Cu_3Sn IMCs) increased linearly. After various days of aging, a comparatively planar IMC layer at the solder/Cu interface was observed than that of the as-soldered joints. The growth of IMC layer during aging for Sn-0.7Cu, Sn-0.7Cu-0.7Bi and Sn-0.7Cu-1.3Bi solders followed the diffusion control mechanism. And the interfacial IMC layers were thicker with higher Bi content in solder alloy since the Bi could result in more chemical bonds between Cu atoms or between Cu and Sn atoms to be broken, which made more Cu and Sn atoms activated (Hu et al., 2014).

Anderson et al. showed that Fe or Co addition to SAC solder alloys decrease Cu_3Sn IMC thickness, however increase Cu_6Sn_5 thickness, and these trends continue by increasing aging time, Figure 2.38.

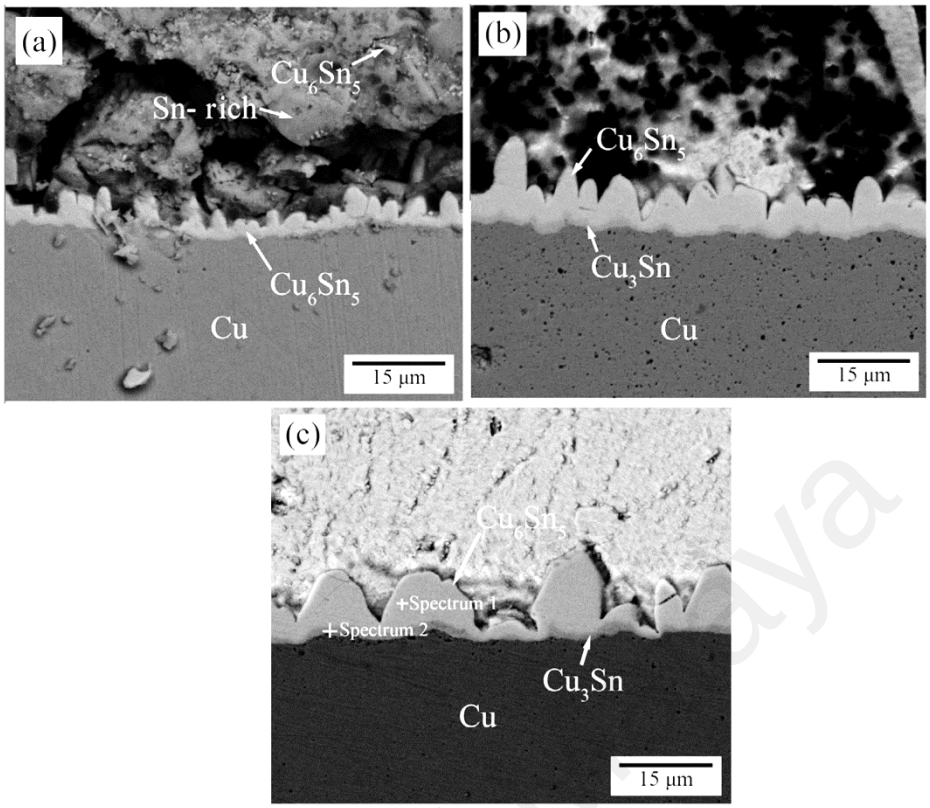

Figure 2.37: BSE SEM micrograph of the (a) Sn0.7Cu/Cu, (b) Sn0.7Cu0.7Bi/Cu and (c) Sn0.7Cu1.3Bi/Cu reaction couples reacted at 240°C for 30 min (Hu et al., 2014).

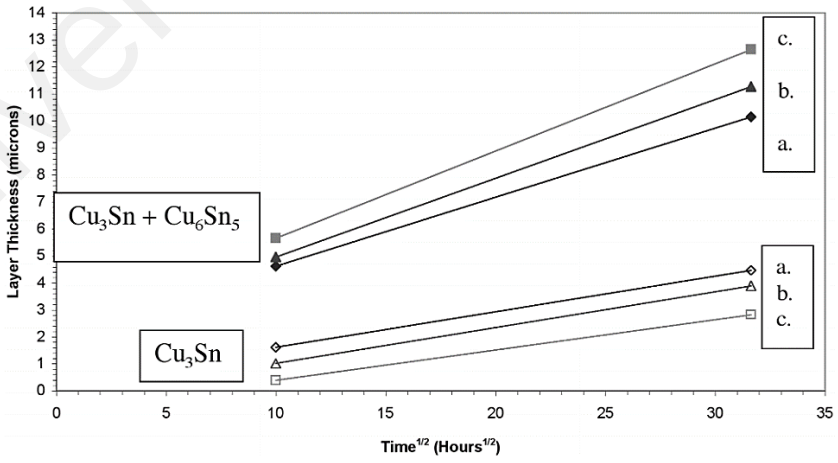

Figure 2.38: Comparison of the Cu_3Sn and (Cu_3Sn+Cu_6Sn_5) intermetallic-interface thickness measurements as a function of isothermal aging time at 150°C for solder joints made from (a) Sn-3.7Ag-0.9Cu, (b) Sn-3.7Ag-0.7Cu-0.2Fe, and (c) Sn-3.7Ag-0.6Cu-0.3Co (Anderson & Harringa, 2004).

2.5.5 Effect of Fe and Bi alloying on electrical resistivity of solder alloys

In microelectronics devices, solder acts as an electrical interconnect whereby electrical currents flowing into and out of the device need to pass through the solder connection. In order to ensure proper functioning of the interconnect, the electrical resistivity of the solder materials has to be low so as to allow current flow.

There are a number of complex factors that determine the net resistivity of solder joints. In alloys containing a fourth-element addition, an additional lattice-scattering term is expected; however, in most of the compositions of interest, the amount of the fourth element added to the alloy is on the order of 0.5 at. % or less. The degree to which lattice-strain scattering becomes a contribution to resistivity depends on whether the addition is dissolved in the solvent or forms secondary phases. The Darken–Gurry criteria is commonly used to estimate solid solubility in alloys; in the case of Bi, for example, the atomic size difference with Sn is less than 7%, and the electronegativity difference is 0.06 (on the Pauling scale). The maximum solubility of Bi in Sn is reported as 13at.%, in accordance with the Darken–Gurry prediction. The increase in resistivity caused by lattice strain scattering (if the solute is assumed to form a substitutional solid solution with β-Sn) is proportional to the square of the valence difference between solute and solvent, $(DV)^2$, according to the Linde-Norbury rule. In the case of fourth-element additions to Sn-Ag-Cu solder alloys, the magnitude of $(DV)^2$ is 1 for Bi, 4 for Fe and Co, and 9 for Cu and Ag. Thus, to a first approximation, a significant amount of Bi substitution in a β-Sn solvent (valence =4) would be required to cause the resistivity to increase significantly, while only a minor amount of Cu or Ag would have the same effect. Indeed, microstructural results indicate that a significant fraction of the Ag and Cu solute forms secondary intermetallic phases, consistent with the limited solid solubility of both, and presumably for Fe and Co as well, in β-Sn (Cook et al., 2002)

Cook et al. observed that the addition of 1 wt.% Bi to Sn–3.7Ag–0.9Cu increased the bulk resistivity by approximately 8% (Cook et al., 2002). This increase was attributed to the solubility effect of Bi in the β-Sn matrix according to the Linde–Norbury rule (Rossiter, 1991).

Table 2.4: Electrical resistivity of specified elements and compounds at 300 K.

Phase or composition	Electrical resistivity (300 K) (μΩ cm)
Sn	12
Ag	1.59
Cu	1.66
Fe	10
Cu_6Sn_5	17.5
Ag_3Sn	6.08
$FeSn_2$	100
63Sn–37Pb	14.5
96.5Sn–3.5Ag	12.5
96.5Sn–3Ag–0.5Cu	12.34

Amin et.al showed that the electrical resistivity decreases with increasing the Ag content from 1.0 wt.% to 3.0 wt.%. This is because the number of low resistivity Ag_3Sn IMCs increases with an increase in the content of Ag. Electrical resistivity of specified elements and compounds at 300 K are shown in Table 2.4 (Amin et al., 2014).

As shown in Figure 2.39, the electrical resistivity of Fe-modified Sn–1Ag–0.5Cu solder alloys decrease initially with the addition of 0.1 wt.% Fe, and then gradually increase with increasing the amount of Fe addition. The initial decrease in electrical resistivity was attributed to the low resistivity of Fe compared to Sn. The gradual increase in electrical resistivity was attributed to the presence of a large number of high resistivity $FeSn_2$ IMCs. The electrical resistivity of the Fe-bearing Sn–1Ag–0.5Cu solder alloys is comparable with the resistivity of the Sn–1Ag–0.5Cu solder alloy, and is sufficient for a normal operation of the electrical circuit. In other words, the differences are neither too

high nor too low to significantly affect the overall functionality of any electronic circuit in current use within the context of electrical performance.

Sabri et.al showed that the electrical resistivity for 0.1 wt.%, 0.3 wt.%, and 0.5 wt.% Fe-bearing SAC105 solder alloys decreased by 25%, 11%, and 17% respectively, showing a rather stable reduction in resistivity. This can be correlated to the stabilisation of the microstructure of the Fe-added SAC 105 after thermal aging. Thus, the stability of Fe-added SAC formulation under thermal aging, demonstrates its reliability in applications which undergo thermal stress (Sabri et al., 2015).

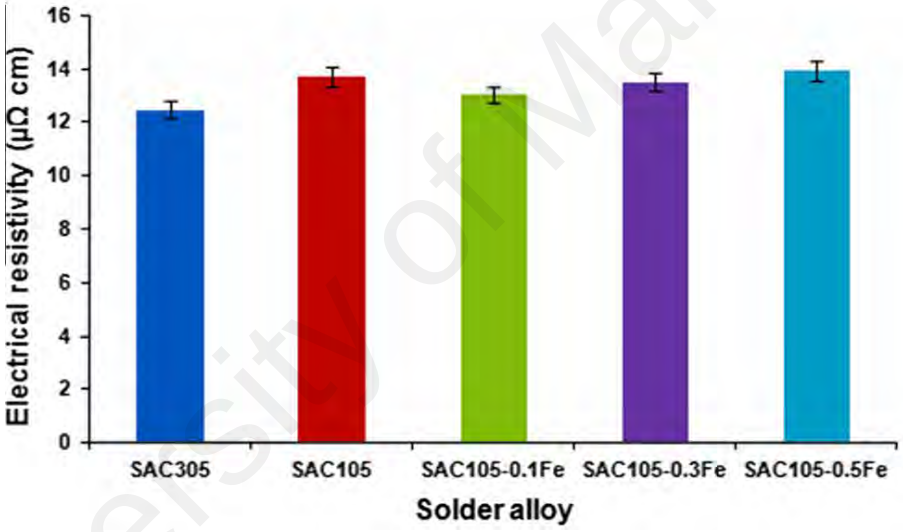

Figure 2.39: Electrical resistivity of the SAC305, SAC105, SAC105–0.1Fe, SAC105–0.3Fe, and SAC105–0.5Fe solder alloys(Amin et al., 2014).

2.6 Summary

The importance of microelectronic packaging and soldering technology elaborated in detail in this chapter. Pb-Free solder alloys as a replacement of Sn-Pb soldering was introduced by standards due to the toxicity of Pb(lead). The Sn-0.7Cu solder and low-Ag SAC solder alloy are the most reliable and affordable solder alloys. Properties of lead-free solder alloy which play an important role include mechanical, microstructure, thermal, isothermal aging, wetting and interfacial reaction elaborated in details in this

chapter. The addition of alloying elements as one of the methods to improve solder alloy reliability is discussed in this chapter. In details, the role of Fe and Bi addition on the properties of solder alloy illustrated.

CHAPTER 3: METHODOLOGY

3.1 Bulk solder specimen preparation

Details of samples composition are shown in table 3.1.

Table 3.1: Samples composition.

Sn-Cu based	Sn-Ag-Cu based
Sn-0.7 Cu (SC07)	Sn-1Ag-0.5 Cu (SAC105)
Sn-0.7 Cu-0.05Fe (SC07-Fe)	Sn-1Ag-0.5 Cu-0.05 Fe-1 Bi (SAC105-Fe-1Bi)
Sn-0.7 Cu-0.05 Fe-1 Bi (SC07-Fe-1Bi)	Sn-1Ag-0.5 Cu-0.05 Fe-2 Bi (SAC105-Fe-2Bi)
Sn-0.7 Cu-0.05 Fe-2 Bi (SC07-Fe-2Bi)	

Solder bar production process are shown in Figure 3.1. The alloys were prepared by melting pure ingots of Sn, Ag, Cu, Fe and Bi in an induction furnace at more than 1000ºC for 40 min. The molten alloys were cast to disk shaped ingots and sent to a third-party lab (SGS Taiwan) to analyze element concentration by spark Atomic emission spectroscopy (AES) to ensure that all elements of the alloy composition met the specifications (per JIS-Z-3282:1999, Table 3.2 and Table 3.3). Next, the solder bar remelted into the molten solder and keep the temperature at 285±5°C. Then, the molten solder alloys were poured into stainless steel molds that were pre-heated at 130±10°C, and the molds were air cooled naturally to room temperature (25°C). The molds were disassembled, and the dog bone samples were removed and visually inspected to ensure that the surface of the parallel area was without damage or voids.

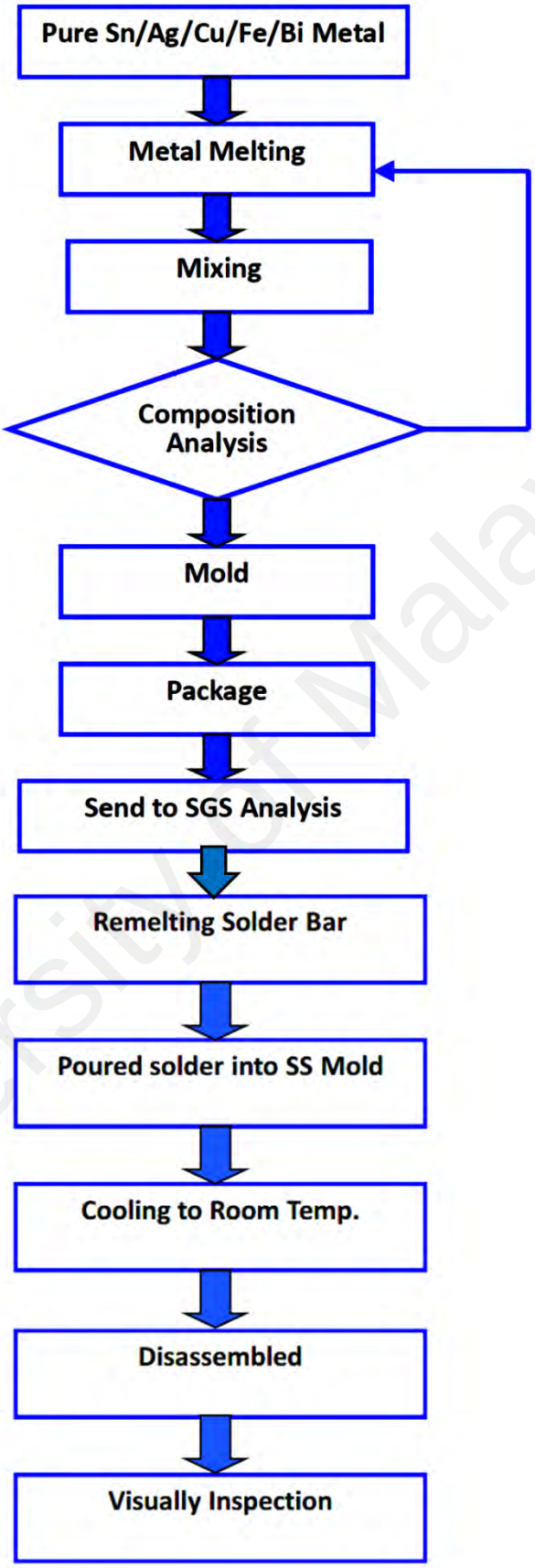

Figure 3.1: Solder bar production process.

Table 3.2: Chemical composition of SC07 and (Fe and Bi)-bearing SC07 solder alloys.

Quality	SC07	SC07-Fe	SC07-Fe-1Bi	SC07-Fe-2Bi
Ag	0.0002	0.0018	0.0001	0.0001
Al	0.0005	0.0005	0.0005	0.0005
As	0.0008	0.0008	0.0008	0.0008
Bi	0.0016	0.0021	1.0763	1.9354
Cd	0.0001	0.0000	0.0001	0.0002
Co	0.0004	0.0006	0.0006	0.0006
Cu	0.7141	0.7335	0.7283	0.7252
Fe	0.0007	0.0507	0.0535	0.0520
In	0.0014	0.0013	0.0013	0.0014
Ni	0.0000	0.0000	0.0004	0.0003
Pb	0.0032	0.0040	0.0050	0.0060
Sb	0.0036	0.0036	0.0038	0.0039
Zn	0.0001	0.0001	0.0001	0.0001
Sn	99.2733	99.201	98.1292	97.2735

Table 3.3: Chemical composition of SAC105 and (Fe and Bi)-bearing SAC105 solder alloys.

Quality	SAC105	SAC105-Fe-1Bi	SAC105-Fe-2Bi
Ag	0.9401	1.0105	0.9159
Al	0.0005	0.0005	0.0005
As	0.0008	0.0008	0.0008
Bi	0.0016	1.0124	1.9510
Cd	0.0001	0.0001	0.0002
Co	0.0004	0.0006	0.0006
Cu	0.4947	0.4960	0.4747
Fe	0.0005	0.0460	0.0503
In	0.0013	0.0013	0.0013
Ni	0.0002	0.0000	0.0000
Pb	0.0039	0.0047	0.0045
Sb	0.0034	0.0038	0.0039
Zn	0.0001	0.0001	0.0001
Sn	98.5524	97.4232	96.5962

All samples prepared in dog bone shape as shown in Figure 3.2.

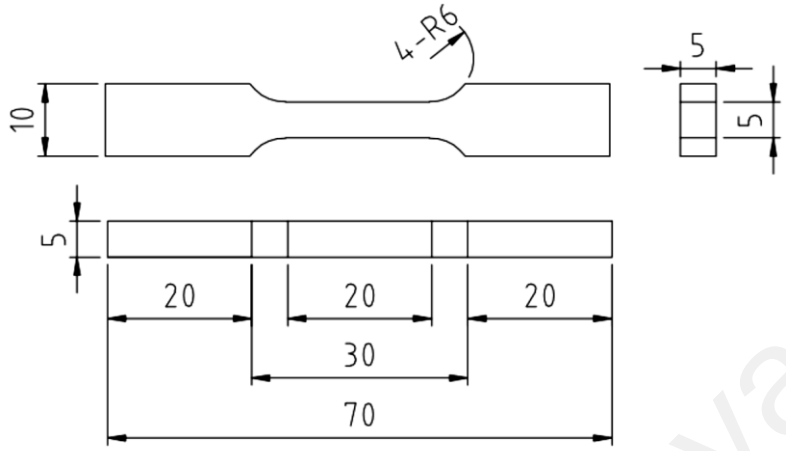

Figure 3.2: Dog bone sample(mm).

3.2 Characterization of Solder

3.2.1 Microstructure analysis

Dog bone samples diced with dicing machine and cold mounted for embedding and impregnation of metallographic specimens. For cold mounting, 15 parts of resin and 2 parts of hardener by volume mixed and stirred for approximately 2 minutes without introducing too many air bubble. Next, rest epoxy for 2 minutes and then pour it carefully over the specimens. Finally, leave it at room temperature for 12 to 24 hours to be harden.

Specimens grinded and polished with Struers TegraPol-21(Figure 3.3) to be prepared for metallographic purpose. As it is shown in Table 3.4, grinding start with 800 grit (the number of grains of silicon carbide per square inch of abrasive paper) silicon carbide (SiC) paper and then #1200, #2400 and #4000 SiC papers. Duration time for each step is 5±1min. The rotation direction of the specimen holder should be same as the direction of the grinding disc for soft nonferrous materials (complementary). Disk and head speed selected 100/100 rpm, to prevent smearing effect on soft materials.

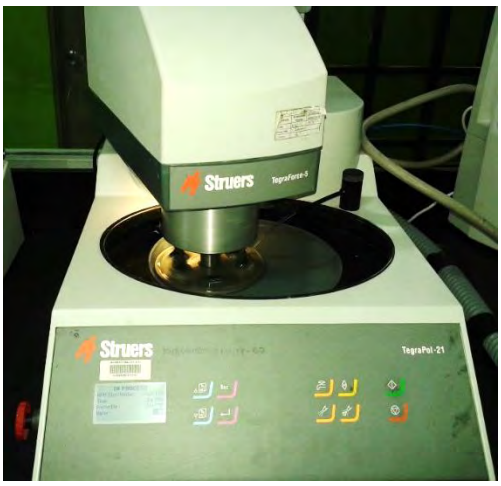

Figure 3.3: Struers TegraPol-21.

Table 3.4: Grinding and polishing process.

Grit	Paper type	Duration, min	Force, N	Disk and Head speed, rpm	Lubricant
800	SiC	5±1	10	100/100	Water
1200	SiC	5±1	10	100/100	Water
2400	SiC	5±1	10	100/100	Water
4000	SiC	5±1	10	100/100	Water
MD-MOL polishing cloth	woven wool	5±1	10	100/100	3.0 μm diamond suspension
MD-CHEM polishing cloth	Porous neoprene	5±1	10	100/100	0.04 μm colloidal silica suspension

After grinding with #4000, the polishing process began with water based diamond suspension containing a high performance diamonds (3.0 μm) and cooling lubricant on MD-MOL polishing cloth. Then, for final polishing a colloidal silica suspension (0.04 μm) used on MD-CHEM polishing cloth.

After polishing, distilled water and ethanol was applied on sample surface for cleaning and then surface dried with air blower. Due to aging effect and oxidation, samples should not keep for long time after preparation. So, samples microstructure evaluated shortly after preparation.

A field-emission scanning electron microscope (FESEM; FEI Helios NanoLab 650, Figure 3.4) with a concentric backscatter detector (CBS) was used to take backscatter electron imaging and examine the microstructures. Additionally, energy dispersive X-ray spectroscopy (EDX or EDS) on an Oxford Instruments X-Max 80 mm^2 SDD-EDS detector were adopted to determine the phase compositions.

Figure 3.4: FEI Helios NanoLab 650 dual beam.

After tapping samples to decrease electron discharge, sample put in dual beam chamber. Generally, the setting for Dual Beam was: HV=20KV; Det=CBS

(All=A+B+C+D); WD=5m; beam current=1.6nA after chamber vacuumed. Basically CBS imaging took at 3 proper area on each sample and 5 magnifications (100X, 500X, 1000X, 2000X, and 5000X) at each area. Elemental mapping at 2 area at 2000X or 1000X magnification and 2 times point EDX and/or area EDX at each composition or element were applied (setting: HV= 15KV or 20KV, beam current=0.4 nA or 0.8nA).

3.2.2 X-ray Diffraction (XRD)

XRD samples cut from middle of dog bone sample with size of 10mm to 5mm , then goes through cleaning procedure, 5 min in acetone, 1 min in distilled water, 1 min in HCL and finally 5min in ethyl alcohol. Next, samples etch with natal 2% (HNO_3 in ethanol) for 30s.

Bruker-AXS D8 Advance X-ray Diffractometer (XRD) (Figure 3.5) was used to identify the presented phase in structure. XRD testing condition was 2 theta scale, scanning type: start 20°- End 80°, scanning speed: step 0.02° deg/sec, and step time 1 sec.

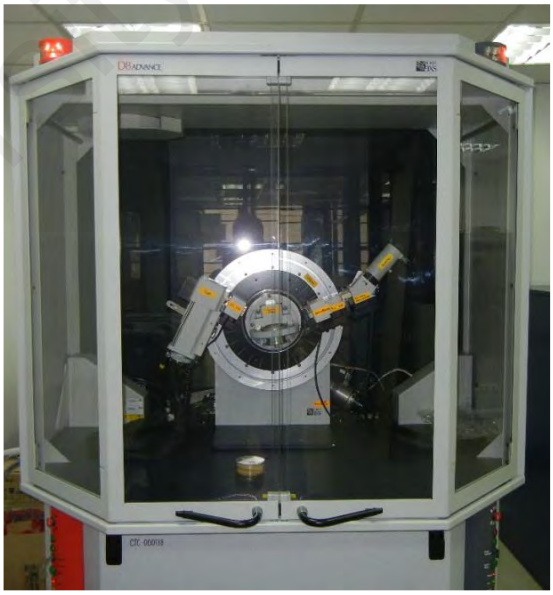

Figure 3.5: Bruker-AXS D8 Advance XRD.

3.2.3 Transmission electron microscopy(TEM)

The Transmission Electron Microscope (TEM) characterization was performed using FEI Tecnai G2 F20 High Resolution Transmission Electron Microscope (Figure 3.6) system for an elemental identification. The TEM lamella was prepared by using FEI Helios NanoLab 650 Dual Beam system (Figure 3.4). It has both High Resolution Electron Beam and Finely Focused Ion Beam incorporated into the system. The TEM lamella was lifted out from the bulk sample and attached onto the Molybdenum grid finger using an in-situ lift out technique by means of Omniprobe needle. The TEM lamella was then thinned down to the electron transparency with the thickness of less than 100nm.

Figure 3.6: FEI Tecnai G2 F20 High Resolution Transmission Electron Microscope.

3.2.4 Fracture Analysis

The fracture surfaces of the tensile test samples were cleaned with acetone and ethanol and then checked with HITACHI SU8030 FESEM (Figure 3.7).

Figure 3.7: HITACHI SU8030 FESEM.

3.2.5 Differential Scanning Calorimetry (DSC)

Differential scanning calorimetry (DSC), Perkin Elmer (DSC-8000) in Figure 3.8, utilized to investigate the melting behavior of solder alloys. DSC applied with the scanning rate 5˚C/min from 30˚C up to 300˚C on 10mg samples. The test was repeated 5 times for each solder alloy.

Figure 3.8: Differential Scanning Calorimetry, Perkin Elmer (DSC-8000).

3.2.6 Isothermal aging treatment

The specimens were aged in universal oven memmert (Model 100-800) at 125°C for 30days and 180°C for 1 day to evaluate the effect of aging on microstructural and mechanical properties of solder alloys.

3.2.7 Tensile testing of specimens

Dog bone sample was set onto a testing grip at two ends of the specimen using an Instron 5569A universal testing machine, Figure 3.9. An extensometer was secured onto the specimen surface to measure the strain of the solder. In this study, a length of 10 mm was used as a gauge length. The tensile force applied to the specimen was measured by a load cell for stress calculation. Five samples were tested under the same testing conditions for each solder specimen and the tensile properties were obtained by averaging the test data. The tensile tests were conducted at room temperature (25 °C) for all solders composition under a strain rate of 10^{-3} s^{-1} to investigate the effects of the addition of Fe and Bi to SAC105 and SC07 on the mechanical properties of the solder, yield stress, ultimate tensile strength (UTS), and elongation. Typical stress-strain behavior diagram shown in Figure 3.10. The UTS is indicated at point M. The proportional limit P, and the yield strength as determined using the 0.002 strain.

Figure 3.9: Instron 5569A universal testing machine with 10mm extensometer.

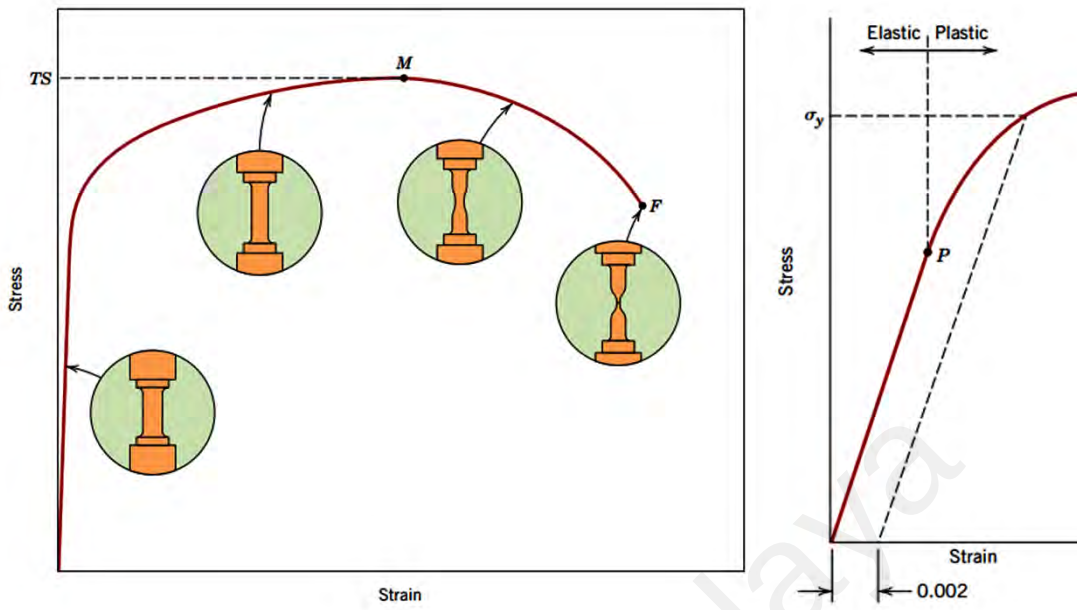

Figure 3.10: Typical engineering stress– strain behavior to fracture, point F. The UTS is indicated at point M. The proportional limit P, and the yield strength as determined using the 0.002 strain (Callister et al., 2007).

In this work, the yield stress of the solder was considered to be the stress value at which 0.2% plastic strain occurred. The UTS of the solder was considered to be the maximum stress in the stress–strain curve. Universal testing machine setting was: Cross head speed= gauge length× strain rate=$10mm\times10^{-3}\times60sec = 0.6\ \frac{mm}{min}$, Cross section area=25 mm^2.

3.2.8 Nanoindentation

Measurements of hardness and young's modulus were made by nanomechanical test instrument, Hysitron Ubi TI 750 (Figure 3.11), using a Berkovich indenting tip. The integrated in-situ Scanning Probe Microscopy (SPM) used to locate and record testing result. Prior to each experiment the indenter head was calibrated to ensure stage movement accuracy and the precise placement of the indenter tip. Indentations were performed at load controlled under loading rate 200μN/s, holding time 2s and maximum

load 1mN-7mN. Five times of indentation have done on each sample and by averaging the result hardness and young's modulus were obtained.

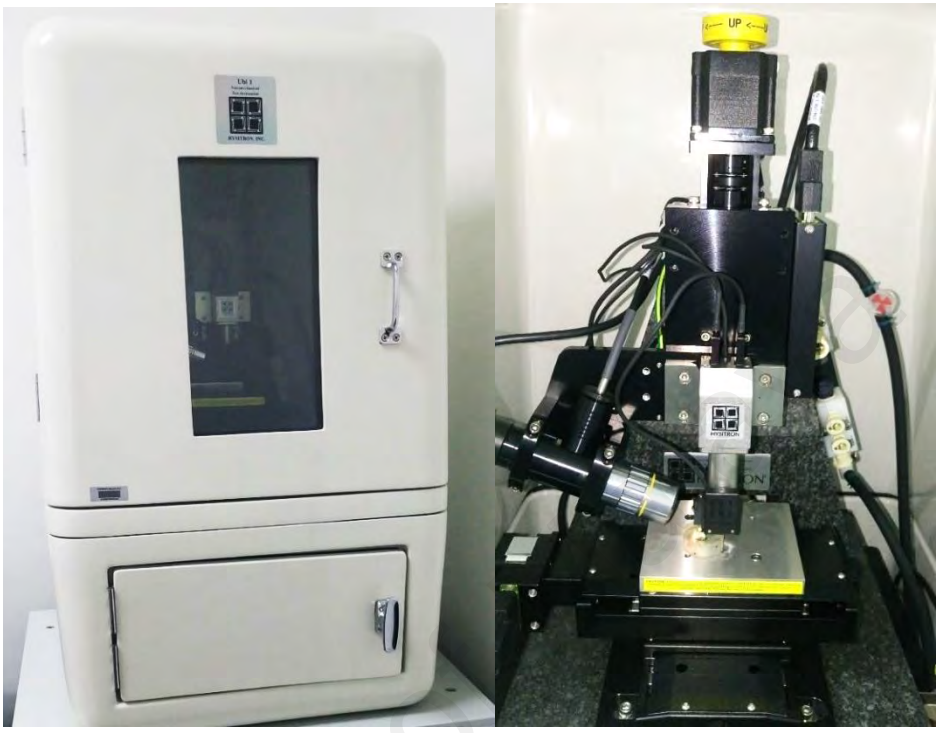

Figure 3.11: Hysitron Ubi TI 750 nanoindentor.

3.2.9 Wetting test (Spreading Rate and Wetting Angle)

The Cu substrates (30mm × 30mm × 0.3mm) cleaned by acetone followed by 10 s pickled in distilled water and 10s in HCl solution (5 vol.%), and then 5 min left in ethanol, and finally dried.

Dog bone samples were remelted and casted to make a 5mm diameter rod. Then rod sliced to get disc with weight 0.3 g and thickness 2mm. Next, disc was soaked with RMA (rosin mildly activated) flux and placed on the Cu substrate on a hot plate maintained at 250°C for 50 s and allowed to cooling in room temperature. The spreading rate (SR) of the solder was calculated according to the Japanese Industrial Standard (JIS Z3198-3, 2003), using the equation, SR=((D-H)/D)100. Here is the spreading rate (%), $D=1.24\ V^{1/3}$, D is the diameter when solder used for a test, V is mass/density of the solder sample used

for the test and H is the height of spread solder. Ten samples were tested for each of the compositions and the average value was calculated. After the spreading rate measurement, the specimens were sectioned with electrical discharge wire cutter and polished for metallographic examination. The wetting angle was measured under an optical microscope with the aid of Video Tool Box Pro software (Zarbeco, USA).

3.2.10 Microhardness

The Shimadzu hardness tester HMV-G21 used to measure Vickers hardness, Figure 3.12. The indentation picture of test surface taken by CCD camera, system perform automatic measurement of the diagonal length of indentation, and calculate Vickers hardness. Machine setting was 245.2mN force and 10s holding time. Calculation is based on the following formula:

$$HV = 0.1891\frac{F}{d^2} \qquad \textbf{3-1}$$

HV: Vickers hardness, F: Test force(N), d: Average length of diagonal lines of indentation (mm).

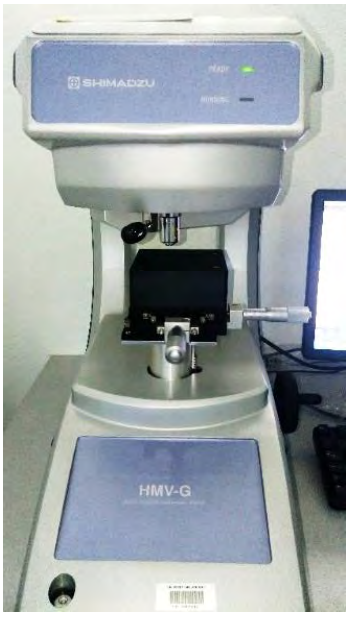

Figure 3.12: Shimadzu hardness tester HMV-G21.

3.2.11 Density

Electronic Densimeter MDS-300 Alfamirage was utilized to measure density of solder composition, Figure 3.13. The resolution of this device is a 0.001 g/Cm^3. First put sample gently on sensor by tweezers, then weight of sample memorized by device. Next sample should put on the center of tray in water, which measure weight of sample in water. Finally, device calculate density of sample.

Figure 3.13: Electronic densimeter MDS-300.

3.3 Summary

In this chapter, the dog bone sample preparation procedure is explained. Then all characterization technique which used during the experiment is elaborated. Microstructure analysis, x-ray diffraction (XRD), transmission electron microscopy (TEM), fracture analysis, differential scanning calorimetry (DSC), isothermal aging treatment, tensile testing of specimens, nanoindentation, wetting test, microhardness, and density tests utilized to characterize solder alloys.

CHAPTER 4: RESULTS AND DISSCUSION

4.1 Sn-1Ag-0.5Cu solder alloy bearing Fe and Bi

4.1.1 Mechanical properties

The stress–strain curves of the as-cast SAC105, SAC105-Fe-1Bi and SAC105-Fe-2Bi solder alloys under a strain rate of 10^{-3} s^{-1} are shown in Figure 4.1. The mechanical properties of solder alloys yield stress, ultimate tensile strength (UTS), and total elongation are shown in Figure 4.2. The result showed 21.1 MPa Yield strength, 27.5MPa UTS and 60% total elongation for SAC105, which is in agreement with previous work by Che et al. (Che et al., 2007).

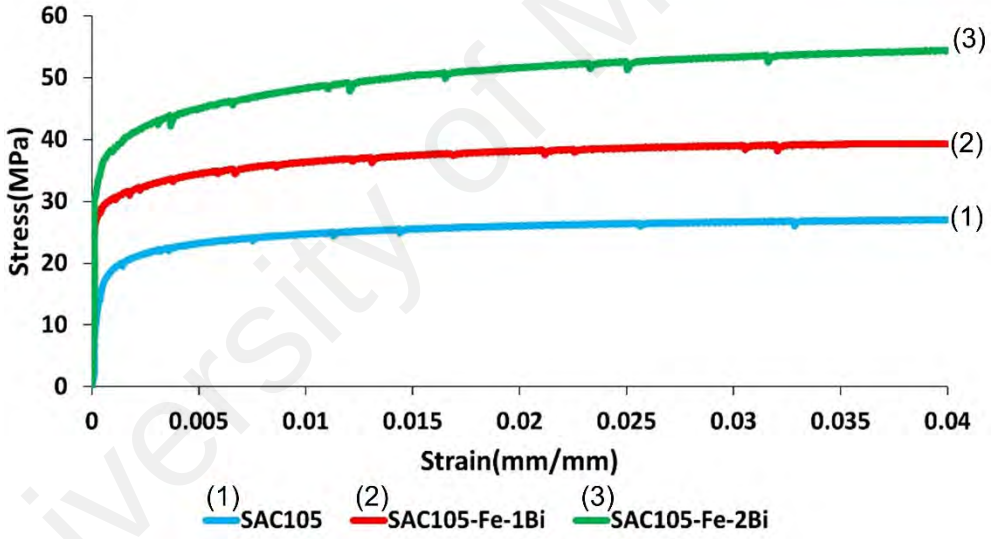

Figure 4.1: Stress- strain curves of SAC105, SAC105-Fe-1Bi and SAC105-Fe-2Bi solders.

As illustrated, doping 0.05 wt.% Fe and 1 wt.% Bi to SAC105 solder increased the yield strength to 31.7MPa and increased UTS to 40.5 MPa, whilst the total elongation was slightly decreased to 43%. By increasing Bi to 2wt% the same trends continue, increase yield strength to 41.8 MPa and UTS to 56 MPa, and also total elongation decrease to 33.8%. Jie Zhao, et al. (Zhao et al., 2004) and also Xiaowu Hua et al. (Hu et

al., 2015) showed the similar effect in mechanical properties by adding Bi to Sn-Ag-Cu and Sn-0.7Cu respectively. Also previous works showed that just by adding 0.1wt%Fe to SAC yield stress and UTS decreased, while total elongation maintained at the SAC105 level (Laurila et al., 2009).

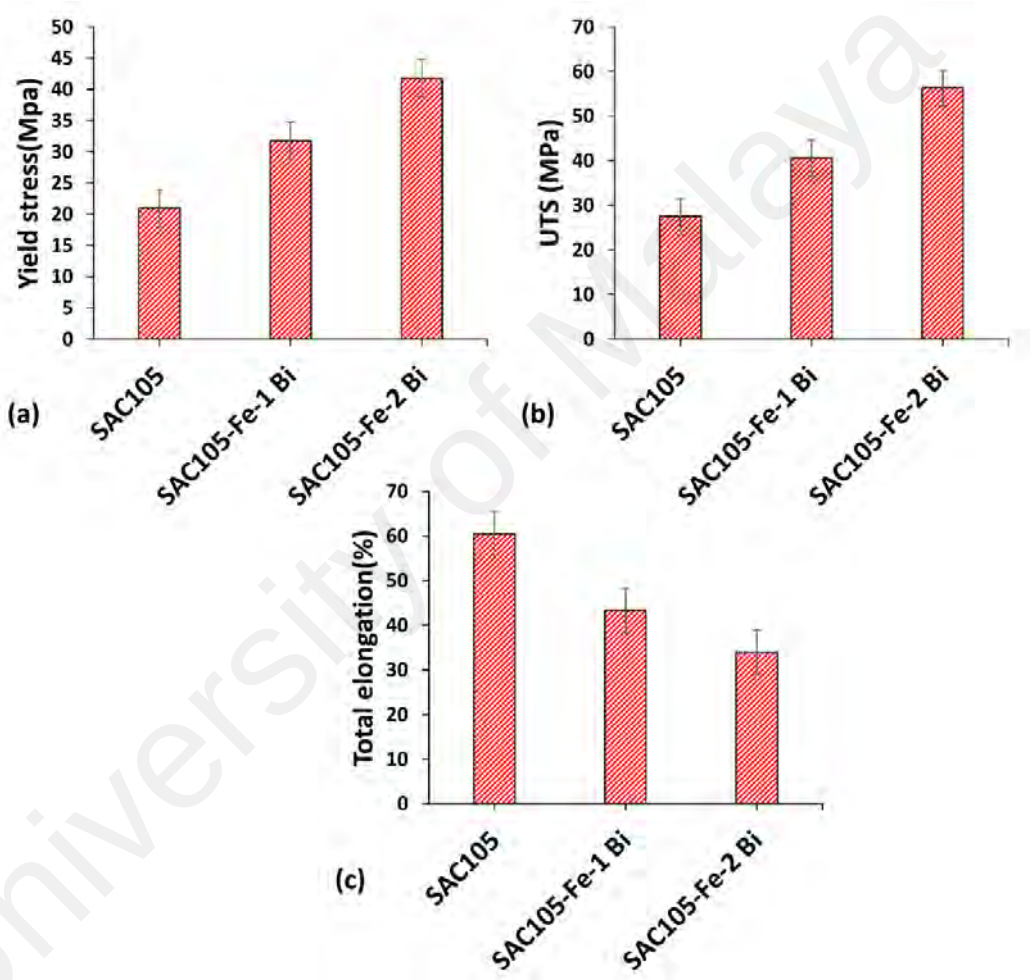

Figure 4.2: Tensile properties of SAC105, SAC105-Fe-1Bi and SAC105-Fe-2Bi solders: (a) yield stress, (b) UTS, and (c) total elongation.

4.1.2 Microstructure properties

The as-cast microstructures of the standard SAC105, SAC105-Fe-1Bi, and SAC105-Fe-2Bi alloys are shown in Figure 4.3 (a), (b), and (c). The microstructures of SAC105 in Figure 4.3 (a) include β-Sn dendrites and interdendritic regions consisting of Cu_6Sn_5 and Ag_3Sn intermetallic compounds (IMCs) particle dispersed within a Sn-rich matrix. Also, Figure 4.4 shows X-ray Diffraction (XRD) result of composition in the solder alloys. Figure 4.3 (b) shows SAC105-Fe-1Bi which contain β-Sn, Cu_6Sn_5 and Ag_3Sn. Moreover, addition of 0.05wt%Fe and 1 wt% Bi to SAC105 makes $FeSn_2$ in bulk of solder and 1 wt% Bi scatter on whole bulk of solder. On the basis of the phase diagrams of Bi-Ag, Bi-Sn, Bi-Cu and Bi-Fe, Bi cannot make any intermetallic compound with other element, so there is not any Bi compound in solder. Also, by adding 2wt% Bi to SAC105-Fe $FeSn_2$, Ag_3Sn, and Cu_6Sn_5 detected in the solder bulk, Figure 4.3(c). Elemental mapping of SAC105, SAC105-Fe-1Bi, and SAC105-Fe-2Bi solder alloys are shown in Figure 4.5, Figure 4.6 and Figure 4.7 respectively. Huang et al. showed that the solid solubility limit of Bi in the Sn-Ag–based solder is about 4 wt.% at room temperature, and with a higher Bi addition, the supersaturated Bi would precipitate in the form of the pure Bi phase from the Sn matrix. So it is not possible to show one point as a Bi in the FESEM image with 1 and 2wt% Bi (Liu et al., 2014).

Also, based on following calculation at.% of Bi is 1.77 in 97.45Sn-1Ag-0.5Cu-0.05Fe-1Bi, atomic mass Bi is 209 g/mol and atomic mass Sn is 119 g/mol, therefore at.% Bi in Sn is, at.% Bi=((1×209)/((1×209)+(97.45×119)))×100=1.77. Therefore, the role of 1wt.% Bi at atomic level is higher and can have more effect on the crystal structure of Sn. Similarly, at.% of Bi in 96.45Sn-1Ag-0.5Cu-0.0Fe-2Bi is 3.51.

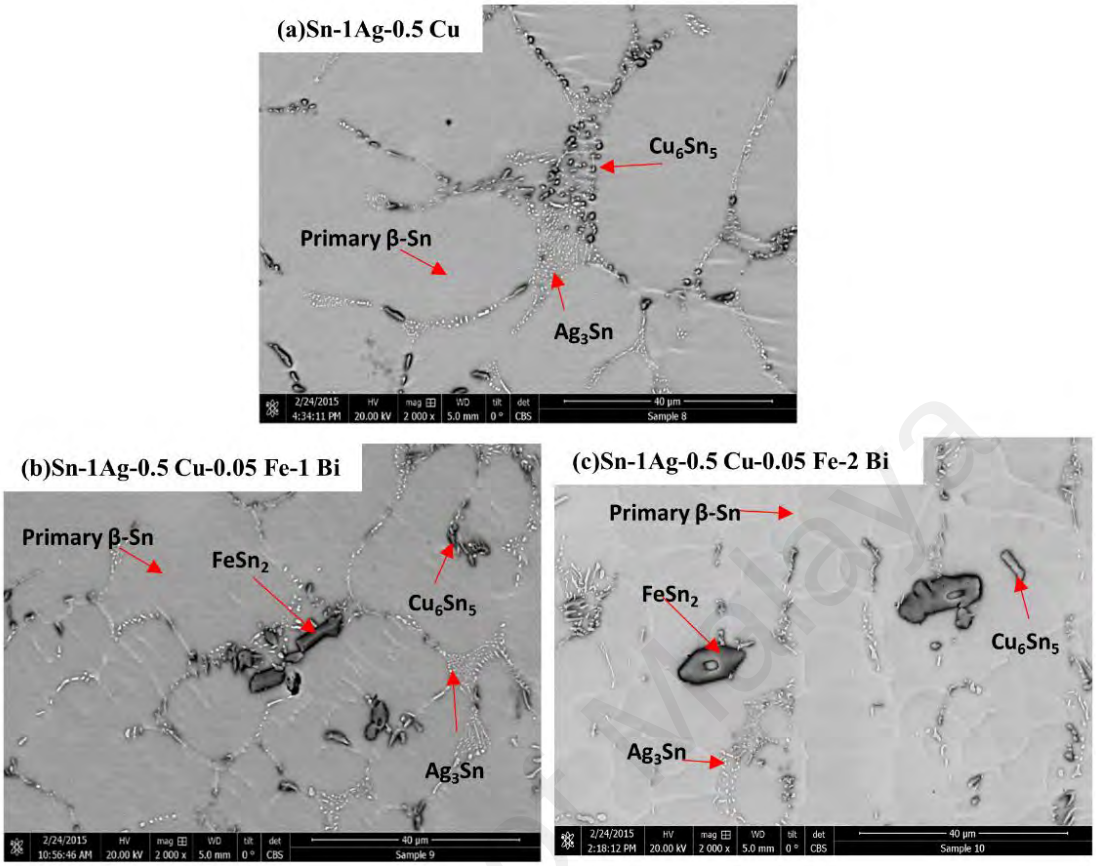

Figure 4.3: FESEM micrographs of as-cast SAC105, SAC105-Fe-1Bi and SAC105-Fe-2Bi solder alloys.

Adding Bi to SAC105-Fe increase β-Sn and decrease Cu_6Sn_5. As it is clear in Figure 4.3 (b) and (c) eutectic regions degenerated into a chain-like arrangement. Lin et al also showed the same result by adding Mn and Ti to Sn-Ag-Cu solder(Lin et al., 2009). Vianco et al. showed that the Bi particles in Sn-3.5Ag solder pinned several grain boundaries (Vianco et al., 1999). Grain boundary pinning would contribute to the high mechanical strength of this particular composition, which attributed to solid-solution and precipitation strengthening effects by Bi in the Sn-rich phase.

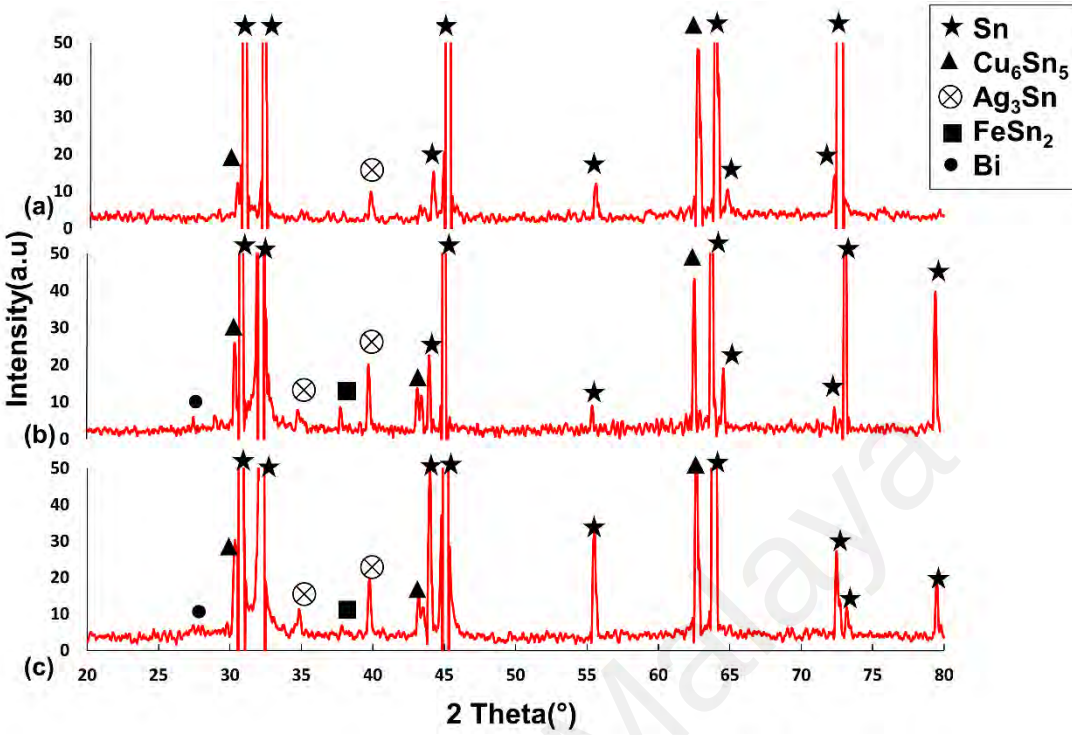

Figure 4.4: XRD result: (a) SAC105, (b) SAC105-Fe-1Bi, and (c) SAC105-Fe-2Bi solder alloys.

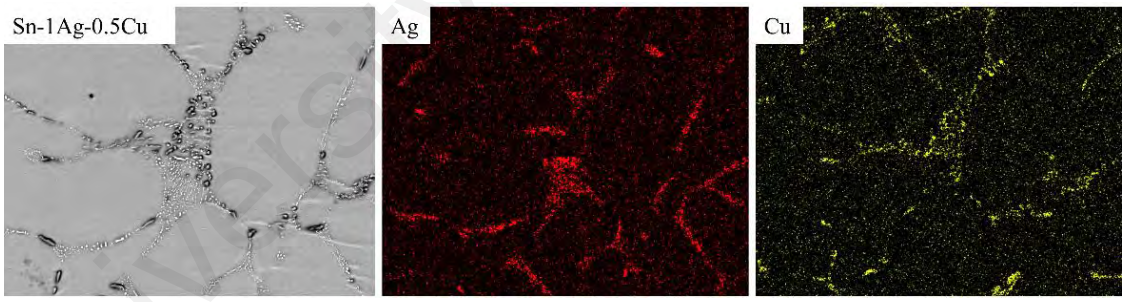

Figure 4.5: Elemental mapping analysis of SAC105 solder alloy.

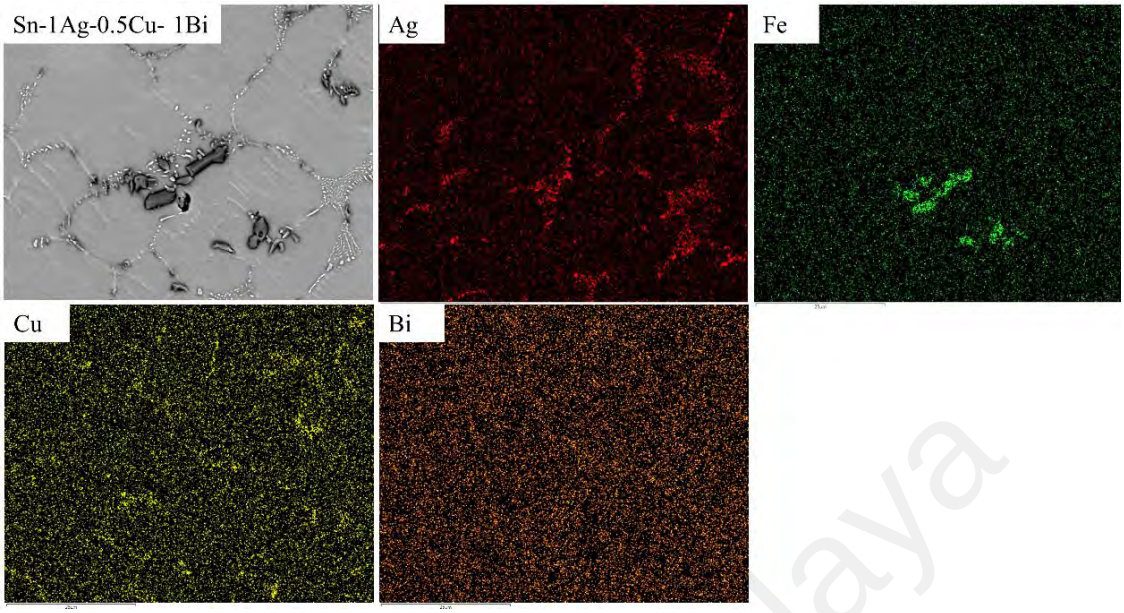

Figure 4.6: Elemental mapping analysis of SAC105-Fe-1Bi solder alloy.

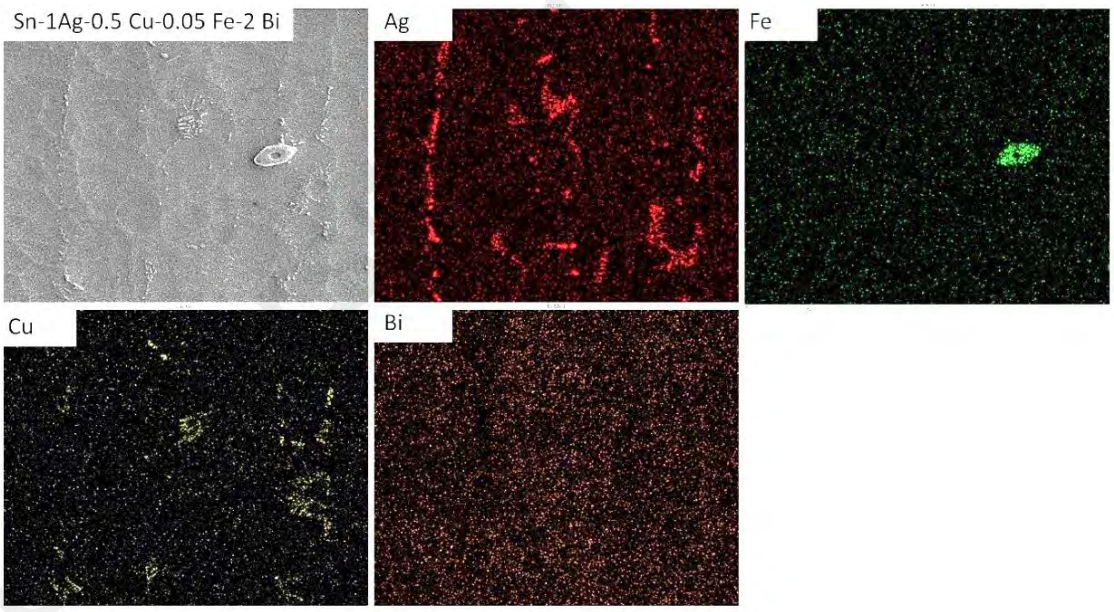

Figure 4.7: Elemental mapping analysis of SAC105-Fe-2Bi solder alloy.

4.1.3 Fracture behavior

To further study the effect of Bi and Fe addition to the SAC105 bulk solder, the fracture surfaces were examined after tensile tests. Figure 4.8 shows SEM micrographs of the fracture surfaces of alloys after tensile tests. The fractograph of the SAC105, SAC105-Fe-1Bi, and SAC105-Fe-2Bi alloys (Figure 4.8) shows different cross-sectionals areas. For the standard SAC105 solder cross-sectional area shows necking. The fracture surface of the SAC105 alloy consists of large ductile dimples as shown in Figure 4.8 (b).

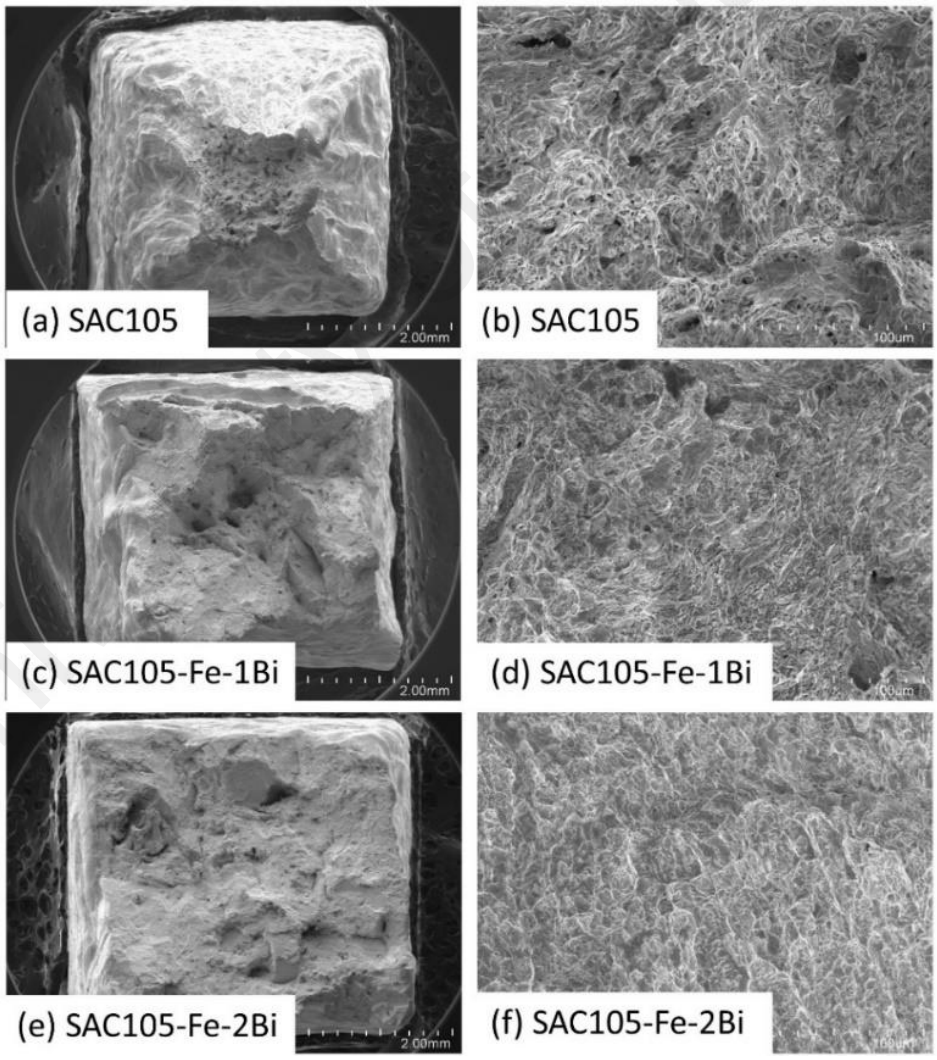

Figure 4.8: SEM fractographs of the alloys after tensile tests (a) and (b) SAC105, (c) and (d) SAC105-Fe-1Bi, (e) and (f) SAC105-Fe-2Bi.

These results demonstrate that the fracture mechanism for SAC105 is ductile. As shown in Figure .4.8 (c) adding 0.05wt Fe and 1wt% Bi make the fracture surface clearly brittle with very little plastic deformation and no necking. Also, Figure 4.8 (d) shows that the number of dimples decrease in compare to Figure 4.8 (b). By increasing Bi to 2wt% the surface become more brittle, Figure 4.8 (e), and there is not any dimple on the surface, Figure 4.8 (f). Previous works showed that adding 0.3Wt%Fe to SAC105 make large circular $FeSn_2$ IMC particles inside the bulk of solder which can be nucleation sites for failure, even though does not have effect on mode of ductile fracture for SAC105 (Kantarcıoğlu et al., 2014). Whereas in the present work by adding just 0.05%wt Fe there is few $FeSn_2$ IMC particles inside the β-Sn. Therefore, this non ductile fracture behavior can be attributed to Bi, which is scatter in β-Sn and prevent solder to deform in β-Sn. Also, the reduction of elongation of the SAC105-Fe-1Bi, and SAC105-Fe-2Bi alloys can be justified by Bi brittle properties.

4.1.4 Thermal behavior

Due to thermodynamic considerations, the melting point of the alloy may be depressed and/or additional eutectic and peritectic reactions can occur, where the two-phase solid transforms to a single phase liquid at a single temperature, much like a pure element, is called the eutectic temperature. Otherwise, when the composition deviate from eutectic composition the change from solid to liquid occur over a range of temperatures which referred as a mushy/pasty zone. The solder microstructure affected by nonequilibrium cooling due to undercooling effects into the solidification process. In order to form a solid embryo, liquid should be cooled below its solidification temperature to obtain sufficient free energy for solidification (Kang et al., 2007; Lee et al., 2015).

Differential scanning calorimetry (DSC) analysis was carried out to determine the effects of the Fe and Bi additions on the melting temperature and pasty range of the

SAC105 alloy. The solidus and liquidus temperatures and pasty range of the solder alloys were measured as shown in Figure 4.9 and are listed in Table 4.1. Figure 4.9 shows heat flow during heating and solidification for SAC105-Fe-1Bi. DSC test shows decrease in solidus temperature from 219.33°C for SAC105 to 214°C for SAC105-0.05Fe-2Bi. Adding 0.05wt%Fe and 2wt% Bi to SAC105 decreased undercooling from 12.3 to 9.8. These results are in agreement with previous work (El-Daly et al., 2015) which showed 6°C decrease of melting temperature by adding 3wt%Bi to SAC157and decreased undercooling 4°C. Moreover, previous works (Shnawah et al., 2012) showed that Fe does not have considerable effect on pasty range, solidus and liquidus temperature, while can increase undercooling slightly.

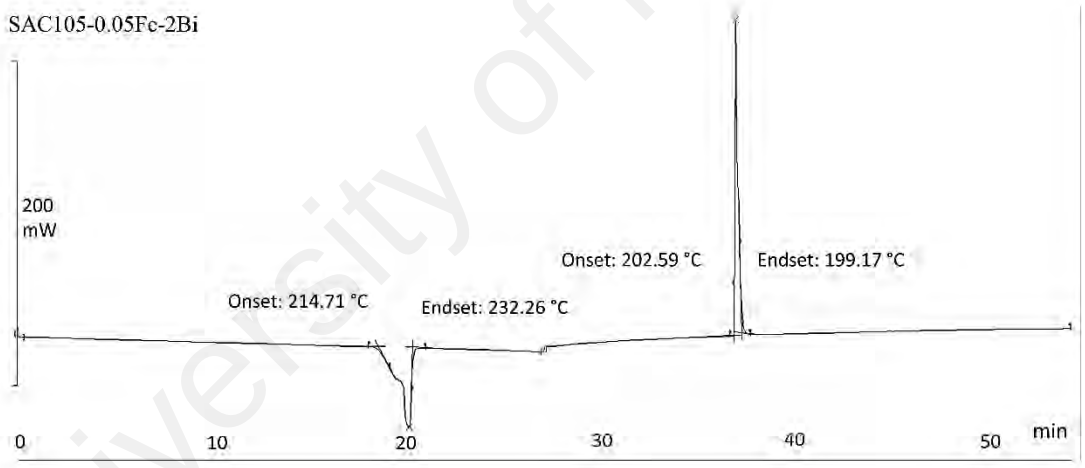

Figure 4.9: DSC thermograph of SAC105-Fe-2Bi solder alloy.

Table 4.1: Differential scanning calorimetry (DSC) test results of the alloys.

Alloys	Solidus temp. Ts (◦C)	Liquidus temp. Tl (◦C)	Pasty range	Onset soldifi. temp. Tc (◦C)	Under cooling, Ts −Tc (◦C)
SAC105	219.3	231.7	12.4	207	12.3
SAC105-0.05 Fe-1 Bi	217.6	230	12.4	207.5	10.1
SAC105-0.05 Fe-2 Bi	214	229	15	204.2	9.8

4.1.5 Aging effect

4.1.5.1 Microstructure properties

The FESEM micrographs of the as-cast and aged microstructures of the SAC105 solder alloy illustrated in Figure 4.10 (a) and (c) for as cast solder, (b) and (d) are after aging at 125°C for 30 days ((a) and (b) at 1000 magnification, (c) and (d) at 2000 magnification). Elemental mapping of SAC105 solder after aging at 125°C for 30 days illustrated in Figure 4.11. The composition of IMC particles verified by EDX. Table 4.2 shows EDX analysis results with wt.% and at.% of elements for IMCs in the bulk of solder. Also, Figure 4.4a shows XRD result for SAC105.

The microstructures of the as cast SAC105 solder consist of thick interdendritic regions of Cu_6Sn_5 and Ag_3Sn IMC particles within a β-Sn matrix. For as cast samples, the addition of 0.05 wt.% Fe does not significantly affect the microstructural properties of the SAC105. Whereas Bi addition lead to the remarkable microstructural changes which contribute to strengthen the solder alloy, such as the extended area fraction of the primary β-Sn with dissolved Bi, the degenerated eutectic regions, and the coarsened and less-packed Cu_6Sn_5 and Ag_3Sn IMC particles. The addition of Bi results in a lower area fraction of the eutectic Cu_6Sn_5 and Ag_3Sn IMCs as well as a higher area fraction of the β-Sn dendrites. It is therefore supposed that Bi super-saturated dissolved in the primary β-Sn phase. This can be attributed to the high solubility of Bi in Sn as the solid solubility limit of Bi in Sn at 120˚C is below 3% (Kattner et al., 1994). Lin et al. also showed the same result by adding Mn and Ti to SAC solder (Lin et al., 2009). Vianco and Rejent (Vianco & Rejent, 1999) illustrated the grain boundary pinning of Bi as a result of precipitation strengthening and solid-solution effects by Bi in the Sn-rich phase in Sn-3.5Ag solder which lead to the high mechanical strength of this composition.

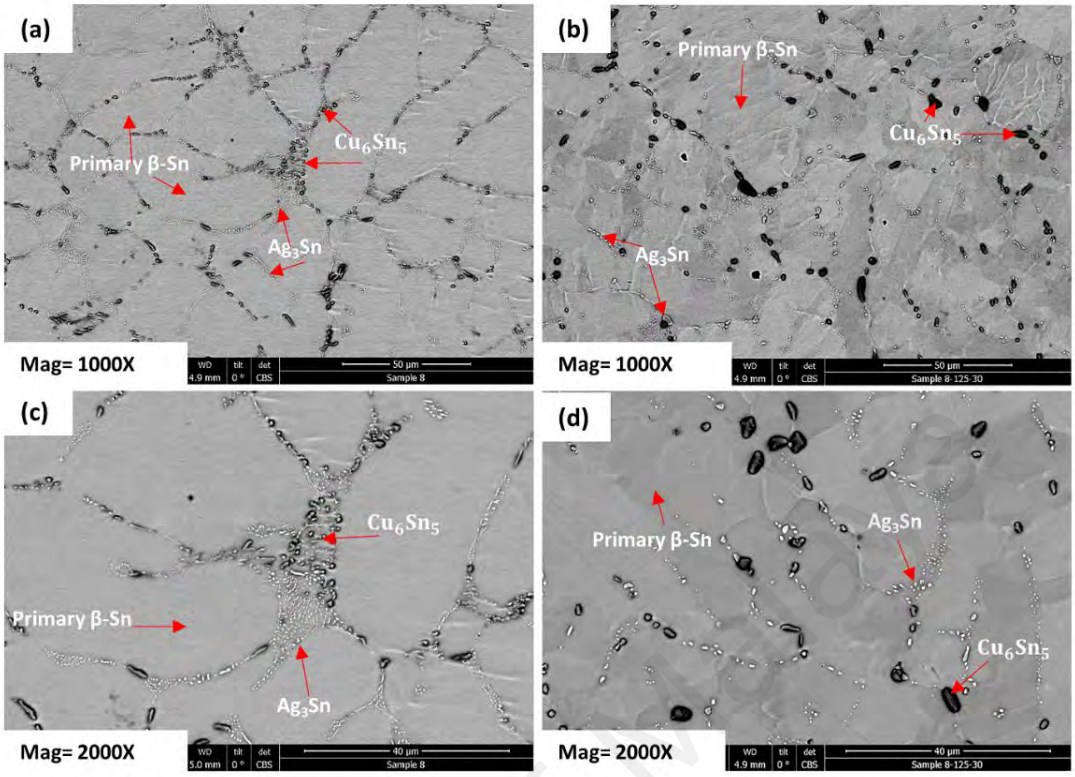

Figure 4.10: FESEM results for SAC105, (a)1000x and (c)2000x for as cast solder, (b)1000x and (d)2000x are after aging at 125°C for 30 days.

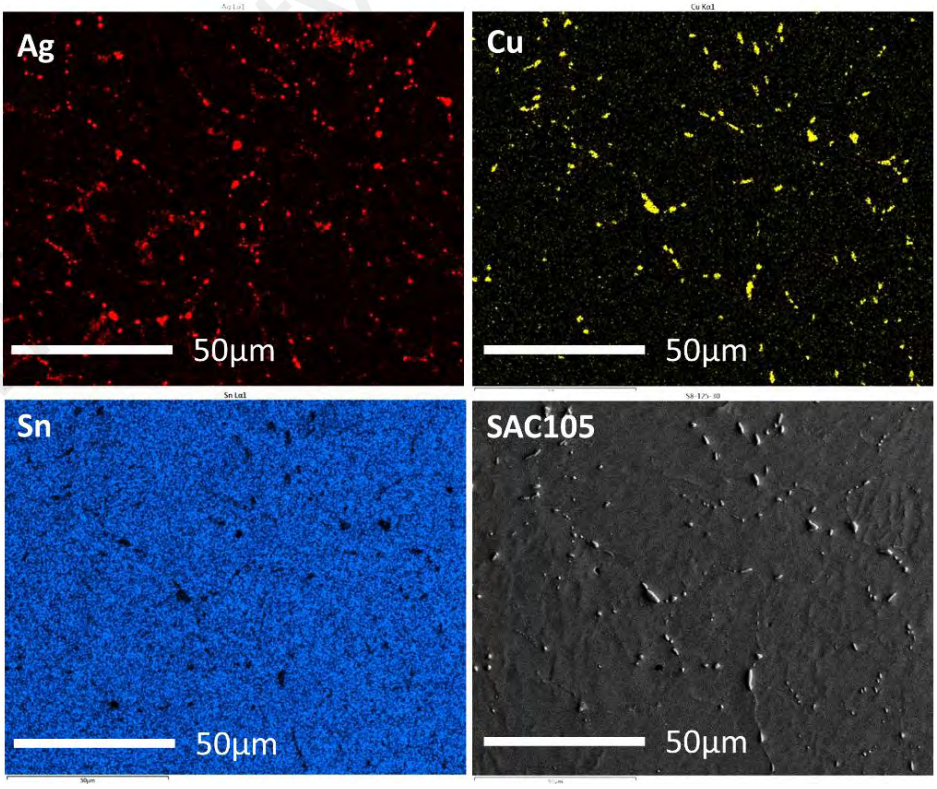

Figure 4.11: Elemental mapping of SAC105 after aging at 125°C for 30 days.

Table 4.2: EDX analysis results for IMC particles.

Composition	IMCs	Sn	Ag	Cu	Fe
SAC105	Cu_6Sn_5	64.37 wt.% 49.17 at.%	-	35.63 wt.% 50.83 at.%	-
	Ag_3Sn	65.83 wt.% 63.71 at.%	34.17 wt.% 36.29 at.%	-	-
SAC105-Fe-1Bi	Cu_6Sn_5	65.26 wt.% 50.14 at.%	-	34.74 wt.% 49.86 at.%	-
	Ag_3Sn	64.65 wt.% 62.44 at.%	35.35 wt.% 37.56 at.%	-	-
	$FeSn_2$	82.72 wt.% 69.25 at.%	-	-	17.28 wt.% 30.75 at.%
SAC105-Fe-2Bi	Cu_6Sn_5	64.54 wt.% 49.36 at.%	-	35.46 wt.% 50.64 at.%	-
	Ag_3Sn	63.96 wt.% 61.57 at.%	36.04 wt.% 38.43 at.%	-	-
	$FeSn_2$	82.29 wt.% 68.61 at.%	-	-	17.71 wt.% 31.39 at.%

Therefore, on one hand the amount of Sn increase which consider soft as its metallic bonding and the amount of Cu_6Sn_5 and Ag_3Sn decrease which are hard and brittle particle due to the strong covalent bonding of these IMCs. So it would seem that an increase in the amount of Sn and decrease in the amount of Cu_6Sn_5 and Ag_3Sn would make the solder more ductile. But on the other hand, the crystal lattice of primary β-Sn distorts by the addition of Bi atoms and increase unit cell volume. Table 4.3 shows the lattice constants of the Sn phases in the solder alloys. Sn crystal structure is tetragonal, by knowing miller indices (h, k, l) from XRD result, lattice parameter (a, b, and c) can be calculated from crystal geometry equation 4-1:

$$\frac{1}{d^2} = \frac{h^2 + k^2}{a^2} + \frac{l^2}{c^2}, \qquad (a = b) \qquad 4\text{-}1$$

In this case, (200) and (101) Sn peaks selected and on the basis of *d* (spacing) from XRD database, lattice parameter (a, b and c) calculated. The lattice constant of the Sn phase in SAC105-Fe-1Bi and SAC105-Fe-2Bi slightly differs from that of the SAC105. This result agrees with phase diagrams which show that the solubility of Cu and Fe in Sn is very low (Massalski et al., 1986), and Bi solutes in the Sn phase and causes solid solution hardening of the Sn phase. The dissolution of Bi atoms in the β-Sn lattice distort the latter, thereby causing a local stress fields that act as a barrier to the mobility of dislocations which in turn make the solder exhibit higher yield strength and UTS. Therefore, the addition of Bi makes the solder alloy stronger by solute mechanism.

Table 4.3: Effect of Fe and Bi on lattice constant of Sn phase.

Solder composition	Lattice Parameter a=b (Å)	Lattice Parameter c (Å)	c/a	Volume of the unit cell $(Å)^3$
SAC105	5.77	3.177	0.5506	105.77
SAC105-Fe-1Bi	5.81	3.169	0.5454	106.97
SAC105-Fe-2Bi	5.83	3.174	0.5444	107.88

It is observed for SAC105 after aging, Figure. 4.10 (b) and (d), the growth and spheroidization of Cu_6Sn_5 and Ag_3Sn controlled by Gibbs-Thomson effect and Ostwald ripening process (Fix et al., 2008; Song et al., 2003). On the basis of Ostwald ripening small crystal redeposits onto larger crystals which are more energetically favorable. Therefore, IMCs and β-Sn grains coarsen. Consequently, the numbers of Ag_3Sn and Cu_6Sn_5 IMC particles in the SAC105 solder decrease after aging. Thus after aging total elongation for SAC105 increased because the number of IMCs decreased as it is clear in Figure 4.10 while UTS and yield strength decrease because dislocation are more able to move (Anderson, 2007). Gibbs-Thomson effect consider that the surface free energy of the intermetallic phase decrease as result of the spheroidization and growth of Cu_6Sn_5 and

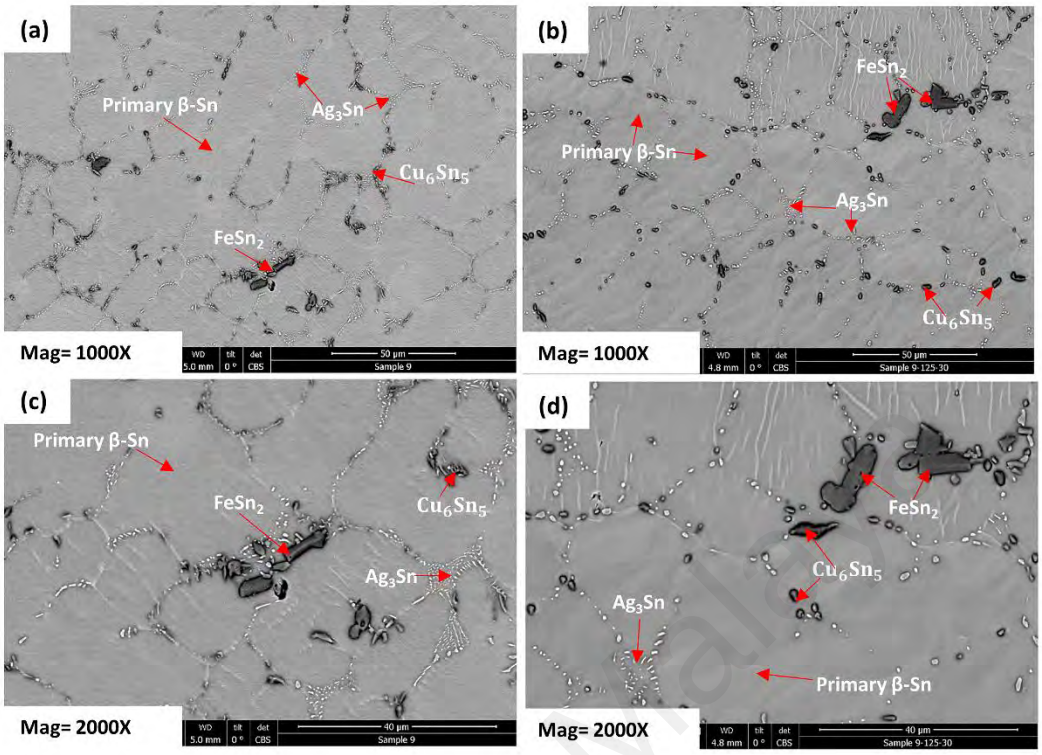

Figure 4.12: FESEM results for SAC105-Fe-1Bi, (a)1000x and (c)2000x for as cast solder, (b)1000x and (d)2000x are after aging at 125°C for 30 days.

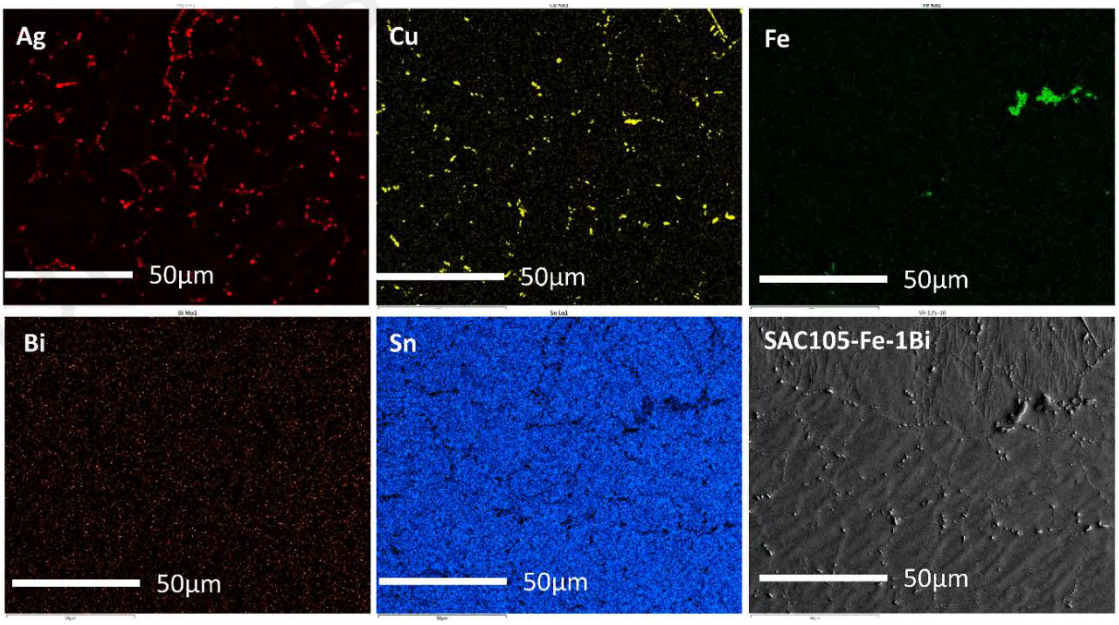

Figure 4.13: Elemental mapping SAC105-Fe-1Bi after aging at 125°C for 30 days.

Ag_3Sn. The interface of Cu_6Sn_5 and Sn matrix prepare a heterogeneous region for the interaction between Cu and Sn and similarly between Ag and Sn for Ag_3Sn. The Cu or Ag dissolved in Sn-rich phase and resulted in the growth of Cu_6Sn_5 or Ag_3Sn. It illustrates that Cu and Sn segregates at the surrounding of the Cu_6Sn_5 intermetallic phase, also similarly Ag and Sn segregates at the surrounding of the Ag_3Sn and then forms the new intermetallic phase at the determined concentration. This procedure leaded to the growth of IMCs (Hsuan et al., 2007).

Then by the addition of 0.05 wt.% Fe and 1 wt.% Bi to SAC105, few $FeSn_2$ IMC particles form in the interdendritic regions, whereas Bi scatter on the whole of the β-Sn area, Figure 4.12 and Figure 4.13 show FESEM and elemental mapping of SAC105-Fe-1Bi respectively. Figure 4.4 (b) shows XRD result for SAC105-Fe-1Bi. Because of the low solubility of Fe in the β-Sn majority of the Fe precipitates as the $FeSn_2$ phase or in the eutectic regions. It is clearly the size of Cu_6Sn_5 (3μm) in SAC105-Fe-1Bi after aging, Figure 4.12 (b), is smaller in compare to the size of Cu_6Sn_5 (2.5 μm) in SAC105 after aging, Figure 4.9 (b). Figure 4.14 (a) shows average IMC size and Figure 4.14 (b) shows IMC area percentage of solder alloys before and after aging.

Based on previous work by, Fe addition to SAC105 solder suppress the coarsening of Ag_3Sn. The lattice strain in the Ag_3Sn intermetallic and blocking effect on Ag diffusivity in the Sn matrix are the possible mechanism for coarsening suppression of Ag_3Sn in the Fe modified solder alloys (Anderson et al. 2007).

The combined analysis of atomic radii and electronegativity which is known as the Darken-Gurry ellipse used to predict elements that would dissolve in solid solution, Figure 4.15 (Anderson et al., 2006; Kotadia et al., 2014). Fe falls inside the Darken-Gurry ellipse for substitution in place of Cu. Therefore, Fe can partially substitute into the

Cu_6Sn_5 IMC particles. Fe atoms have -0.31% mismatch with Cu atoms. This partial substitution might produce increased lattice strain in the Cu_6Sn_5 IMC particles and reduce the vacancy diffusion rate. Thus, it decreases microstructure coarsening rate (Anderson & Harringa, 2004). For SAC105-Fe-1Bi UTS slightly increased after aging and yield strength decreased a little, however due to the effect of Fe yield strength drops less in compare to SAC105.

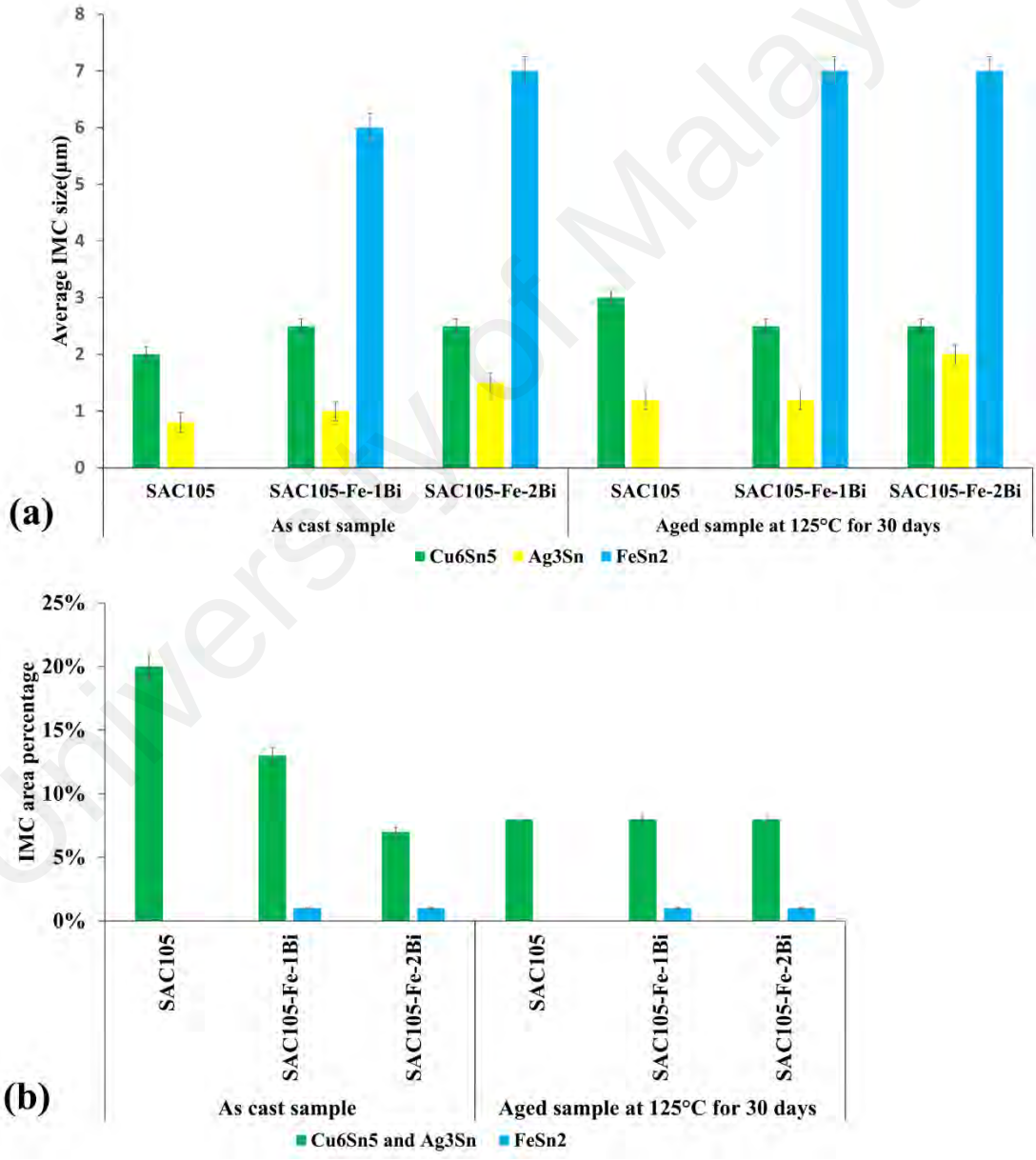

Figure 4.14: (a) Average IMC size and (b)shows IMC area percentage of solder alloys before and after aging at 125°C for 30 days.

After aging, Bi prevented coarsening of IMCs. The existence of Bi within the β-Sn matrix reduce the activity of Sn involved in the chemical reaction between Sn and Cu, or Sn and Ag during the solidification and hence reduces the amount of Cu_6Sn_5 and Ag_3Sn IMC particles.

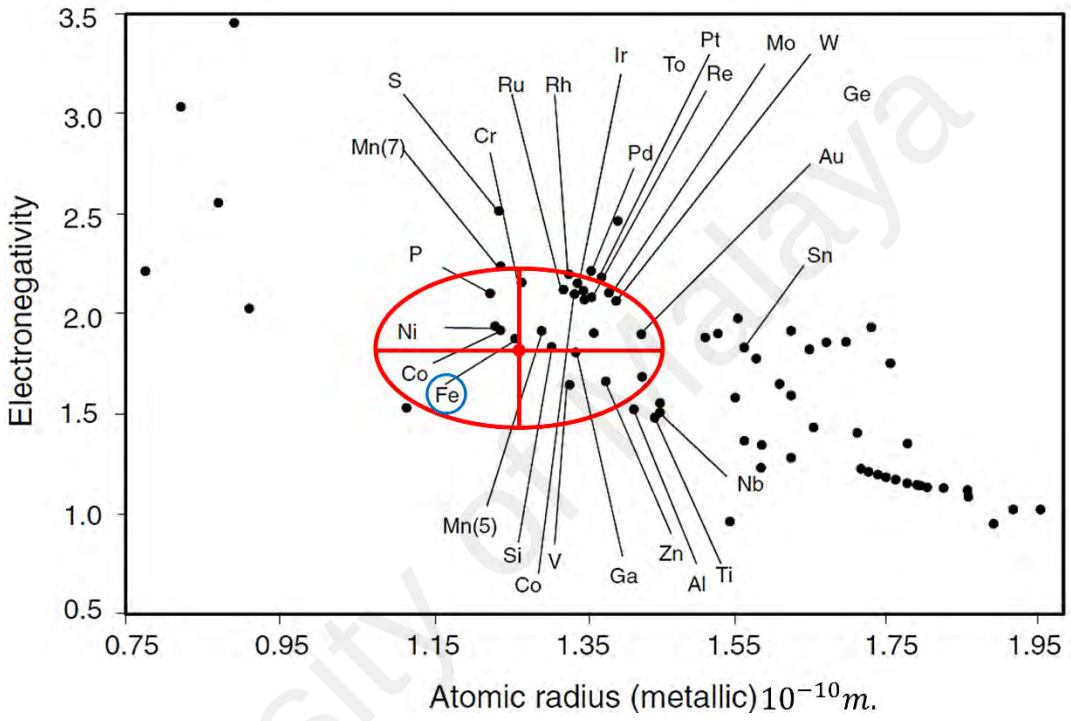

Figure 4.15: A Darken–Gurry ellipse plot with Cu as the central atom, where the elements in the ellipse are exhibit high solid solubility in Cu (up to 5 at.%) (Kotadia et al., 2014).

For SAC105-Fe-2Bi sample, FESEM results show in Figure 4.16. Figure 4.4 (c) shows XRD result for SAC105-Fe-2Bi. Increasing Bi to 2wt.% degenerated eutectic region more. In Figure 4.17 mapping result clearly shows scatter and chain-like arrangement of Ag and Cu in solder bulk. For SAC105-Fe-(1 or 2)Bi samples total elongation after aging are approximately constant. The mutual effect of Bi by solid solution and solder bulk softening due to the decrease of IMCs plus partial substitution of Fe in IMCs all together can result in stable total elongation after aging.

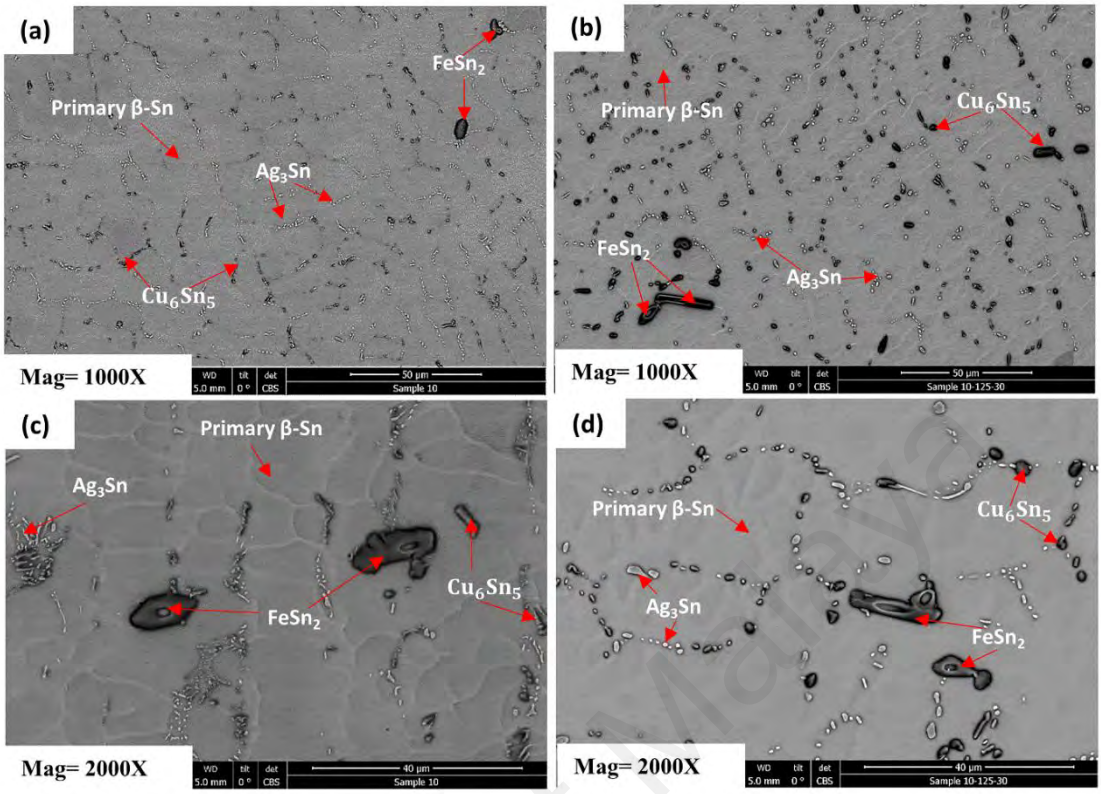

Figure 4.16: FESEM results for SAC105-Fe-2Bi, a(1000x) and c(2000x) for as cast solder, b(1000x) and d (2000x) are after aging at 125°C for 30 days.

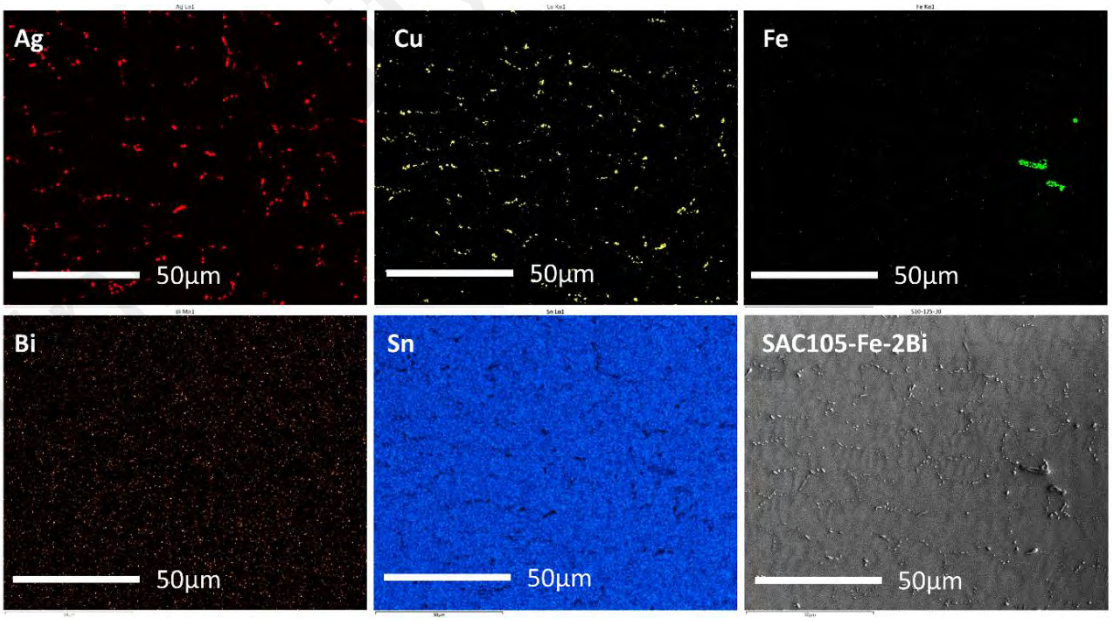

Figure 4.17: Elemental mapping SAC105-Fe-2Bi after aging at 125°C for 30 days.

4.1.5.2 Mechanical Properties

The stress–strain curves of the as-cast and aged at 125 °C for 30-days of samples SAC105, SAC105-Fe-1Bi and SAC105-Fe-2Bi solder alloys under a strain rate of 10^{-3} s^{-1} are shown in Figure 4.18. It is obvious that for samples with Fe and Bi, stress-strain curve after aging is above the as cast samples.

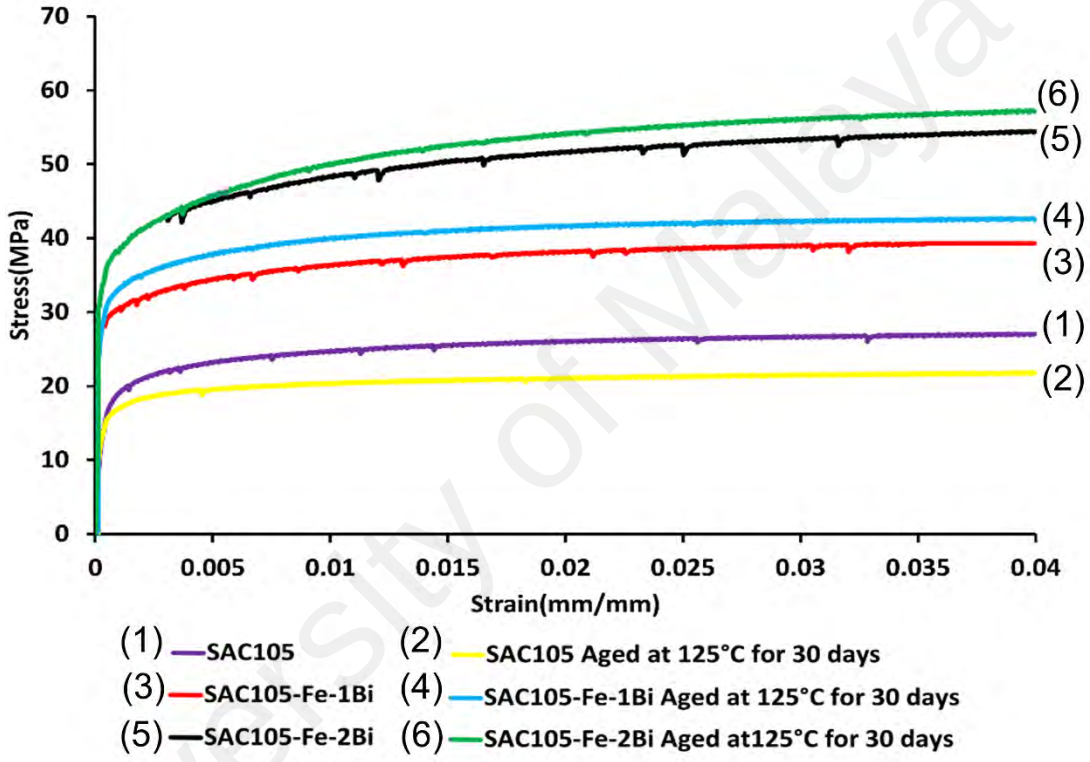

Figure 4.18: stress-strain curve for as cast solder alloys and solder alloys after aging at 125°C for 30 days.

The mechanical properties of solder alloys include yield strength, ultimate tensile strength (UTS), and total elongation for as cast, aged at 125 °C for 30-days and aged at 180 °C for 1-day solder alloys are shown in Figure 4.19. The results for samples aged at 180 °C for 1-day shown for comparison with higher temperature aging.

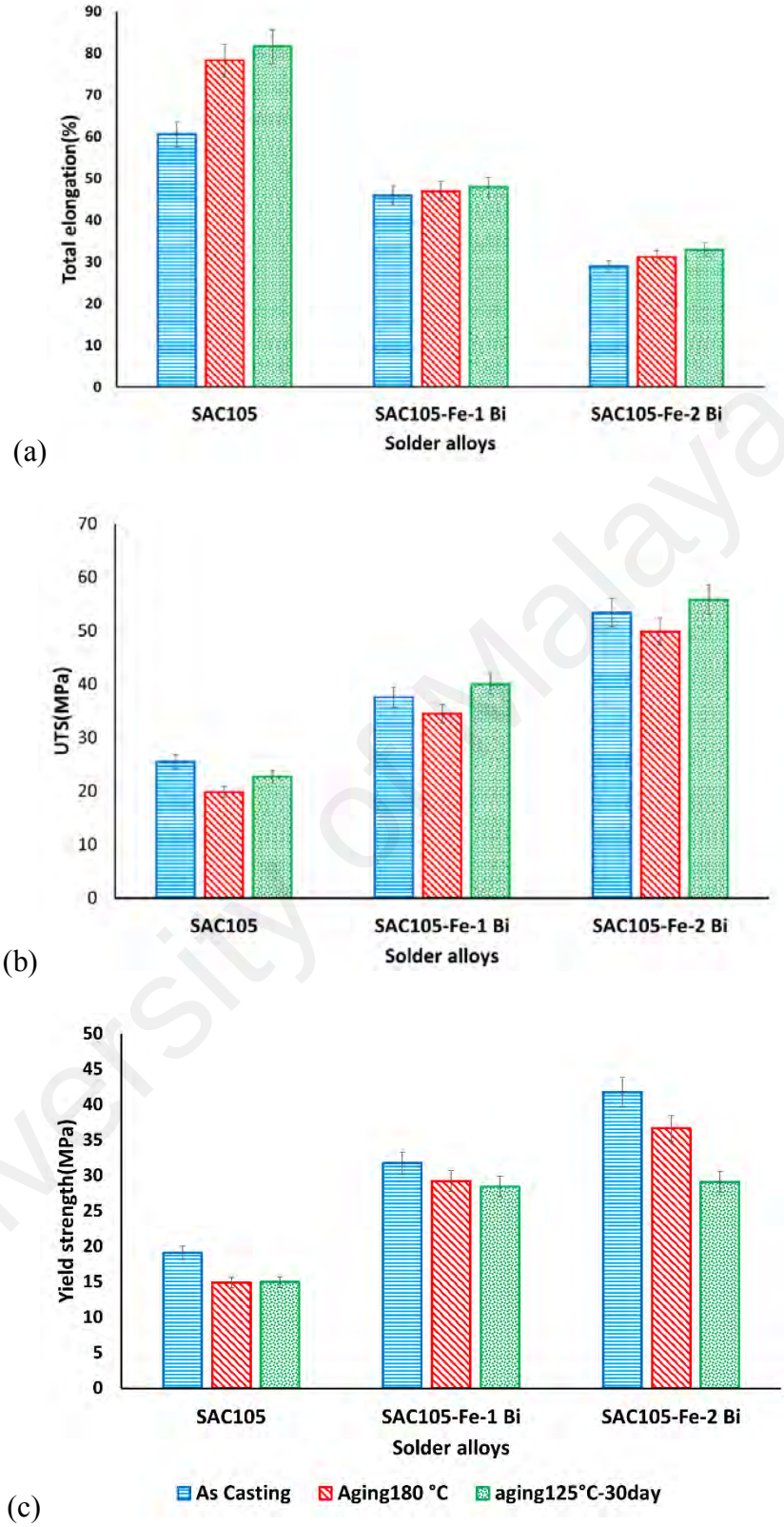

Figure 4.19: Mechanical properties of solder alloys, (a)total elongation, (b)UTS, (c) Yield strength.

As illustrated in Figure 4.19 for as cast samples, doping 0.05 wt.% Fe and 1 or 2wt.%Bi to SAC105 solder increased UTS, from 27.5 MPa for SAC105 to 56MPa for SAC105-Fe-2Bi, and increased yield strength from 21 MPa for SAC105 to 41.8 MPa for SAC105-Fe-2Bi whereas total elongation decreased from 60 % to 34% respectively for SAC105 and SAC105-Fe-2Bi. Jie Zhao et al. (Zhao et al., 2004) and Xiaowu Hu et al. (Hu et al., 2015) showed the similar effect in mechanical properties by adding Bi to SAC and Sn-0.7Cu respectively.

After SAC105 aged at 125°C for 30 days, UTS decreased from 25.5MPa to 22.5 MPa and yield strength decreased from 19MPa to 15MPa. Total elongation for SAC105 increased after aging from 60.5% to 81.5% whereas for sample with 1wt.%Bi UTS slightly increased from 37MPa to 40MPa, yield strength slightly decreased from 31MPa to 27MPa and total elongation (46%) is approximately constant in comparison for as cast and aged sample at 125°C for 30 days. Bi prevent the Cu and Sn to interact with each other, therefore spheroidization and growth of IMCs after aging slowed down and decreased the rate of IMCs coarsening. Thus, SAC105-Fe-1Bi solder alloy have stabilized mechanical properties after aging which approximately the properties after aging remain stable. Then by increasing Bi to 2wt.%, after aging total elongation is roughly stable, although yield strength decreased from 41MPa to 29MPa and UTS increased from 53MPa to 55MPa. Aging at 180°C for 1-day have a similar trend like 125°C aged for 30-days samples, yield strength decreased and total elongation increased whereas UTS is less than as cast samples and aged samples at 125°C aged for 30-days, which can be related to the harsh coarsening of IMC after high temperature aging.

4.1.6 Microhardness

The measurement of hardness, especially Vickers microhardness, is regarded as one of the most principal ways to characterize the mechanical performance of lead-free solder alloy. The solder microhardness is often related to how the metallic material resists wearing or abrasion (Hu et al., 2013).

Figure 4.20 shows microhardness indentation of (a) SAC105, (b) SAC105-1Bi, (c) SAC105-2Bi solder alloys. Table 4.4 shows UTS and microhardness of solder composition in MPa and HV. There is a general correlation between strength (UTS) and hardness (HV ≈ 3 UTS) (Boyer et al., 1985; Callister & Rethwisch, 2007). However, this relation is lower than 3 in the materials with good ductility, due to the hardness represents a hardened state of materials without fully hardened (Pavlina et al., 2008; Zhang et al., 2011). To investigate this relation vicker hardness can be converted to MPa (HV× 9.807≈ hardness in MPa) (Cahoon et al., 1971). Table 4.4 shows microhardness and UTS in MPa which is approximately UTS is 3 time of microhardness, however for SAC105 this correlation is less than 3 time which is because of its more ductility in compare to samples with Fe and Bi.

Bi increases hardness due to solid solution hardening mechanism which is consistent with previous works by Huang et.al (Huang & Wang, 2005; Vianco et al., 1999). Fe does not have considerable effect on bulk hardness, as it exists in bulk of solder as $FeSn_2$. $FeSn_2$ has high hardness, but it can be find in just less than 1% area fraction of solder, it does not have effect of overall hardness of solder. Moreover, the limited amount of Fe goes inside the Cu_6Sn_5, which have a little effect on increasing hardness of solder.

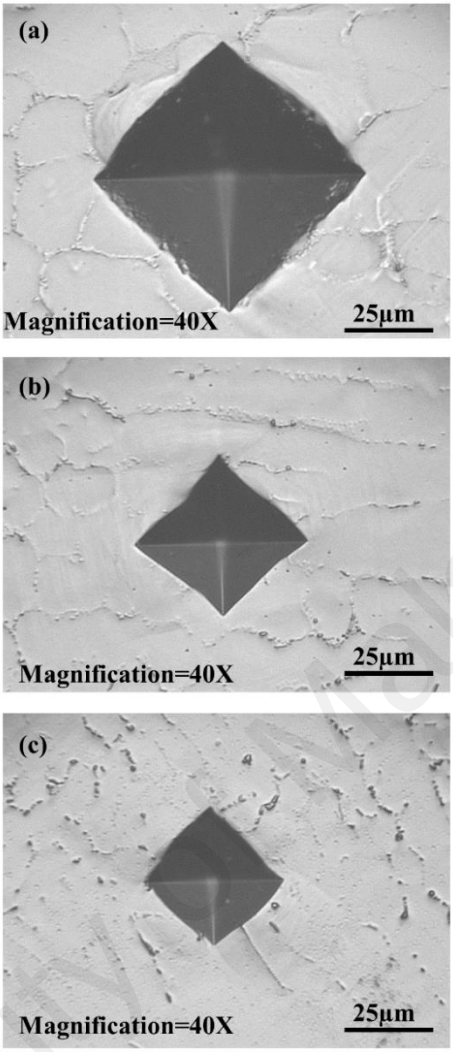

Figure 4.20: Microhardness indentation of (a) SAC105, (b) SAC105-1Bi, (c) SAC105-2Bi.

Table 4.4: UTS and microhardness of solder composition in MPa and HV.

Solder composition	UTS (MPa)	Microhardness (MPa)	Microhardness (HV)
SAC105	27	59	6.02
SAC105-Fe-1Bi	41	110	11.22
SAC105-Fe-2Bi	57	140	14.28

4.1.7 Nanoindentation

Nanoindentation applied to calculate young modulus and hardness of solders composition. Measurements of hardness and young's modulus were made by nanomechanical test instrument, Hysitron Ubi TI 750, using a Berkovich indenting tip. The integrated in-situ Scanning Probe Microscopy (SPM) used to locate and record testing result. Indentations were performed at load controlled under loading rate 200μN/s, holding time 2s and maximum load 1mN-7mN. Five times of indentation have done on each sample and by averaging the result hardness and young's modulus were obtained.

E_r (reduced modulus) is related to Young's modulus E_s of the test specimen with equation 4-2:

$$\frac{1}{E_r} = \frac{(1-\nu_i{}^2)}{E_i} - \frac{(1-\nu_s{}^2)}{E_s} \qquad \textbf{4-2}$$

The subscript i specify a property of the indenter material and v is Poisson's ratio. For a diamond indenter tip, Ei is 1140 GPa and vi is 0.07. Poisson's ratio of the specimen, vs considered 0.35.

Hardness calculated by equation 4-3, maximum load over projected area.

$$H = \frac{P_{Max}}{A_c} \qquad \textbf{4-3}$$

Figure 4.21 (a) shows scanning probe microscopy (SPM) of SAC105 which include Ag_3Sn and Cu_6Sn_5. Figure 4.21 (c) shows β-Sn area. Figure 4.21 (b) and (d) show

indentation and position of indents in eutectic region (Ag_3Sn and Cu_6Sn_5) and β-Sn respectively. Figure 4.22 shows Load-Displacement curve for SAC105 in eutectic region and in β-Sn which is include loading, creep deformation and unloading. The onset slope of unloading curve shows reduced Young's modulus. Figure 4.23 shows SPM of SAC105-Fe-2Bi (a) before, (b) after nanoindentation and (c) position of indent. Figure 4.24 illustrate Load-Displacement curve for SC07-Fe-2Bi in eutectic region and in β-Sn. Table 4.5 and Table 4.6 illustrate Young's modulus and hardness of solder compositions respectively.

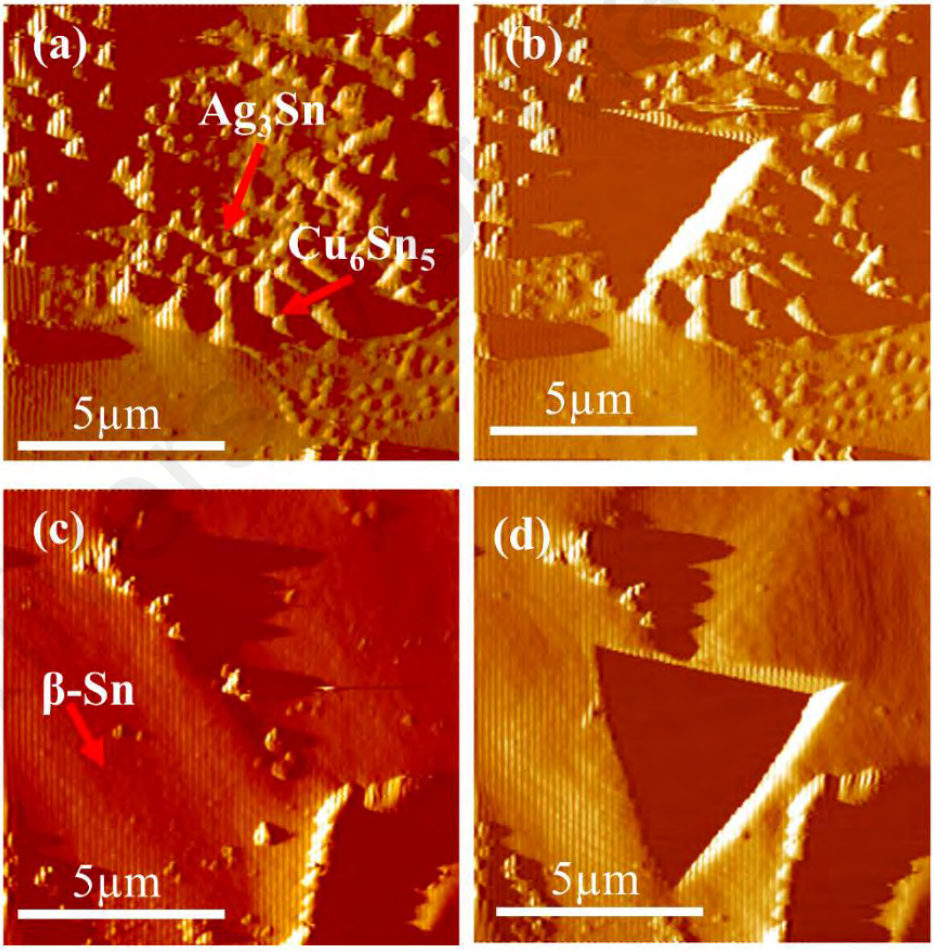

Figure 4.21: SPM of SAC105 (a) before and (b) after nanoindentation in Cu_6Sn_5. (c) before and (d) after nanoindentation in β-Sn.

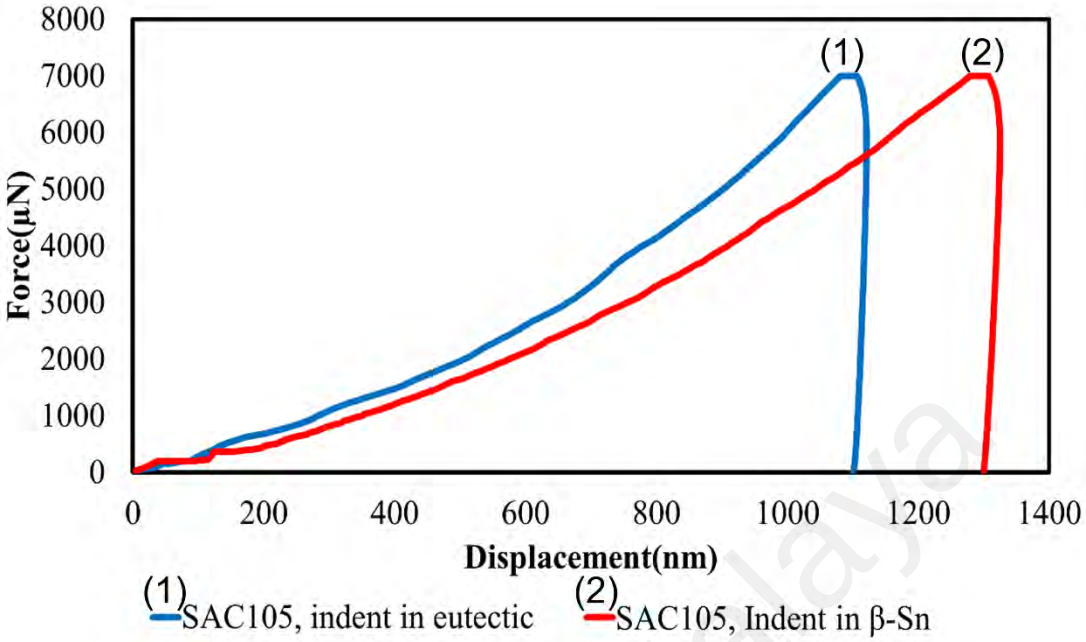

Figure 4.22: Load-Displacement curve for SAC105 in eutectic region and in β-Sn.

The indenting result shows that E_r (reduced modulus) for SAC105 is 71GPa and 59GPa in the β-Sn and (Cu_6Sn_5+ Ag_3Sn) respectively. Then for sample SAC105-Fe-2Bi, Er increased to 112GPa and 92GPa respectively in β-Sn and (Cu_6Sn_5+Ag_3Sn) which attributed to the solid solution effect of Bi and distortion of lattice parameter. Also due to the Darken-Gurry ellipsis few Fe can substitute with Cu in Cu_6Sn_5 which result in increasing Er. Also there is same trend for hardness which hardness of SAC105 in β-Sn from 166.4 MPa increased to 391MPa for SAC105-Fe-2Bi. Moreover, hardness in (Cu_6Sn_5+Ag_3Sn) increase from 212Mpa for SAC105 to 396MPa for SAC105-Fe-2Bi.

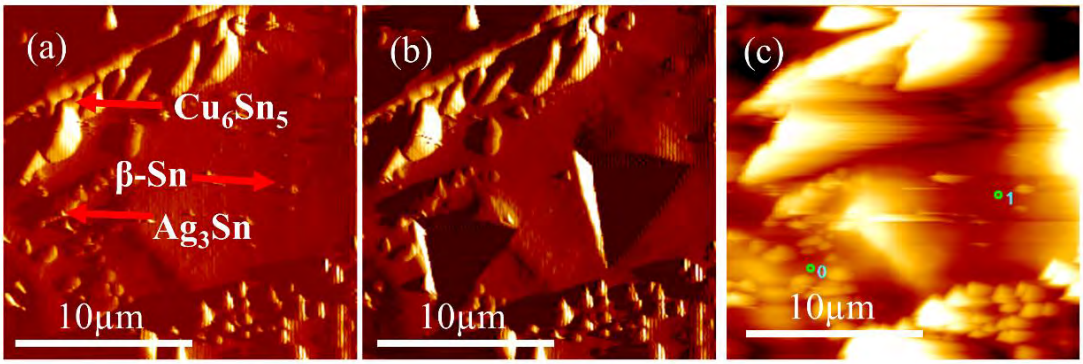

Figure 4.23: SPM of SAC105-Fe-2Bi (a) before, (b) after nanoindentation and (c) position of indent.

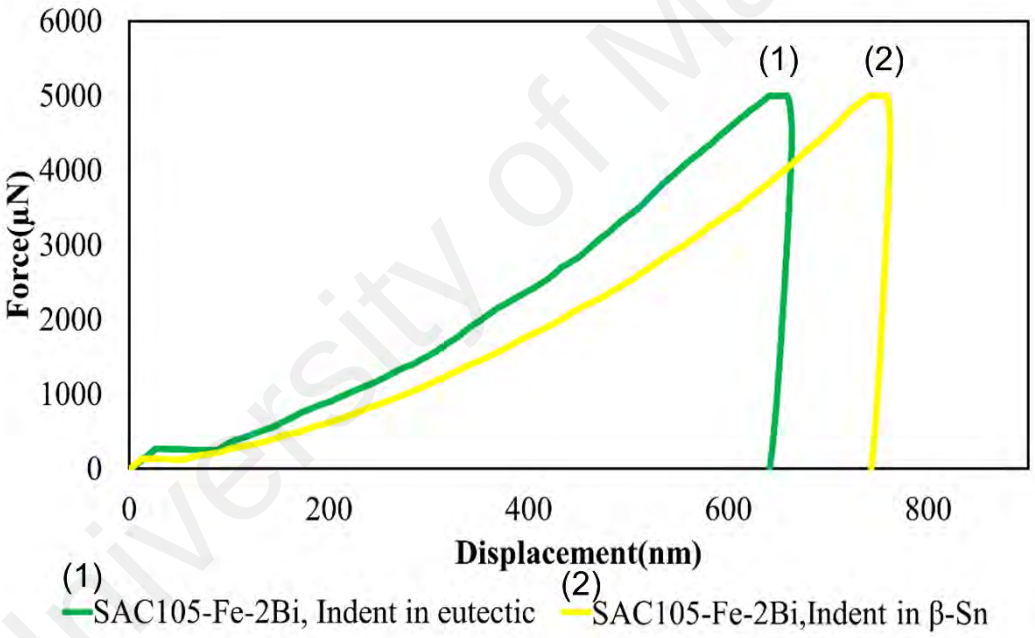

Figure 4.24: Load-Displacement curve for SAC105-Fe-2Bi in eutectic region and in β-Sn

Table 4.5: Reduced Young's modulus of solder composition.

Solder composition	Er (GPa)	
	β-Sn	Cu_6Sn_5+Ag_3Sn
SAC105	71	59
SAC105-0.05Fe-1Bi	97.4	85.5
SAC105-0.05Fe-2Bi	112.5	92

Table 4.6: Hardness(MPa) of solder composition

Solder composition	Hardness(MPa)	
	β-Sn	Cu_6Sn_5+Ag_3Sn
SAC105	166.4	212
SAC105-0.05Fe-1Bi	244	281
SAC105-0.05Fe-2Bi	391	396

4.1.8 Wetting angle and spreading rate

Many factors have effect on wetting properties, such as flux, temperature, substrate conditions, and soldering condition. However, spreading rate and wetting angle are considered to measure the solderability of solder alloy. Generally higher spreading rate with a lower wetting angle is desired during reflow. Figure 4.25 shows Wetting angle for SAC105, SAC105-Fe-1Bi and SAC105-Fe-2Bi solder alloys. Wetting angle and spreading rate for SAC105 with RMA (Rosin Mildly Activated) flux are 38° and 65.4% respectively, as shown in Figure 4.26, by adding 0.05 wt% Fe and 2wt% Bi contact angle decrease to 31° and spreading rate rises to 68.1%. The wetting angle $30° < \theta < 40°$ is considered acceptable (Kripesh et al., 2001).

Bi addition to SAC solder improve wetting (Huang & Lee, 1999), presumably due to the low surface tension of Bi (0.376 N/m for Bi versus 0.537 N/m for Sn) (Lee, 2007). Furthermore, Bi addition improved solder wetting properties because of better solder spreading as a result of the segregation of Bi on the solder surface in the liquid state by decreasing the surface tension of the molten solder (Pandher et al., 2007). It is reported that the first intermetallic compound (IMC) formed at the interface play important role on the wetting properties, because the molten solder is in contact with the IMC at the interface, not the original substrate (Chen et al., 2002; Choi et al., 1999; de Gennes, 1985). Therefore, Bi-doped SAC solder has better wettability due to the growth suppression of

the Cu_3Sn IMC layers (Pandher & Healey, 2008; Pandher et al., 2007). Moreover addition of Fe improve wetting slightly, because Fe can decrease the size of IMC in interface by retarding the growth of interfacial Cu_6Sn_5 and Cu_3Sn layer during liquid state and slightly decreased the total IMC layer thickness (Laurila et al., 2009).

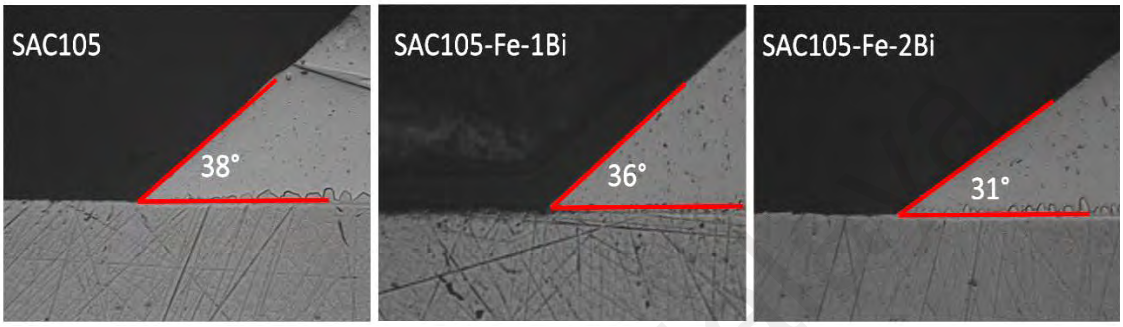

Figure 4.25: Wetting angle for SAC105, SAC105-Fe-1Bi and SAC105-Fe-2Bi solder alloys.

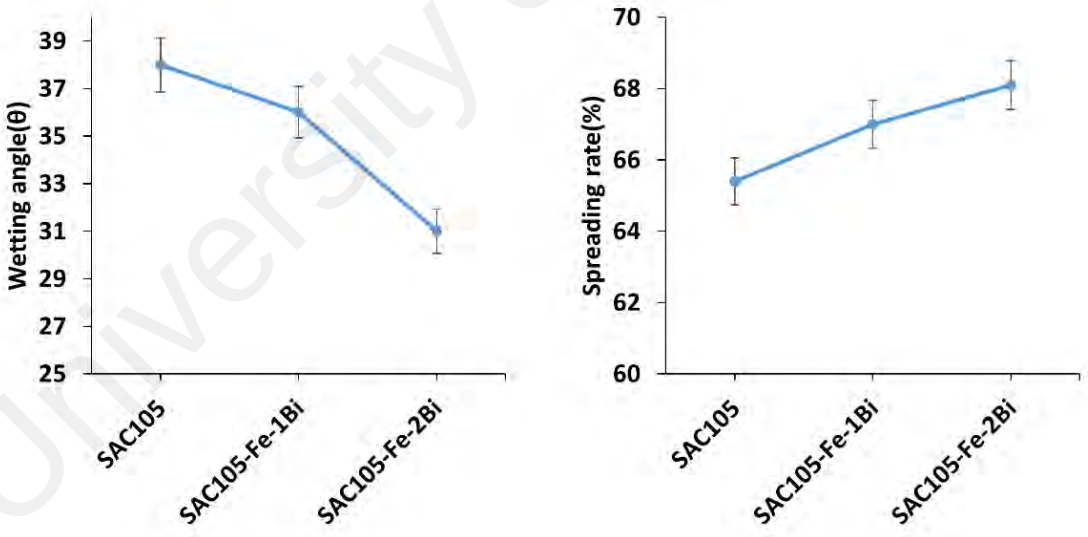

Figure 4.26: wetting angle and spreading rate of SAC105, SAC105-Fe-1Bi, and SAC105-Fe-2Bi solder alloys.

4.1.9 Density

Electronic Densimeter was utilized to measure density of solder composition with the resolution of a 0.001 g/cm^3. Table 4.7 shows density of SAC105, SAC105-Fe-1Bi and SAC105-Fe-2Bi. It can interpret that due to effect of Bi on bulk of solder by solid solution effect, which Bi scatter in whole of bulk of solder therefore density of SAC105 solder increased slightly after addition of 0.05wt%Fe and 1wt.%Bi from 7.38 g/Cm^3 to 7.4 g/Cm^3 and consequently by increasing Bi to 2wt.% density become 7.41 g/Cm^3.

Table 4.7: Density of SAC105, SAC105-Fe-1Bi and SAC105-Fe-2Bi

Solder composition	Density(g/Cm^3)
SAC105	7.38
SAC105-0.05 Fe-1 Bi	7.4
SAC105-0.05 Fe-2 Bi	7.41

4.2 Sn-0.7Cu solder alloy bearing Fe and Bi

4.2.1 Mechanical properties

Figure 4.27 shows the stress–strain curves of the as-cast SC07, SC07-Fe, SC07-Fe-1Bi, andSC07-Fe-2Bi solder alloys. The yield stress, ultimate tensile strength (UTS), and total elongation for the four solder alloys tested are shown in Figure 4.28. It is clear that

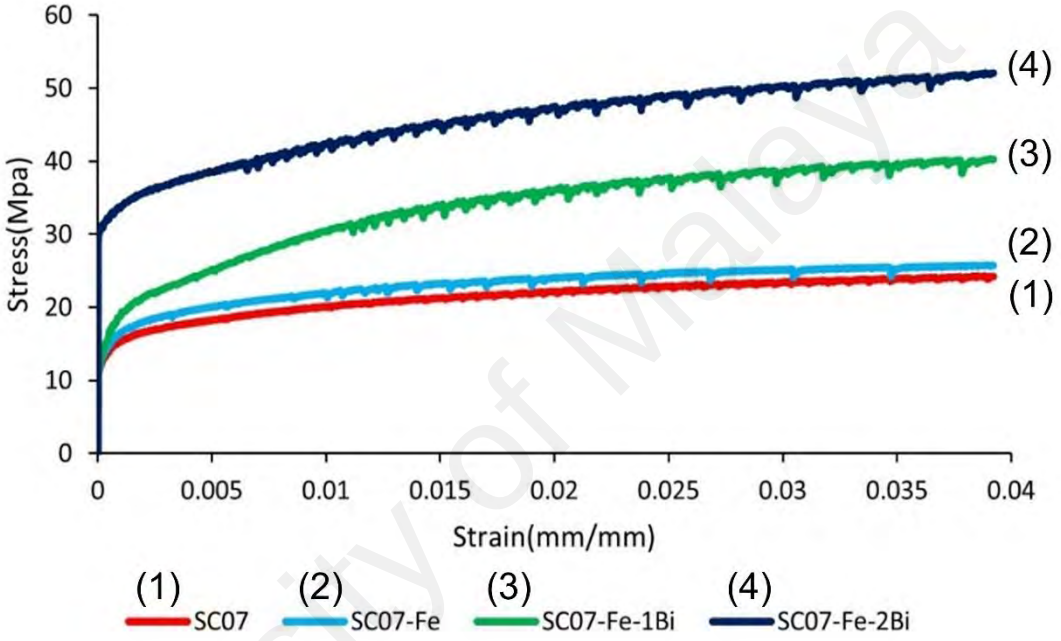

Figure 4.27: Stress- strain curves of SC07, SC07-Fe, SC07-Fe-1Bi and SC07-Fe-2Bi solders.

the addition of 0.05 wt.% Fe does not significantly affect the mechanical properties of the SC07 solder alloy. The addition of Fe increases the yield strength from 16.7MPa to 19.7MPa and keeps the UTS almost the same, whilst the total elongation is slightly decreased from 50% to 48%. On the other hand, the addition of Bi to the Fe-added SC07 solder alloy significantly affects the mechanical properties. The addition of 1 wt.% Bi increase the yield strength from 19.7MPa to 32.5MPa with 64% rise and increase the UTS two times from 27.4MPa to 55.64MPa, whilst the total elongation is significantly decreased from 48.5% to 40.4% with 20% drop. Increasing the amount of Bi to 2 wt%

increases the strengthening effect of Bi. The yield strength and UTS are further increased to 38.84MPa and 55.64MPa, respectively, while the total elongation is further decreased to 28%.

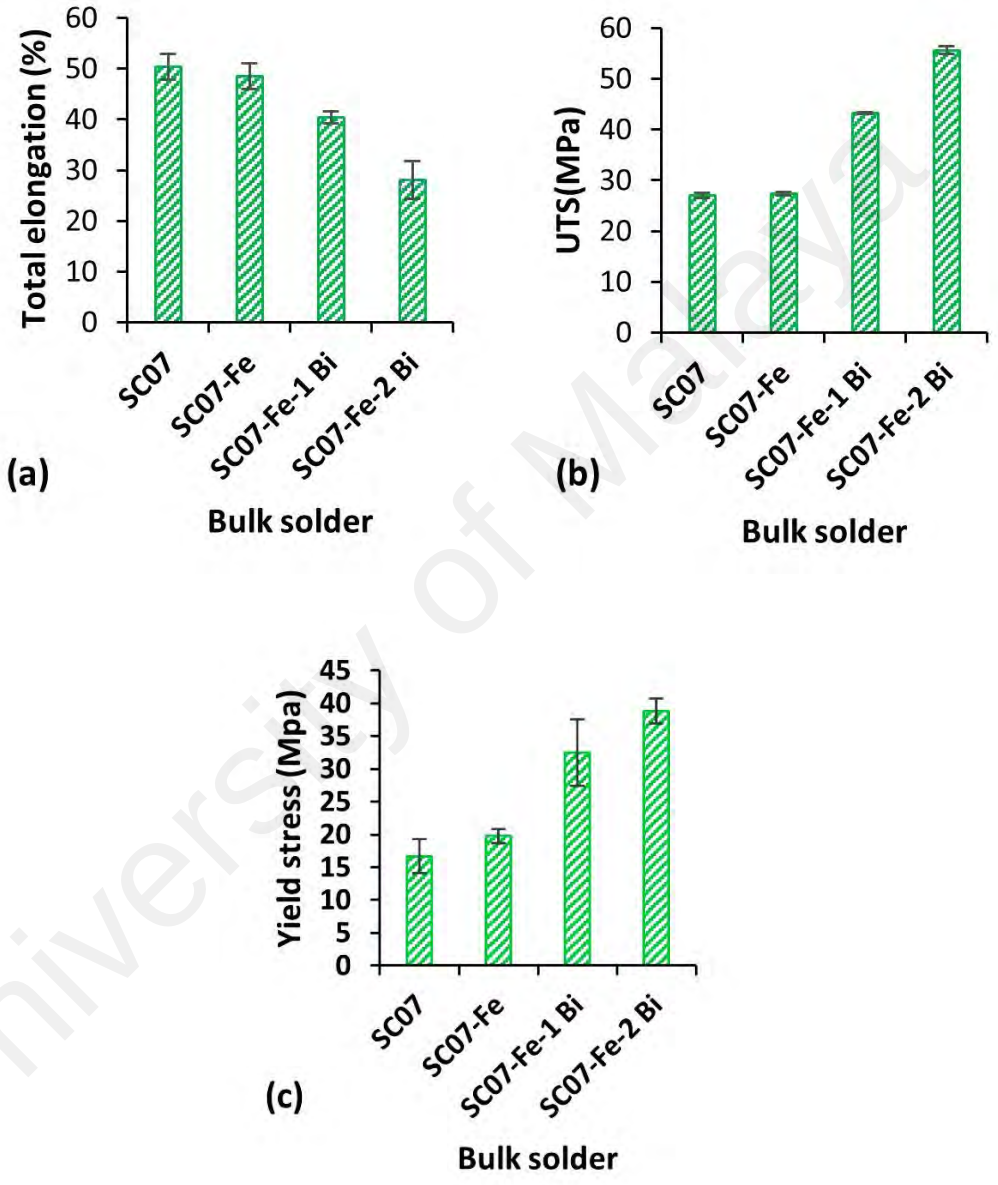

Figure 4.28: Tensile properties of SC07, SC07-Fe, SC07-Fe-1Bi and SC07-Fe-2Bi solders: (a) yield stress, (b) UTS, and (c) total elongation.

4.2.2 Microstructure properties

The FESEM micrographs of the as-cast microstructures of the SC07 and 0.05 wt.% Fe-added SC07 solder alloys are shown in Figure 4.29 (a) and (b). The microstructures of the two solder consist of primary β-Sn dendrites and thick interdendritic regions consisting of Cu_6Sn_5 IMC particles dispersed within a Sn-rich matrix. It is seen that the addition of 0.05 wt.% Fe does not change the type of IMC particles. However, it leads to form few $FeSn_2$ IMC particles in the interdendritic regions. The composition of IMC particles in the two samples was confirmed by EDX and XRD analyses, as shown in Table 4.8 and Figure 4.30 (a) and (b). Because of the low solubility of Fe in the β-Sn most of the Fe precipitates as the $FeSn_2$ phase or in the eutectic regions. The scanning element mapping in Figure 4.31 illustrates that the concentrations of Fe increase at the location of the $FeSn_2$, whereas the remaining Fe is distributed homogeneously within the microstructure, indicating a possible dissolution of Fe in the Cu_6Sn_5 IMC particles. However, EDX results did not show the presence of Fe in the Cu_6Sn_5 IMC particles (Table 4.8). Therefore, TEM observation was carried out (Figure 4.32 and 4.33) to investigate the inclusion of Fe into Cu_6Sn_5 IMC particles. Figure 4.32 shown TEM sample preparation in FEI. The TEM lamella was prepared by using FEI Helios NanoLab 650 Dual Beam system. It has both High Resolution Electron Beam and Finely Focused Ion Beam incorporated into the system. The TEM lamella was lifted out from the bulk sample and attached onto the Molybdenum grid finger using an in-situ lift out technique by means of Omniprobe needle. The TEM lamella was then thinned down to the electron transparency with the thickness of less than 100nm. Figure 4.33 shows a cross-sectioned TEM photograph of the as-cast SC07-Fe solder alloy with micro-electron-beam diffraction pattern. Micro-element analysis were utilized to determine IMC particles and primary β-Sn. EDX analysis and element mapping determined a small amount of Fe in Cu_6Sn_5 IMC particles. These observations are in agreement with the other studies on

microstructural properties of SAC105 solder alloy containing Fe in the range of 0.1 to 0.5 wt.% (Shnawah et al., 2015). The combined analysis of atomic radii and electronegativity which is known as the Darken–Gurry ellipse used to predict elements that would dissolve in solid solution (Anderson & Harringa, 2006). Fe falls inside the Darken-Gurry ellipse for substitution in place of Cu which in turn promotes the partial substitution of Fe into the Cu_6Sn_5 IMC particles. Fe atoms have -0.31% mismatch with Cu atoms. This partial substitution might produce increased lattice strain in the Cu_6Sn_5 IMC particles and, thus, to reduce the vacancy diffusion rate, resulting in a slowing of the microstructure coarsening rate (Anderson & Harringa, 2004).

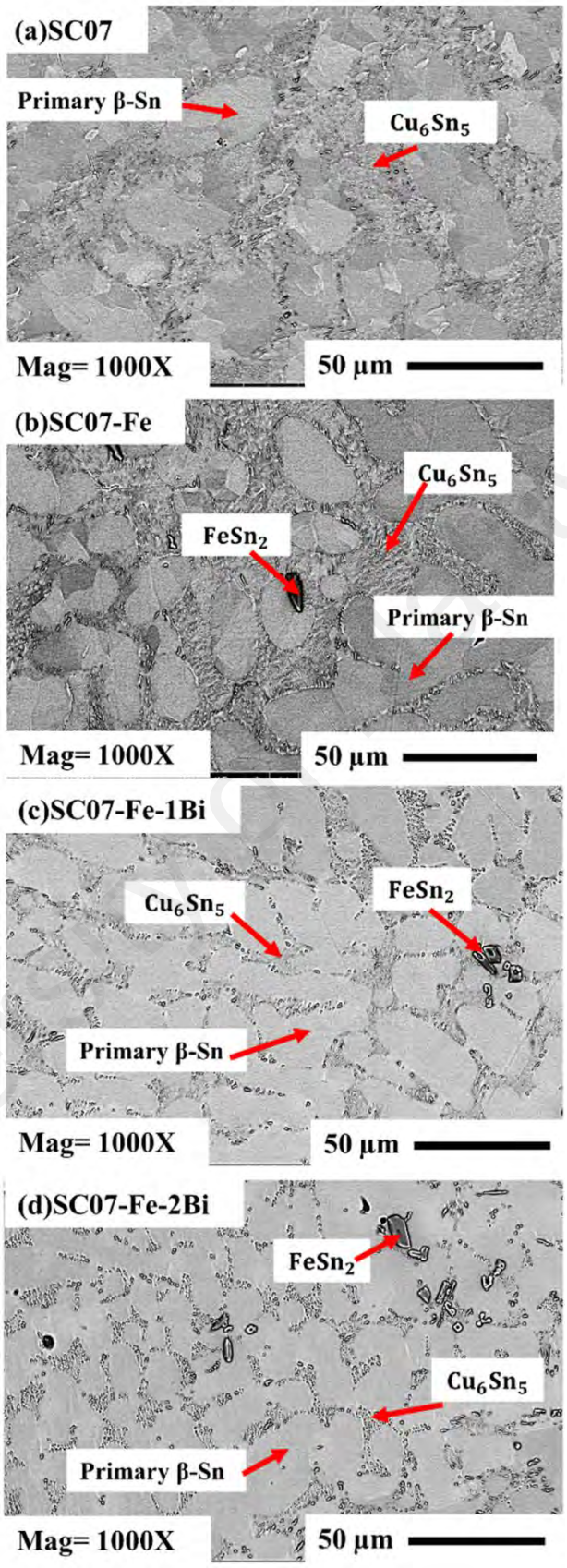

Figure 4.29: FESEM micrographs of as-cast SC07, SC07-Fe, SC07-Fe-1Bi and SC07-Fe-2Bi solder alloys.

Table 4.8: Chemical composition of IMCs in the SC07, SC07-Fe solders.

Composition	IMCs	Cu	Sn	Fe
SC07	Cu_6Sn_5	42.35 wt.% 57.84 at.%	57.65 wt.% 42.16 at.%	-
SC07-Fe	Cu_6Sn_5	41.64 wt.% 57.13 at.%	58.36 wt.% 42.87 at.%	-
	$FeSn_2$	-	76.36 wt.% 60.32 at.%	23.64 wt.% 39.68 at.%

Table 4.9: Chemical composition of IMCs in the SC07-Fe-1Bi and SC07-Fe-2Bi solders

Composition	IMCs	Cu	Sn	Fe
SC07-Fe-1Bi	Cu_6Sn_5	42.35 wt.% 57.84 at.%	57.65 wt.% 42.16 at.%	-
	$FeSn_2$	-	81.68 wt.% 67.86 at.%	18.32 wt.% 32.14 at.%
SC07-Fe-2Bi	Cu_6Sn_5	41.64 wt.% 57.13 at.%	58.36 wt.% 42.87 at.%	-
	$FeSn_2$	-	82.08 wt.% 68.42 at.%	17.92 wt.% 31.59 at.%

Figure 4.29 (c) and (d) shows the FESEM micrographs of the as-cast microstructures of the Fe-added SC07 solder alloy containing 1 and 2 wt.% Bi. The addition of Bi also does not change the type of IMC particles as shown in Table 4.9 and Figure 4.30 (c) and (d). However, the addition of Bi leads to a progressive degeneration in the interdendritic regions and a significant refinement in the primary β-Sn dendrites. The Cu_6Sn_5 IMCs become less-packed and its amount significantly decreases. Remarkably, the network-like eutectic regions degenerated into a chain-like arrangement. Experimental results obtained in the EDX element mapping shows that Bi is homogeneously distributed within the β-Sn matrix (Figure 4.31). The existence of Bi within the β-Sn matrix might reduce

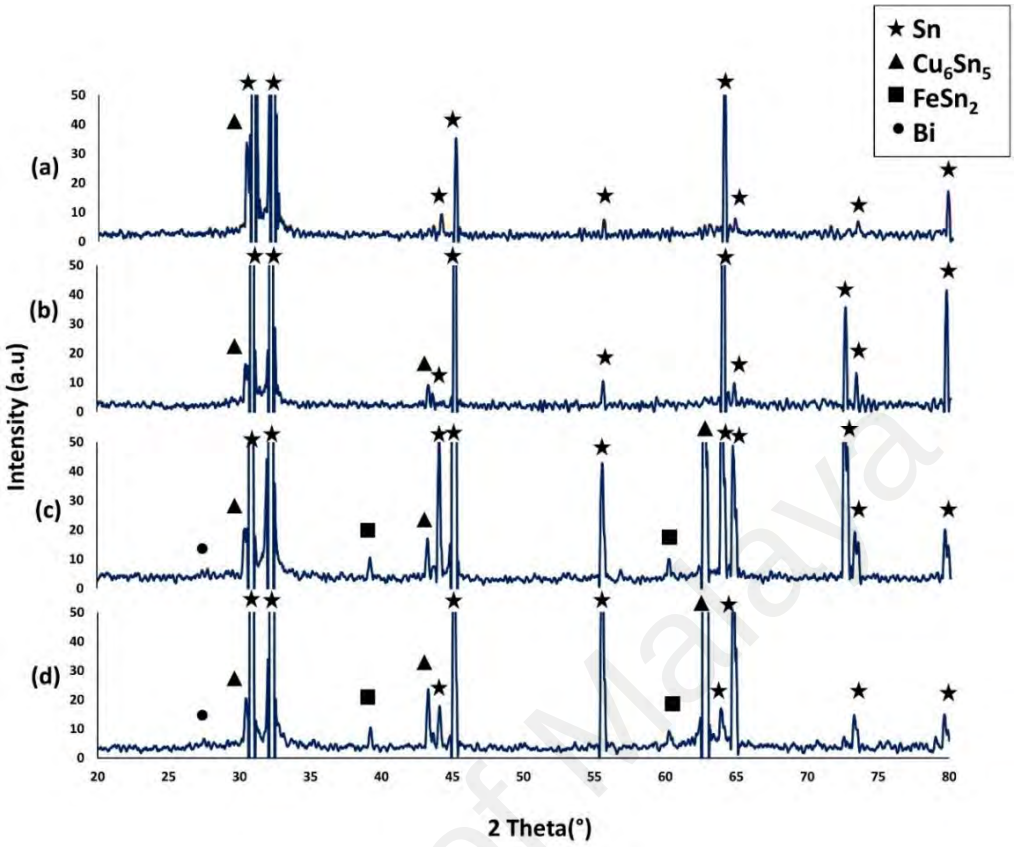

Figure 4.30: XRD result: (a) SC07, (b) SC07-Fe, (c) SC07-Fe-1Bi, and (d) SC07-Fe-2Bi solders

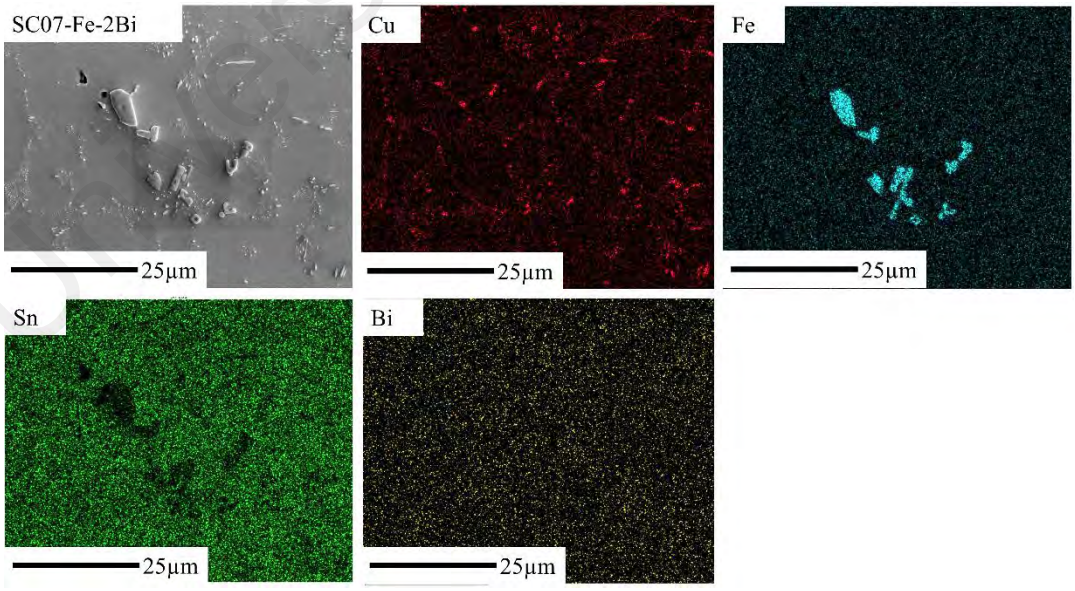

Figure 4.31: Elemental mapping analysis of SC07-Fe-2Bi solder alloy.

the activity of Sn involved in the chemical reaction between Sn and Cu during the solidification and hence reduces the amount of Cu_6Sn_5 IMC particles. However, there was not observed precipitation of Bi-rich particles in the solder alloys. It is therefore supposed that Bi super-saturated dissolved in the primary β-Sn phase and hence the microstructure of the Bi containing solder alloys is composed of β-Sn phase and Cu-Sn IMC. This can be attributed to the high solubility of Bi in Sn as the solid solubility limit of Bi in Sn at 120˚C is below 3% (Kattner & Boettinger, 1994). The quantitative data of the microstructural changes shown in Figure 4.34(a) demonstrate the observation above. The addition of Bi results in a lower area fraction of the eutectic Cu_6Sn_5 IMC as well as a higher area fraction of the β-Sn dendrites but a reduced dendritic size as shown in Figure 4.34(b). In Figure 4.35(a) shows the procedure of calculation of area percentage of Sn dendrites and IMCs in sample SC07-Fe-1Bi, and in Figure 4.35(b) shows the calculation of SDAS (secondary dendrite arm spacing) in sample SC07-Fe-1Bi. This method of calculation utilized for all samples and repeated 5 times for each composition and averaged the results.

It is obvious that the microstructural characteristics of an alloy determine its mechanical performance. Therefore, any change in the microstructural properties of an alloy will affect its mechanical performance.

The addition of 0.05 wt.% Fe does not significantly affect the microstructural properties of the SC07 solder alloy Figure 4.29a and b which is in agreement with the result of corresponding mechanical properties shown in Figure 4.28.

On the other hand, the significant microstructural changes resulted from Bi addition, such as the extended area fraction of the primary β-Sn with Bi dissolved, degenerated eutectic regions, coarsened and less-packed Cu_6Sn_5 IMC particles all contribute to strengthen the solder alloy. It is worthy to note that since Sn is considered to be soft due to its metallic bonding, whereas Cu_6Sn_5 IMCs are hard particles due to the strong covalent

bonding of these IMCs, it would seem that an increase in the amount of Sn and decrease in the amount of Cu_6Sn_5 in the present study would make the solder more ductile. However, the results stated above do not support this. There are two possible mechanisms which Bi strengthens the solder alloy. First, the refinement effect of Bi on the primary β-Sn dendrites resulted in finer microstructure. Second, the crystal lattice of primary β-Sn were distorted by the addition of Bi atoms. Table 4.10 shows the lattice constants of the Sn phases in the solder alloys. The lattice constant of Sn phase in the SC07 and SC07-Fe solders is almost the same. This indicates that the primary β-Sn phases in the SC07 and SC07-Fe solders are consists of almost entirely of Sn. This result agrees with Sn–Cu and Sn-Fe phase diagrams which show that the solubility of Cu and Fe in Sn is very low (Massalski et al., 1986). The lattice constant of the Sn phase in SC07-Fe-1Bi and SC07-Fe-2Bi slightly differs from that of the SC07. From the fact that the solubility of Cu and Fe in Sn is very low again, and from the Sn–Bi phase diagram (Massalski et al., 1986), it is considered that Bi solutes in the Sn phase and causes solid solution hardening of the Sn phase. The dissolution of Bi atoms in the β-Sn lattice distort the latter, thereby causing a local stress fields that act as a barrier to the mobility of dislocations which in turn make the solder exhibit higher yield strength and UTS. Therefore, the addition of Bi make the solder alloy stronger by solute mechanism.

Also, based on following calculation at.% of Bi is 1.75 in 98.25Sn-0.7Cu-0.05Fe-1Bi, atomic mass Bi is 209 g/mol and atomic mass Sn is 119 g/mol, therefore at.% Bi in Sn is: at.% Bi=((1×209)/((1×209)+(98.25×119)))×100=1.75. Therefore, the role of 1wt.% Bi at atomic level is higher and can have more effect on the crystal structure of Sn. Similarly, at.% of Bi in 98.25Sn-0.7Cu-0.0Fe-2Bi is 3.48.

Table 4.10: Lattice constants of the Sn phases in the solder alloys.

Solder composition	Lattice Parameter a=b (Å)	Lattice Parameter c (Å)	c/a	Volume of the unit cell Å^3
Sn-0.7Cu	5.8049	3.1698	0.54605592	106.8123
Sn-0.7Cu-0.05Fe	5.8014	3.1494	0.54286896	105.997
Sn-0.7Cu-0.05Fe-1Bi	5.8243	3.1570	0.54203939	107.0932
Sn-0.7Cu-0.05Fe-2Bi	5.8571	3.1640	0.54019907	108.543

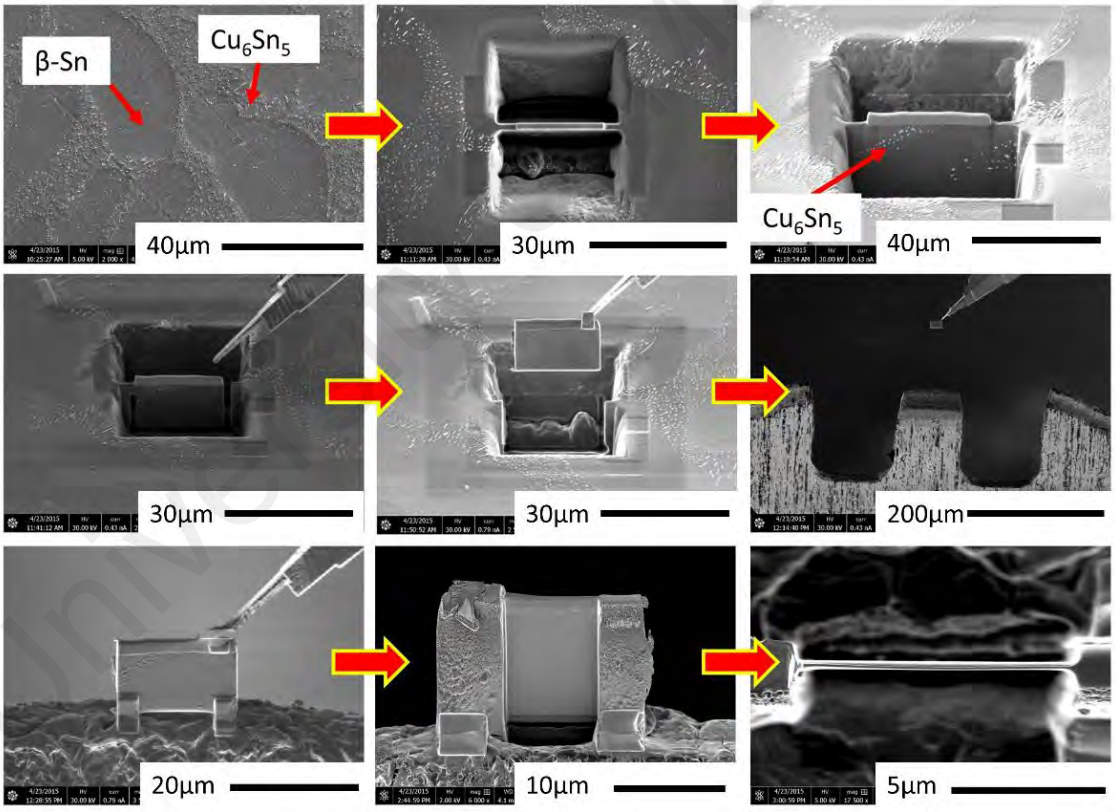

Figure 4.32: TEM sample preparation in a FEI.

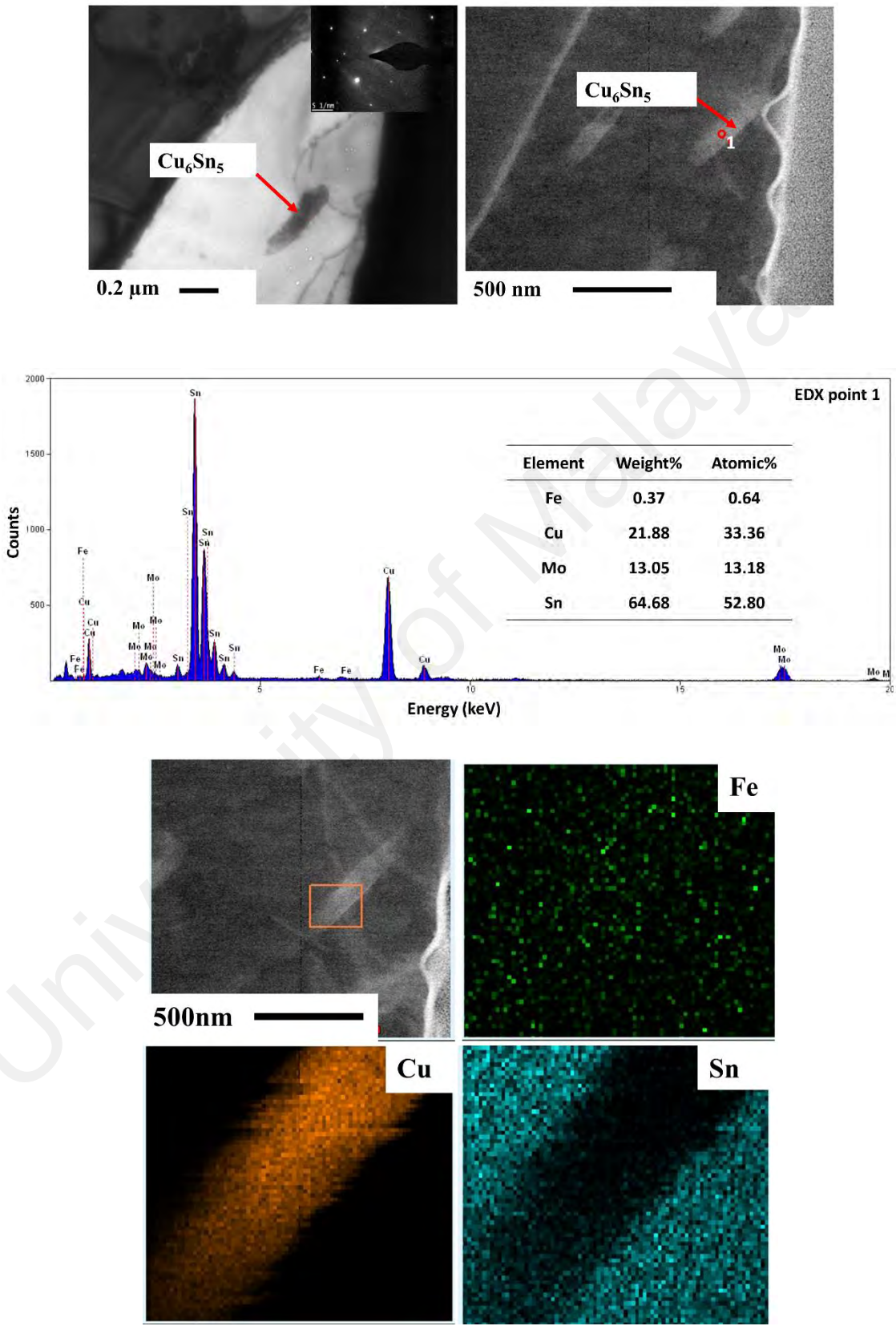

Figure 4.33: Bright field STEM image of SC07-Fe sample and corresponding EDX and elemental maps.

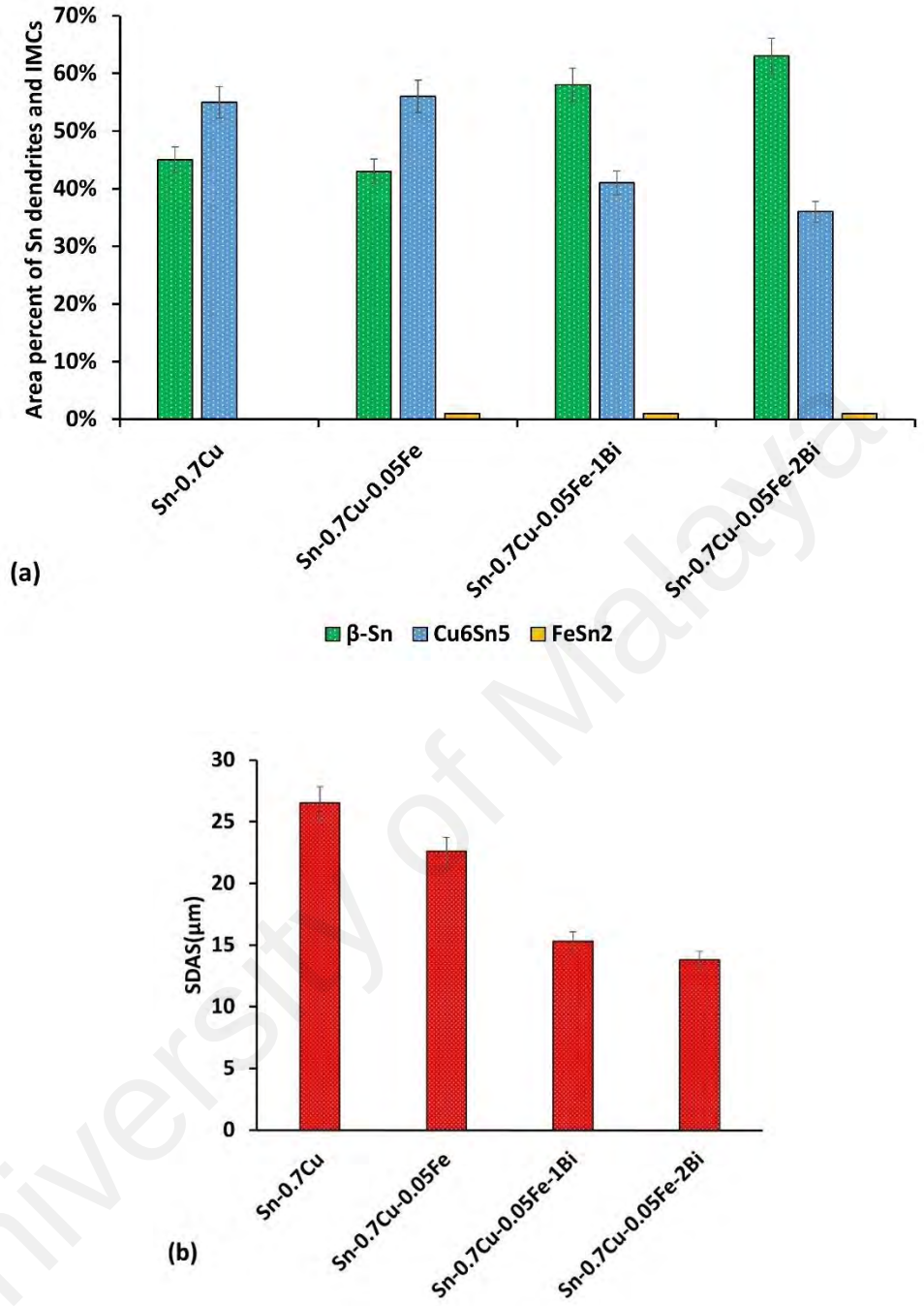

Figure 4.34: Quantitative data of the microstructure of the solders: (a) area fractions of the phases and (b) secondary dendrite arm spacing (SDAS) of Sn dendrites.

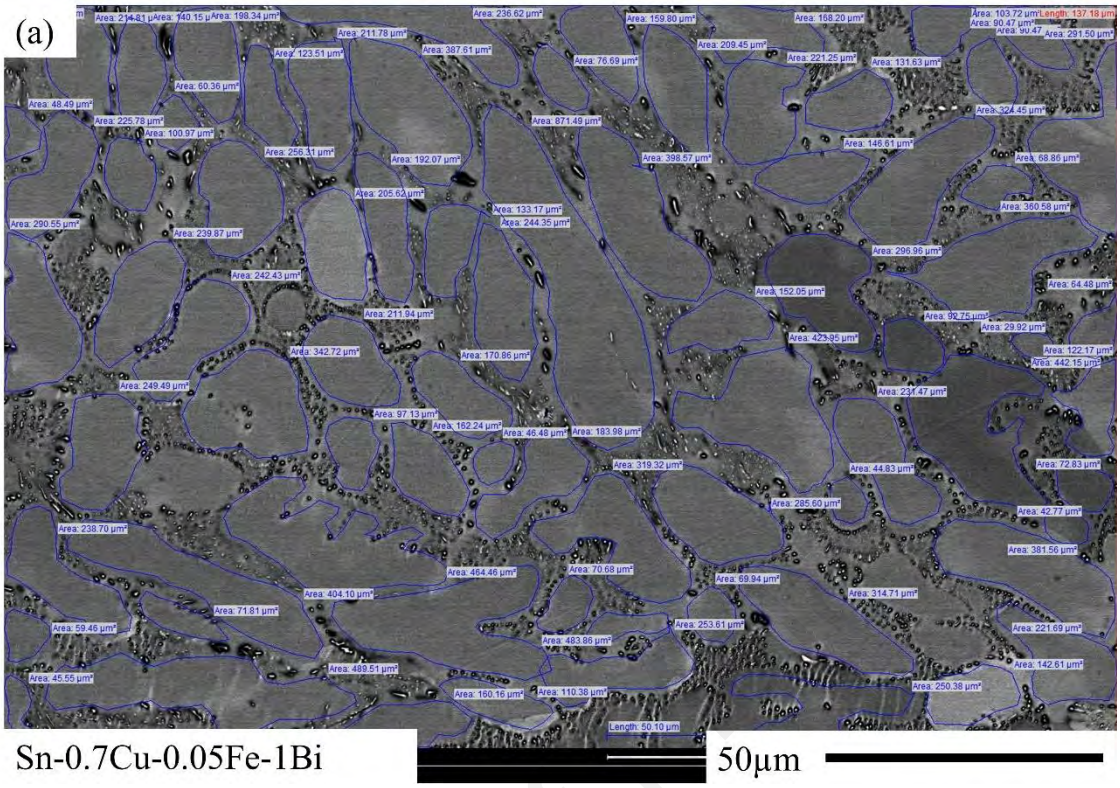

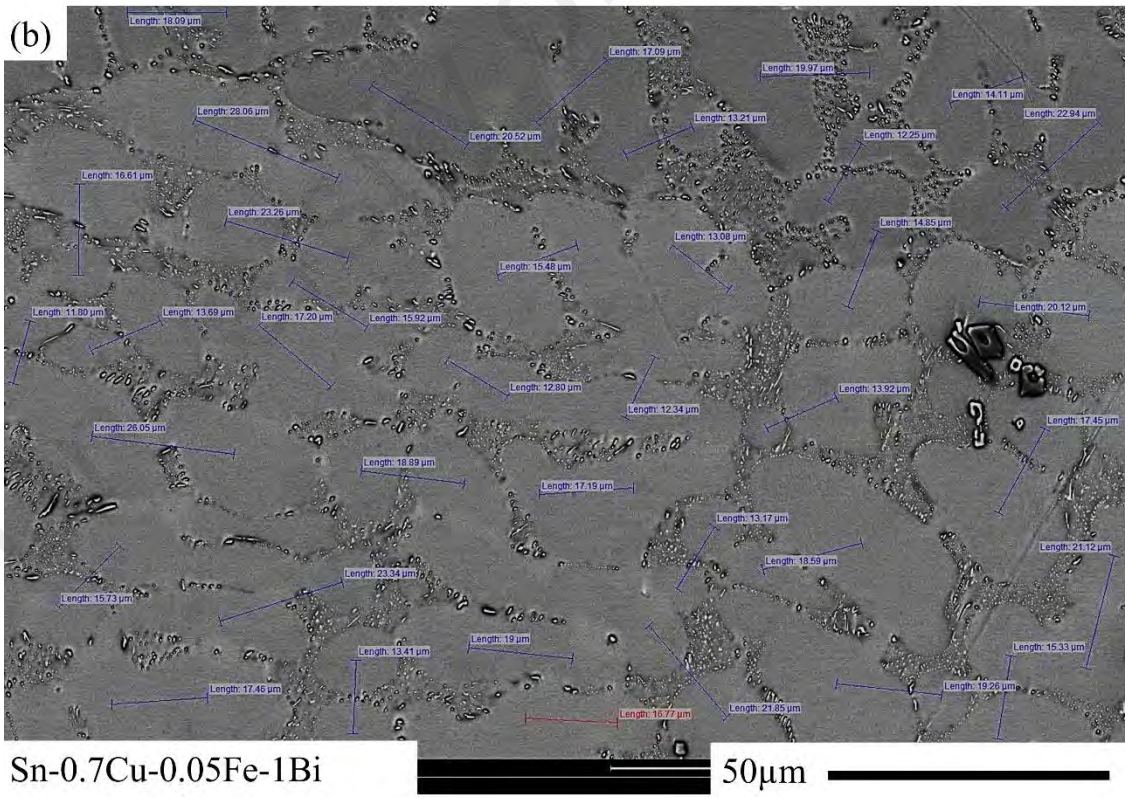

Figure 4.35: (a)Calculation of area fractions of the phases, (b) Calculation of secondary dendrite arm spacing (SDAS) of Sn dendrites.

4.2.3 Fracture behavior

The fracture surfaces of the tensile test samples were checked after tensile test to study the effects of Bi and Fe additions to the SC07 solder alloy. The necking clearly occurs in the SC07 and Fe-added SC07 specimens, specifying that the fracture is ductile (Figure 4.36 (a) and (c)). The FESEM micrographs of the fracture surfaces of the SC07 and Fe added SC07 solder alloys are shown in Figure 4.36 b and d. It can clearly recognize the large ductile-dimples on the fracture surface of the two solders owing to a microvoid formation. The microvoids coalesce to form cracks, and then cracks propagate through the necking, finally leading to failure. In these solder alloys, it is quite possible that voids nucleate at the β-Sn/Cu_6Sn_5 IMC interface and make stress concentration around Cu_6Sn_5 IMC particles during the tensile test. The primary β-Sn will become extended along the loading direction during the tensile test. There is internal stress between the matrix and the particles because the plastic deformation of the soft β-Sn matrix is not related to that of the hard Cu_6Sn_5 IMC particles. Stress increases and when it becomes large enough a microvoid nucleates at the interface. So, the source of the microvoids nucleation are IMCs. Then, by applying stress the microvoids grow in both the longitudinal and cross directions and they coalesce until the sample necks down. This indicates that the deformation of SC07 and Fe-added SC07 solders are governed by the plastic deformation of primary β-Sn matrix, which consists almost entirely of Sn. Therefore, the mode of fracture does not affect by the addition of Fe to the SC07 solder alloy. However, the necking is reduced with the addition of 1 wt.% Bi, as shown in Figure 4.36 (e). The FESEM micrograph of the fracture surfaces of the SC07-Fe-1Bi is shown in Figure 4.36 (f). It is clear that the addition of 1 wt.% Bi reduces the number and size of the dimples on the fracture surface which indicates that the addition of 1 wt.% Bi reduces the plastic deformation of the primary β-Sn phase during tensile testing. This can be attributed to the solid solution hardening of the Sn phase by Bi as well as the hard and brittle nature of Bi.

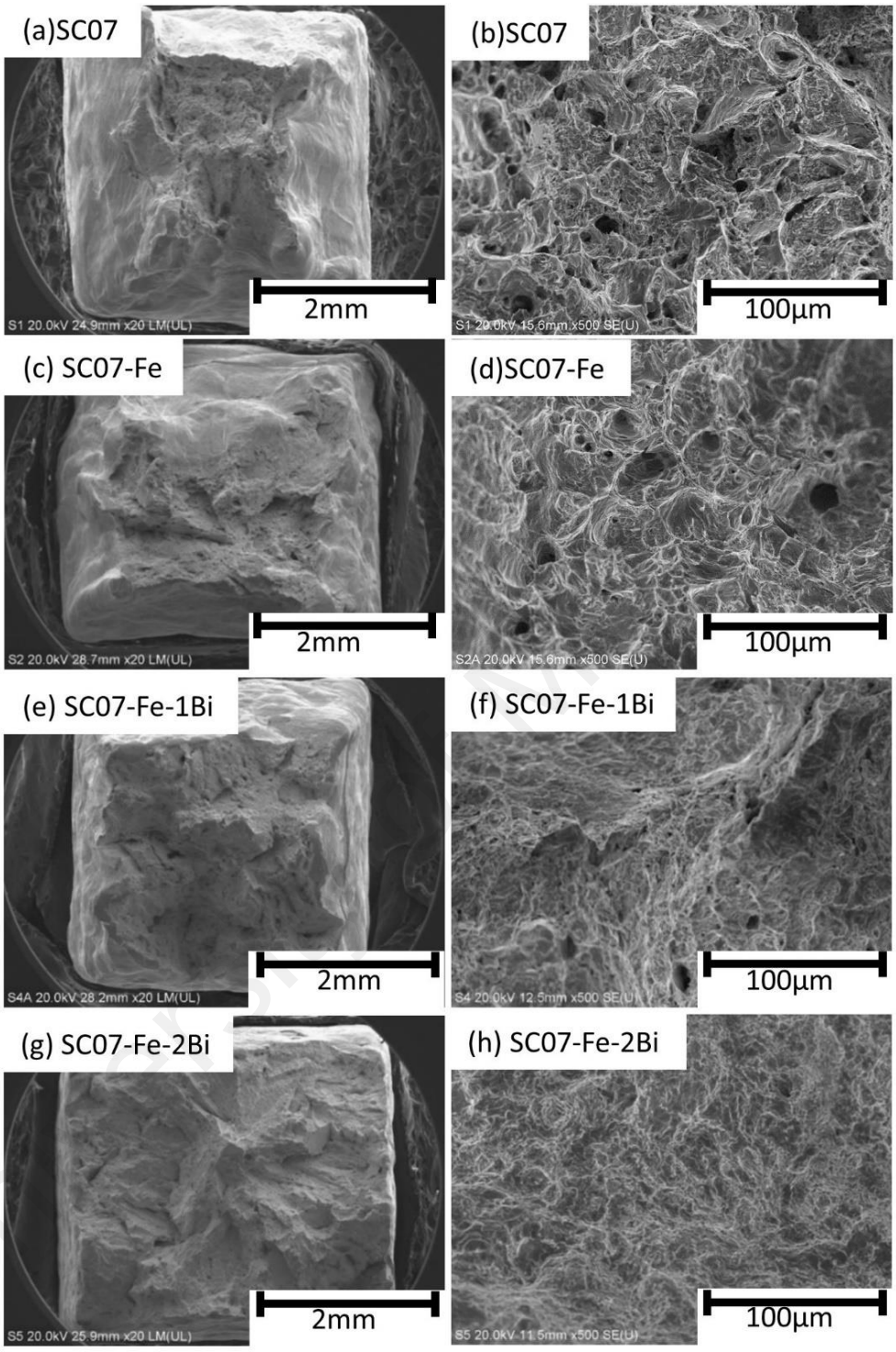

Figure 4.36: SEM fractographs of the alloys after tensile tests (a) and (b) SC07, (c) and (d) SC07-Fe, (e) and (f) SC07-Fe-1Bi, (g) and (h) SC07-Fe-2Bi.

Therefore SC07-Fe-1Bi solder shows lower elongation and higher tensile strength than those of the SC07 and SC07-Fe solders. On the other hand, the tensile test specimens of

the SC07-Fe-2Bi solder do not neck at all (Figure 4.36 (g)) and the fractured surfaces are flat, indicating brittle cleavage fracture, as shown in Figure 4.36 (h). From these observations of the morphology of fractured surfaces, no deformation in the primary β-Sn phase occurred in the SC07-Fe-2Bi solder. This can be attributed to increase the amount of Bi atoms in the primary β-Sn phase which makes the solder do not deform in the β-Sn phase during testing. Therefore, the addition of 2 wt.% Bi further decreases the elongation, whereas the tensile strength is further increased.

4.2.4 Thermal behavior

DSC analysis were utilized to investigate the effect of Fe and Bi additions on the melting behavior of the SC07 solder alloy. Figure 4.37 shows the endothermic DSC peaks of the samples upon heating. The heating curves in Figure 4.37 reveal that SC07-Fe, SC07-Fe-1Bi, andSC07-Fe-2Bi solder alloys exhibit one endothermic peak similar to that of the SC07 solder. However, the addition of Bi shifted the endothermic peak to the left. Table 4.11 shows the solidus and liquidus temperatures and the pasty range of the solder alloys. As illustrated, Fe addition has a negligible effect on the melting behavior. On the other hand, the addition of Bi reduces the solidus and liquidus temperatures and the pasty range. The addition of 1 wt.% Bi decreases the liquidus temperature from 232.3˚C to 228.9˚C, the solidus temperature from 227.6˚C to 224.5˚C, and the pasty range is decreased from 4.7 to 4.4. The addition of 2 wt.% Bi further decreases the liquidus, and solidus temperatures and the pasty range to 228.1˚C, 223.8˚C, and 4.3 respectively. Thus, the addition of Bi to the Fe-modified SC07 solder alloy decreases the melting point.

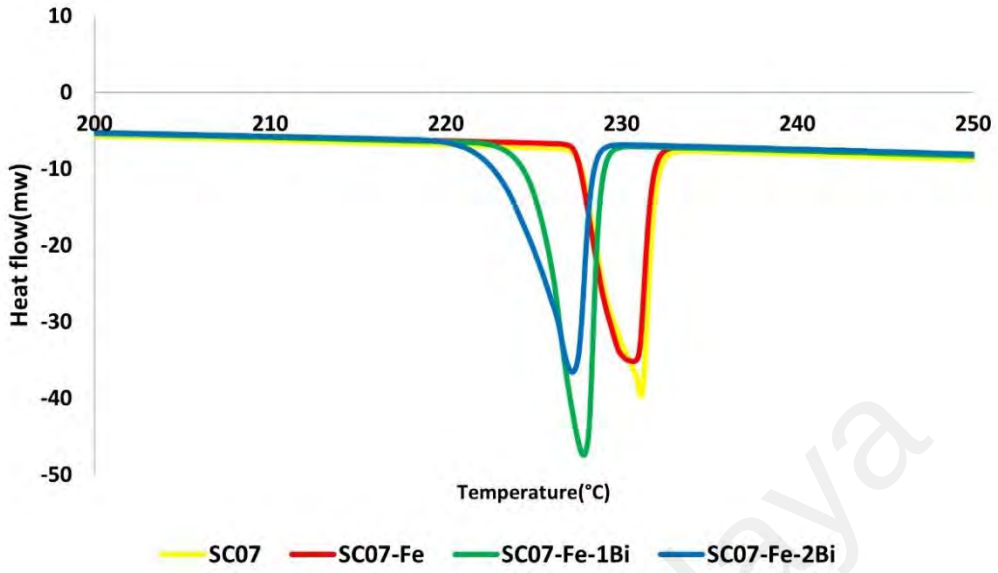

Figure 4.37: DSC thermographs of SC07, SC07-Fe, SC07-Fe-1Bi, and SC07-Fe-2Bi solders.

Table 4.11: Differential scanning calorimetry (DSC) test results of the alloys.

Alloys	Solidus temp. Ts (˚C)	Liquidus temp. Tl (˚C)	Pasty range
SC07	227.6	232.3	4.7
SC07-Fe	227.4	232.1	4.7
SC07-Fe-1Bi	224.5	228.9	4.4
SC07-Fe-2Bi	223.8	228.1	4.3

4.2.5 Aging effect

4.2.5.1 Mechanical properties

The mechanical properties of solder alloys include yield stress, ultimate tensile strength (UTS), and total elongation for as cast, aged at 125 °C for 30-days and aged at 180 °C for 1-day solder alloys are shown and compared in Figure 4.38. Aging at 180 °C for 1-day determine solders properties in automobile application. The current work focuses on aging at 125 °C for 30-days which is more common in electronic application.

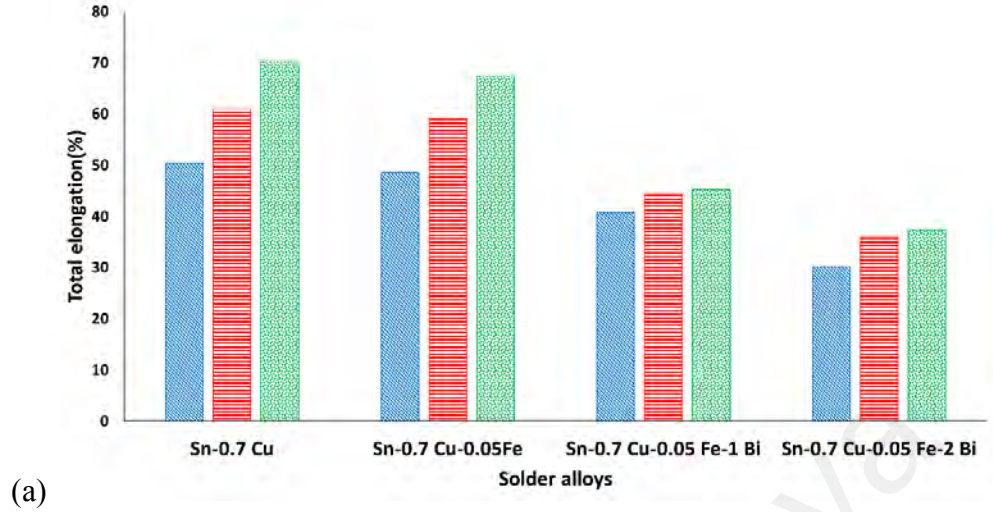

(a)

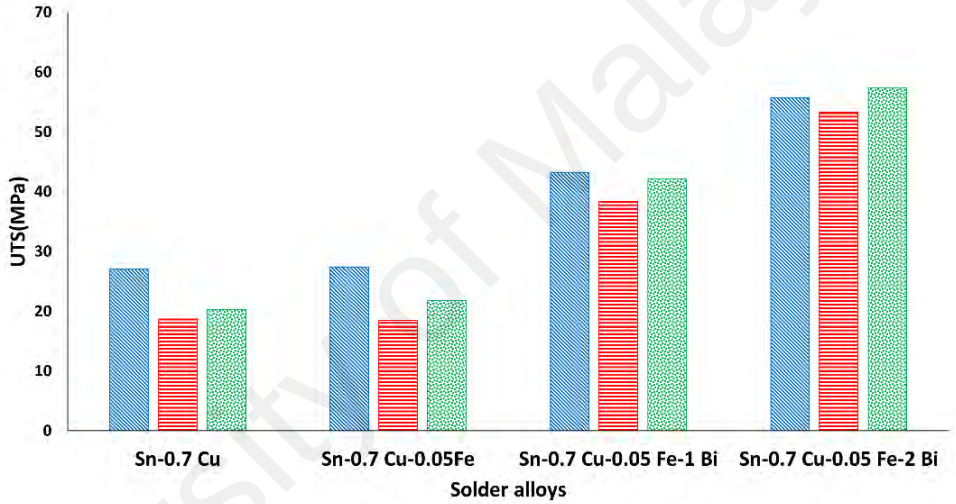

(b)

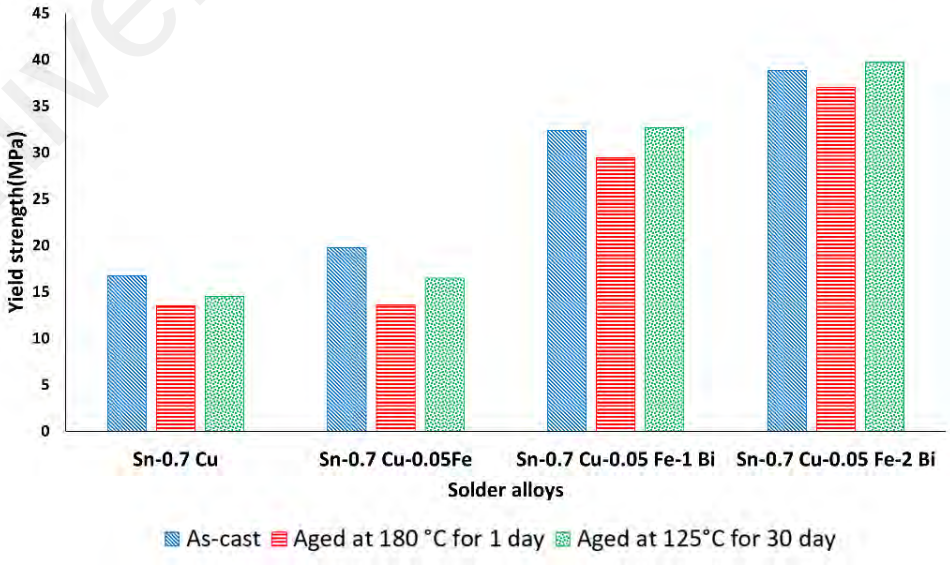

(c)

Figure 4.38: (a)total elongation, (b) ultimate tensile strength (UTS), (c) yield stress, for as cast, aged at 125 °C for 30-days and aged at 180 °C for 1-day solders.

For as cast samples, adding Fe to SC07 does not have considerable effect on UTS, yield strength and total elongation of SC07. But, by adding Bi to SC07-Fe UTS and yield strength increased whereas total elongation decreased. It is considered that Bi solutes in the Sn phase and causes solid solution hardening of the Sn phase. The dissolution of Bi atoms in the β-Sn lattice distort the latter, thereby causing a local stress fields that act as a barrier to the mobility of dislocations which in turn make the solder exhibit higher yield strength and UTS.

After SC07 aged at 125°C for 30 days UTS decreased from 27MPa to 20 MPa and yield strength decreased from 16.7MPa to 14MPa. Adding Fe does not have considerable effect on these properties. Total elongation for SC07 and SC07-Fe increased after aging, because the number of second phase decreased, therefore total elongation increased slightly. But UTS, Yield strength and total elongation for sample with Bi are approximately constant. Because Bi prevent the Cu and Sn to interact with each other, therefore spheroidization and growth of IMCs after aging slowed down and decreased the rate of IMCs coarsening.

4.2.5.2 Microstructure properties

The FESEM micrographs of the as-cast and Aged microstructures of the SC07 and 0.05 wt.% Fe-added SC07 solder alloys are illustrated in Figure 4.39. The composition of IMC particles in the two samples was confirmed by EDX and XRD analyses, the elemental mapping results are shown in Figure 4.40. The microstructures of the as cast solder consist of primary β-Sn dendrites and thick interdendritic regions consisting of Cu_6Sn_5 IMC particles dispersed within a Sn-rich matrix. It is seen that the addition of 0.05 wt.% Fe does not change the type of IMC particles. However, it leads to form few $FeSn_2$ IMC particles in the interdendritic regions. Because of the low solubility of Fe in the β-Sn most of the Fe precipitates as the $FeSn_2$ phase or in the eutectic regions.

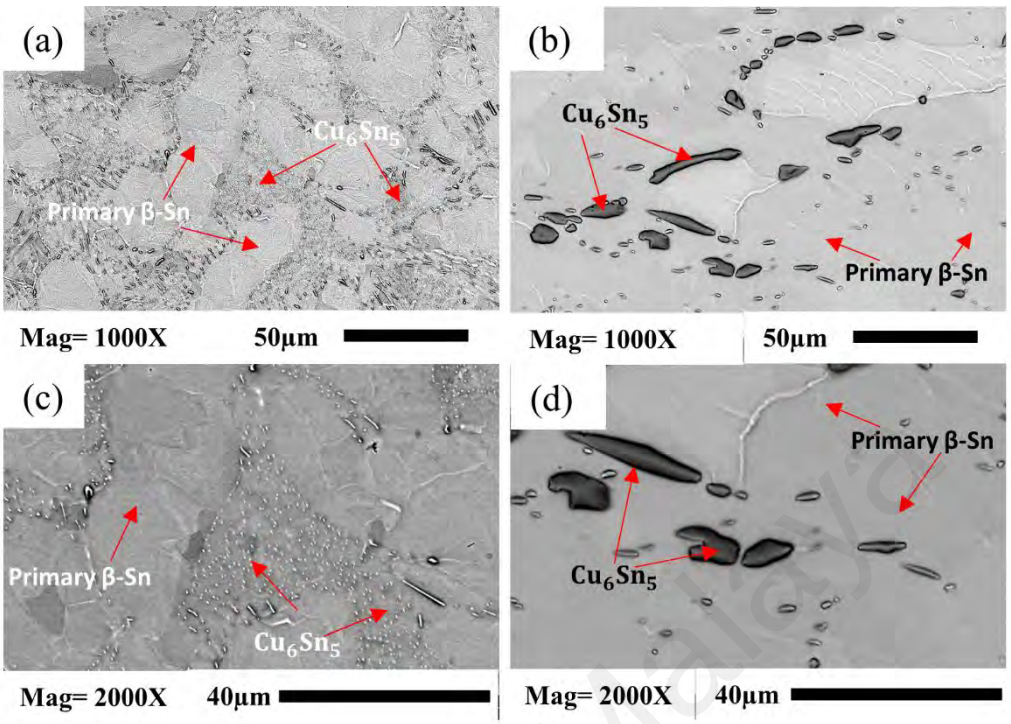

Figure 4.39: FESEM of SC07, (a) and (c) for as cast samples, (b) and (d) for sample after aging at 125°C for 30 days.

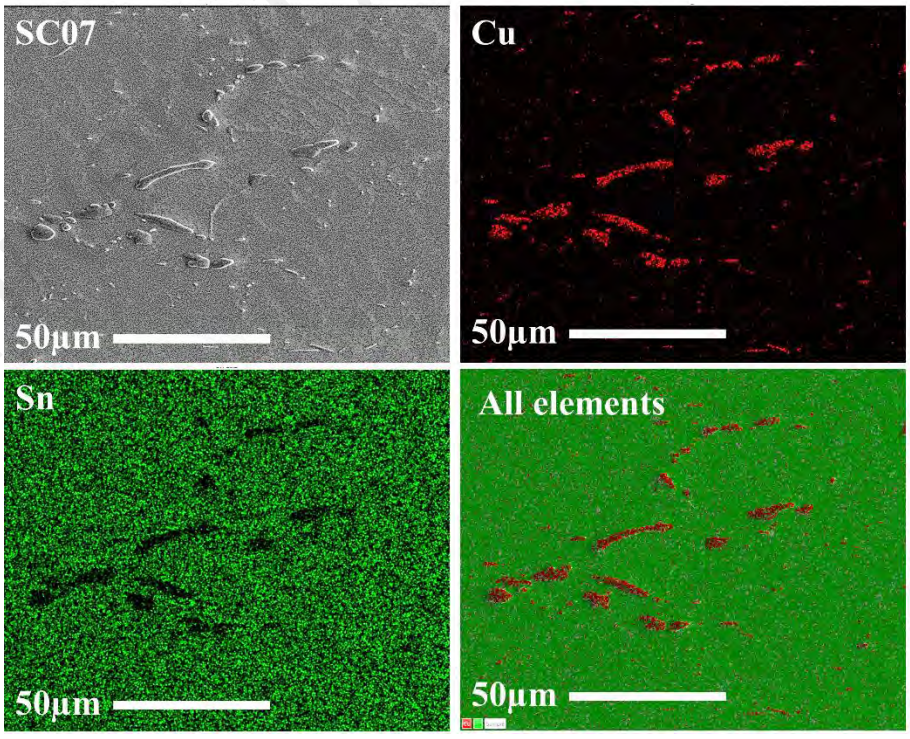

Figure 4.40: Elemental mapping of SC07.

It is observed for SC07 after aging, Figure 4.39(b), the growth and spheroidization of Cu_6Sn_5 controlled by Gibbs–Thomson effect(Song & Lin, 2003) . The surface free energy of the intermetallic phase decrease as result of the spheroidization and growth of Cu_6Sn_5. The interface of Cu_6Sn_5 and Sn matrix prepare a heterogeneous region for the interaction between Cu and Sn. The Cu dissolved in Sn-rich phase and resulted in the growth of Cu_6Sn_5. It illustrates that Cu and Sn segregates at the surrounding of the Cu_6Sn_5 intermetallic phase and then forms the new intermetallic phase at the determined concentration. This procedure leaded to the growth of IMCs(Hsuan & Lin, 2007).

Figure 4.41 shows FESEM result for SC07-Fe before and after aging. Figure 4.42 shows elemental mapping for SC07-Fe. The combined analysis of atomic radii and electronegativity which is known as the Darken–Gurry ellipse used to predict elements that would dissolve in solid solution (Anderson & Harringa, 2006). Fe falls inside the Darken-Gurry ellipse for substitution in place of Cu. Therefore, Fe can partially substitute into the Cu_6Sn_5 IMC particles. Fe atoms have -0.31% mismatch with Cu atoms. This partial substitution might produce increased lattice strain in the Cu_6Sn_5 IMC particles and reduce the vacancy diffusion rate. Thus, it decrease microstructure coarsening rate (Anderson & Harringa, 2004).

Due to the coarsening of IMCs yield strength and UTS decreased for SC07 after aging. For SC07-Fe the trend is same for yield strength and UTS, however because of Fe they drop less in compare to SC07.

Figure 4.43, 4.44, and 4.45 shown the FESEM micrographs and elemental mapping of the as-cast and aged microstructures of the Fe-added SC07 solder alloy containing 1 and 2 wt.% Bi respectively. The addition of Bi also does not change the type of IMC particles. However, Bi leads to a progressive degeneration in the interdendritic regions and a significant refinement in the primary β-Sn dendrites. The Cu_6Sn_5 IMCs become less-packed and its amount significantly decreases. The size Cu_6Sn_5 IMCs decreased

progressively by addition of Fe and Bi to SC07 (from 9μm for SC07 to 2 μm for SC07-Fe-2Bi) as shown in Figure 4.46 which measured from FESEM microstructure result. Remarkably, the network-like eutectic regions degenerated into a chain-like arrangement. It is therefore supposed that Bi super-saturated dissolved in the primary β-Sn phase and hence the microstructure of the Bi containing solder alloys is composed of β-Sn phase and Cu-Sn IMC. This can be attributed to the high solubility of Bi in Sn as the solid solubility limit of Bi in Sn at 120˚C is below 3% (Kattner & Boettinger, 1994). The addition of Bi results in a lower area fraction of the eutectic Cu_6Sn_5 IMC as well as a higher area fraction of the β-Sn dendrites. The correlation between microstructural characteristics and its mechanical performance are obvious. Therefore, any change in the microstructural properties of an alloy will affect its mechanical performance.

After aging, Bi prevented coarsening of IMCs. The existence of Bi within the β-Sn matrix reduce the activity of Sn involved in the chemical reaction between Sn and Cu during the solidification and hence reduces the amount of Cu_6Sn_5 IMC particles.

Figure 4.47 shows area fractions of the phases for as cast samples and aged samples at 125°C for 30 days. Obviously percentage of Cu_6Sn_5 after aging drop for all samples, for SC07 from 55% area fraction as cast to 6% after aging, for SC07-Fe-2Bi from 40% area fraction as cast to 4% after aging. However, for samples with Bi Cu_6Sn_5 scatter in whole are, but for samples without Bi, Cu_6Sn_5 concentrate at some points, therefore the number of Cu_6Sn_5 are higher in samples with Bi in compare to samples without Bi. On the other hand, Sn is considered to be soft due to its metallic bonding, whereas Cu_6Sn_5 IMCs are hard particles due to the strong covalent bonding of these IMCs, it would seem that an increase in the amount of Sn and decrease in the amount of Cu_6Sn_5 in the present study would make the solder more ductile. However, for SC07-Fe-1or2Bi samples total elongation increased a little, which is related to the solid solution hardening mechanism of Bi that make solder strong and brittle.

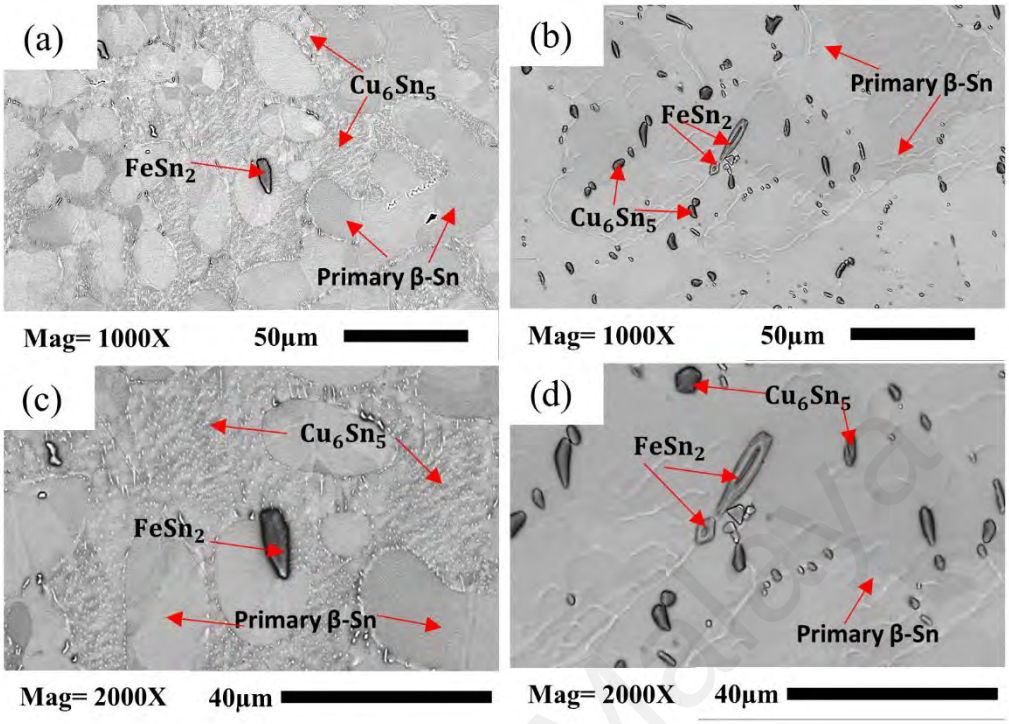

Figure 4.41: FESEM of SC07-Fe, (a) and (c) for as cast samples, (b) and (d) for sample after aging at 125°C for 30 days.

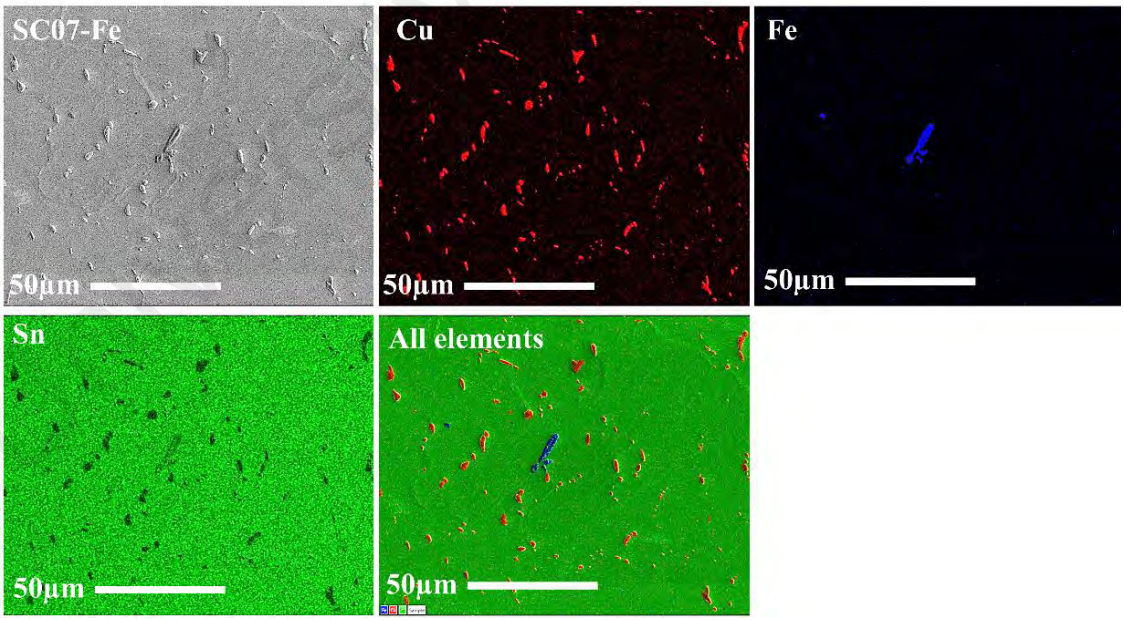

Figure 4.42: Elemental mapping of SC07-Fe.

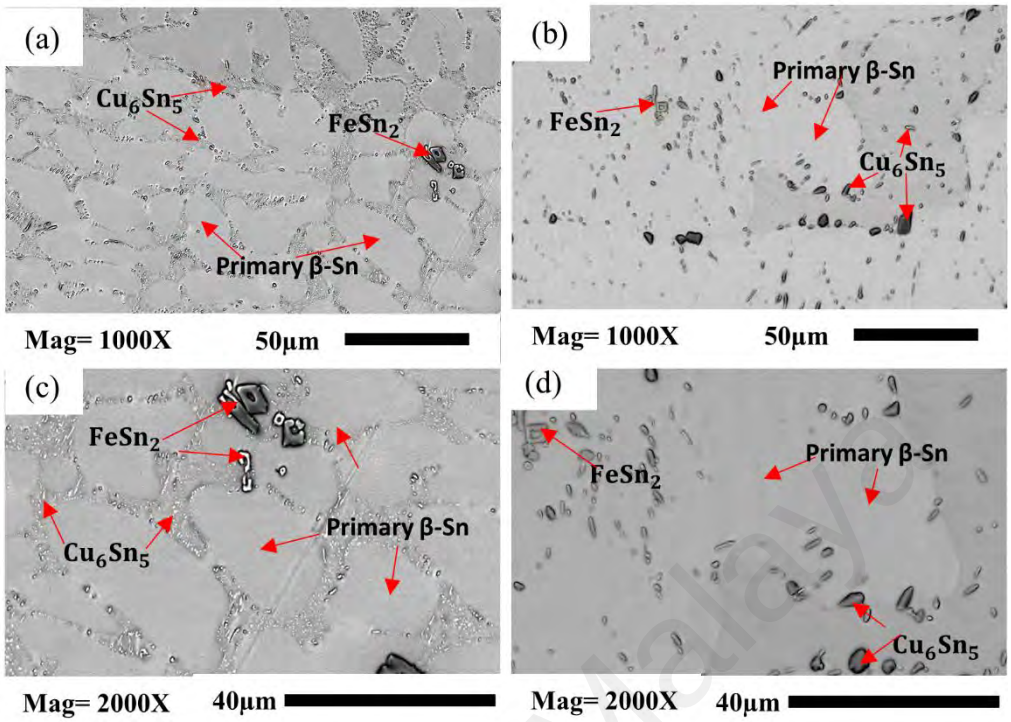

Figure 4.43: FESEM of SC07-Fe-1Bi, (a) and (c) for as cast samples, (b) and (d) for sample after aging at 125°C for 30 days.

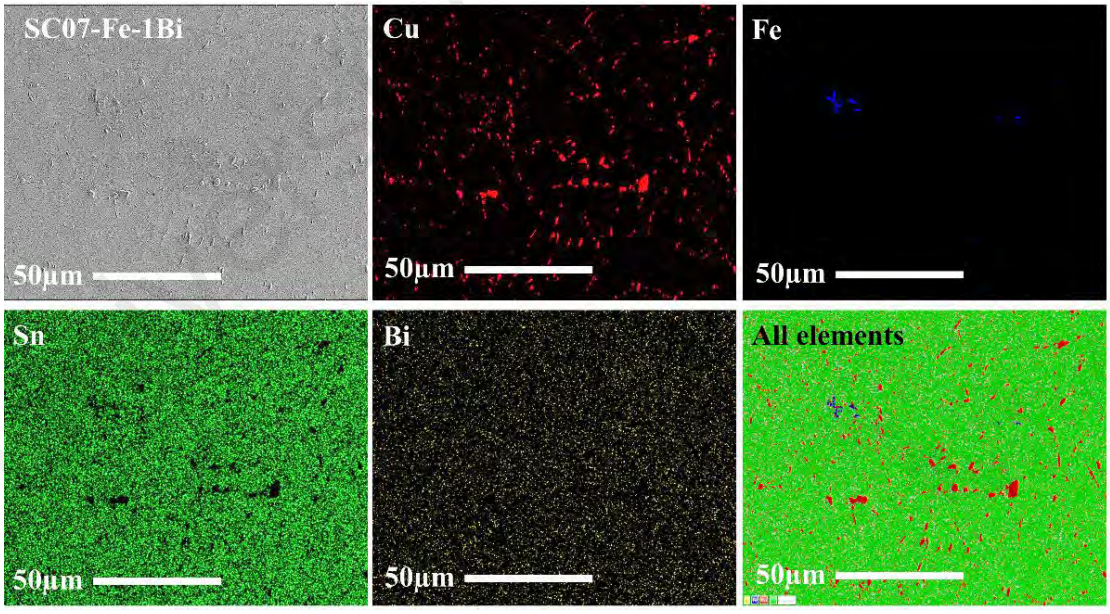

Figure 4.44: Elemental mapping of SC07-Fe-1Bi.

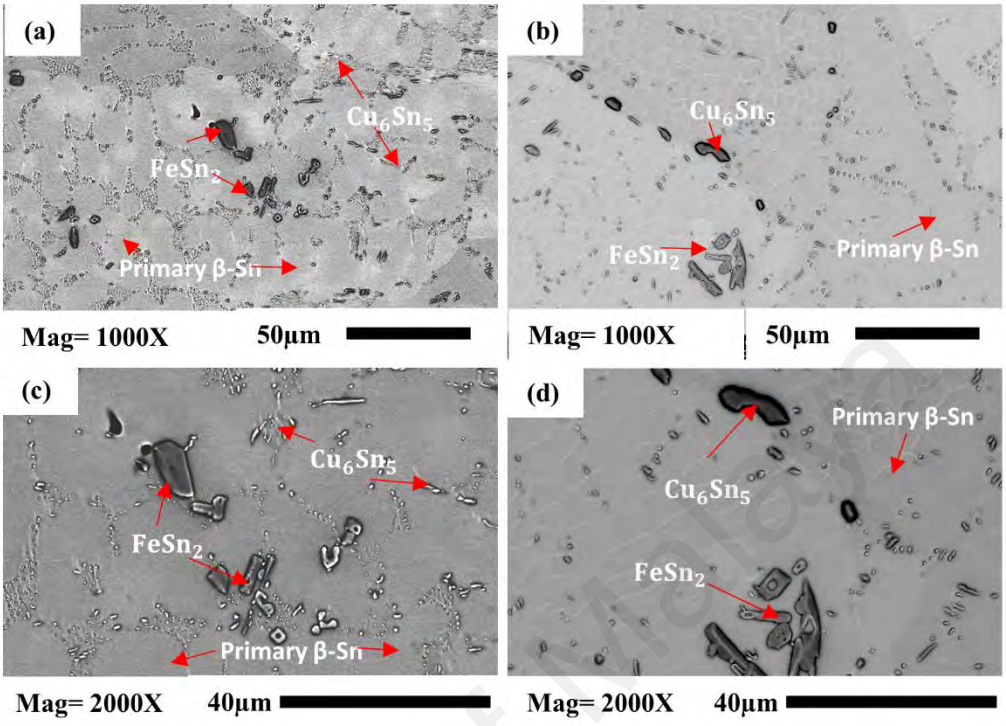

Figure 4.45: FESEM of SC07-Fe-2Bi, (a) and (c) for as cast samples, (b) and (d) for sample after aging at 125°C for 30 days.

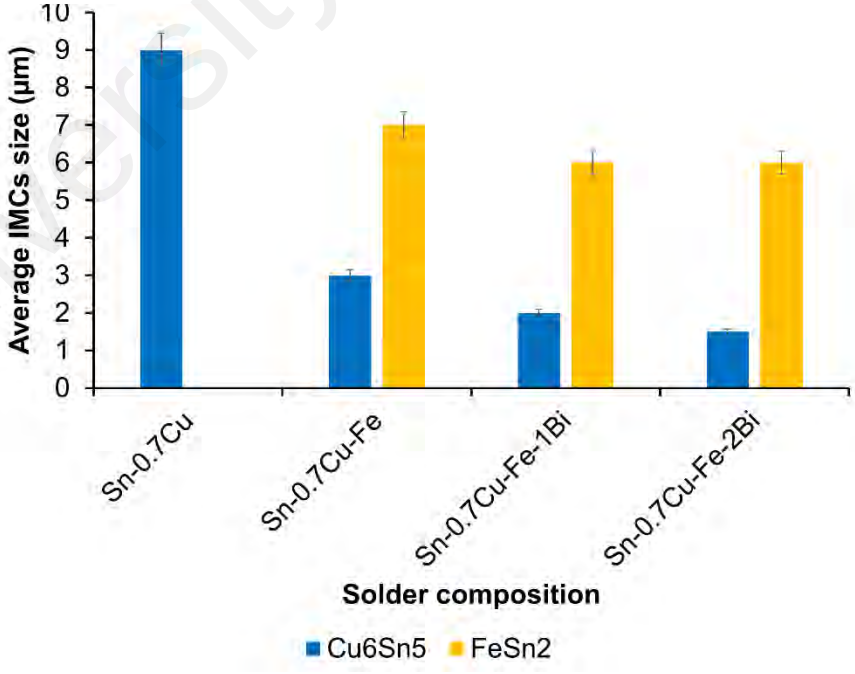

Figure 4.46: Average IMCs size after aging at 125°C for 30 days for SC07, SC07-Fe, SC07-Fe-1Bi and SC07-Fe-2Bi.

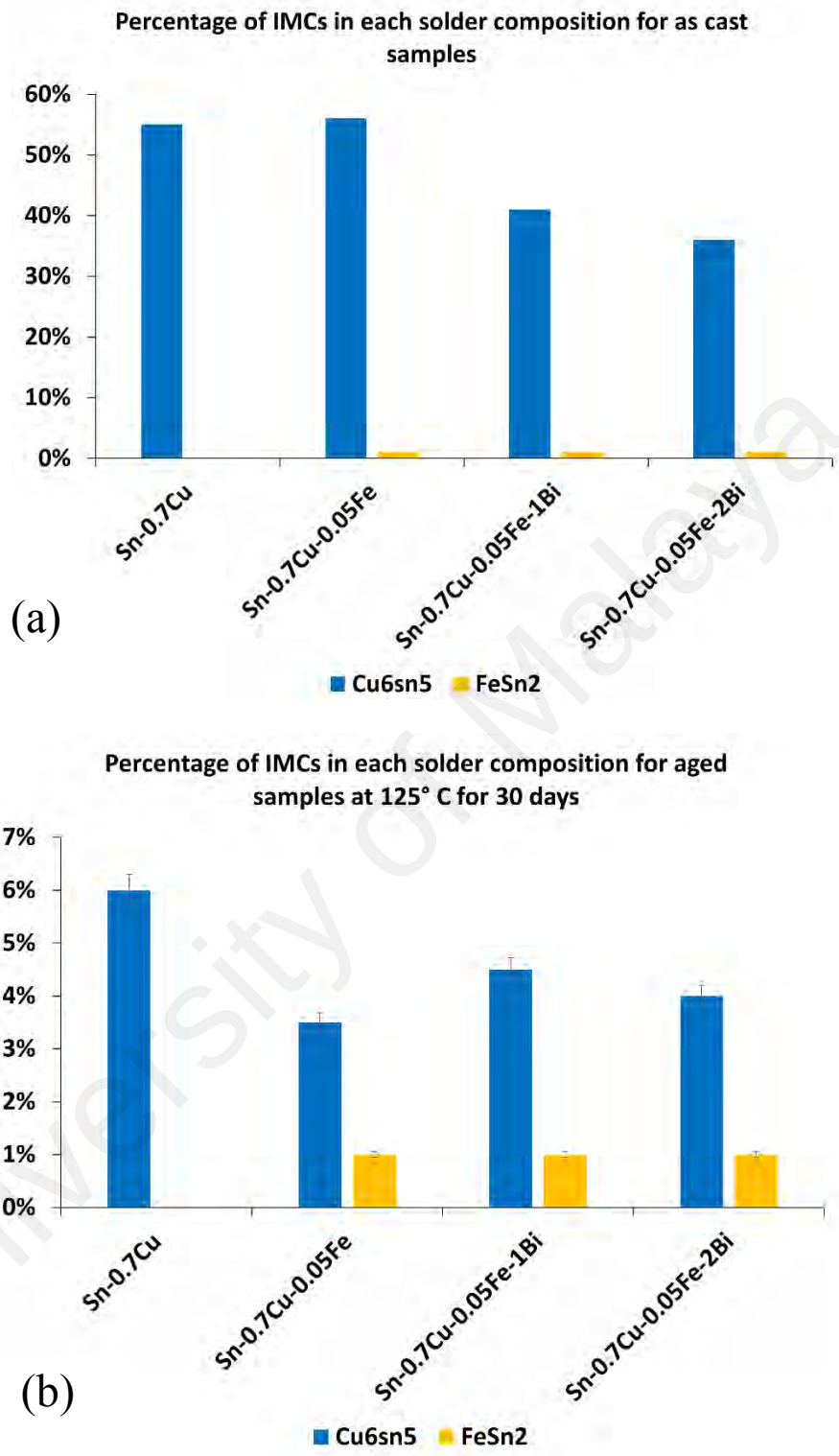

Figure 4.47: Area fractions of the phases (a) for as cast samples (b) for aged samples at 125°C for 30 days.

4.2.6 Microhardness

Vickers microhardness is regarded as one of the most principal ways to characterize the mechanical performance of lead-free solder alloy (Xiao Hu, Chan, Zhang, & Yung, 2013).

Figure 4.48 shows microhardness indentation of (a) SC07, (b)SC07-Fe, (c) SC07-Fe-1Bi, (d) SC07-Fe-2Bi solder alloys. Table 4.12 shows UTS and microhardness of solder composition in MPa and HV. UTS results which is measured by tensile test imported in table 4.12 to compare with hardness test from microharness indentation. There is a general correlation between strength (UTS) and hardness (HV ≈ 3 UTS) (Boyer & Gall, 1985; Callister & Rethwisch, 2007). However, this relation is lower than 3 in the materials with good ductility, due to the hardness represents a hardened state of materials without fully hardened (Pavlina & Van Tyne, 2008; P. Zhang, Li, & Zhang, 2011). To investigate this relation vicker hardness can be converted to MPa (HV× 9.807≈ hardness in MPa) (Cahoon, Broughton, & Kutzak, 1971). Table 4.12 shows microhardness and UTS in MPa which approximately UTS is 3 time of microhardness, however for SC07 this correlation is less than 3 time which is because of its more ductility in compare to samples with Fe and Bi, for other composition this proportion is close to 3.

Microhardness of SC07 increased a little from 6 HV to 7 HV by adding of Fe. Then by addition of 1or 2 wt.% Bi to SC07-Fe microhardness incresed to 12.1 HV and 14.2 HV.

Bi increases hardness due to solid solution hardening mechanism which is consistent with previous works by Huang et.al (M. L. Huang & Wang, 2005; Vianco & Rejent, 1999b). Fe does not have considerable effect on bulk hardness, as it exists in bulk of solder as $FeSn_2$. $FeSn_2$ has high hardness, but it can be find in just less than 1% area

fraction of solder, it does not have effect of overall hardness of solder. Moreover, the limited amount of Fe goes inside the Cu_6Sn_5, which have a little effect on increasing hardness of solder.

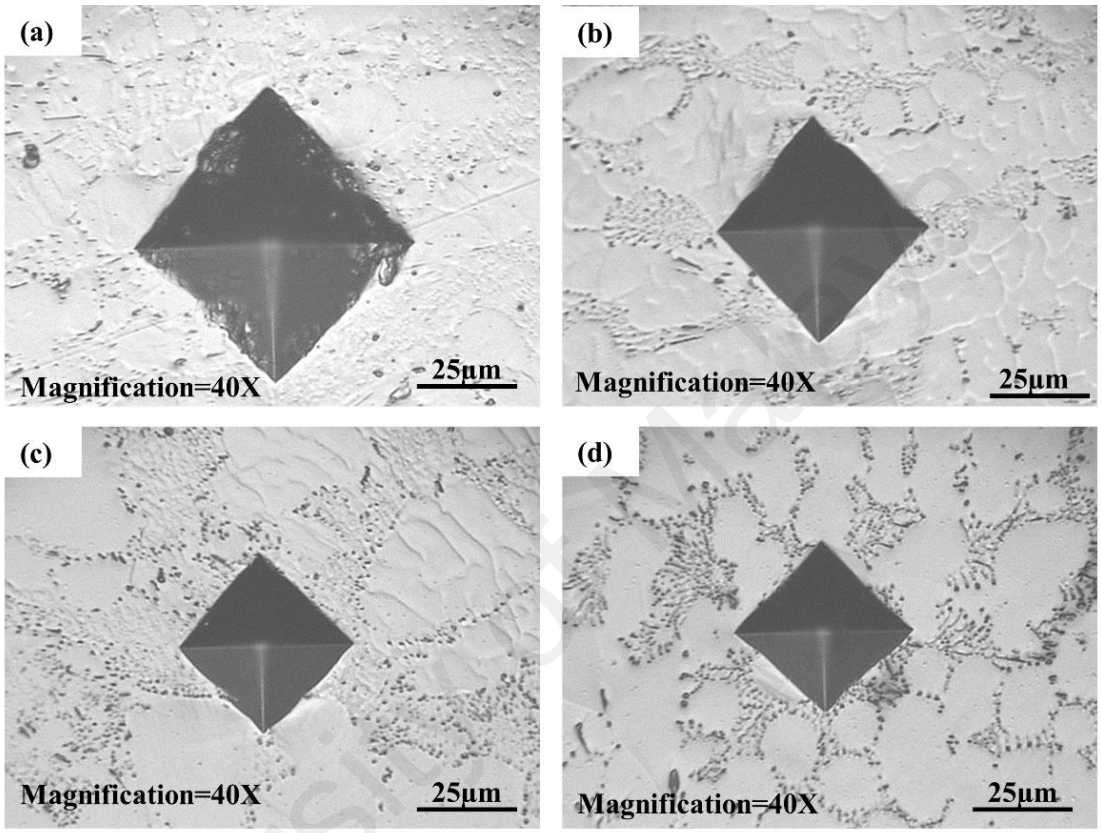

Figure 4.48: Microhardness indentation of (a) SC07 (b) SC07-Fe (c) SC07-Fe-1Bi (d) SC07-Fe-2Bi.

Table 4.12: UTS and Microhardness of solder composition in MPa and HV.

Solder composition	UTS (MPa)	Microhardness (MPa)	Microhardness (HV)
SC07	27	58.8	6
SC07-Fe	28	62.4	7
SC07-Fe-1Bi	42	118.6	12.1
SC07-Fe-2Bi	55	139.3	14.2

4.2.7 Nanoindentation

Nanoindentation applied to calculate young modulus and hardness of solders composition. Measurements of hardness and young's modulus were made by nanomechanical test instrument, Hysitron Ubi TI 750, using a Berkovich indenting tip. The integrated in-situ Scanning Probe Microscopy (SPM) used to locate and record testing result. Indentations were performed at load controlled under loading rate 200μN/s, holding time 2s and maximum load 1mN-7mN. Five times of indentation have done on each sample and by averaging the result hardness and young's modulus were obtained.

Figure 4.49 (a) shows scanning probe microscopy (SPM) of Sn-0.7Cu(SC07) which include β-Sn and Cu6Sn5. Figure 4.49 (b) and (c) show indentation and position of indents in β-Sn and eutectic region(Cu_6Sn_5) respectively. Figure 4.50 shows load-displacement curve for SC07 in eutectic region and in β-Sn which is include loading, creep deformation and unloading. The onset slope of unloading curve shows reduced Young's modulus. Figure 4.51 shows SPM of SC07-Fe-2Bi (a) before and (b) after nanoindentation (c) position of indents. Figure 4.52 illustrate load-displacement curve for SC07-Fe-2Bi in eutectic region and in β-Sn. E_r (reduced modulus) and hardness calculated based on equation 4-2 and 4-3. Table 4.13 and Table 4.14 illustrate Young's modulus and hardness of solder compositions respectively.

The indenting result shows that E_r (reduced modulus) for SC07 is 60GPa and 70GPa in the β-Sn and Cu_6Sn_5 respectively. Then for sample SC07-Fe-2Bi, E_r increased to 85GPa and 77GPa respectively in β-Sn and Cu_6Sn_5 which attributed to the solid solution effect of Bi and distortion of lattice parameter. Also on the basis of Darken-Gurry ellipsis few Fe can substitute with Cu in Cu_6Sn_5 which result in increasing Er. Also there is same trend for hardness which hardness of SC07 in β-Sn increase from 177MPa to 326MPa for SC07-Fe-2Bi and in Cu_6Sn_5 increase from 215Mpa for SC07 to 369MPa for SC07-Fe-2Bi.

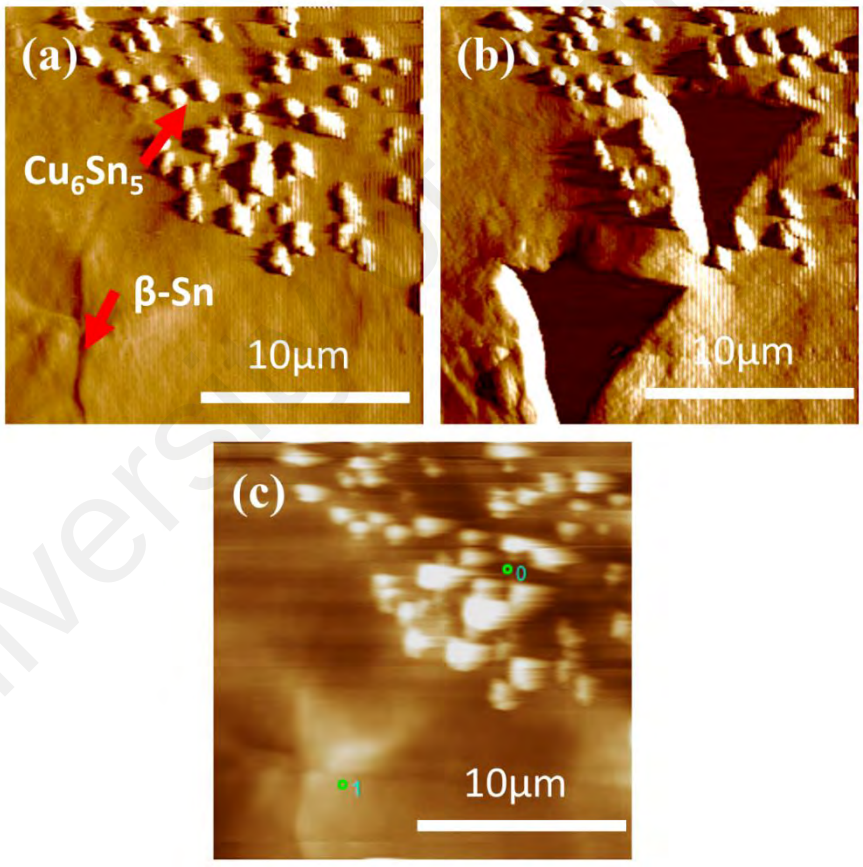

Figure 4.49: SPM of SC07 (a) before and (b) after nanoindentation (c) position of indents.

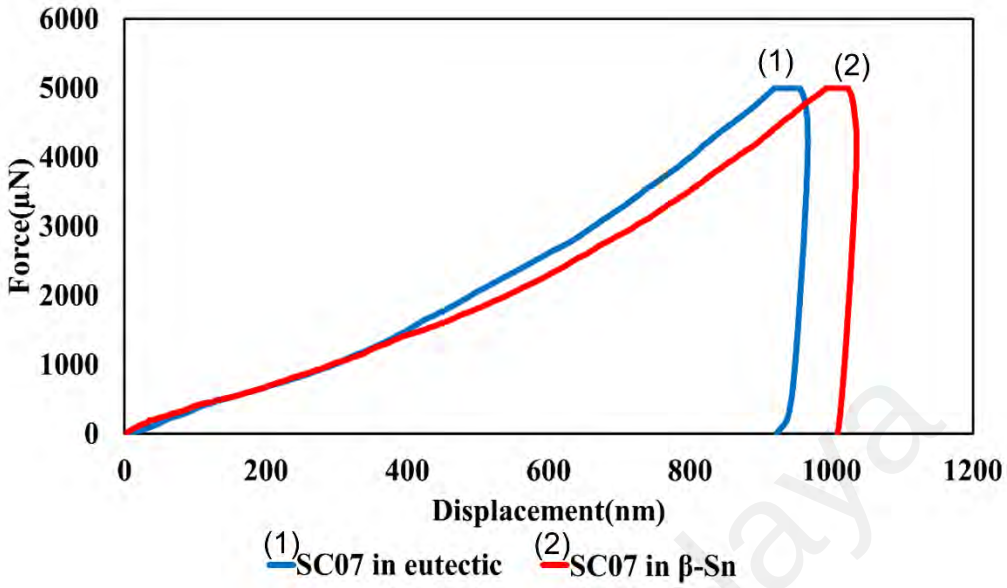

Figure 4.50: Load-Displacement curve for SC07 in eutectic region and in β-Sn.

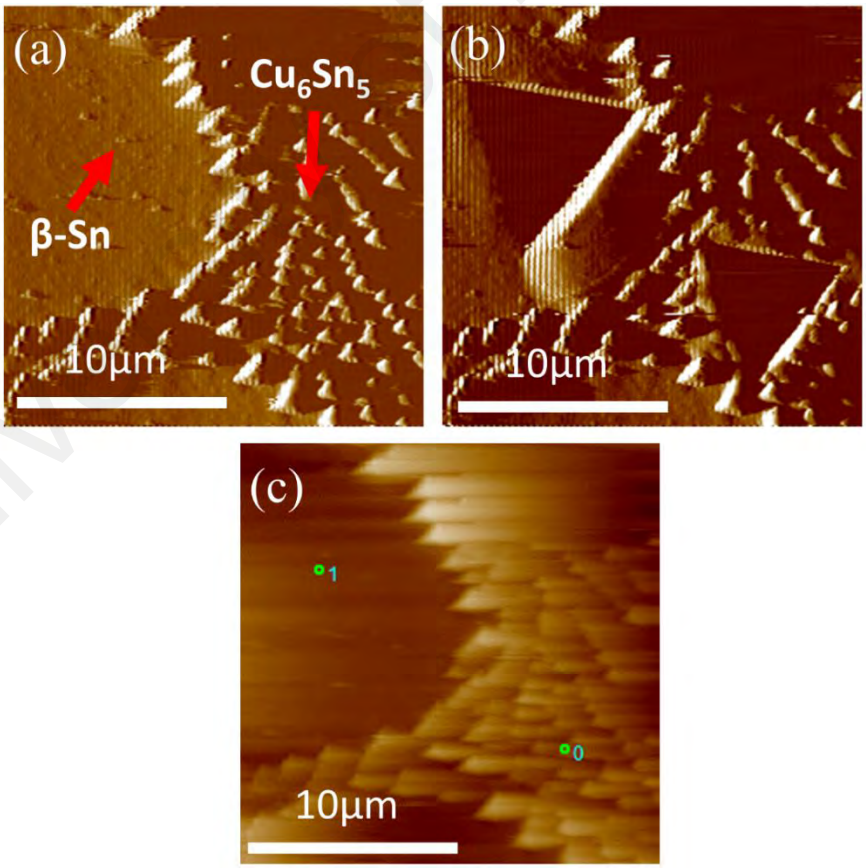

Figure 4.51: SPM of SC07-Fe-2Bi (a) before and (b) after nanoindentation (c) position of indents.

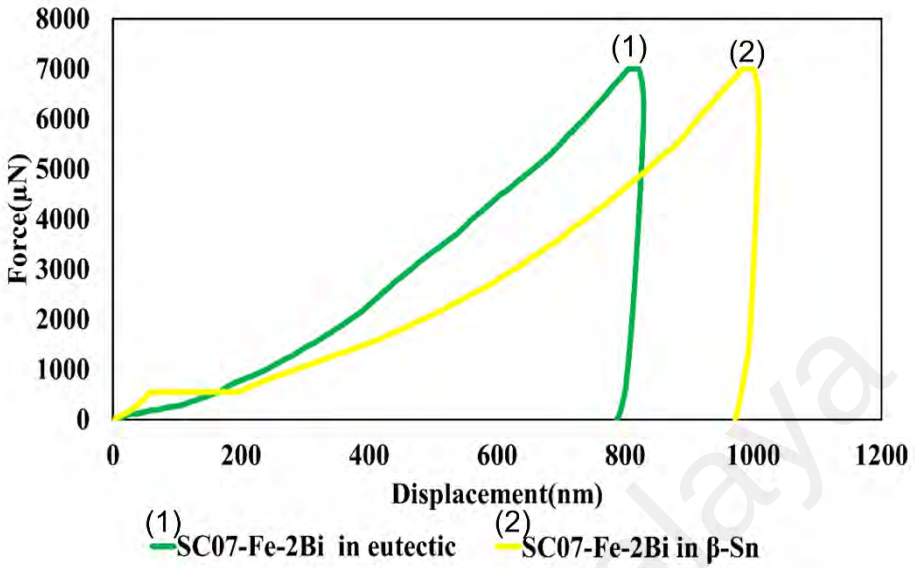

Figure 4.52: Load-Displacement curve for SC07-Fe-2Bi in eutectic region and in β-Sn

Table 4.13: Reduced Young's modulus of solder composition.

Solder composition	Er (GPa)	
	β-Sn	Cu_6Sn_5
Sn-0.7Cu	60	70
Sn-0.7Cu-0.05Fe	71	71
Sn-0.7Cu-0.05Fe-1Bi	75	72
Sn-0.7Cu-0.05Fe-2Bi	85	77

Table 4.14: Hardness(MPa) of solder composition.

Solder composition	Hardness(MPa)	
	β-Sn	Cu_6Sn_5
Sn-0.7Cu	177	215
Sn-0.7Cu-0.05Fe	206	334
Sn-0.7Cu-0.05Fe-1Bi	295	299
Sn-0.7Cu-0.05Fe-2Bi	326	369

4.2.8 Wetting angle and spreading rate

Many factors have effect on wetting properties, such as flux, temperature, substrate conditions, and soldering condition. However, spreading rate and wetting angle are considered to measure the solderability of solder alloy. Generally higher spreading rate with a lower wetting angle is desired during reflow. Figure 4.53 shows wetting angle SC07, SC07-Fe, SC07-Fe-1Bi, and SC07-Fe-2Bi sodler alloys. As shown in Figure 4.54 wetting angle decrease by addition of Fe and Bi to SC07 with RMA flux from 33.5° to 26° for sample with 0.05wt.% Fe and 2wt.% Bi. The wetting angle $20° < \theta < 30°$ and $30° < \theta < 40°$ is considered good and acceptable respectively (Kripesh et al., 2001). Spreading rate increase from 75.3% for SC07 to 78.2% for SC07-0.05Fe-2Bi.

Bi addition to Sac solder improve wetting (Huang & Lee, 1999), presumably due to the low surface tension of Bi (0.376 N/m for Bi versus 0.537 N/m for Sn) (Lee, 2007). Furthermore, Bi addition improved solder wetting properties because of better solder spreading as a result of the segregation of Bi on the solder surface in the liquid state by decreasing the surface tension of the molten solder (Pandher et al., 2007). It is reported that the first intermetallic compound (IMC) formed at the interface play important role on the wetting properties, because the molten solder is in contact with the IMC at the interface, not the original substrate (Chen et al., 2002; Choi & Lee, 1999; de Gennes, 1985). Therefore, Bi-doped solder has better wettability due to the growth suppression of the Cu_3Sn IMC layers (Pandher & Healey, 2008; Pandher et al., 2007). Moreover addition of Fe improve wetting slightly too, because Fe can decrease the size of IMC in interface by retarding the growth of interfacial Cu_6Sn_5 and Cu_3Sn layer during liquid state and slightly decreased the total IMC layer thickness (Laurila et al., 2009).

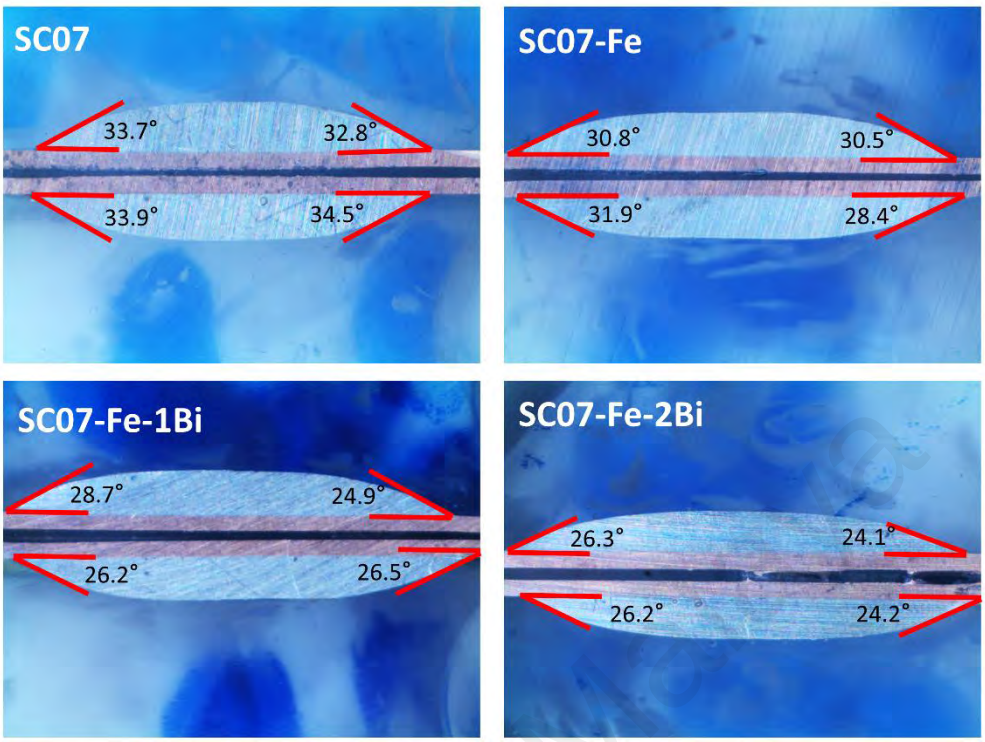

Figure 4.53: wetting angle for SC07, SC07-Fe, SC07-Fe-1Bi, and SC07-Fe-2Bi sodler alloys.

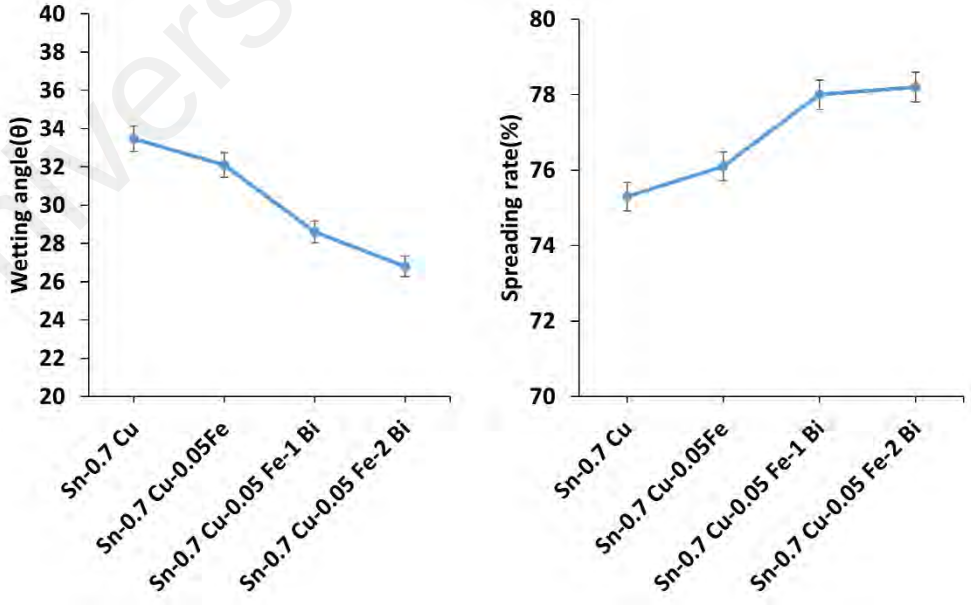

Figure 4.54: wetting angle and percent of spreading rate for SC07, SC07-Fe, SC07-Fe-1Bi, and SC07-Fe-2Bi solder alloys.

4.2.9 Density

Electronic Densimeter was utilized to measure density of solder composition. Table 4.15 shows density of SC07, SC07-Fe, SC07-Fe-1Bi and SC07-Fe-2Bi. The result test shows that addion of Fe and Bi increase density of SC07 solder composition. It can interpret that due to effect of Bi on bulk of solder by solid solution effect, which Bi scatter in whole bulk of solder. Furthermore, Fe has some solid solution effect and make $FeSn_2$ in the bulk of solder. Therefore, density of SC07 solder increased slightly after addition of 0.05wt%Fe from 7.31 g/Cm^3 to 7.35 g/Cm^3 and consequently by adding 1wt.% Bi and 2wt.% Bi increased density to 7.37 g/Cm^3 and 7.38 g/Cm^3 respectively.

Table 4.15: Density of SC07, SC07-Fe, SC07-Fe-1Bi and SC07-Fe-2Bi.

Solder composition	Density(g/Cm^3)
Sn-0.7 Cu	7.31
Sn-0.7 Cu-0.05Fe	7.35
Sn-0.7 Cu-0.05 Fe-1 Bi	7.37
Sn-0.7 Cu-0.05 Fe-2 Bi	7.38

4.2.10 Interfacial reaction

IMCs at interface play important role in solder joint reliability. Top view of IMCs at interface between solder alloys and Cu substrate are shown in Figure 4.55. It is obvious that by addition of Fe to Sn-0.7Cu, IMCs size decreased significantly and then by adding 2wt.% Bi to Sn-0.7Cu-Fe IMCs size decreased more slightly.

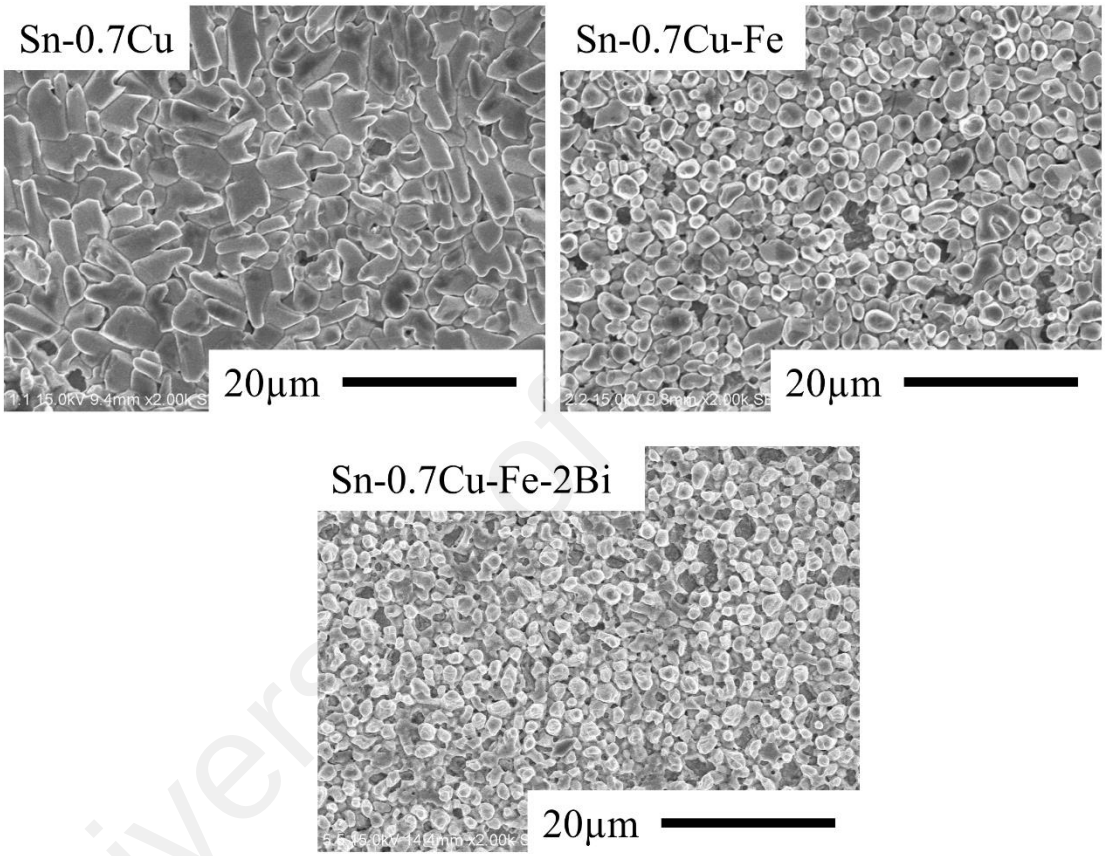

Figure 4.55: Top view of IMCs at interface between solder alloys and Cu substrate.

Based on the solubility of the alloying elements in the IMC layers, Bi does not dissolve in either Cu_6Sn_5 or Cu_3Sn. Whereas Fe has low solubility in Cu_6Sn_5 or Cu_3Sn at interface. Although Fe has more solubility at IMCs at interface in compare to IMCs in bulk of solder. Probably because interfacial Cu_6Sn_5 IMC formed mostly at the reflow temperature of 250 °C, while the formation temperature of the same IMC within the solder should

have been below ~220 °C, the melting temperature of the alloy. With the high temperature as well as a strong preference to react with Cu, Fe may be easily incorporated into the Cu_6Sn_5 at interface (Lee et al., 2015).

Bi which does not dissolve in IMC layer can influence diffusion fluxes in the layers only indirectly through the activity of Sn. While Fe which dissolves in IMC layer can alter its stability and probably also its microstructure, thus influencing the growth kinetics directly (Laurila et al., 2010).

Figure 4.56 shows TEM lamella preparation. Figure 4.57 shows EDX analysis at IMC layer, EDX at area 1 shows concentration of Bi on top of IMC layer and EDX at area 2

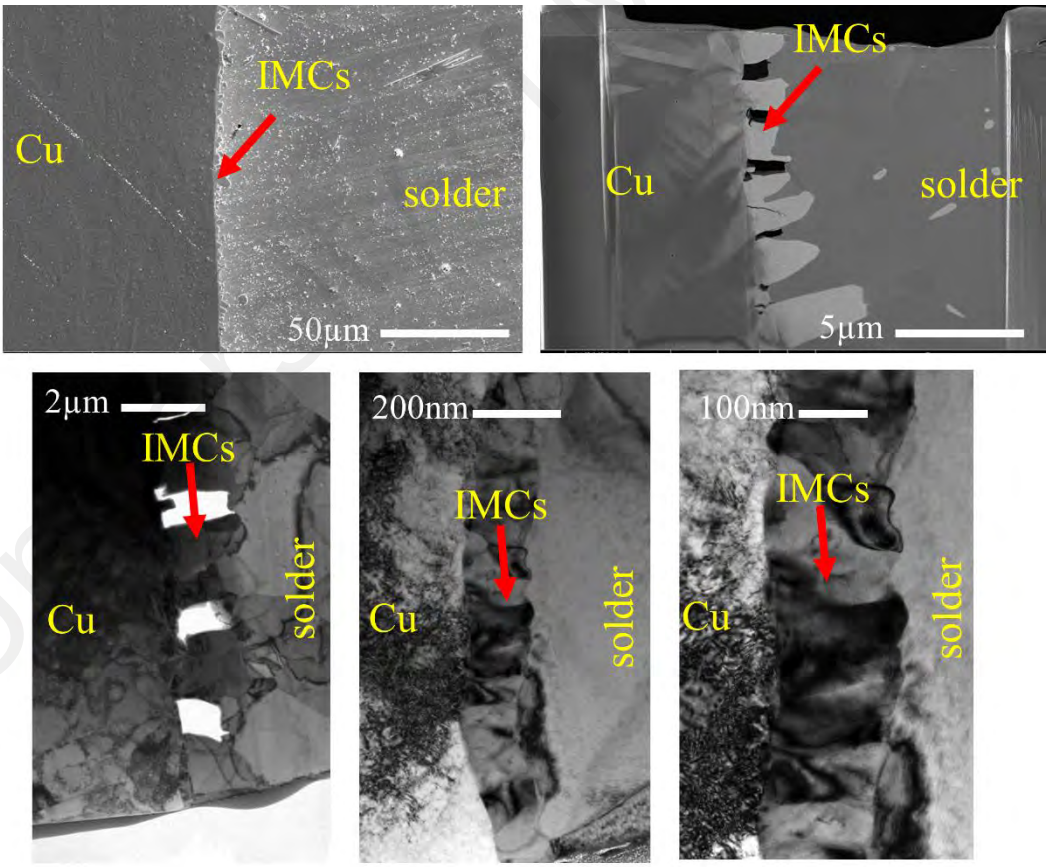

Figure 4.56: TEM lamella prepation of as cast Sn-0.7Cu-0.1Fe-2Bi solder alloy.

shows a little Fe in Cu_6Sn_5. Elemental mapping in Figure 4.58 confirm that Bi scattered on top of IMCs layer and Fe exist inside the IMCs.

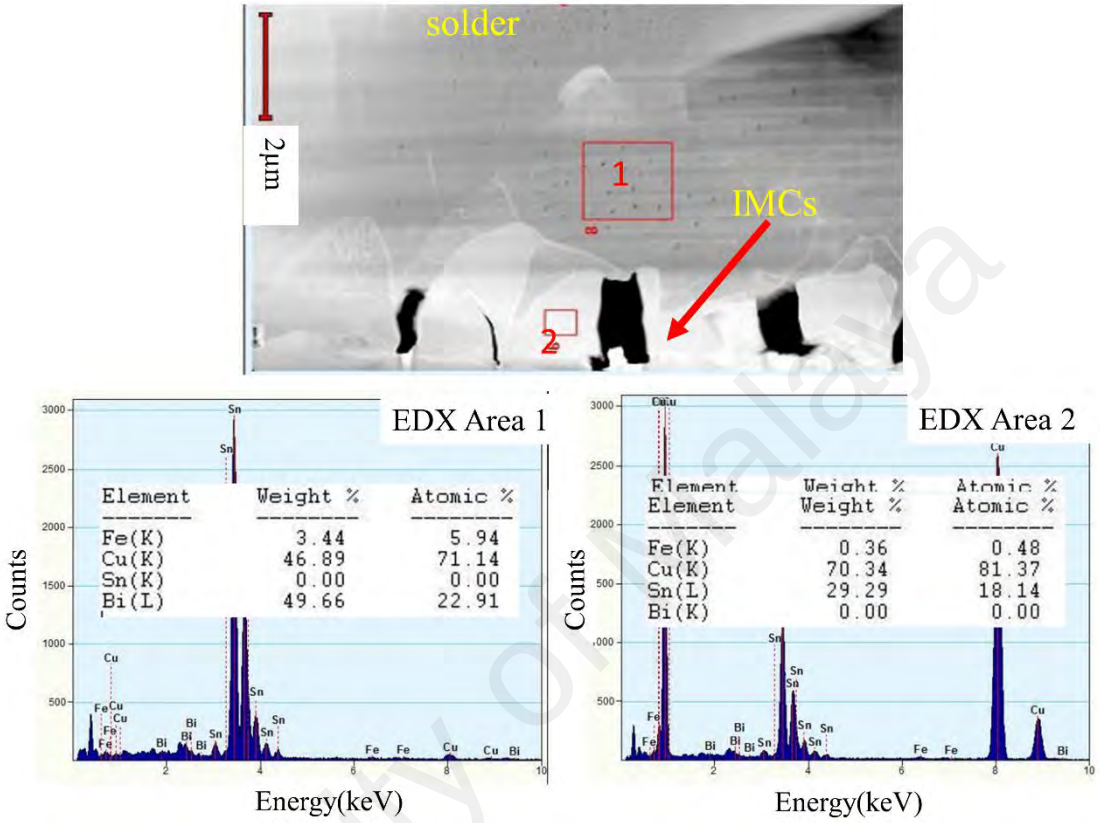

Figure 4.57: EDX at area in (1)solder bulk and (2) IMC Sn-0.7Cu-0.1Fe-2Bi solder alloy.

Hu et al. found that addition of Bi into the Sn-0.7Cu eutectic solder caused the excessive formations of IMCs during the soldering reaction and thereafter in aging condition. Because Bi could result in more chemical bonds between Cu atoms or between Cu and Sn atoms to be broken, which made more Cu and Sn atoms activated, therefore interfacial IMC layers were thicker with higher Bi content in solder alloy (Hu et al., 2014). On the other hand, the key reason for thinner IMC layer is slowing diffusion process. Fe substitution by copper in Cu_6Sn_5 or Cu_3Sn could effectively suppress the flow of tin atoms and retard IMC growth. Therefore, in the current work both of these mechanism effected on thickness of IMCs layer. Figure 4.59 Shows IMC layer on Cu substrate for solder alloy

(a) Sn-0.7Cu, and (b) Sn-0.7Cu-Fe-1Bi which by addition of Bi and Fe to Sn-0.7Cu, thickness of IMC layer and scallop size decreased.

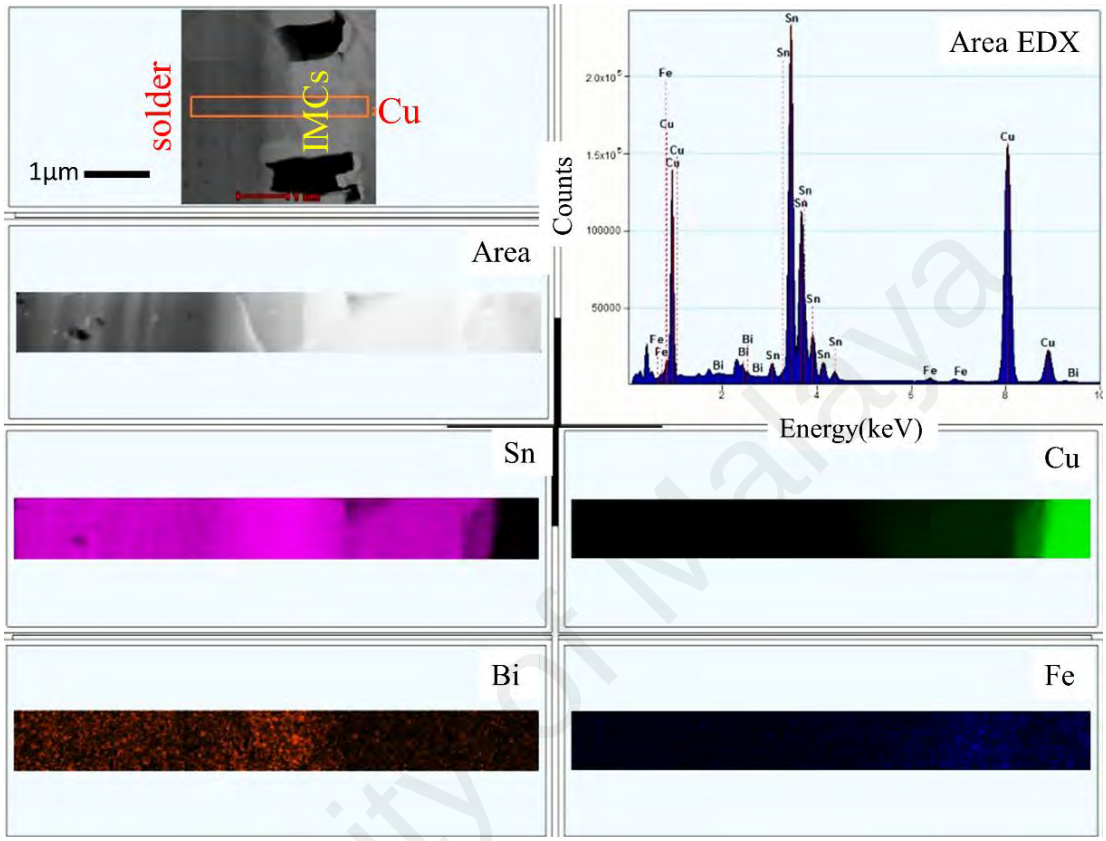

Figure 4.58: Elemental mapping of Sn-0.7Cu-0.1Fe-2Bi at IMC layer at interface.

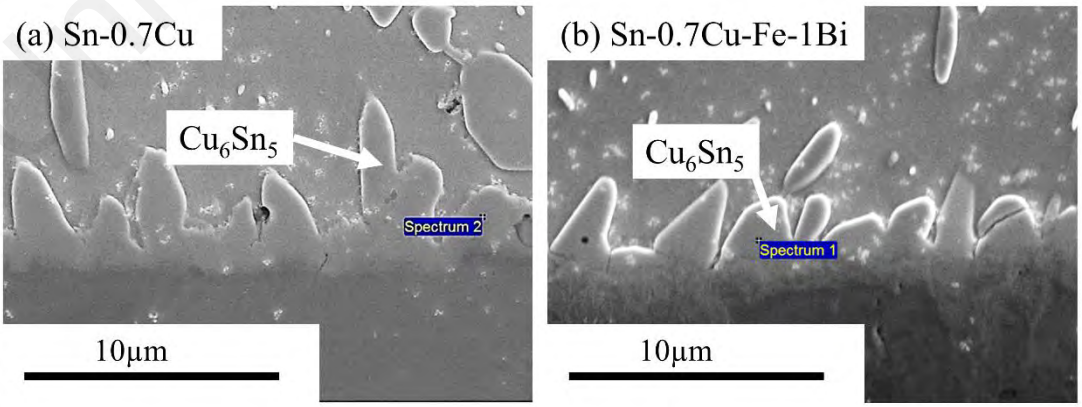

Figure 4.59: IMC layer on Cu substrate for solder alloy (a) Sn-0.7Cu, (b) Sn-0.7Cu-Fe-1Bi.

4.3 Summary

The properties of two group of solder alloys are explained in this chapter. The first group is Sn-1Ag-0.5Cu solder by addition of 0.05wt.%Fe and 1or2wt.% Bi. The second group is Sn-0.7Cu solder by addition of 0.05wt.%Fe and 1or2wt.% Bi. Their mechanical and microstructural properties, fracture, and thermal behavior, aging effect, microhardness, nanoindentation, wetting behavior, density and the interfacial reaction of all composition are analyzed and discussed in this chapter.

CHAPTER 5: CONCLUSION AND RECOMMENDATIONS

5.1 Conclusion

Near eutectic Sn-Ag-Cu lead-free solders, such as Sn-4 wt.%Ag-0.5 wt.% Cu (SAC405) or Sn-3 wt.% Ag-0.5 wt.% Cu (SAC305), suggested as a promising replacement for toxic Sn-Pb solder alloy because of their low melting temperature, and favorable thermal–mechanical fatigue properties. However, because of the rigidity of the high-Ag-content Sn-Ag-Cu (SAC) alloys, portable electronic products that contain these high-Ag-SAC solder joints are more prone to failure due to drop and high impact applications. Moreover, the high Ag content in Sn-Ag-Cu alloys results in a relatively high cost for these solder alloys. Low-Ag-content Sn-Ag-Cu alloys such as Sn-1 wt.%Ag-0.5 wt.% Cu (SAC105) have been considered as a solution to both the cost and poor drop impact reliability issues.

0.05wt%Fe and (1or2 wt%) Bi were added together to the SAC105(Sn-1Ag-0.5Cu) or SC07(Sn-0.7Cu), to investigate the effect of these two elements on the bulk alloy microstructure, tensile and thermal properties. Following shows summary of results:

- Addition of Bi to SAC105-Fe and SC07-Fe increased yield strength and ultimate tensile strength while decreased total elongation. Bi degenerated the eutectic region into a chain-like arrangement, which decreased Cu_6Sn_5 and increase β-Sn in solder. 0.05wt%Fe made few $FeSn_2$ IMC particles in the solder which does not have considerable effect on mechanical and microstructural properties. 1wt% or 2wt%Bi scattered in the whole of solder without concentration at any position and strengthen solder by a solid solution effect. The surface fracture of solder does not show necking by addition of Bi which is related to the Bi brittle properties and prevention of β-Sn deformation by Bi.

- The solidus temperature of SAC105Fe-2Bi is 214°C, which is 5°C less than SAC105, whilst pasty rage increased 3°C. Also undercooling decreased from 12.3 °C to 9.8°C by adding 2wt% Bi to SAC105-Fe. The addition of 2 wt.% Bi to SC07-Fe decreases the solidus temperature of SC07 from 227.6°C to 223.8°C.
- After aging at 125 °C for 30 days, UTS (ultimate tensile strength) and yield strength decreased for SAC105 or SC07 by coarsening of IMCs whereas total elongation increased. Scanning electron microscope (FESEM) and energy dispersive X-ray (EDX) indicated that the growth and spheroidization of Cu_6Sn_5 and Ag_3Sn for SAC105 or Cu_6Sn_5 for SC07 after aging controlled by Gibbs-Thomson effect and Ostwald ripening process. Therefore, IMCs and β-Sn grains coarsen. Addition of Bi strengthen solder by scattering in the bulk of SAC105-Fe solder alloy, increased β-Sn and degenerated Cu_6Sn_5 and Ag_3Sn into a chain-like arrangement due to the solid solution and precipitation strengthening effects by Bi in the Sn-rich phase. Partially substitution of Fe in the Cu_6Sn_5 on the basis of Darken-Gurry ellipse decreased microstructure coarsening rate. UTS, yield strength, and total elongation are approximately constant after aging, because Bi prevent the Cu and Sn to interact with each other, therefore spheroidization and growth of IMCs slowed down and decreased the rate of IMCs coarsening.
- The effect of the addition of Fe and Bi on nanoindetation of SAC105 and SC07 investigated to measure young modulus and hardness of these solder alloys. The nanomechanical test instrument, using a Berkovich indenting tip used for analysis microstructure and measure reduced young modulus and hardness of samples. For Both solder alloys (SC07 and SAC105) addition of Bi and Fe shows a remarkable increase in Er (reduced elastic modulus) and hardness. Bi increase hardness and young modulus by solid solution effect and distortion of lattice parameter of β-

Sn. Furthermore, Fe makes few $FeSn_2$ with high hardness in the matrix and few Fe substitute with Cu in Cu_6Sn_5 which increase hardness.

- Wetting angle and spreading rate for SC07 with RMA (rosin mildly activated) flux are 33.5° and 75.3% respectively, by adding 0.05 wt% Fe and 2wt% Bi contact angle decrease to 26.8° and spreading rate increase to 78.2%. Wetting angle and spreading rate for SAC105 with RMA flux are 38° and 65.4% respectively, by adding 0.05 wt% Fe and 2wt% Bi contact angle decrease to 31° and spreading rate is approximately constant.

5.2 Recommendation

- Sample size and cooling rate play important role in solidification of solder joint microstructure. In the current work dog bone sample studied for mechanical and microstructural properties. It is suggested to investigate solder ball and other surface mount technology solder joints in future works.
- For solder joints, the pad surface finish may change the microstructure drastically. In this present experimental work solders were reflowed on Cu substrate. It is recommended different surface finishes such as electroless Ni(P)/Au, electrolytic Ni/Au, Al/Ni(V)/Cu, Zn(Mo)/Cu etc. These processing techniques are more close to industrial practices in the microelectronics industries.
- The size of bearing elements has role in properties of solder alloy, addition of elements at nanoparticle size can be investigate in future works.
- Investigation on shear strength, creep, fatigue and corrosion behavior of Fe and Bi added SAC105 and SC07 can make more clear the properties of these solder alloys.

REFERENCES

Abbaschian, G. J., & Eslamloo, M. (1975). Solidification kinetics of tin. *Journal of Crystal Growth, 28*(3), 372-374.

Abtew, M., & Selvaduray, G. (2000). Lead-free Solders in Microelectronics. *Materials Science and Engineering: R: Reports, 27*(5–6), 95-141.

Amagai, M., Watanabe, M., Omiya, M., Kishimoto, K., & Shibuya, T. (2002). Mechanical characterization of Sn–Ag-based lead-free solders. *Microelectronics Reliability, 42*(6), 951-966.

Amin, N. A. A. M., Shnawah, D. A., Said, S. M., Sabri, M. F. M., & Arof, H. (2014). Effect of Ag content and the minor alloying element Fe on the electrical resistivity of Sn–Ag–Cu solder alloy. *Journal of Alloys and Compounds, 599*(0), 114-120.

Anderson, I. (2007). Development of Sn-Ag-Cu and Sn-Ag-Cu-X alloys for Pb-free electronic solder applications *Lead-Free Electronic Solders* (pp. 55-76): Springer US.

Anderson, I. E., Foley, J. C., Cook, B. A., Harringa, J., Terpstra, R. L., & Unal, O. (2001). Alloying effects in near-eutectic Sn-Ag-Cu solder alloys for improved microstructural stability. *Journal of Electronic Materials, 30*(9), 1050-1059.

Anderson, I. E., & Harringa, J. L. (2004). Elevated temperature aging of solder joints based on Sn-Ag-Cu: Effects on joint microstructure and shear strength. *Journal of Electronic Materials, 33*(12), 1485-1496.

Anderson, I. E., & Harringa, J. L. (2006). Suppression of void coalescence in thermal aging of tin-silver-copper-X solder joints. *Journal of Electronic Materials, 35*(1), 94-106.

Bader, W. (1975). Lead alloys for high temperature soldering of magnet wire. *Welding Journal, 54*(10), 370s-375s.

Bath, J. (2010). *Lead-Free Soldering*: Springer.

Boettinger, W. J., Johnson, C. E., Bendersky, L. A., Moon, K. W., Williams, M. E., & Stafford, G. R. (2005). Whisker and Hillock formation on Sn, Sn–Cu and Sn–Pb electrodeposits. *Acta Materialia, 53*(19), 5033-5050.

Boyer, H. E., & Gall, T. L. (1985). Metals handbook; desk edition.

Bradley III, E., & Hranisavljevic, J. (2001). Characterization of the melting and wetting of Sn-Ag-X solders. *Electronics Packaging Manufacturing, IEEE Transactions on, 24*(4), 255-260.

Bui, Q. V., & Jung, S. B. (2013). Characterization of low speed shear test reliability of Sn–1.0Ag–XCe/ENEPIG solder joint. *Journal of Alloys and Compounds, 560*(0), 54-61.

Cahoon, J., Broughton, W., & Kutzak, A. (1971). The determination of yield strength from hardness measurements. *Metallurgical Transactions, 2*(7), 1979-1983.

Callister, W. D., & Rethwisch, D. G. (2007). *Materials science and engineering: an introduction* (Vol. 7): Wiley New York.

Che, F. X., Poh, E. C., Zhu, W. H., & Xiong, B. S. (2007, 10-12 Dec. 2007). *Ag Content Effect on Mechanical Properties of Sn-xAg-0.5Cu Solders.* Paper presented at the Electronics Packaging Technology Conference, 2007. EPTC 2007. 9th.

Chen, J., Gu, M., & Pan, F. (2002). Reactive wetting of a metal/ceramic system. *Journal of Materials Research, 17*(04), 911-917.

Chen, W. T., Ho, C. E., & Kao, C. R. (2002). Effect of Cu concentration on the interfacial reactions between Ni and Sn–Cu solders. *Journal of Materials Research, 17*(02), 263-266.

Choi, W., & Lee, H. (1999). Effect of Ni layer thickness and soldering time on intermetallic compound formation at the interface between molten Sn-3.5Ag and Ni/Cu substrate. *Journal of Electronic Materials, 28*(11), 1251-1255.

Cook, B. A., Anderson, I. E., Harringa, J. L., & Terpstra, R. L. (2002). Effect of heat treatment on the electrical resistivity of near-eutectic Sn-Ag-Cu Pb-Free solder alloys. *Journal of Electronic Materials, 31*(11), 1190-1194.

Date, M., Shoji, T., Fujiyoshi, M., & Sato, K. (2005). *Pb-free Solder Ball with Higher Impact Reliability.* Paper presented at the Intel Pb-free Technology Forum.

Datta, M., Osaka, T., & Schultze, J. W. (2004). *Microelectronic packaging*: CRC press.

de Gennes, P. G. (1985). Wetting: statics and dynamics. *Reviews of Modern Physics, 57*(3), 827-863.

El-Daly, A. A., & El-Taher, A. M. (2013). Improved strength of Ni and Zn-doped Sn–2.0Ag–0.5Cu lead-free solder alloys under controlled processing parameters. *Materials & Design, 47*(0), 607-614.

El-Daly, A. A., El-Taher, A. M., & Gouda, S. (2015). Development of new multicomponent Sn–Ag–Cu–Bi lead-free solders for low-cost commercial electronic assembly. *Journal of Alloys and Compounds, 627*(0), 268-275.

El-Daly, A. A., Hammad, A. E., Fawzy, A., & A. Nasrallh, D. (2013). Microstructure, mechanical properties, and deformation behavior of Sn–1.0Ag–0.5Cu solder after Ni and Sb additions. *Materials & Design, 43*(0), 40-49.

Fix, A. R., Nüchter, W., & Wilde, J. (2008). Microstructural changes of lead-free solder joints during long-term ageing, thermal cycling and vibration fatigue. *Soldering & Surface Mount Technology, 20*(1), 13-21.

Frear, D. R. (1996). The mechanical behavior of interconnect materials for electronic packaging. *JOM Journal of the Minerals Metals and Materials Society, 48*(5), 49-53.

Frear, D. R. (1999). Materials issues in area-array microelectronic packaging. *JOM Journal of the Minerals Metals and Materials Society, 51*(3), 22-27.

Frear, D. R. (2007). Issues related to the implementation of Pb-free electronic solders in consumer electronics *Lead-Free Electronic Solders* (pp. 319-330): Springer US.

Glazer, J. (1994). Microstructure and mechanical properties of Pb-free solder alloys for low-cost electronic assembly: A review. *Journal of Electronic Materials, 23*(8), 693-700.

Gong, J., Liu, C., Conway, P. P., & Silberschmidt, V. V. (2009). Initial formation of CuSn intermetallic compounds between molten SnAgCu solder and Cu substrate. *Scripta Materialia, 60*(5), 333-335.

Greig, W. (2007). *Integrated circuit packaging, assembly and interconnections: trends and options*: Springer Science & Business Media.

Guowei, X., Chan, P., Cai, J., Teng, A., & Yuen, W. (2000, 2000). *The effect of Cu stud structure and eutectic solder electroplating on intermetallic growth and reliability of flip-chip solder bump.* Paper presented at the Electronic Components & Technology Conference, 2000. 2000 Proceedings. 50th.

Hammad, A. E. (2013). Evolution of microstructure, thermal and creep properties of Ni-doped Sn–0.5Ag–0.7Cu low-Ag solder alloys for electronic applications. *Materials & Design, 52*(0), 663-670.

Harrison, M., Vincent, J., & Steen, H. (2001). Lead-free reflow soldering for electronics assembly. *Soldering & surface mount technology, 13*(3), 21-38.

He, M., & Acoff, V. L. (2006). Effect of reflow and thermal aging on the microstructure and microhardness of Sn-3.7Ag-xBi solder alloys. *Journal of Electronic Materials, 35*(12), 2098-2106.

Ho, C., Lin, Y., Yang, S., Kao, C., & Jiang, D. (2006). Effects of limited Cu supply on soldering reactions between SnAgCu and Ni. *Journal of Electronic Materials, 35*(5), 1017-1024.

Ho, C., Tsai, R., Lin, Y., & Kao, C. (2002). Effect of Cu concentration on the reactions between Sn-Ag-Cu solders and Ni. *Journal of Electronic Materials, 31*(6), 584-590.

Hodúlová, E., Palcut, M., Lechovič, E., Šimeková, B., & Ulrich, K. (2011). Kinetics of intermetallic phase formation at the interface of Sn–Ag–Cu–X (X=Bi, In) solders with Cu substrate. *Journal of Alloys and Compounds, 509*(25), 7052-7059.

Hsuan, T.-C., & Lin, K.-L. (2007). Effects of aging treatment on mechanical properties and microstructure of Sn–8.5Zn–0.5Ag–0.01Al–0.1Ga Solder. *Materials Science and Engineering: A, 456*(1–2), 202-209.

Hu, X., Chan, Y. C., Zhang, K., & Yung, K. C. (2013). Effect of graphene doping on microstructural and mechanical properties of Sn–8Zn–3Bi solder joints together with electromigration analysis. *Journal of Alloys and Compounds, 580*, 162-171.

Hu, X., Li, K., & Min, Z. (2013). Microstructure evolution and mechanical properties of Sn0.7Cu0.7Bi lead-free solders produced by directional solidification. *Journal of Alloys and Compounds, 566*(0), 239-245.

Hu, X., Li, Y., Liu, Y., & Min, Z. (2015). Developments of high strength Bi-containing Sn0.7Cu lead-free solder alloys prepared by directional solidification. *Journal of Alloys and Compounds, 625*(0), 241-250.

Hu, X., Li, Y., & Min, Z. (2014). Interfacial reaction and IMC growth between Bi-containing Sn0.7Cu solders and Cu substrate during soldering and aging. *Journal of Alloys and Compounds, 582*(0), 341-347.

Huang, B., & Lee, N.-C. (1999). *Prospect of lead free alternatives for reflow soldering.* Paper presented at the SPIE proceedings series.

Huang, M. L., & Wang, L. (2005). Effects of Cu, Bi, and In on microstructure and tensile properties of Sn-Ag-X(Cu, Bi, In) solders. *Metallurgical and Materials Transactions A, 36*(6), 1439-1446.

Huh, S.-H., Kim, K.-S., & Suganuma, K. (2001). Effect of Ag addition on the microstructural and mechanical properties of Sn-Cu eutectic solder. *Materials Transactions-JIM, 42*(5), 739-744.

Humpston, G., & Jacobson, D. M. (2004). *Principles of Soldering*: Asm International.

Hunt, C., & Lea, D. (2000). Solderability of lead-free alloys. *Proceedings of Apex, 1238*.

Jianbiao, P., Tonkay, G. L., Storer, R. H., Sallade, R. M., & Leandri, D. J. (2004). Critical variables of solder paste stencil printing for micro-BGA and fine-pitch QFP. *Electronics Packaging Manufacturing, IEEE Transactions on, 27*(2), 125-132.

Kang, S., & Sarkhel, A. (1994). Lead (Pb)-free solders for electronic packaging. *Journal of Electronic Materials, 23*(8), 701-707.

Kang, S. K., Cho, M. G., Lauro, P., & Shih, D. Y. (2007, May 29 2007-June 1 2007). *Critical Factors Affecting the Undercooling of Pb-free, Flip-Chip Solder Bumps and In-situ Observation of Solidification Process.* Paper presented at the Electronic Components and Technology Conference, 2007. ECTC '07. Proceedings. 57th.

Kang, S. K., Moon Gi, C., Lauro, P., & Da-Yuan, S. (2007, May 29 2007-June 1 2007). *Critical Factors Affecting the Undercooling of Pb-free, Flip-Chip Solder Bumps and In-situ Observation of Solidification Process.* Paper presented at the Electronic Components and Technology Conference, 2007. ECTC '07. Proceedings. 57th.

Kantarcıoğlu, A., & Kalay, Y. E. (2014). Effects of Al and Fe additions on microstructure and mechanical properties of SnAgCu eutectic lead-free solders. *Materials Science and Engineering: A, 593*(0), 79-84.

Karakaya, I., & Thompson, W. T. (1987). The Ag-Sn (Silver-Tin) system. *Bulletin of Alloy Phase Diagrams, 8*(4), 340-347.

Kariya, Y., & Otsuka, M. (1998). Mechanical fatigue characteristics of Sn-3.5Ag-X (X=Bi, Cu, Zn and In) solder alloys. *Journal of Electronic Materials, 27*(11), 1229-1235.

Kattner, U., & Boettinger, W. (1994). On the Sn-Bi-Ag ternary phase diagram. *Journal of Electronic Materials, 23*(7), 603-610.

Kerr, M., & Chawla, N. (2004). Creep deformation behavior of Sn–3.5Ag solder/Cu couple at small length scales. *Acta Materialia, 52*(15), 4527-4535.

Kim, D., Suh, D., Millard, T., Kim, H., Kumar, C., Zhu, M., & Xu, Y. (2007, May 29 2007-June 1 2007). *Evaluation of High Compliant Low Ag Solder Alloys on OSP as a Drop Solution for the 2nd Level Pb-Free Interconnection.* Paper presented at the 2007 Proceedings 57th Electronic Components and Technology Conference.

Kim, H., Zhang, M., Kumar, C. M., Suh, D., Liu, P., Kim, D., . . . Wang, Z. (2007, May 29 2007-June 1 2007). *Improved Drop Reliability Performance with Lead Free Solders of Low Ag Content and Their Failure Modes.* Paper presented at the 2007 Proceedings 57th Electronic Components and Technology Conference.

Kim, J., & Yu, J. (2008). Effects of residual impurities in electroplated Cu on the Kirkendall void formation during soldering. *Applied Physics Letters, 92*(9), 092109.

Kim, K., Huh, S., & Suganuma, K. (2003). Effects of intermetallic compounds on properties of Sn–Ag–Cu lead-free soldered joints. *Journal of Alloys and Compounds, 352*(1), 226-236.

Kim, K. S., Huh, S. H., & Suganuma, K. (2003). Effects of fourth alloying additive on microstructures and tensile properties of Sn–Ag–Cu alloy and joints with Cu. *Microelectronics Reliability, 43*(2), 259-267.

Kim, S. H., & Yu, J. (2013). Fe addition to Sn-3.5Ag solder for the suppression of Kirkendall void formation. *Scripta Materialia, 69*(3), 254-257.

Kotadia, H. R., Howes, P. D., & Mannan, S. H. (2014). A review: On the development of low melting temperature Pb-free solders. *Microelectronics Reliability, 54*(6–7), 1253-1273.

Kripesh, V., Teo, P.-S., Tai, C., Vishwanadam, G., & Mui, Y. C. (2001). *Development of a lead free chip scale package for wireless applications.* Paper presented at the Electronic Components and Technology Conference, 2001. Proceedings., 51st.

Lampe, B. (1976). Room temperature aging properties of some solder alloys. *Welding Journal, 55*(10), 330.

Lau, J., Wong, C., Lee, N., & Lee, S. R. (2003). Electronics manufacturing with leadfree halogen-free, and conductive–adhesive handbooks: McGraw-Hill.

Laurila, T., Hurtig, J., Vuorinen, V., & Kivilahti, J. K. (2009). Effect of Ag, Fe, Au and Ni on the growth kinetics of Sn–Cu intermetallic compound layers. *Microelectronics Reliability, 49*(3), 242-247.

Laurila, T., Vuorinen, V., & Kivilahti, J. K. (2005). Interfacial reactions between lead-free solders and common base materials. *Materials Science and Engineering: R: Reports, 49*(1–2), 1-60.

Laurila, T., Vuorinen, V., & Paulasto-Kröckel, M. (2010). Impurity and alloying effects on interfacial reaction layers in Pb-free soldering. *Materials Science and Engineering: R: Reports, 68*(1–2), 1-38.

Lea, C. (1993). Solderability and its measurement. *Engineering Science & Education Journal, 2*(2), 77-84.

Lee, B.-J., Hwang, N. M., & Lee, H. M. (1997). Prediction of interface reaction products between Cu and various solder alloys by thermodynamic calculation. *Acta Materialia, 45*(5), 1867-1874.

Lee, H.-T., Lin, H.-S., Lee, C.-S., & Chen, P.-W. (2005). Reliability of Sn–Ag–Sb lead-free solder joints. *Materials Science and Engineering: A, 407*(1–2), 36-44.

Lee, J. C. B., Chen, P. C., & Lai, Y. S. (2007, 14-17 Aug. 2007). *The Effect of SnxAgCu and SnAgCuX on the Mechanical Drop Performance in Lead Free CSP Package.* Paper presented at the Electronic Packaging Technology, 2007. ICEPT 2007. 8th International Conference on.

Lee, N.-C. (2007). *Future lead-free solder alloys and fluxes-meeting challenges of miniaturization.* Paper presented at the Microsystems, Packaging, Assembly and Circuits Technology, 2007. IMPACT 2007. International.

Lee, N. C. (2009). Lead-free soldering *Materials for Advanced Packaging* (pp. 181-218): Springer.

Lee, T.-K., Bieler, T. R., Kim, C.-U., & Ma, H. (2015). *Fundamentals of Lead-Free Solder Interconnect Technology*: Springer.

Lehman, L. P., Athavale, S. N., Fullem, T. Z., Giamis, A. C., Kinyanjui, R. K., Lowenstein, M., Cotts, E. J. (2004). Growth of Sn and intermetallic compounds in Sn-Ag-Cu solder. *Journal of Electronic Materials, 33*(12), 1429-1439.

Li, G.-y., & SHI, X.-q. (2006). Effects of bismuth on growth of intermetallic compounds in Sn-Ag-Cu Pb-free solder joints. *Transactions of Nonferrous Metals Society of China, 16*, s739-s743.

Lin, L.-W., Song, J.-M., Lai, Y.-S., Chiu, Y.-T., Lee, N.-C., & Uan, J.-Y. (2009). Alloying modification of Sn–Ag–Cu solders by manganese and titanium. *Microelectronics Reliability, 49*(3), 235-241.

Liu, W., & Lee, N.-C. (2006). Novel SACX solders with superior drop test performance. *SMTAI, Chicago, IL*.

Liu, Y., Sun, F., & Liu, X. (2010, 13-15 Oct. 2010). *Improving Sn-0.3Ag-0.7Cu low-Ag lead-free solder performance by adding Bi element.* Paper presented at the Strategic Technology (IFOST), 2010 International Forum on.

Liu, Y., Sun, F., Liu, Y., & Li, X. (2014). Effect of Ni, Bi concentration on the microstructure and shear behavior of low-Ag SAC–Bi–Ni/Cu solder joints. *Journal of Materials Science: Materials in Electronics, 25*(6), 2627-2633.

Liu, Y., Sun, F., Zhang, H., & Wang, Y. (2011, 22-24 Aug. 2011). *Influence of Ag, Cu and additive Bi elements on the thermal property of low-Ag SAC solder alloys.* Paper presented at the Strategic Technology (IFOST), 2011 6th International Forum on.

Liu, Y., Sun, F. L., Yan, T. L., & Hu, W. G. (2008, 28-31 July 2008). *Effects of Bi and Ni addition on wettability and melting point of Sn-0.3Ag-0.7Cu Low-Ag Pb-free solder.* Paper presented at the Electronic Packaging Technology & High Density Packaging, 2008. ICEPT-HDP 2008. International Conference on.

Liu, Y. C., Teo, J. W. R., Tung, S. K., & Lam, K. H. (2008). High-temperature creep and hardness of eutectic 80Au/20Sn solder. *Journal of Alloys and Compounds, 448*(1–2), 340-343.

Lu, D., & Wong, C. (2009). *Materials for advanced packaging* (Vol. 181): Springer.

M. Arden, W. (2002). The International Technology Roadmap for Semiconductors—Perspectives and challenges for the next 15 years. *Current Opinion in Solid State and Materials Science, 6*(5), 371-377.

Ma, H. (2009). Constitutive models of creep for lead-free solders. *Journal of materials science, 44*(14), 3841-3851.

Ma, H., & Suhling, J. (2009). A review of mechanical properties of lead-free solders for electronic packaging. *Journal of Materials Science, 44*(5), 1141-1158.

Ma, H., Suhling, J. C., Zhang, Y., Lall, P., & Bozack, M. J. (2007). *The influence of elevated temperature aging on reliability of lead free solder joints.* Paper presented at the Electronic Components and Technology Conference, 2007. ECTC'07. Proceedings. 57th.

Massalski, T. B., Okamoto, H., Subramanian, P., Kacprzak, L., & Scott, W. W. (1986). *Binary alloy phase diagrams* (Vol. 1): American Society for Metals Metals Park, OH.

Mathew, M. D., Yang, H., Movva, S., & Murty, K. L. (2005). Creep deformation characteristics of tin and tin-based electronic solder alloys. *Metallurgical and Materials Transactions A, 36*(1), 99-105.

Medvedev, A. (1956). Aging of Tin-Lead Solders and Joints Soldered by Them. *Metallovedenie i Obrabotka Metallov*(7), 16-23.

Moon, K., Boettinger, W., Kattner, U., Biancaniello, F., & Handwerker, C. (2000). Experimental and thermodynamic assessment of Sn-Ag-Cu solder alloys. *Journal of Electronic Materials, 29*(10), 1122-1136.

Moon, K. W., Boettinger, W. J., Kattner, U. R., Biancaniello, F. S., & Handwerker, C. A. (2000). Experimental and thermodynamic assessment of Sn-Ag-Cu solder alloys. *Journal of Electronic Materials, 29*(10), 1122-1136.

Nogita, K., & Nishimura, T. (2008). Nickel-stabilized hexagonal (Cu, Ni) 6 Sn 5 in Sn–Cu–Ni lead-free solder alloys. *Scripta Materialia, 59*(2), 191-194.

Okamoto, H. (2002). *Phase diagrams of dilute binary alloys* (Vol. 157): ASM International Materials Park, OH.

Osório, W. R., Peixoto, L. C., Garcia, L. R., Mangelinck-Noël, N., & Garcia, A. (2013). Microstructure and mechanical properties of Sn–Bi, Sn–Ag and Sn–Zn lead-free solder alloys. *Journal of Alloys and Compounds, 572*(0), 97-106.

Pandher, R., & Healey, R. (2008, 27-30 May 2008). *Reliability of Pb-free solder alloys in demanding BGA and CSP applications.* Paper presented at the Electronic Components and Technology Conference, 2008. ECTC 2008. 58th.

Pandher, R. S., Lewis, B. G., Vangaveti, R., & Singh, B. (2007, May 29 2007-June 1 2007). *Drop Shock Reliability of Lead-Free Alloys - Effect of Micro-Additives.* Paper presented at the Electronic Components and Technology Conference, 2007. ECTC '07. Proceedings. 57th.

Pang, J. H., Xu, L., Shi, X., Zhou, W., & Ngoh, S. (2004). Intermetallic growth studies on Sn-Ag-Cu lead-free solder joints. *Journal of Electronic Materials, 33*(10), 1219-1226.

Pang, J. H. L., & Che, F. X. (2006, 0-0 0). *Drop impact analysis of Sn-Ag-Cu solder joints using dynamic high-strain rate plastic strain as the impact damage driving force.* Paper presented at the Electronic Components and Technology Conference, 2006. Proceedings. 56th.

Pang, J. H. L., Low, T. H., Xiong, B. S., Luhua, X., & Neo, C. C. (2004). Thermal cycling aging effects on Sn–Ag–Cu solder joint microstructure, IMC and strength. *Thin Solid Films, 462–463*(0), 370-375.

Park, J.-Y., Kabade, R., Kim, C.-U., Carper, T., Dunford, S., & Puligandla, V. (2003). Influence of Au addition on the phase equilibria of near-eutectic Sn-3.8 Ag-0.7 Cu Pb-free solder alloy. *Journal of Electronic Materials, 32*(12), 1474-1482.

Pavlina, E. J., & Van Tyne, C. J. (2008). Correlation of Yield Strength and Tensile Strength with Hardness for Steels. *Journal of Materials Engineering and Performance, 17*(6), 888-893.

Peng, W., Monlevade, E., & Marques, M. E. (2007). Effect of thermal aging on the interfacial structure of SnAgCu solder joints on Cu. *Microelectronics Reliability, 47*(12), 2161-2168.

Puttlitz, K. J., & Stalter, K. A. (2004). *Handbook of lead-free solder technology for microelectronic assemblies*: CRC Press.

Ritchie, R. O. (1988). Workshop on the Mechanics and Physics of Crack Growth: Application to Life PredictionMechanisms of fatigue crack propagation in metals, ceramics and composites: Role of crack tip shielding. *Materials Science and Engineering: A, 103*(1), 15-28.

Rizvi, M., Bailey, C., Chan, Y., Islam, M., & Lu, H. (2007). Effect of adding 0.3 wt% Ni into the Sn–0.7 wt% Cu solder: Part II. Growth of intermetallic layer with Cu during wetting and aging. *Journal of Alloys and Compounds, 438*(1), 122-128.

Rosenberg, A., & Winegard, W. (1954). The rate of growth of dendrites in supercooled tin. *Acta Metallurgica, 2*(2), 342-343.

Rossiter, P. L. (1991). *The electrical resistivity of metals and alloys*: Cambridge University Press.

Sabri, M. F. M., Nordin, N. I. M., Said, S. M., Amin, N. A. A. M., Arof, H., Jauhari, I., . . . Weide-Zaage, K. (2015). Effect of thermal aging on the electrical resistivity of Fe-added SAC105 solder alloys. *Microelectronics Reliability, 55*(9–10), 1882-1885.

Schoeller, H., Bansal, S., Knobloch, A., Shaddock, D., & Cho, J. (2009). Microstructure Evolution and the Constitutive Relations of High-Temperature Solders. *Journal of Electronic Materials, 38*(6), 802-809.

Seo, S.-K., Kang, S. K., Shih, D.-Y., & Lee, H. M. (2008). An Investigation of Microstructure and Microhardness of Sn-Cu and Sn-Ag Solders as Functions of Alloy Composition and Cooling Rate. *Journal of Electronic Materials, 38*(2), 257-265.

Shang, P. J., Liu, Z. Q., Pang, X. Y., Li, D. X., & Shang, J. K. (2009). Growth mechanisms of Cu3Sn on polycrystalline and single crystalline Cu substrates. *Acta Materialia, 57*(16), 4697-4706.

Shangguan, D. (2005). *Lead-Free Solder Interconnect Reliability*: Asm International.

Shen, J., & Chan, Y. C. (2009). Research advances in nano-composite solders. *Microelectronics Reliability, 49*(3), 223-234.

Shimotomai, M., Hasiguti, R., & Umeyama, S. (1978). Dissociative diffusion of Fe 57 in β-Sn as observed by Mössbauer effect. *Physical Review B, 18*(5), 2097.

Shnawah, D., Sabri, M., Badruddin, I., Said, S., Ariga, T., & Che, F. (2013). Effect of Ag Content and the Minor Alloying Element Fe on the Mechanical Properties and Microstructural Stability of Sn-Ag-Cu Solder Alloy Under High-Temperature Annealing. *Journal of Electronic Materials, 42*(3), 470-484.

Shnawah, D. A., Sabri, M. F. M., Badruddin, I. A., Said, S. B. M., Bashir, M. B. A., Sharif, N. M., & Elsheikh, M. H. (2015). Study on coarsening of Ag3Sn intermetallic compound in the Fe-modified Sn–1Ag–0.5Cu solder alloys. *Journal of Alloys and Compounds, 622*(0), 184-188.

Sivasubramaniam, V., Bosco, N. S., Janczak-Rusch, J., Cugnoni, J., & Botsis, J. (2008). Interfacial Intermetallic Growth and Strength of Composite Lead-Free Solder Alloy Through Isothermal Aging. *Journal of Electronic Materials, 37*(10), 1598-1604.

Song, H. Y., Zhu, Q. S., Wang, Z. G., Shang, J. K., & Lu, M. (2010). Effects of Zn addition on microstructure and tensile properties of Sn–1Ag–0.5Cu alloy. *Materials Science and Engineering: A, 527*(6), 1343-1350.

Song, J. M., & Lin, K. L. (2003). Behavior of intermetallics in liquid Sn–Zn–Ag solder alloys. *Journal of Materials Research, 18*(09), 2060-2067.

Suganuma, K. (2001). Advances in lead-free electronics soldering. *Current Opinion in Solid State and Materials Science, 5*(1), 55-64.

Suganuma, K. (2003). *Lead-Free Soldering in Electronics: Science, Technology, and Environmental Impact*: CRC Press.

Suh, D., Kim, D. W., Liu, P., Kim, H., Weninger, J. A., Kumar, C. M., . . . Tejada, H. B. (2007). Effects of Ag content on fracture resistance of Sn–Ag–Cu lead-free solders under high-strain rate conditions. *Materials Science and Engineering: A, 460–461*, 595-603.

Swenson, D. (2007). The effects of suppressed beta tin nucleation on the microstructural evolution of lead-free solder joints *Lead-Free Electronic Solders* (pp. 39-54): Springer US.

Syed, A., Kim, T. S., Cho, Y. M., Kim, C. W., & Yoo, M. (2006, 6-8 Dec. 2006). *Alloying effect of Ni, Co, and Sb in SAC solder for improved drop performance of chip scale packages with Cu OSP pad finish.* Paper presented at the 2006 8th Electronics Packaging Technology Conference.

Telang, A. U., & Bieler, T. R. (2005). The orientation imaging microscopy of lead-free Sn-Ag solder joints. *JOM Journal of the Minerals Metals and Materials Society, 57*(6), 44-49.

Terashima, S., Kariya, Y., & Tanaka, M. (2004). Improvement on thermal fatigue properties of Sn-1. 2 Ag-0. 5 Cu flip chip interconnects by nickel addition. *Materials Transactions, 45*(3), 673-680.

Tu, K.-N. (2007). *Solder joint technology*: Springer.

Tu, K. N. (2010). *Solder Joint Technology: Materials, Properties, and Reliability*: Springer.

Vianco, P. T., & Rejent, J. A. (1999). Properties of ternary Sn-Ag-Bi solder alloys: Part I—Thermal properties and microstructural analysis. *Journal of Electronic Materials, 28*(10), 1127-1137.

Vianco, P. T., & Rejent, J. A. (1999). Properties of ternary Sn-Ag-Bi solder alloys: Part II—Wettability and mechanical properties analyses. *Journal of Electronic Materials, 28*(10), 1138-1143.

Wade, N., Wu, K., Kunii, J., Yamada, S., & Miyahara, K. (2001). Effects of Cu, Ag and Sb on the creep-rupture strength of lead-free solder alloys. *Journal of Electronic Materials, 30*(9), 1228-1231.

Wang, Y., Lin, Y., Tu, C., & Kao, C. (2009). Effects of minor Fe, Co, and Ni additions on the reaction between SnAgCu solder and Cu. *Journal of Alloys and Compounds, 478*(1), 121-127.

Wang, Y. W., Lin, Y. W., Tu, C. T., & Kao, C. R. (2009). Effects of minor Fe, Co, and Ni additions on the reaction between SnAgCu solder and Cu. *Journal of Alloys and Compounds, 478*(1–2), 121-127.

White, D. (1971). The surface tensions of Pb, Sn, and Pb-Sn alloys. *Metallurgical and Materials Transactions B, 2*(11), 3067-3071.

Wood, E. P., & Nimmo, K. L. (1994). In search of new lead-free electronic solders. *Journal of Electronic Materials, 23*(8), 709-713.

Wu, C. M. L., Yu, D. Q., Law, C. M. T., & Wang, L. (2002). Microstructure and mechanical properties of new lead-free Sn-Cu-RE solder alloys. *Journal of Electronic Materials, 31*(9), 928-932.

Xiao, Q., Bailey, H. J., & Armstrong, W. D. (2004). Aging effects on microstructure and tensile property of Sn3. 9Ag0. 6Cu solder alloy. *Journal of Electronic Packaging, 126*(2), 208-212.

Xie, H., Chawla, N., & Mirpuri, K. (2012). Thermal and Mechanical Stability of Ce-Containing Sn-3.9Ag-0.7Cu Lead-Free Solder on Cu and Electroless Ni-P Metallizations. *Journal of Electronic Materials, 41*(12), 3249-3258.

Xie, Y., & Zhang, X. (1998). Phase diagram and thermodynamic properties of Ag−Cu alloys. *Science in China Series E: Technological Sciences, 41*(4), 348-356.

Yang, L. (2013). Effects of Ag particles content on properties of Sn0.7Cu solder. *Journal of Materials Science: Materials in Electronics, 24*(5), 1405-1409.

Yang, L., Zhang, Y., Dai, J., Jing, Y., Ge, J., & Zhang, N. (2015). Microstructure, interfacial IMC and mechanical properties of Sn–0.7Cu–xAl (x = 0–0.075) lead-free solder alloy. *Materials & Design, 67*(0), 209-216.

Yazzie, K., Williams, J., Phillips, N., De Carlo, F., & Chawla, N. (2012). Multiscale microstructural characterization of Sn-rich alloys by three dimensional (3D) X-ray synchrotron tomography and focused ion beam (FIB) tomography. *Materials Characterization, 70*, 33-41.

You, T., Kim, Y., Kim, J., Lee, J., Jung, B., Moon, J., & Choe, H. (2009). Predicting the Drop Performance of Solder Joints by Evaluating the Elastic Strain Energy from High-Speed Ball Pull Tests. *Journal of Electronic Materials, 38*(3), 410-414.

Yu, J., & Kim, J. Y. (2008). Effects of residual S on Kirkendall void formation at Cu/Sn–3.5Ag solder joints. *Acta Materialia, 56*(19), 5514-5523.

Zakel, E., Azdasht, G., & Reichl, H. (1991). Investigations of laser soldered TAB inner lead contacts. *Components, Hybrids, and Manufacturing Technology, IEEE Transactions on, 14*(4), 672-679.

Zeng, G., Xue, S., Zhang, L., Gao, L., Dai, W., & Luo, J. (2010). A review on the interfacial intermetallic compounds between Sn–Ag–Cu based solders and substrates. *Journal of Materials Science: Materials in Electronics, 21*(5), 421-440.

Zhang, P., Li, S. X., & Zhang, Z. F. (2011). General relationship between strength and hardness. *Materials Science and Engineering: A, 529*, 62-73.

Zhang, Q. (2015). *Investigations on Microstructure and Mechanical Properties of the Cu/Pb-free Solder Joint Interfaces*: Springer.

Zhao, J., Qi, L., Wang, X.-m., & Wang, L. (2004). Influence of Bi on microstructures evolution and mechanical properties in Sn–Ag–Cu lead-free solder. *Journal of Alloys and Compounds, 375*(1–2), 196-201.

Zhou, J., Sun, Y., & Xue, F. (2005). Properties of low melting point Sn–Zn–Bi solders. *Journal of Alloys and Compounds, 397*(1–2), 260-264.

Zhou, Q., Zhou, B., Lee, T.-K., & Bieler, T. (2016). Microstructural Evolution of SAC305 Solder Joints in Wafer Level Chip-Scale Packaging (WLCSP) with Continuous and Interrupted Accelerated Thermal Cycling. *Journal of Electronic Materials, 45*(6), 3013-3024.

Zhuo-Ming, G., Guo-Xun, L., & Tao, L. (2000). Kinetics of interface reaction in 40Sn-Bi/Cu and 40Sn-Bi-2Ag/Cu systems during aging in solid state. *IEEE Transactions on Advanced Packaging, 23*(4), 737-742.

Zribi, A., Clark, A., Zavalij, L., Borgesen, P., & Cotts, E. (2001). The growth of intermetallic compounds at Sn-Ag-Cu solder/Cu and Sn-Ag-Cu solder/Ni interfaces and the associated evolution of the solder microstructure. *Journal of Electronic Materials, 30*(9), 1157-1164.

Zribi, A., Clark, A., Zavalij, L., Borgesen, P., & Cotts, E. J. (2001). The growth of intermetallic compounds at Sn-Ag-Cu solder/Cu and Sn-Ag-Cu solder/Ni interfaces and the associated evolution of the solder microstructure. *Journal of Electronic Materials, 30*(9), 1157-1164.

LIST OF PUBLICATIONS AND PAPERS PRESENTED

1. **Mahdavifard, M. H**., Sabri, M. F. M., Said, S. M., Shnawah, D. A., Badruddin, I. A., & Rozali, S. (2016). Effects of Fe and Bi Minor Alloying on Mechanical, Thermal, and Microstructural Properties of Sn-0.7Cu Solder Alloy. Journal of Electronic Materials, 1-10 (*ISI-indexed*).

2. **Mahdavifard, M. H**., Sabri, M. F. M., Shnawah, D. A., Said, S. M., Badruddin, I. A., & Rozali, S. (2015). The effect of iron and bismuth addition on the microstructural, mechanical, and thermal properties of Sn–1Ag–0.5Cu solder alloy. Microelectronics Reliability, 55(9–10), 1886-1890 (*ISI-indexed*).

3. **Mahdavifard. M. H**, M. F. M. Sabri, S.M. Said, I.A. Badruddin, S. Rozali, Effect of aging on mechanical properties of Sn-Cu-Fe-Bi solder alloy, proceeding the 2nd International Science, Technology and Engineering Conference (2nd ISTEC), 2016, Penang, Malaysia.